Theoretical Approach to the Tunneling Current across an Interacting Quantum Dot: The Dressed-Second-Order Diagram Selection

DISSERTATION ZUR ERLANGUNG DES DOKTORGRADES DER NATURWISSENSCHAFTEN (DR. RER. NAT.) DER FAKULTÄT FÜR PHYSIK

DER UNIVERSITÄT REGENSBURG

vorgelegt von
Johannes Kern aus
Freyung
im Jahr 2021.

Die Arbeit wurde von Prof. Dr. Milena Grifoni angeleitet.
Das Promotionsgesuch wurde am 25.08.2021 eingereicht.
Das Kolloquium fand am 27.10.2022 statt.
Prüfungsausschuss:

Vorsitzender:	Prof. Dr. Jascha Repp
1. Gutachter:	Prof. Dr. Milena Grifoni
2. Gutachter:	Prof. Dr. Jaroslav Fabian
weiterer Prüfer:	PD Dr. Andreas K. Hüttel

Abstract:

The topic of this work is the theoretical description of the tunneling current across an interacting quantum dot. The quantum dot is tunnel-coupled to metallic contacts at different chemical potentials – a bias voltage is applied between the two contacts. The discrete energy levels of the quantum dot are tuned by a gate voltage. We here use the term *(energy) level* both as a short term for one-electron levels on the quantum dot, and for the difference of energies of many-electron states of the quantum dot with neighbouring particle-number, while we use the term *chemical potential* only for the contacts. Within the method we apply, the density matrix of the quantum dot, and, in a second step, the current across the quantum dot are calculated making use of a *quantum master equation*. The integral kernel appearing in the quantum master equation is a convergent power series in the parameter characterizing the strength of the tunneling coupling between the quantum dot and the leads, and the coefficients of each of the orders of this power series have an expansion as a sum of contributions we refer to – and actually depict – as *diagrams*, where each diagram represents a collection of tunneling events. In the general-theoretical part of this work, the transport theory, we shall give a derivation of the quantum master equation, and we present and explain the diagrammatic language, by the use of which we formulate tunneling processes as graphic objects.

Within the present thesis we study the transport across a quantum dot according to the single impurity Anderson model (SIAM), which consists of one spin-degenerate one-electron level. The energy of the doubly occupied many-electron state includes the Coulomb-repulsion between the two electrons. The exact and complete sum of all diagrams of all orders has not been calculated, nor has the transport problem been solved exactly by another theory, but approximations are obtained by calculating the sums of all diagrams within diagram selections. In the second main part of this work, where we apply the transport theory, one particular diagram selection is discussed: the *dressed-second-order* (DSO) diagram selection. The DSO selection contains diagrams to all orders in the tunneling coupling; its effect is to "dress" the perturbative second order rates with a finite life time. Specifically, in the DSO-diagrams, the tunneling of a single electron from one lead to the quantum dot (or vice versa) is accompanied by spin- and charge-fluctuations. The second order alone is a natural approximation scheme to describe sequential tunneling across a single electron transistor (SET): An electron with fit energy tunnels from one lead onto the quantum dot; then, this electron tunnels from the quantum dot into a non-occupied level with fit energy of the opposite lead, which has lower chemical potential. These sequential processes are

responsible for the current-voltage characteristics in the sequential tunneling regime: A maximum of the differential conductance vs. the bias at that position, where one of the contacts' chemical potentials meets the energy level of the SET – in the main chapters of this work we shall refer to the latter quantity as the energy difference between the occupied and the non-occupied many-electron states of the quantum dot – is seen by the second order. The width of this resonance, obtained by the second order, is given exclusively by the thermal energy k_BT. However, with decreased temperature, the width of the resonance gets determined no more by the temperature, but rather by the tunneling coupling. This behaviour is covered by the DSO-diagram selection, but not by the un-dressed second order.

In addition, if applied to the SIAM, and if the degenerate level of the SIAM lies *below* the Fermi level of the contacts, the DSO produces a resonance at zero bias which is getting more and more pronounced with decreasing temperature. We show that the DSO describes the onset of the Kondo effect in quantum dots qualitatively correctly. We compare the results of a numerical implementation of the DSO to the results of a closely related theoretical approach – the *resonant tunneling approximation* – as well as to the results of experiments.

Contents

Chapter 1

Introduction

The tunneling of electrons across potential barriers has attracted the interest of theoretical as well as experimental physicists since the phenomenon became known. According to quantum mechanics, the dualism of particle and wave implies that a particle can cross a forbidden region with high potential energy, even if, classically, the particle's energy does not suffice to ever be present in the barrier-region. Exemplarily, one early experiment on the effect investigates the electric current through a thin insulating layer, Ref. [1]. An aluminum-oxide film around $50\mathring{A}$ thick is sandwiched between aluminum metal films in this experiment; the current starts to grow linearly with the voltage between the Al-electrodes; at higher voltages, the current increases exponentially with voltage. The measurements could be brought into line with an adapted theory for tunneling through thin vacuum layers (cp. Fig. 1.1), while alternative transport-mechanisms, such as ionic conduction, as well as electric current via small metal bridges, could be excluded.

Later experiments contain two metallic electrodes, and, within the oxide which fills the space between these electrodes, a small amount of another conducting material. In the experiment [2], layers of small tin-particles, embedded in aluminum-oxide, are placed between two aluminum-electrodes – the electron here tunnels from one Al-film to a Sn-particle, becomes localized on the particle, and then in turn tunnels on to the other Al-film. The dynamical resistance dV/dI vs. the voltage V displays a maximum at zero bias in this experiment. In Ref. [2], the $Al - Sn - Al$ tunneling-junction is viewed as a sequence of two capacitors in series (cp. Fig. 1.2). Due to large Coulomb-interaction on the small tin-particles (neglecting the level spacing), the energy levels on the particle are in general not aligned with the Fermi level of the electrodes; hence, an activation energy has to be paid to allow current to flow. This causes the minimum of the differential conductance dI/dV as function of the bias V at zero bias. On the other hand,

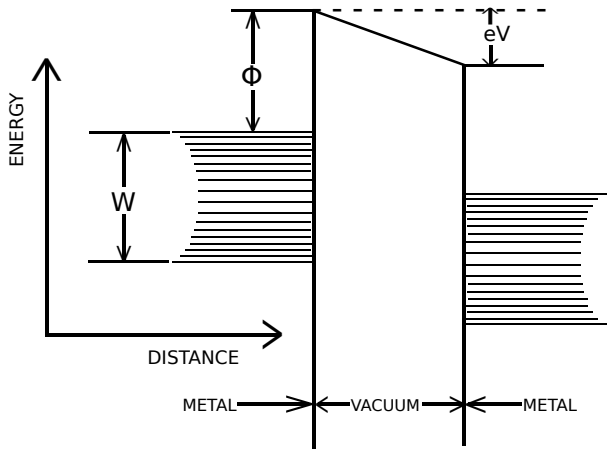

Figure 1.1: Potential energy diagram for the analysis of tunneling through a thin vacuum layer (cp. Fig. 5 in Ref. [1]). The quantity Φ is the work function, while V is the voltage between two electrodes of the same metal.

a temperature-dependent *maximum* of the differential conductance at zero bias has been observed in metal-insulator-metal junctions. This maximum has been attributed to the scattering of the tunneling electrons by localized magnetic impurities inside the insulating layer or near the insulator-metal interface [3].

Modern experiments on tunneling across a metallic or semi-conducting island include a gate-electrode which serves to shift the discrete energy levels of the island up- and downward (Fig. 1.3). For example, the island – which we refer to as "quantum dot" in this context – can be realized as a tiny metallic particle, as a region within plane semi-conducting material, as a carbon nanotube, as a molecule, etc.. The quantum dot is so small that, in contrast to the contacts with their continuous density of electron levels, the many-body energies necessary to add one more electron on the dot are quantized. Plots of the differential conductance dI/dV_b as function of the bias- and the gate voltage – *stability diagrams* – reveal regions of Coulomb-blockade, where sequential tunneling is excluded, since none of the quantum dot's discrete energy levels lies in the window between the electrodes' chemical potentials; electric current is strongly suppressed within these "Coulomb diamonds". *Resonant* transport, on the other hand, sets in as soon as one of the differences $E_{N+1} - E_N$ between ground state energies of the quantum dot is pushed through the bias-window by the gate voltage. Note: We here consider *all* contributions to the energy of a N-electron quantum dot state, such as Coulomb-interaction, level spacing, gate-dependent part, exchange

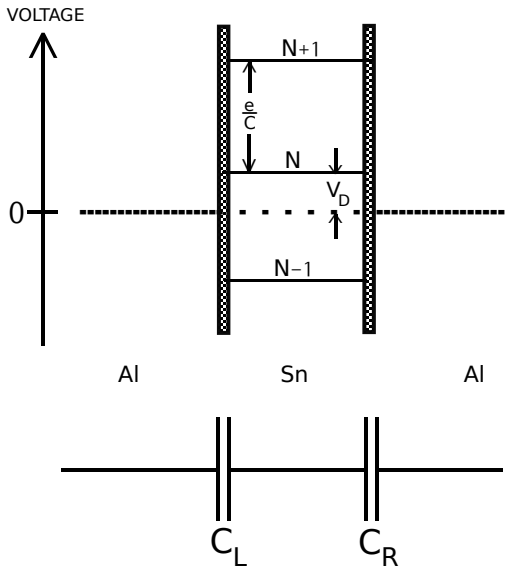

Figure 1.2: (Cp. Fig. 12 in Ref. [2].) Energy scheme of an $Al - Sn - Al$ based metallic island. There is an integer number of electrons on the Sn-particle. Changing this number by one electron changes the voltage of the particle by e/C, where $C = C_R + C_L$ is the particle's capacitance. The quantity eV_D (e the electron charge), on the other hand, is the difference between the electrodes' Fermi level, and the nearest-lying discrete energy level of the particle.

energy etc. to be per definition contained in the quantity E_N; thus, the latter quantity corresponds to the energy E_a assigned to a many-electron state a by the quantum dot Hamiltonian (Eq. (2.4)) within the main chapters of this thesis.

Transport experiments with quantum dots encompass a variety of phenomena (examples are taken from Ref. [4]): In carbon nanotubes, the fourfold-periodicity in the successive occupation of one-electron levels is confirmed. Co-tunneling – a coherent tunneling process in which two electrons are involved – is recovered in the stability diagram in the form of areas within the Coulomb diamonds whose boundaries are lines of constant bias [5]. In transport experiments with molecules, the effect of vibrations of the nuclei, as well as of center-of-mass oscillations between the contacts, is visible in the stability diagram as lines running parallel to the Coulomb diamonds' boundaries [6, 7]. Finally, the Kondo effect in quantum dots gives rise to a temperature-dependent peak of the differential conductance at zero bias [8, 9].

The present work is theoretical, and it is based on a rich history of theoretical models designed – or transferred from related problems – to study the tunneling current across interacting quantum dots. We work in the second quantization formalism, thus starting out with *many*-electron states rather than describing the tunneling of a single electron. The Hamilton operator of the overall system, consisting of two leads (also referred to as contacts, electrodes, source and drain, or reservoirs), and the quantum dot, contains the Hamiltonian of each isolated sub-system as an additive contribution. An extra term, the tunneling Hamiltonian, establishes the coupling between one-electron levels on the leads, on the one hand, and on the quantum dot, on the other hand. The contacts' different chemical potentials enter into the theory via their *density matrix* at thermal equilibrium [10], while the gate electrode's influence is incorporated in the energies assigned to the quantum dot states.

The tunneling current across a single impurity Anderson model quantum dot has been addressed by various methods. An overview of a selection of these approaches is given in Ref. [11], where the authors compare the equations of motion method, the slave boson approximation, and the numerical renormalization group technique. Within the *equations of motion* method, time-derivatives of the quantum dot- and leads Green's functions are taken to generate a set of coupled equations of motion. The hierarchy of equations is infinite, and one needs to truncate the equations by physical arguments [11, 12]. In the *slave boson approximation*, on the other hand, the quantum dot's creation operator is rewritten by the use of bosonic auxiliary- or pseudo-particle operators. The quantum dot Green's function is expressed by the

pseudo-particle Green's functions, where the latter are calculated by a diagrammatic theory perturbative in the tunneling coupling [11, 13]. The terms *non-* and *one-crossing approximation* refer to numbers of vertex corrections taken into account within these approximations [11]. Finally, the *numerical renormalization group* method involves a logarithmic discretization in energy of the contacts' non-interacting Hamiltonian [11, 14].

We here present a *quantum master equation* approach [15] to calculate the tunneling current via the stationary reduced density matrix of the island, and we shall assume the single impurity Anderson model for the quantum dot, which possesses only one spin-degenerate level. By a diagrammatic analysis, and, in particular, by a diagram *selection* first applied in Ref. [16], we describe correctly resonant transport. At the same time, the diagram selection is able to address the onset of the Kondo peak, as well as its splitting in magnetic field.

The work is structured as follows: *Chapter 2* contains the derivation of the general transport theory, including the quantum master equation. The stationary density matrix and current are determined by an integral kernel, and we give a complete diagrammatic analysis of all contributions to this kernel. In the following applied *Chapter 3*, being based on Ref. [17], on the other hand, we choose a particular diagram selection, the *dressed-second-order*, and test its performance compared to other theoretical approaches, as well as to experimental results. In a number of appendices to this work, we give mathematical background, and intermediate steps in sequences of equations, too lengthy to be included in the main chapters. We summarize the benefit of this work in the final conclusions.

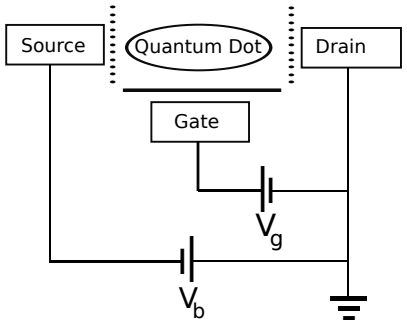

Figure 1.3: Basic setup of transport experiments with quantum dots. Two metallic electrodes (source and drain) are tunnel-coupled to a nanoscopic device. Electrons tunnel sequentially from source to quantum dot, then from quantum dot to drain, or, else, several electrons may tunnel in one coherent process between the electrodes and the quantum dot. The current is driven by a bias voltage V_b, while a gate voltage V_g serves to tune the energy differences $E_{N+1} - E_N$ between quantum dot states with neighbouring particle-number.

Chapter 2

Transport Theory

In this chapter we outline the general theory we apply to describe the electron-transport across quantum dots. Central to this theory are the quantum master equation for the dot reduced density operator, and a diagrammatic language, by which we depict the tunneling of electrons between contacts and quantum dot. At the level of the diagrams it is equivalent to the transport theory developed in the 1990-s by J. König, H. Schoeller, and G. Schön [18]. Independently, an approach perturbative in the tunneling coupling has been formulated by M. Leijnse, M. Wegewijs, M. Grifoni, and S. Koller [19]. The theory of the present work, however, is exact, and contains this perturbative approach.

2.1 Hamilton Operator

The system under consideration contains a quantum dot and two metallic leads (also referred to as contacts or reservoirs); its Hamilton operator reads:

$$\hat{H} = \hat{H}_R + \hat{H}_\odot + \hat{H}_T. \tag{2.1}$$

$\hat{H}_R$ and $\hat{H}_\odot$ rule the time evolution of the reservoirs and of the quantum dot, respectively, as long as these are separate. The connection between the two sub-systems is established by the tunneling contribution $\hat{H}_T$. We assume:

$$\hat{H}_R = \sum_{l\in\mathcal{L},\sigma\in\mathcal{S},\mathbf{k}\in\mathcal{K}_l} \varepsilon_{l\sigma\mathbf{k}} \hat{c}^\dagger_{l\sigma\mathbf{k}} \hat{c}_{l\sigma\mathbf{k}}. \tag{2.2}$$

Implicitly, the vector space of many-electron states, on which the Hamiltonian $\hat{H}$, as well as its constituent parts, operate, is generated by a set of one-electron levels (cp. Fig. (2.1)). In the formula for $\hat{H}_R$ (2.2), the index $l \in \mathcal{L}$ denotes the lead and takes all values within a set $\mathcal{L}$ of – within this

work: always two – contacts, while the spin-index σ is taken from a two-elementary set $\mathcal{S} = \{\uparrow, \downarrow\}$. Else, to study the theoretically relevant case of a spinless quantum dot, $\mathcal{S}$ is assumed to consist of only *one* element, $\mathcal{S} = \{\sigma_o\}$. For any fixed value of l, $\mathcal{K}_l$ denotes a set of allowed wave vectors of electron levels in lead l. To each electron level in one of the leads defined by the three indices $l\sigma\mathbf{k}$, $\varepsilon_{l\sigma\mathbf{k}}$ is the band energy assigned to this electron level. Finally, $\hat{c}^{(\dagger)}_{l\sigma\mathbf{k}}$ is the annihilation (creation) operator of the level $l\sigma\mathbf{k}$. For simplicity, we take into account only one band in each of the contacts, and assume the set $\mathcal{K}_l$ of allowed wave vectors is finite.

The theoretical models of quantum dots considered within this work are the spinless quantum dot with only one non-degenerate one-electron level, on the one hand, and the single impurity Anderson model (SIAM), on the other hand. The Hamiltonian of the spinless quantum dot reads:

$$\hat{H}_\odot \quad = \quad E_{\sigma_o} \hat{d}^\dagger_{\sigma_o} \hat{d}_{\sigma_o}, \tag{2.3}$$

where $\hat{d}_{\sigma_o}$ is the annihilation operator of the only one-electron level on the quantum dot, and E_{σ_o} is the corresponding energy of the occupied state. The Hamiltonian of the SIAM, on the other hand, is

$$\hat{H}_\odot \quad = \quad \sum_{\sigma\in\{\uparrow,\downarrow\}} E_\sigma \hat{d}^\dagger_\sigma \hat{d}_\sigma \quad + \quad U \hat{d}^\dagger_\uparrow \hat{d}_\uparrow \hat{d}^\dagger_\downarrow \hat{d}_\downarrow, \tag{2.4}$$

with $U \geq 0$ the energy due to Coulomb-repulsion. Implicitly, the state vector space of the quantum dot in the case of the SIAM is spanned by four states: An empty state, a doubly occupied state, and two singly occupied states with spins $\uparrow$, and $\downarrow$.

Finally, the interaction between dot and leads is given by the tunneling Hamiltonian:

$$\hat{H}_T = \sum_{l\in\mathcal{L},\sigma\in\mathcal{S},\mathbf{k}\in\mathcal{K}_l} T_{l\sigma\mathbf{k}} \hat{c}^\dagger_{l\sigma\mathbf{k}} \hat{d}_\sigma + T^*_{l\sigma\mathbf{k}} \hat{d}^\dagger_\sigma \hat{c}_{l\sigma\mathbf{k}}. \tag{2.5}$$

The coefficients $T_{l\sigma\mathbf{k}}$ contain, via their magnitude, the strength of the tunneling coupling. Let $T^*_{l\sigma\mathbf{k}}$ denote their complex conjugates.

2.2 Density matrix

The configuration of the total system containing the leads and the quantum dot is described by a density operator or *density matrix* [10] $\hat{\rho}(t)$. We assume there is an initial time t_0, at which the sub-systems are independent, and at which the contacts are in thermal equilibrium. The total density matrix $\hat{\rho}(t_0)$

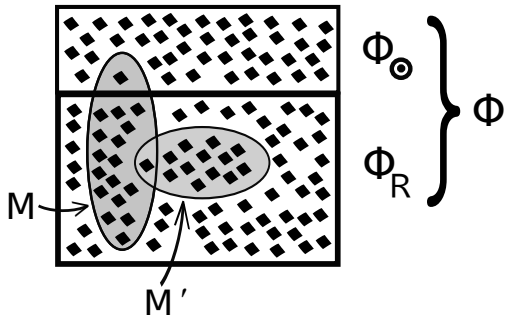

Figure 2.1: The structure of the vector space which the Hamiltonian (2.1) operates on (cp. App. A (Product States)). All many-electron states are constructed from a finite set Φ of one-electron levels. These one-electron levels here are depicted by the little black squares. To each subset $M \subset \Phi$, including the empty set $\emptyset$, there is one normalized many-electron state $\pi(M)$. While $\hat{H}_R$ and $\hat{H}_\odot$ are diagonal in the states $\pi(M)$, the tunneling Hamiltonian $\hat{H}_T$ maps a state $\pi(M)$ to a linear combination of states $\pi(M')$ with $|M'| = |M|$, $|M' \cap M| = |M| - 1$. So, $\pi(M')$ has the same number of elements as $\pi(M)$, but the two many-electron states differ by one one-electron level.

is then a product of the density matrices of the reservoirs and the quantum dot,

$$\hat{\rho}(t_0) \quad = \quad \hat{\rho}_R \otimes \hat{\rho}_\odot(t_0), \tag{2.6}$$

where

$$\hat{\rho}_R \quad = \quad \bigotimes_{l \in \mathcal{L}} \hat{\rho}_l. \tag{2.7}$$

One possible realization of the present product of vector spaces and operators is given in App. A (Product States).

To each of the leads, the operator $\hat{\rho}_l$ is the density matrix of lead l in thermal equilibrium at temperature T, and at possibly spin-dependent chemical potentials $\mu_{l\sigma}$:

$$\hat{\rho}_l \quad := \quad \frac{1}{\mathcal{N}_l} \exp\left(\frac{-1}{k_B T} \sum_{\sigma \in \mathcal{S}, \mathbf{k} \in \mathcal{K}_l} (\varepsilon_{l\sigma\mathbf{k}} - \mu_{l\sigma}) \hat{c}^\dagger_{l\sigma\mathbf{k}} \hat{c}_{l\sigma\mathbf{k}} \right) \Bigg|_{V_l}, \tag{2.8}$$

(cp. Fig. 2.2) with V_l the state vector space of lead l, where the vertical bar denotes the restriction of the map to the domain's subset V_l, and where the factor $1/\mathcal{N}_l$ ensures the normalization of the density operator to unity trace,

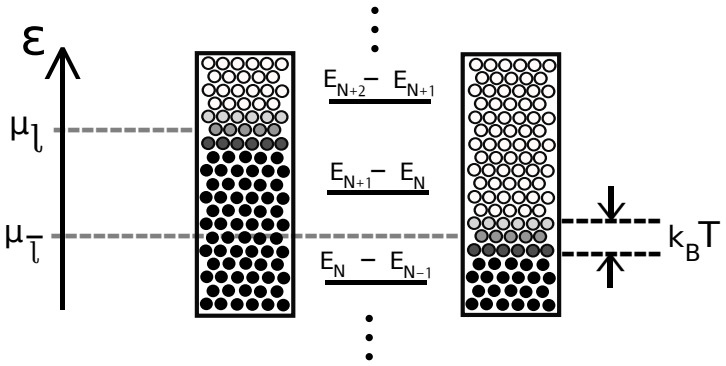

Figure 2.2: Energy scheme with contacts and central device. The density matrix $\hat{\rho}_l$ (2.8) of contact l at thermal equilibrium with chemical potential μ_l [for simplicity we omit the spin-index "σ" in case the chemical potential is independent of the spin] implies that the occupation-probability of a one-electron level in contact l with energy ε is given by $f\left((\varepsilon-\mu_l)/k_BT\right)$, with f the parameter-free Fermi-Dirac distribution. The differences $E_{N+1}-E_N$ between the energies of quantum dot states with neighbouring particle-number contain a gate-dependent contribution $\alpha e V_{gate}$, with α a conversion factor, which is independent of N. Hence, by changing the gate voltage the latter energy differences are uniformly shifted up- or downward. Moreover, to add one more electron to the quantum dot, provided there is already a number of N electrons on it, costs the energy NU, with U the energy of Coulomb-repulsion between two electrons on the dot. While the energy E_N of a particular N-electron state depends on its specific structure, the differences $E_{N+1}-E_N$ appear approximately equidistant – as far as the Coulomb-repulsion yields the dominant contribution.

$$\mathcal{N}_l \quad = \quad \prod_{\sigma\in\mathcal{S},\mathbf{k}\in\mathcal{K}_l} \left\{1+\exp\left(\frac{-1}{k_BT}(\varepsilon_{l\sigma\mathbf{k}}-\mu_{l\sigma})\right)\right\}. \tag{2.9}$$

The operator $\hat{\rho}_\odot(t_0)$ is some initial density matrix of the quantum dot; its shape is not relevant for the *stationary* reduced density matrix of the quantum dot, nor for the stationary current flowing across it, and so, since we shall determine and calculate only stationary quantities, we do not further specify $\hat{\rho}_\odot(t_0)$.

After the time t_0, the time evolution of the density matrix is ruled by the total Hamiltonian according to the Liouville-von Neumann Equation:

$$i\hbar\,\dot{\hat{\rho}}(t) = [\hat{H},\hat{\rho}(t)]. \tag{2.10}$$

The total density matrix will then cease to have product form, but the *reduced density matrix* (Ref. [10]) $\hat{\rho}_{\odot}(t)$ of the quantum dot can be defined by tracing out the degrees of freedom of the reservoirs:

$$\hat{\rho}_{\odot}(t) \quad := \quad Tr_R\{\hat{\rho}(t)\}. \tag{2.11}$$

The expectation value $\mathcal{E}(\hat{N}_l)(t)$ of the particle-counting operator of lead l,

$$\hat{N}_l \; := \sum_{\sigma\in\mathcal{S},\mathbf{k}\in\mathcal{K}_l} \hat{c}^{\dagger}_{l\sigma\mathbf{k}}\hat{c}_{l\sigma\mathbf{k}}, \tag{2.12}$$

at time t is obtained by taking the full trace of its product with the density matrix [10],

$$\mathcal{E}(\hat{N}_l)(t) \; := \; Tr\left\{\hat{N}_l\hat{\rho}(t)\right\}. \tag{2.13}$$

Thus, applying the cyclicity of the trace, the particle *current* onto lead l at time t is:

$$\begin{aligned}\frac{d}{dt}\mathcal{E}(\hat{N}_l)(t) &= Tr\left\{\hat{N}_l\dot{\hat{\rho}}(t)\right\} = -\frac{i}{\hbar}Tr\left\{\hat{N}_l\left[\hat{H},\hat{\rho}(t)\right]\right\}\\ &= Tr\left\{\hat{I}_l\hat{\rho}(t)\right\}\\ &=: \mathcal{E}(\hat{I}_l)(t),\end{aligned} \tag{2.14}$$

with $\hat{I}_l$ the operator of the particle-current onto lead l,

$$\begin{aligned}\hat{I}_l \quad &:= \quad \frac{i}{\hbar}[\hat{H},\hat{N}_l] \\ &= \quad \frac{i}{\hbar}\sum_{\sigma\in\mathcal{S},\mathbf{k}\in\mathcal{K}_l} T^{*}_{l\sigma\mathbf{k}}\hat{d}^{\dagger}_{\sigma}\hat{c}_{l\sigma\mathbf{k}} - T_{l\sigma\mathbf{k}}\hat{c}^{\dagger}_{l\sigma\mathbf{k}}\hat{d}_{\sigma}.\end{aligned} \tag{2.15}$$

In the applied part of this work we will determine the *stationary* current $\boldsymbol{I_l}$ according to the definition

$$\boldsymbol{I_l} \quad := \quad \lim_{\lambda\to 0+}\lambda\int_{t_0}^{\infty} e^{-\lambda(t-t_0)}\mathcal{E}(\hat{I}_l)(t)dt. \tag{2.16}$$

(Cp. Fig. 2.3.)

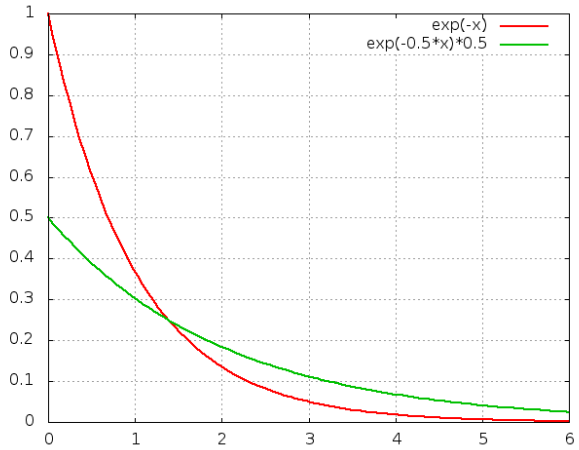

Figure 2.3: Plots of the probability density $d_\lambda(x) = \lambda \exp(-\lambda x)$ in the cases $\lambda = 1$, and $\lambda = 0.5$. The integral $\int_0^\infty dx d_\lambda(x)$ has the value 1 for all $\lambda > 0$. However, with smaller and smaller value of λ, the probability is distributed more and more evenly over the positive x-axis, and so we can form a long-term average- or stationary value of a function $f(x)$ by taking the limit $\lim_{\lambda \to 0+} \int_0^\infty dx\ f(x) d_\lambda(x)$, as it is done for the stationary current (2.16).

2.3 Quantum Master Equation

2.3.1 Time Evolution in the Interaction Picture

To focus on the effect of the tunneling, which establishes the interaction between the sub-systems, we define

$$\hat{H}_0 \quad := \quad \hat{H}_R + \hat{H}_\odot, \tag{2.17}$$

the non-interacting part of the complete Hamiltonian (2.1); to any operator $\hat{z}$ we define the transform

$$\mathcal{W}(t)\hat{z} \ := \ \exp\left(\frac{i}{\hbar}\hat{H}_0 t\right)\ \hat{z}\ \exp\left(-\frac{i}{\hbar}\hat{H}_0 t\right), \tag{2.18}$$

and, analogously, for linear maps $\hat{y}$ operating only on the sub-space $V_\odot$ spanned by the many-electron states of the quantum dot:

$$\mathcal{W}_\odot(t)\hat{y} \ := \ \exp\left(\frac{i}{\hbar}\hat{H}_\odot|_{V_\odot} t\right)\ \hat{y}\ \exp\left(-\frac{i}{\hbar}\hat{H}_\odot|_{V_\odot} t\right), \tag{2.19}$$

where $\hat{H}_\odot|_{V_\odot}$ is the restriction of $\hat{H}_\odot$ to $V_\odot$. We note the relation

$$Tr_R\{\mathcal{W}(t)\hat{z}\} \quad = \quad \mathcal{W}_\odot(t) Tr_R\{\hat{z}\}. \tag{2.20}$$

Now, we consider the time evolution of the transformed density matrix

$$\hat{\sigma}(t) \quad := \quad \mathcal{W}(t)\hat{\rho}(t_0 + t), \tag{2.21}$$

the density matrix *in the interaction picture*. In analogy to Eq. (2.11), we define

$$\hat{\sigma}_{\odot}(t) \quad := \quad Tr_R\{\hat{\sigma}(t)\}. \tag{2.22}$$

The translation of the Liouville-von Neumann equation (2.10) into the interaction picture yields the following kinetic equation for the total density matrix in the interaction picture $\hat{\sigma}(t)$:

$$\dot{\hat{\sigma}}(t) \quad = \quad \mathcal{L}(t)\hat{\sigma}(t), \tag{2.23}$$

where the Liouvillian appearing in this equation is given by

$$\mathcal{L}(t)\hat{z} \quad = \quad \frac{-i}{\hbar}[\mathcal{W}(t)\hat{H}_T, \hat{z}]. \tag{2.24}$$

We note the relation

$$\mathcal{W}(s)\mathcal{L}(t) \quad = \quad \mathcal{L}(s+t)\mathcal{W}(s). \tag{2.25}$$

The solution to Eq. (2.23) can be written as a series:

$$\begin{aligned} \hat{\sigma}(t) \;=\; & \hat{\sigma}(0) \quad + \\ & \int_{0\le\tau_1\le t} \mathcal{L}(\tau_1)\hat{\sigma}(0) \quad + \\ & \int\int_{0\le\tau_1\le\tau_2\le t} \mathcal{L}(\tau_2)\mathcal{L}(\tau_1)\hat{\sigma}(0) \quad + \\ & \vdots \quad . \end{aligned} \tag{2.26}$$

The n-th integral in this sum is taken over a set of measure $t^n/n!$, since there are $n!$ possibilities to order a number of n real numbers; hence the sum converges, and this ansatz for $\hat{\sigma}(t)$ indeed solves the equation (2.23).

Let

$$\hat{N}_R \;:=\; \sum_{l\in\mathcal{L}} \hat{N}_l \tag{2.27}$$

be the particle-counting operator of the reservoirs, and for any $N \in \mathbb{N}_0$, let

$$\mathrm{eig}\left(\hat{N}_R, N\right) \;:=\; \ker\left(\hat{N}_R - N\hat{1}\right) \tag{2.28}$$

be the eigenspace of $\hat{N}_R$ with eigenvalue N. The operators $\hat{H}_0$ and $\hat{\sigma}(0) = \hat{\rho}(t_0)$, Eq. (2.6), do not change the particle-number, but $\hat{H}_T$ maps elements in eig $\left(\hat{N}_R, N\right)$ to sums of elements in eig $\left(\hat{N}_R, N+1\right)$ and eig $\left(\hat{N}_R, N-1\right)$. Hence, the reduced operator of any of the integrals with an odd number of Liouvillians vanishes:

$$\begin{aligned} \hat{\sigma}_\odot(t) &= \hat{\sigma}_\odot(0) \quad + \\ &\int\int_{0\le\tau_1\le\tau_2\le t} A^{(2)}(\tau_2,\tau_1)\hat{\sigma}_\odot(0) \quad + \\ &\int\dots\int_{0\le\tau_1\le\dots\le\tau_4\le t} A^{(4)}(\tau_4,\dots,\tau_1)\hat{\sigma}_\odot(0) \quad + \\ &\quad\vdots \quad , \end{aligned} \tag{2.29}$$

where

$$A^{(2n)}(\tau_{2n},\dots,\tau_1)\hat{y} \quad := \quad Tr_R\left\{\mathcal{L}(\tau_{2n})\dots\mathcal{L}(\tau_1)(\hat{\rho}_R\otimes\hat{y})\right\} \tag{2.30}$$

for any linear map $\hat{y}$ operating on the vector space of the quantum dot.

2.3.2 Memory Equation for the Reduced Density Matrix and for the Current

The map $A^{(2n+2)}$ of the last definition has the decomposition

$$\begin{aligned} A^{(2n+2)}(\tau_{2n+2},\dots,\tau_1) &= I^{(2n+2)}(\tau_{2n+2},\dots,\tau_1) \quad + \\ &\quad I^{(2n)}(\tau_{2n+2},\dots,\tau_3)A^{(2)}(\tau_2,\tau_1) \quad + \\ &\qquad\vdots \\ &\quad I^{(2)}(\tau_{2n+2},\tau_{2n+1})A^{(2n)}(\tau_{2n},\dots,\tau_1), \end{aligned} \tag{2.31}$$

with $I^{(2n+2)}(\tau_{2n+2},\dots,\tau_1)$ being defined recursively by

$$I^{(2)} \quad := \quad A^{(2)}, \tag{2.32}$$

and by the condition that the above equality is satisfied:

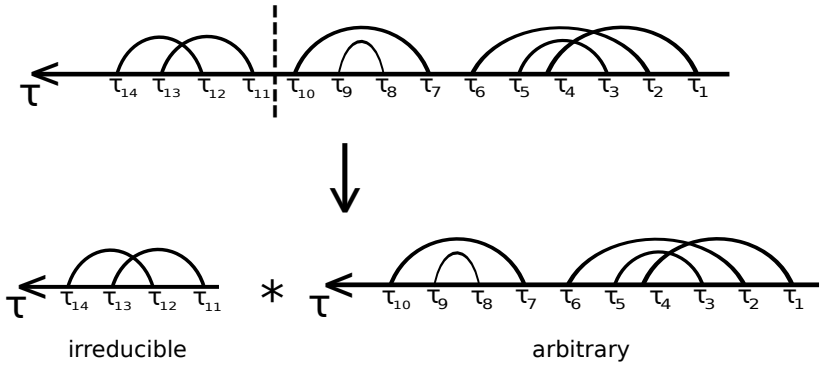

Figure 2.4: As we show in App. C (Decomposition of the Kernel), all the contributions to $A^{(2n+2)}(\tau_{2n+2},\ldots,\tau_1)$ are characterized by what we shall refer to as "pair formations": Ways of grouping a number of $2n+2$ ordered objects into pairs; in the present example-figure, this is a number of 14 subsequent points on a time axis, each connected to one further point by a bent line. The diagram is split into two parts by a vertical cut which does not cut through any of the bent lines. After the splitting, the leading component can be arbitrary, while the final component is *irreducible* in the sense that no further splitting of this component is possible.

$$
\begin{aligned}
I^{(2n+2)}(\tau_{2n+2},\ldots,\tau_1) \;:=\; & A^{(2n+2)}(\tau_{2n+2},\ldots,\tau_1) \quad - \\
& \Big\{\; I^{(2n)}(\tau_{2n+2},\ldots,\tau_3)A^{(2)}(\tau_2,\tau_1) + \\
& I^{(2n-2)}(\tau_{2n+2},\ldots,\tau_5)A^{(4)}(\tau_4,\ldots,\tau_1) + \\
& \qquad\vdots \\
& I^{(2)}(\tau_{2n+2},\tau_{2n+1})A^{(2n)}(\tau_{2n},\ldots,\tau_1)\Big\}\;.
\end{aligned}
\tag{2.33}
$$

As we shall see later, the present decomposition of $A^{(2n+2)}$ corresponds to a splitting of "pair formations" into an arbitrary, possibly *reducible*, component, and an *irreducible* component; within the map $I^{(2n)}$, we take the sum over all irreducible pair formations, while, within the map $A^{(2n)}$, the sum over all arbitrary pair formations is taken (cp. Fig. 2.4).

Applying this decomposition of $A^{(2n+2)}$ (2.31), we can rearrange the sum (2.29):

$$\hat{\sigma}_\odot(t) = \hat{\sigma}_\odot(0) \quad + \tag{2.34}$$

$$\int\int_{0\le s_1\le s_2\le t} I^{(2)}(s_2,s_1) \qquad \{\hat{\sigma}_\odot(0)+$$
$$\int\int_{0\le\tau_1\le\tau_2\le s_1} A^{(2)}(\tau_2,\tau_1)\hat{\sigma}_\odot(0)+$$
$$\int\ldots\int_{0\le\tau_1\le\cdots\le\tau_4\le s_1}$$
$$A^{(4)}(\tau_4,\ldots,\tau_1)\hat{\sigma}_\odot(0)+$$
$$\vdots \quad \} \quad +$$
$$\int\ldots\int_{0\le s_1\le\cdots\le s_4\le t} I^{(4)}(s_4,\ldots,s_1) \qquad \{\hat{\sigma}_\odot(0)+$$
$$\int\int_{0\le\tau_1\le\tau_2\le s_1} A^{(2)}(\tau_2,\tau_1)\hat{\sigma}_\odot(0)+$$
$$\int\ldots\int_{0\le\tau_1\le\cdots\le\tau_4\le s_1}$$
$$A^{(4)}(\tau_4,\ldots,\tau_1)\hat{\sigma}_\odot(0)+$$
$$\vdots \quad \} \quad +$$
$$\vdots \quad ,$$

so

$$\hat{\sigma}_\odot(t) \quad = \quad \hat{\sigma}_\odot(0) + \int_0^t ds\ \kappa(t,s)\hat{\sigma}_\odot(s), \tag{2.35}$$

with the integral kernel

$$\kappa(t,s) \ := \ \int_{s\le s_2\le t} I^{(2)}(s_2,s) \quad +$$
$$\int\int\int_{s\le s_2\le s_3\le s_4\le t} I^{(4)}(s_4,s_3,s_2,s) \quad +$$
$$\vdots \quad . \tag{2.36}$$

Back-Transformation to the Schrödinger Picture

The back-transformation of this equation to the Schrödinger picture is performed by going back to definition (2.21). By Eq. (2.20) we obtain

$$\hat{\rho}_\odot(t_0+t) = \mathcal{W}_\odot(-t)\hat{\sigma}_\odot(0) + \int_0^t ds\ \mathcal{W}_\odot(-t)\kappa(t,s)\hat{\sigma}_\odot(s). \tag{2.37}$$

Applying Eq. (2.25), we find that generally

$$\begin{aligned} & \mathcal{W}_\odot(-\tau)A^{(2n)}(\tau_{2n},\ldots,\tau_1) \\ = \quad & A^{(2n)}(\tau_{2n}-\tau,\ldots,\tau_1-\tau)\mathcal{W}_\odot(-\tau), \end{aligned} \tag{2.38}$$

and hence

$$\begin{aligned} & \mathcal{W}_\odot(-\tau)I^{(2n)}(\tau_{2n},\ldots,\tau_1) \\ = \quad & I^{(2n)}(\tau_{2n}-\tau,\ldots,\tau_1-\tau)\mathcal{W}_\odot(-\tau). \end{aligned} \tag{2.39}$$

As a consequence, the kernel (2.36) has the property

$$\begin{aligned} \mathcal{W}_\odot(-t)\kappa(t,s) &= \mathcal{W}_\odot\left(-(t-s)\right)\mathcal{W}_\odot\left(-s\right)\kappa(t,s) \\ &= \mathcal{W}_\odot\left(-(t-s)\right)\kappa(t-s,0)\mathcal{W}_\odot\left(-s\right), \end{aligned} \tag{2.40}$$

and we obtain the following equation for the reduced density matrix of the quantum dot at time t:

$$\hat{\rho}_\odot(t) = \mathcal{W}_\odot(-(t-t_0))\hat{\rho}_\odot(t_0) + \int_{t_0}^t ds\ \overline{K}(t-s)\hat{\rho}_\odot(s), \tag{2.41}$$

where

$$\overline{K}(\tau) := \mathcal{W}_\odot(-\tau)\kappa(\tau,0). \tag{2.42}$$

Differentiation of this Equation: Quantum Master Equation

Differentiating both sides of Eq. (2.41) with respect to the time t we obtain:

$$\begin{aligned} \dot{\hat{\rho}}_\odot(t) &= \frac{d}{dt}\mathcal{W}_\odot\left(-(t-t_0)\right)\hat{\rho}_\odot(t_0) \\ &+ \lim_{t'\to t}\frac{1}{t'-t}\left\{\int_{t_0}^{t'} ds\overline{K}\left(t'-s\right)\hat{\rho}_\odot(s) - \int_{t_0}^{t} ds\overline{K}\left(t-s\right)\hat{\rho}_\odot(s)\right\} \end{aligned} \tag{2.43}$$

$$
\begin{aligned}
&= -\frac{i}{\hbar}\left[\hat{H}_\odot|_{V_\odot}, \mathcal{W}_\odot\left(-(t-t_0)\right)\hat{\rho}_\odot(t_0)\right] \; + \\
&\quad \lim_{t'\to t}\frac{1}{t'-t}\left\{\int_{t_0}^{t} ds\left(\overline{K}(t'-s)-\overline{K}(t-s)\right)\hat{\rho}_\odot(s)+\int_{t}^{t'} ds\overline{K}(t'-s)\hat{\rho}_\odot(s)\right\} \\
&= -\frac{i}{\hbar}\left[\hat{H}_\odot|_{V_\odot}, \mathcal{W}_\odot\left(-(t-t_0)\right)\hat{\rho}_\odot(t_0)\right]+\int_{t_0}^{t} ds\dot{\overline{K}}(t-s)\hat{\rho}_\odot(s),
\end{aligned}
$$

since $\overline{K}(0)=\kappa(0,0)=0$. Moreover, with Defs. (2.36), (2.42) we obtain

$$
\frac{d}{dt}\overline{K}(t)\hat{y} = -\frac{i}{\hbar}\left[\hat{H}_\odot|_{V_\odot}, \mathcal{W}_\odot(-t)\kappa(t,0)\hat{y}\right]+\mathcal{W}_\odot(-t)\frac{\partial\kappa}{\partial t}(t,0)\hat{y}, \tag{2.44}
$$

and, inserting this into Eq. (2.43), we arrive at the *quantum master equation*:

$$
\dot{\hat{\rho}}_\odot(t) \quad = \quad \frac{i}{\hbar}[\hat{\rho}_\odot(t), \hat{H}_\odot|_{V_\odot}]+\int_{t_0}^{t} ds\; K(t-s)\hat{\rho}_\odot(s). \tag{2.45}
$$

Orders of the Density Matrix Kernel

The integral kernel $K(\tau) := \mathcal{W}_\odot(-\tau)\frac{\partial\kappa}{\partial\tau}(\tau,0)$ is given by the sum

$$
K(\tau) \quad = \quad \sum_{n=1}^{\infty} K^{(2n)}(\tau), \tag{2.46}
$$

with

$$
K^{(2)}(\tau) \quad = \quad \mathcal{W}_\odot(-\tau)I^{(2)}(\tau,0), \tag{2.47}
$$

and for $n \geq 2$:

$$
K^{(2n)}(\tau) = \int\ldots\int_{0\leq s_2\leq\cdots\leq s_{2n-1}\leq\tau} I_{\tau_{(2)}}^{(2n-1)}(s_{2n-1},\ldots,s_2), \tag{2.48}
$$

where

$$
I_{\tau_{(2)}}^{(2n-1)}(s_{2n-1},\ldots,s_2) \;:=\; \mathcal{W}_\odot(-\tau)I^{(2n)}(\tau,s_{2n-1},\ldots,s_2,0). \quad \square \tag{2.49}
$$

We shall use the quantum master equation to determine the stationary reduced density matrix of the quantum dot by calculating a corresponding transform of the integral kernel K. Analogously, we obtain the stationary current by applying a transformation to the current as a function of time, Eq. (2.16).

Current Kernel

In a way perfectly analogous to the way in which the present memory equation for the reduced density matrix of the quantum dot, Eq.(2.45), has been derived, we obtain a memory equation for the current $\mathcal{E}(\hat{I}_l)(t)$, Def. (2.14). The shape of this equation is

$$Tr_R\{\hat{I}_l\hat{\rho}(t)\} \quad = \quad \int_{t_0}^{t} ds \quad K_{curr,l}(t-s)\hat{\rho}_{\odot}(s), \tag{2.50}$$

where the kernel $K_{curr,l}(\tau)$ is derived and given in App. B (Memory Equation for the Current), Eq. (B.11). [We take the full trace on both sides of the present equation to obtain the expectation value $\mathcal{E}(\hat{I}_l)(t)$ of the particle-current onto lead l at time t.]

2.4 Diagrammatic Expansion

The kernel $K(\tau)$ of the quantum master equation (2.45) has an expansion

$$K(\tau) \;=\; \sum_{D\in\mathcal{D}} K(D)(\tau), \tag{2.51}$$

(Eq. D.97) where the objects within the set $\mathcal{D}$ can be nicely visualized as diagrams. The kernel's expansion is in this sense *diagrammatic*. We give the detailed steps on the way to this expansion in Apps. C (Decomposition of the Integral Kernel), and D (Diagrammatic Expansion), while in the present section we only describe these steps, and show the actual depiction as diagrams of the elements of the set $\mathcal{D}$.

2.4.1 Steps in the Kernel's Analysis

The kernel's analysis is to a large extent a matter of finding appropriate terminology and variables, clever re-indexing, recognizing the emerging mathematical objects, and applying useful manipulations. The analysis is too

technical to fully enter into the main part of this work; at the same time, it is an integral part. The present section is intended to form a bridge to the appendices C, and D, where we carry out the steps in the kernel's analysis.

The $2n$-th order of the density matrix kernel is given by an integral (2.48) into which the map $I^{(2n)}(\tau_{2n},\ldots,\tau_1)$ (2.33), being closely related to the map $A^{(2n)}(\tau_{2n},\ldots,\tau_1)$ (2.30), enters. For the analysis of the contributions to the density matrix kernel we write the tunneling Hamiltonian (2.5) in the form

$$\hat{H}_T \quad = \quad \sum_{\nu\in\mathcal{I}} v_\nu \hat{C}_\nu \hat{D}_\nu, \tag{2.52}$$

with $\mathcal{I}$ (Def. (C.4)) a set of indices $\nu = ((l,\sigma,\mathbf{k}), v_\nu)$ consisting of the components that define a particular electron level in the leads, and a sign v_ν. [The explicit definition of the operators $\hat{D}_\nu, \hat{C}_\nu$ is given in Eqs. (C.7), (C.9).] We note that the coefficients of the tunneling Hamiltonian, $T_{l\sigma\mathbf{k}}$, are chosen to be included in the operators $\hat{D}_\nu$, while the $\hat{C}_\nu$ are pure creation- or annihilation operators, without any pre-factor. The multi-commutator contained in $A^{(2n)}(\tau_{2n},\ldots,\tau_1)$ (2.30) takes the form of a sum of terms

$$Tr_R\left\{\hat{H}_T(\tau_{i_1})\ldots\hat{H}_T(\tau_{i_k})\ (\hat{\rho}_R\otimes\hat{y})\ \hat{H}_T(\tau_{i_{k+1}})\ldots\hat{H}_T(\tau_{i_{2n}})\right\}. \tag{2.53}$$

Upon inserting (2.52) into the present expression, we decompose this reduced operator into a product of an operator with domain $V_\odot$, an exponential function into whose argument the times τ_{i_j} enter, and a scalar given by a full trace

$$\begin{aligned} & Tr\left\{\hat{\mathrm{C}}_{\nu_{i_1}}\ldots\hat{\mathrm{C}}_{\nu_{i_k}}\ \hat{\rho}_R\ \hat{\mathrm{C}}_{\nu_{i_{k+1}}}\ldots\hat{\mathrm{C}}_{\nu_{i_{2n}}}\right\} \\ = \ & Tr\left\{\hat{\mathrm{C}}_{\nu_{i_{k+1}}}\ldots\hat{\mathrm{C}}_{\nu_{i_{2n}}}\ \hat{\mathrm{C}}_{\nu_{i_1}}\ldots\hat{\mathrm{C}}_{\nu_{i_k}}\ \hat{\rho}_R\right\}. \end{aligned} \tag{2.54}$$

Evaluation of Traces

According to App. C.2 (Evaluation of Traces), Eq. (C.87), a trace of the form $Tr\left\{\hat{\mathrm{C}}_{\mu_1}\ldots\hat{\mathrm{C}}_{\mu_{2n}}\ \hat{\rho}_R\right\}$ can be written as a linear combination of products

$$\prod_{i=1}^{n} Tr\left\{\hat{\mathrm{C}}_{\mu_{p_i}}\hat{\mathrm{C}}_{\mu_{q_i}}\ \hat{\rho}_R\right\}, \tag{2.55}$$

where the pairs $(p_i,q_i), i=1,\ldots,n$, satisfying $p_i<q_i$, are arbitrary, but cover the set $\{1,\ldots,2n\}$ completely, and represent in this sense a *pair formation* $\mathcal{P}$ of this set, "$\mathcal{P}\in PF\{1,\ldots,2n\}$" (Def. (C.81)). The sum runs over all

such pair formations, and the contribution of each pair formation $\mathcal{P}$ takes a sign $sign(\mathcal{P})$ that can be deduced from a graphic representation (Fig. C.3).

The indices $2n \geq i_1 \geq \cdots \geq i_k \geq 1$ within the expression (2.53) appear in *decreasing* order, while the complementary indices $1 \leq i_{k+1} \leq \cdots \leq i_{2n} \leq 2n$ appear in *increasing* order; the number k can take all integer values between 0 and $2n$. The sum we obtain by expanding the multi-commutator within $A^{(2n)}(\tau_{2n}, \ldots, \tau_1)$ (2.30) goes over all possibilities to choose the indices $i_1, \ldots, i_k, i_{k+1}, \ldots, i_{2n}$ in agreement with the latter order-condition. In alternative formulation, this sum goes over all $k \in \{0, \ldots, 2n\}$, and all subsets $S \subset \{1, \ldots, 2n\}$, with $|S| = k$: To each such set S we define then a map φ_S by $\varphi_S(j) := i_j$, where the indices $i_1, \ldots, i_k$ count the elements of S in decreasing order, and where $i_{k+1}, \ldots, i_{2n}$ count the elements of the set's complement $S^c = \{1 \ldots, 2n\} \setminus S$ in increasing order (Def. (C.13) within App. C.1 (Expansion of Commutators)).

By the map φ_S, we rewrite Eq. (2.54):

$$\begin{aligned} & Tr\left\{\hat{\mathrm{C}}_{\nu_{i_1}} \ldots \hat{\mathrm{C}}_{\nu_{i_k}}\ \hat{\rho}_R\ \hat{\mathrm{C}}_{\nu_{i_{k+1}}} \ldots \hat{\mathrm{C}}_{\nu_{i_{2n}}}\right\} \\ = \ & Tr\left\{\hat{\mathrm{C}}_{\nu_{\varphi_S(1)}} \ldots \hat{\mathrm{C}}_{\nu_{\varphi_S(k)}}\ \hat{\rho}_R\ \hat{\mathrm{C}}_{\nu_{\varphi_S(k+1)}} \ldots \hat{\mathrm{C}}_{\nu_{\varphi_S(2n)}}\right\} \\ = \ & Tr\left\{\hat{\mathrm{C}}_{\nu_{\varphi_S(k+1)}} \ldots \hat{\mathrm{C}}_{\nu_{\varphi_S(2n)}}\ \hat{\mathrm{C}}_{\nu_{\varphi_S(1)}} \ldots \hat{\mathrm{C}}_{\nu_{\varphi_S(k)}}\ \hat{\rho}_R\right\}, \end{aligned} \tag{2.56}$$

and so

$$\begin{aligned} & Tr\left\{\hat{\mathrm{C}}_{\nu_{i_1}} \ldots \hat{\mathrm{C}}_{\nu_{i_k}}\ \hat{\rho}_R\ \hat{\mathrm{C}}_{\nu_{i_{k+1}}} \ldots \hat{\mathrm{C}}_{\nu_{i_{2n}}}\right\} \\ = \ & Tr\left\{\hat{\mathrm{C}}_{\nu_{\varphi_S(\zeta_{(+)}^k(1))}} \ldots \hat{\mathrm{C}}_{\nu_{\varphi_S(\zeta_{(+)}^k(2n))}}\ \hat{\rho}_R\right\}, \end{aligned} \tag{2.57}$$

where we have used the cyclic permutation

$$\zeta_{(+)}(j) \ := \begin{cases} j+1 & (j < 2n) \\ 1 & (j = 2n). \end{cases} \tag{2.58}$$

Hence, in the expansion of the present trace into a linear combination of contributions

$$\prod_{i=1}^{n} Tr\left\{\hat{\mathrm{C}}_{\nu_{p_i}} \hat{\mathrm{C}}_{\nu_{q_i}}\ \hat{\rho}_R\right\}, \tag{2.59}$$

the pairs (p_i, q_i) have to satisfy the demand

$$p_i \ <_{\varphi_S \circ \zeta_{(+)}^k} \ q_i, \tag{2.60}$$

i.e., p_i appears before q_i within the list

$$\varphi_S \circ \zeta_{(+)}^k(1), \ \ldots \ , \varphi_S \circ \zeta_{(+)}^k(2n), \tag{2.61}$$

or else:

$$\left\{\varphi_S \circ \zeta_{(+)}^k\right\}^{-1}(p_i) \ < \ \left\{\varphi_S \circ \zeta_{(+)}^k\right\}^{-1}(q_i). \tag{2.62}$$

In addition, as we noted above, the sum we obtain in the expansion of the map $A^{(2n)}(\tau_{2n}, \ldots, \tau_1)$ (2.30) goes over *all* pair formations, while the sum we obtain in the expansion of $I^{(2n)}(\tau_{2n}, \ldots, \tau_1)$ (2.33) goes only over the *irreducible* pair formations. So, as a second condition, the pair formation

$$\mathcal{P} \ = \ \{\{p_i, q_i\} : i = 1, \ldots, n\} \tag{2.63}$$

is required to be irreducible *in the natural order*, since the indices "i_j" of the ν_{i_j} within Eq. (2.54) are also the indices of the naturally ordered times τ_{i_j} within (2.53).

Away from the Time-Order as Index-Number

However, to derive the diagrammatic language from the equation for $I^{(2n)}(\tau_{2n}, \ldots, \tau_1)\hat{y}$, we apply a different formulation: We re-number the indices

$$\nu_{i_j} \ =: \ \mu_j, \tag{2.64}$$

so we write the trace (2.54) in the form

$$\begin{aligned} & Tr\left\{\hat{\mathrm{C}}_{\nu_{i_1}} \ldots \hat{\mathrm{C}}_{\nu_{i_k}} \ \hat{\rho}_R \ \hat{\mathrm{C}}_{\nu_{i_{k+1}}} \ldots \hat{\mathrm{C}}_{\nu_{i_{2n}}}\right\} \\ = \ & Tr\left\{\hat{\mathrm{C}}_{\mu_1} \ldots \hat{\mathrm{C}}_{\mu_k} \ \hat{\rho}_R \ \hat{\mathrm{C}}_{\mu_{k+1}} \ldots \hat{\mathrm{C}}_{\mu_{2n}}\right\} \\ = \ & Tr\left\{\hat{\mathrm{C}}_{\mu_{k+1}} \ldots \hat{\mathrm{C}}_{\mu_{2n}} \ \hat{\mathrm{C}}_{\mu_1} \ldots \hat{\mathrm{C}}_{\mu_k} \hat{\rho}_R\right\}. \end{aligned} \tag{2.65}$$

The latter trace we expand into a sum over pair formations to obtain

$$\begin{aligned} & Tr\left\{\hat{\mathrm{C}}_{\nu_{i_1}} \ldots \hat{\mathrm{C}}_{\nu_{i_k}} \ \hat{\rho}_R \ \hat{\mathrm{C}}_{\nu_{i_{k+1}}} \ldots \hat{\mathrm{C}}_{\nu_{i_{2n}}}\right\} \\ = \ & \sum_{\mathcal{P}'=\{\{p'_\iota, q'_\iota\}:\iota=1,\ldots,n\}} \mathrm{sign}(\mathcal{P}') \ \prod_{\iota=1}^{n} Tr\left\{\hat{\mathrm{C}}_{\mu_{p'_\iota}} \hat{\mathrm{C}}_{\mu_{q'_\iota}} \hat{\rho}_R\right\}, \end{aligned} \tag{2.66}$$

where each of the pairs (p'_ι, q'_ι) satisfies one of the order-conditions

$$\left\{ \begin{array}{c} 1 \leq p'_\iota \leq q'_\iota \leq k, \\ k+1 \leq p'_\iota \leq q'_\iota \leq 2n, \text{ or} \\ q'_\iota \leq k, \ k+1 \leq p'_\iota. \end{array} \right\} \tag{2.67}$$

In addition, since

$$\mu_j \mathrel{\widehat{=}} \nu_{i_j} \ = \ \nu_{\varphi_S(j)}, \tag{2.68}$$

the pair (p'_ι, q'_ι) of indices of μ corresponds to the pair $(\varphi_S(p'_\iota), \varphi_S(q'_\iota))$ of indices of ν. Hence, it is the *image* of the pair formation $\mathcal{P}'$ under the map φ_S which is required to be irreducible in the natural order when we expand the quantity $I^{(2n)}(\tau_{2n}, \ldots, \tau_1)$:

$$\varphi_S(\mathcal{P}') \ \in \ PF_{irr}\{1, \ldots, 2n\}. \tag{2.69}$$

In other words, when we expand $I^{(2n)}(\tau_{2n}, \ldots, \tau_1)$, the sum on the right-hand side of Eq. (2.66) runs exclusively over all pair formations $\mathcal{P}'$ that satisfy

$$\mathcal{P}' \ \in \ \varphi_S^{-1} PF_{irr}\{1, \ldots, 2n\}. \tag{2.70}$$

Remark: Physical Interpretation of Multiplicative Decomposition

The present manipulations are technical, so we want to point out one aspect accessible to interpretation: As it becomes clear within the proof of Eq. (C.39) within App. C.2 (Evaluation of Traces), the generally valid multiplicative decomposition

$$Tr\left\{\hat{\mathrm{C}}_{\lambda_1} \ldots \hat{\mathrm{C}}_{\lambda_{2n}} \ \hat{\rho}_R\right\} \ = \ \sum_{\mathcal{P} \in PF\{1,\ldots,2n\}} \mathrm{sign}(\mathcal{P}) \prod_{i=1}^{n} Tr\left\{\hat{\mathrm{C}}_{\lambda_{p_i}} \hat{\mathrm{C}}_{\lambda_{q_i}} \hat{\rho}_R\right\} \tag{2.71}$$

(cp. Eq. (C.87)), which we exploited in the previous subsection, has the following implication: The probability to find a certain selection of one-electron levels $(l, \sigma, \mathbf{k})$ (non-)occupied, provided the contacts are in thermal equilibrium in the definition by the density matrix $\hat{\rho}_R$ (Def. 2.7), is given by the *product* of the probabilities to find each of the levels within the selection (non-)occupied. Hence, it is the *independence of occupation probabilities* which is contained in the present equation (2.71).

Expansion to the Level of Eq. (C.117)

Up to now, we have described the steps that lead us to the expansion of the kernel in the form of Eq. (C.117). Within this equation, the elements that determine a particular contribution to the kernel are:

- A natural number n, $k \in \{0, \ldots, 2n\}$, and a set $S \subset \{1, \ldots, 2n\}$ with $|S| = k$.
- A pair formation $\mathcal{P}' \in \varphi_S^{-1} PF_{irr}\{1, \ldots, 2n\}$, and indices $\mu_1, \ldots, \mu_{2n} \in \mathcal{I}$.
- An exponential function $\exp\left(\frac{i}{\hbar}\sum_{j=1}^{2n} \tau_{\varphi_S(j)}\varepsilon_{\mu_j}\right)$ (cp. Eq. (C.32) – creation operator in the interaction picture), and the product of traces $\prod_{\iota=1}^{n} Tr\left\{\hat{\mathrm{C}}_{\mu_{p'_\iota}}\hat{\mathrm{C}}_{\mu_{q'_\iota}}\hat{\rho}_R\right\}$, where the pairs (p'_ι, q'_ι) are ordered according to (2.67).
- An overall sign-factor $(-1)^{n+k}\mathrm{sign}(\mathcal{P}')$, and:
- A composition of operators

$$\hat{\mathrm{D}}_{\mu_1}\left(\tau_{\varphi_S(1)}\right)\ldots\hat{\mathrm{D}}_{\mu_k}\left(\tau_{\varphi_S(k)}\right)\hat{y}\;\hat{\mathrm{D}}_{\mu_{k+1}}\left(\tau_{\varphi_S(k+1)}\right)\ldots\hat{\mathrm{D}}_{\mu_{2n}}\left(\tau_{\varphi_S(2n)}\right) \tag{2.72}$$

with domain $V_\odot$.

Quantum Dot Operators as Matrices

We write each of the operators $\hat{\mathrm{D}}_\mu(\tau)$ within the product (2.72), as well as $\hat{y}$, as a matrix in a basis $\mathcal{B}$ consisting of eigenvectors of the quantum dot's Hamiltonian:

$$\hat{\mathrm{D}}_\mu(\tau) = \sum_{a,b\in\mathcal{B}} \exp\left(\frac{i}{\hbar}\tau\left(E_a - E_b\right)\right)\langle a|\hat{\mathrm{D}}_\mu(b)\rangle\;|a><b| \tag{2.73}$$

according to Eq. (D.2) within App. D (Complete Decomposition and Diagrammatic Expansion of the Kernel), where the energies E_a, E_b are the eigenvalues of the quantum dot's Hamiltonian. Since the operators appear in a product, the sum with respect to the basis states can be reduced (cp. Fig. 2.5). In this way, we obtain the representation of the product (2.72) explicitly given in Eq. (D.4).

Kernel as Integral over *Non*-Ordered Times

The $2n$-th order of the *integrated* integral kernel $\int_0^\tau dsK(s)$ can be written as an integral with a number of $2n-1$ ordered integration variables

$$0 \le \tau_1 \le \cdots \le \tau_{2n-1} \le \tau, \tag{2.74}$$

or, alternatively (Fig. D.3), as an integral with $2n-1$ *non*-ordered positive integration variables $0 \le \overline{\tau}_1, \ldots, \overline{\tau}_{2n-1}$ satisfying

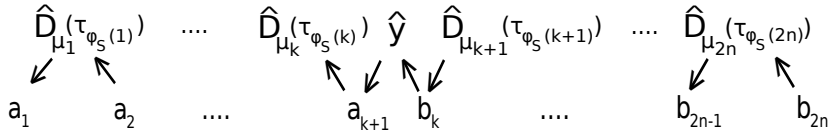

Figure 2.5: Representing all of the operators $\hat{\mathrm{D}}_\mu(\tau)$ as a linear combination of maps $|a><b|$, where a, b are eigenvectors of $\hat{\mathrm{H}}_\odot$ taken from an orthonormal basis, we obtain a corresponding representation of the product of operators in Eq. (C.117). Since $|a_i><b_i|\,|a_{i+1}><b_{i+1}| = 0$ if $b_i \neq a_{i+1}$, the sum can be reduced to a sum over $a_1, \ldots, a_{k+1}$, and $b_k, \ldots, b_{2n}$.

$$\overline{\tau}_1 + \cdots + \overline{\tau}_{2n-1} \leq \tau. \tag{2.75}$$

For the further analysis we choose the latter integration variables, and so we note the equation for the $2n$-th order of the integrated kernel as an integral with respect to $\overline{\tau}_1, \ldots, \overline{\tau}_{2n-1}$:

$$\int_0^\tau ds K^{(2n)}(s) \;=\; \int_{\left\{S^{(2n-1)} \leq \tau\right\}} \overline{I}^{(2n-1)}\left(\overline{\tau}_{2n-1}, \ldots, \overline{\tau}_1\right), \tag{2.76}$$

with

$$\left\{S^{(2n-1)} \leq \tau\right\} \;:=\; \left\{(\overline{\tau}_{2n-1}, \ldots, \overline{\tau}_1) :\; \overline{\tau}_1, \ldots, \overline{\tau}_{2n-1} \geq 0, \sum_{j=1}^{2n-1} \overline{\tau}_j \leq \tau\right\}, \tag{2.77}$$

and with $\overline{I}^{(2n-1)}$ defined in App. D (Diagrammatic Expansion) (Eq. (D.30)).

To obtain an equation for the *non*-integrated $2n$-th order of the kernel itself, we transform the right-hand side of Eq. (2.76) as described in Fig. 2.6:

$$\int_0^\tau ds K^{(2n)}(s) \;=\; \frac{1}{\sqrt{2n-1}} \int_0^\tau ds \int_{\left\{S^{(2n-1)}=s\right\}} dF \quad \overline{I}^{(2n-1)}(\overline{\tau}_{2n-1}, \ldots, \overline{\tau}_1), \tag{2.78}$$

and so

$$K^{(2n)}(s) \;=\; \frac{1}{\sqrt{2n-1}} \int_{\left\{S^{(2n-1)}=s\right\}} dF \quad \overline{I}^{(2n-1)}(\overline{\tau}_{2n-1}, \ldots, \overline{\tau}_1). \tag{2.79}$$

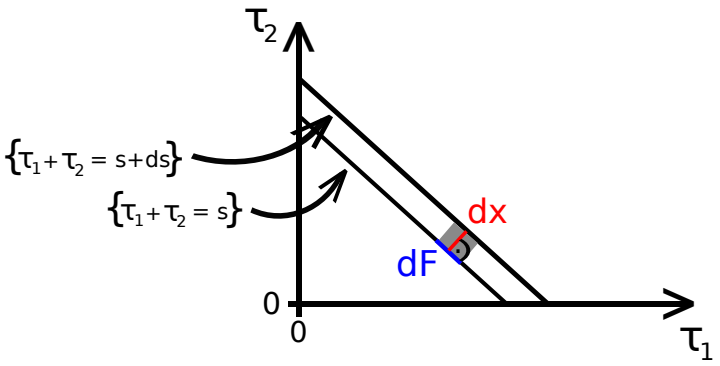

Figure 2.6: An integral $\int_0^\infty d\overline{\tau}_1 \ldots \int_0^\infty d\overline{\tau}_k \quad g(\overline{\tau}_1, \ldots, \overline{\tau}_k)$ with a number of k positive integration variables can be transformed as indicated in the present figure (in this case, $k = 2$). We take infinitesimal elements dF of surfaces $\left\{S^{(k)} = s\right\}$ of constant value s of the sum-function $S^{(k)}(\overline{\tau}_1, \ldots, \overline{\tau}_k) = \overline{\tau}_1 + \cdots + \overline{\tau}_k$. The elements' size-measure dF is multiplied by their distance dx to the surface $\left\{S^{(k)} = s + ds\right\}$ with infinitesimally increased function-value, and so the complete integration-area is divided up into infinitesimal parts of size $dFdx$. The distance dx is in general a function of the position $(\overline{\tau}_1, \ldots, \overline{\tau}_k)$, and of ds. Since locally everywhere $\nabla S^{(k)} \perp \left\{S^{(k)} = s\right\}$, we note: $dx \left|\nabla S^{(k)}\right| = ds$, and so the transformed integral reads $\int\int dFdx \quad g(\overline{\tau}_1, \ldots, \overline{\tau}_k) = \int_0^\infty ds \int_{\left\{S^{(k)}=s\right\}} dF \frac{g}{\left|\nabla S^{(k)}\right|}(\overline{\tau}_1, \ldots, \overline{\tau}_k)$. For the sum-function $S^{(k)}$ we have: $\left|\nabla S^{(k)}\right| = const = \sqrt{k}$.

Reduction of the Sum over $\mu_1, \ldots, \mu_{2n} \in \mathcal{I}$

Our next step in the kernel's analysis is the reduction of the sum over $\mu_1, \ldots, \mu_{2n} \in \mathcal{I}$ within the right-hand side of Eq. (C.117) whose constituent elements we itemized (p. 23 ff.): We note that, generally, $Tr\left\{\hat{\mathrm{C}}_\mu \hat{\mathrm{C}}_\nu \hat{\rho}_R\right\} =: \left\langle \hat{\mathrm{C}}_\mu \hat{\mathrm{C}}_\nu \right\rangle = 0$ if μ and ν are not complementary indices, $\mu \neq \overline{\nu}$ (D.16). Due to the emergence of the product of traces

$$\prod_{M' \in \mathcal{P}} \left\langle \hat{\mathrm{C}}_{\mu_{p\left(M', <_{\zeta^k_{(+)}}\right)}} \hat{\mathrm{C}}_{\mu_{q\left(M', <_{\zeta^k_{(+)}}\right)}} \right\rangle \tag{2.80}$$

in (C.117), we assume without restriction that, to each two-elementary set M' within the previously chosen pair formation $\mathcal{P}$, the indices $\mu_{p(M')}$ and $\mu_{q(M')}$ are complementary. We note that $p(M')$ ($q(M')$) is the minimum (maximum) of the set M' in the *natural* order, while $p\left(M', <_{\zeta^k_{(+)}}\right)$ and $q\left(M', <_{\zeta^k_{(+)}}\right)$ are the same two numbers, however ordered according to the condition (2.67). Hence, we split the present product of traces into three products:

$$\begin{aligned} &\prod_{M' \in \mathcal{P}: 1 \leq p(M') \leq q(M') \leq k} \left\langle \hat{\mathrm{C}}_{\mu_{p(M')}} \hat{\mathrm{C}}_{\overline{\mu}_{p(M')}} \right\rangle \\ &\prod_{M' \in \mathcal{P}: k+1 \leq p(M') \leq q(M') \leq 2n} \left\langle \hat{\mathrm{C}}_{\mu_{p(M')}} \hat{\mathrm{C}}_{\overline{\mu}_{p(M')}} \right\rangle \\ &\prod_{M' \in \mathcal{P}: p(M') \leq k, k+1 \leq q(M')} \left\langle \hat{\mathrm{C}}_{\overline{\mu}_{p(M')}} \hat{\mathrm{C}}_{\mu_{p(M')}} \right\rangle . \end{aligned} \tag{2.81}$$

The reduction of the number of indices $\mu_1, \ldots, \mu_{2n}$ is relevant also for the product of operators (2.72), whose replacement by the right-hand side of Eq. (D.4) we discussed. In the latter expression, the two products

$$\prod_{j=1}^{k} \left\langle a_j | \hat{\mathrm{D}}_{\mu_j}(a_{j+1}) \right\rangle \prod_{j=k+1}^{2n} \left\langle b_{j-1} | \hat{\mathrm{D}}_{\mu_j}(b_j) \right\rangle \tag{2.82}$$

appear, and upon applying the complementarity $\mu_{q(M')} = \overline{\mu}_{p(M')}$, we rewrite these in the form

$$\prod_{M'\in\mathcal{P}:1\leq p(M')\leq q(M')\leq k} \left\langle a_{p(M')}|\hat{\mathrm{D}}_{\mu_{p(M')}}(a_{p(M')+1})\right\rangle \left\langle a_{q(M')}|\hat{\mathrm{D}}_{\overline{\mu}_{p(M')}}(a_{q(M')+1})\right\rangle$$
$$\prod_{M'\in\mathcal{P}:k+1\leq p(M')\leq q(M')\leq 2n} \left\langle b_{p(M')-1}|\hat{\mathrm{D}}_{\mu_{p(M')}}(b_{p(M')})\right\rangle \left\langle b_{q(M')-1}|\hat{\mathrm{D}}_{\overline{\mu}_{p(M')}}(b_{q(M')})\right\rangle$$
$$\prod_{M'\in\mathcal{P}:p(M')\leq k,k+1\leq q(M')} \left\langle a_{p(M')}|\hat{\mathrm{D}}_{\mu_{p(M')}}(a_{p(M')+1})\right\rangle \left\langle b_{q(M')-1}|\hat{\mathrm{D}}_{\overline{\mu}_{p(M')}}(b_{q(M')})\right\rangle . \tag{2.83}$$

We now group the first (second/third) line within (2.81) to the first (second/third) line within (2.83); upon replacing "M'" by "M", and "$\mu_{p(M)}$" by "μ_M", we obtain for the product of the two first lines:

$$\prod_{M\in\mathcal{P}:1\leq p(M)\leq q(M)\leq k} \left\langle \hat{\mathrm{C}}_{\mu_M}\hat{\mathrm{C}}_{\overline{\mu}_M}\right\rangle$$
$$\left\langle a_{p(M)}|\hat{\mathrm{D}}_{\mu_M}(a_{p(M)+1})\right\rangle \left\langle a_{q(M)}|\hat{\mathrm{D}}_{\overline{\mu}_M}(a_{q(M)+1})\right\rangle . \tag{2.84}$$

We write any index μ within the set $\mathcal{I}$ (Def. (C.4)) in the form $\mu = ((l,\sigma,\mathbf{k})_\mu, v_\mu) = (\eta_\mu, v_\mu)$, so we gather those three components of μ defining a particular electron level of the leads in η_μ. Generally, the trace $\left\langle \hat{\mathrm{C}}_\mu\hat{\mathrm{C}}_{\overline{\mu}}\right\rangle$ gives the occupation-probability (one minus this probability) of the level η_μ:

$$\left\langle \hat{\mathrm{C}}_\mu\hat{\mathrm{C}}_{\overline{\mu}}\right\rangle \;=\; Tr\left\{\hat{\mathrm{C}}_\mu\hat{\mathrm{C}}_{\overline{\mu}}\hat{\rho}_R\right\} \;=\; f(\beta_\mu) \tag{2.85}$$

(Eq. (C.79)), with $f(x)$ the parameter-free Fermi-Dirac distribution, and with

$$\beta_\mu \;=\; v_\mu\,\frac{1}{k_BT}\,(\varepsilon_{l\sigma\mathbf{k}} - \mu_{l\sigma}) \tag{2.86}$$

(Defs. (C.71), (C.73); for brevity we here omit the index "μ" in the components of η_μ). The operators $\hat{\mathrm{D}}_\mu$ contain the coefficients of the tunneling Hamiltonian – explicitly: $\hat{\mathrm{D}}_\mu = \hat{\mathrm{D}}_{l\sigma\mathbf{k}v} = T^{(v)}_{l\sigma\mathbf{k}}\hat{\mathrm{d}}^{(v)}_\sigma$ according to Eq. (D.18), where $\hat{\mathrm{d}}^{(+1)}_\sigma$ is the annihilator of the quantum dot level σ, and where $\hat{\mathrm{d}}^{(-1)}_\sigma$ is the creator. Upon applying the present replacement, and inserting the right-hand side of Eq. (2.85) into (2.84), the product (2.84) reads:

$$\prod_{M\in\mathcal{P}:1\leq p(M)\leq q(M)\leq k} f(\beta_{\mu_M})\;\left|T_{(l\sigma\mathbf{k})_{\mu_M}}\right|^2$$
$$\left\langle a_{p(M)}|\hat{\mathrm{d}}^{(v_{\mu_M})}_{\sigma_{\mu_M}}(a_{p(M)+1})\right\rangle \left\langle a_{q(M)}|\hat{\mathrm{d}}^{(-v_{\mu_M})}_{\sigma_{\mu_M}}(a_{q(M)+1})\right\rangle . \tag{2.87}$$

The second line within the present expression either vanishes, or it gives a sign ± 1. Within the first line, on the other hand, we emphasize at this stage the expression's dependence on the wave vector $\mathbf{k}$, replacing it by a function $A^{(v_{\mu_M})}_{(l\sigma)_{\mu_M}}(\mathbf{k}_{\mu_M})$ (Def. (D.32)). In summary, by the manipulations of the present section we obtain the three products on the right-hand side of Eq. (D.31) within App. D.

Dependence on the Non-Ordered Times $\overline{\tau}_1, \ldots, \overline{\tau}_{2n-1}$

As we noted (p. 23 ff.), the dependence of the quantity $I^{(2n)}(\tau_{2n}, \ldots, \tau_1)\hat{y}$ on the set of ordered times $\tau_1, \ldots, \tau_{2n}$ is given by two factors:

1. $\exp\left(\frac{i}{\hbar}\sum_{j=1}^{2n} \tau_{\varphi_S(j)} \varepsilon_{\mu_j}\right)$.

2. The term

$$\exp\left(\frac{i}{\hbar}\left\{\left[\sum_{j=1}^{k} \tau_{\varphi_S(j)}\left(E_{a_j} - E_{a_{j+1}}\right)\right] + \left[\sum_{j=k+1}^{2n} \tau_{\varphi_S(j)}\left(E_{b_{j-1}} - E_{b_j}\right)\right]\right\}\right), \tag{2.88}$$

originating from the composition of operators (2.72), which we obtain from the right-hand side of Eq. (D.4).

At this stage we implement the transformation to the *non*-ordered times $\overline{\tau}_j$ explicitly shown in App. D, Eqs. (D.5) ff.. Within the map $\overline{I}^{(2n-1)}(\overline{\tau}_{2n-1}, \ldots, \overline{\tau}_1)$, by whose integral the $2n$-th order of the kernel is given (Eq. (2.79)), we in addition apply the map $\mathcal{W}_{\odot}\left(-\sum_{j=1}^{2n-1}\overline{\tau}_j\right)$ (cp. Defs. (D.30), (D.11)), so we arrive at that dependence of the contributions to the integral kernel on the non-ordered times $\overline{\tau}_1, \ldots, \overline{\tau}_{2n-1}$ explicitly given by the exponential function within the right-hand side of Eq. (D.31). □

Finally, we replace the sums over the wave vector within Eq. (D.31) by integrals (cp. Fig. D.5), which yields integrands step-wise constant as function of the wave vector, and, in a second step, we insert continuous integrands instead of these step-wise constant functions. Next, we replace the integral over the wave vector by one over energy, and so we arrive at the representation of the integral kernel in the form of Eq. (D.42), and finally in the form of (D.64).

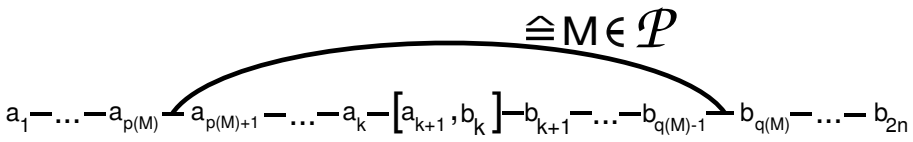

Figure 2.7: This first example-diagram of the present figure shows how we depict a part of the elements of the diagram $\overline{D}$ (2.89): The sequences of quantum dot states $(a_j)_{j=1}^{k+1}$, and $(b_j)_{j=k}^{2n}$, appear listed according to the order of their indices along one straight line. The states a_{k+1}, and b_k, are enclosed in square brackets, and separated by a comma, while in the space between all other neighbouring states we draw one horizontal line. The number of these horizontal lines is $2n$, and it is these horizontal lines, which, in the present transformed diagram, are grouped into pairs by a pair formation $\mathcal{P}$.

2.4.2 Graphic Representation of Diagrams

We gather the parameters that determine a particular contribution to the density matrix kernel according to Eq. (D.64) in tuples

$$\overline{D} \;=\; \left(n, k, J, \mathcal{P}, (a_j)_{j=1}^{k+1}, (b_j)_{j=k}^{2n}, (l_M, \sigma_M, v_M)_{M\in\mathcal{P}}\right), \tag{2.89}$$

which we shall refer to as *diagrams*. There are two equivalent sets of diagrams, for which we shall use the notation "$\mathcal{D}$", and "$\overline{\mathcal{D}}$" (Defs. (D.92), (D.89)). When we want to explicitly distinguish between the two diagram-versions, we refer to the elements of the set $\overline{\mathcal{D}}$ as *transformed* diagrams; the transformation-map T_{diag} is given in (D.88).

We first discuss how we depict the diagrams in the form of elements $\overline{D}$ of the set $\overline{\mathcal{D}}$ (Fig. 2.7), and, at this stage, we have to make a concrete choice of the orthonormal basis $\mathcal{B}$ of the vector space $V_\odot$ of the quantum dot states applied for a complete decomposition of the density matrix kernel (Fig. 2.5). We choose

$$\mathcal{B} \;:=\; \{\mathbf{0}, \boldsymbol{\sigma_o}\}, \tag{2.90}$$

where $\mathbf{0}$ is a normalized empty state, and $\boldsymbol{\sigma_o} := \hat{\mathrm{d}}^\dagger_{\sigma_o}(\mathbf{0})$, in the case of the spinless quantum dot (2.3), and

$$\mathcal{B} \;:=\; \{\mathbf{0}, \uparrow, \downarrow, \mathbf{2}\} \tag{2.91}$$

in the case of the SIAM (2.4), where for $\sigma \in \{\uparrow, \downarrow\}$:

$$\boldsymbol{\sigma} \;:=\; \hat{\mathrm{d}}^\dagger_{\sigma}(\mathbf{0}), \tag{2.92}$$

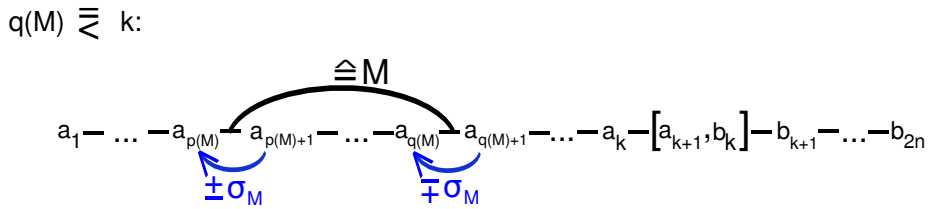

Figure 2.8: In case $q(M) \leq k$, we obtain the quantum dot state $a_{q(M)}$ from the state $a_{q(M)+1}$ by adding (or removing) one electron of the spin σ_M, while we obtain the quantum dot state $a_{p(M)}$ from the state $a_{p(M)+1}$ by removing (or adding) one electron of the same spin σ_M, respectively.

with

$$\hat{\mathrm{d}}_\sigma \;:=\; \hat{\mathrm{d}}_\sigma^{(+1)} \;:=\; \hat{d}_\sigma\Big|_{V_\odot}\,, \tag{2.93}$$

the annihilation operator adjoint to the creator $\hat{\mathrm{d}}_\sigma^\dagger$ (cp. Def. (D.20)), and where

$$\mathbf{2} \;:=\; \hat{\mathrm{d}}_\uparrow^\dagger \hat{\mathrm{d}}_\downarrow^\dagger(\mathbf{0}). \tag{2.94}$$

Tunneling Lines

We note that, for any sequences $(a_j)_{j=1}^{k+1}$ and $(b_j)_{j=k}^{2n}$ of elements in $\mathcal{B}$, as contained in the tuple $\overline{D} \in \overline{\mathcal{D}}$ (2.89), the quantity

$$\mathrm{sg}^{(1)}\ \left\{n, k, \mathcal{P},\ (a_j)_{j=1}^{k+1},\ (b_j)_{j=k}^{2n},\ (\sigma_M, v_M)_{M\in\mathcal{P}}\right\}, \tag{2.95}$$

defined in (D.39), appears as a factor in the expression by which we calculate the contribution of a particular diagram to the density matrix kernel (D.67). The quantity can take only the values $1, -1$, and 0, where in the latter case the diagram is excluded from the set $\overline{\mathcal{D}}$ per definition (D.89). Due to the presence of the scalar products $\langle a_{p(M)}|\hat{\mathrm{d}}_{\sigma_M}^{(v_M)} a_{p(M)+1}\rangle$, etc., the quantity's value is non-zero only if for any $M = \{p(M), q(M)\} \in \mathcal{P}$:

$$\begin{aligned} &q(M) \;\leq\; k \;\Rightarrow \\ &\quad a_{p(M)} \in \{\pm\hat{\mathrm{d}}_{\sigma_M}^{(v_M)}\left(a_{p(M)+1}\right)\},\ a_{q(M)} \in \{\pm\hat{\mathrm{d}}_{\sigma_M}^{(-v_M)}\left(a_{q(M)+1}\right)\}, \end{aligned} \tag{2.96}$$

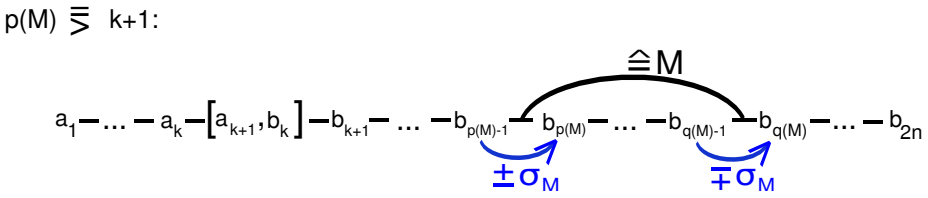

Figure 2.9: In case $p(M) \geq k+1$, we obtain the quantum dot state $b_{p(M)}$ from the state $b_{p(M)-1}$ by adding (or removing) one electron of the spin σ_M, while we obtain the quantum dot state $b_{q(M)}$ from the state $b_{q(M)-1}$ by removing (or adding) one electron of the same spin σ_M, respectively.

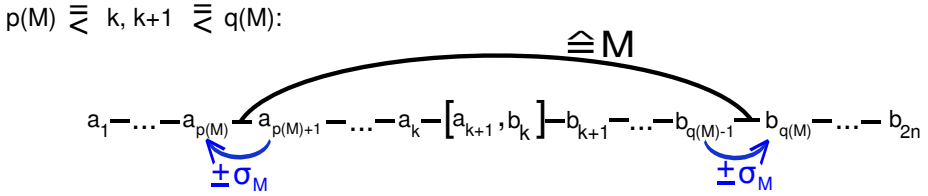

Figure 2.10: In case the "tunneling line" (the line representing the set $M = \{p(M), q(M)\} \subset \{1, \ldots, 2n\}$) stretches over the square brackets containing the states a_{k+1}, b_k of the diagram's *initial* matrix $|a_{k+1} >< b_k|$, we obtain the quantum dot state $a_{p(M)}$ from the state $a_{p(M)+1}$ by adding (or removing) one electron of the spin σ_M, and we obtain the quantum dot state $b_{q(M)}$ from the state $b_{q(M)-1}$ by adding (or removing) one electron of the same spin σ_M, respectively.

$$k+1 \leq p(M) \;\Rightarrow \tag{2.97}$$
$$b_{p(M)-1} \in \{\pm \hat{\mathrm{d}}_{\sigma_M}^{(v_M)}\left(b_{p(M)}\right)\},\; b_{q(M)-1} \in \{\pm \hat{\mathrm{d}}_{\sigma_M}^{(-v_M)}\left(b_{q(M)}\right)\},$$

as well as

$$p(M) \leq k, \quad k+1 \leq q(M) \;\Rightarrow \tag{2.98}$$
$$a_{p(M)} \in \{\pm \hat{\mathrm{d}}_{\sigma_M}^{(v_M)}\left(a_{p(M)+1}\right)\},\; b_{q(M)-1} \in \{\pm \hat{\mathrm{d}}_{\sigma_M}^{(-v_M)}\left(b_{q(M)}\right)\}.$$

Defining, to any $\sigma \in \mathcal{S}$ and $c \in V_{\odot}$:

$$\langle \hat{\mathrm{N}}_\sigma \rangle(c) \;:=\; \langle c|\hat{\mathrm{N}}_\sigma(c)\rangle, \tag{2.99}$$

with $\hat{\mathrm{N}}_\sigma = \hat{\mathrm{d}}_\sigma^\dagger \hat{\mathrm{d}}_\sigma$, the operator of the occupation-number of the level σ on the quantum dot, we note the equality:

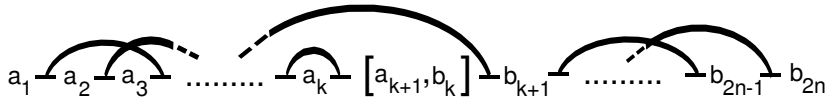

Figure 2.11: A diagram containing the sequences of quantum dot states $(a_j)_{j=1}^{k+1}$, $(b_j)_{j=k}^{2n}$, as well as – via the (bent) *tunneling lines*, each connecting two of the horizontal lines filling the space between the quantum dot states – a pair formation $\mathcal{P} \in PF\{1,\ldots,2n\}$.

$$\langle \hat{\mathrm{N}}_\sigma \rangle (a_1) \; - \; \langle \hat{\mathrm{N}}_\sigma \rangle (a_{k+1}) \; = \; \langle \hat{\mathrm{N}}_\sigma \rangle (b_{2n}) \; - \; \langle \hat{\mathrm{N}}_\sigma \rangle (b_k). \tag{2.100}$$

The overall change of each spin-number is equal on both sides of the diagram, since

$$\begin{aligned} & \sum_{M:\; p(M)\leq k, k+1\leq q(M)} \langle \hat{\mathrm{N}}_\sigma \rangle \left(a_{p(M)}\right) - \langle \hat{\mathrm{N}}_\sigma \rangle \left(a_{p(M)+1}\right) \\ = & \sum_{M:\; p(M)\leq k, k+1\leq q(M)} \langle \hat{\mathrm{N}}_\sigma \rangle \left(b_{q(M)}\right) - \langle \hat{\mathrm{N}}_\sigma \rangle \left(b_{q(M)-1}\right). \end{aligned} \tag{2.101}$$

We depict the elements $n, k, (a_j)_{j=1}^{k+1}$, $(b_j)_{j=k}^{2n}$, and $\mathcal{P}$, of the diagram $\overline{D}$, Eq. (2.89), in the form of Fig. 2.11. The $2n$ horizontal lines are counted from the left to the right, and thus, the bent lines, which we shall refer to as *tunneling lines*, each connecting two of the horizontal lines, represent a pair formation $\mathcal{P} \in PF\{1,\ldots,2n\}$. The operator $|a_{k+1} >< b_k|$ shall be referred to as the *initial matrix* of the diagram, while $|a_1 >< b_{2n}|$ is its *final matrix*.

Inclusion of the Interval Sequence J

Within any tunneling process visualized by the present diagrams, the initial matrix changes to the final matrix in a number of $2n$ steps. The concrete order which these steps happen in is given by an additional element we did not discuss so far: The diagram's matrix after the j-th step is $|a_{min(J(j))} >< b_{max(J(j))}|$, with $J(1) \subset J(2) ... \subset J(2n) = \{1,\ldots,2n\}$ a sequence of integer intervals satisfying $|J(j)| = j$, where $J(0) = \{k\}$, or $J(0) = \{k+1\}$.

To replace the general quantum dot states $a_1,\ldots,a_{k+1},b_k,\ldots,b_{2n}$ by concrete elements of the basis $\mathcal{B} = \{\mathbf{0},\uparrow,\downarrow,\mathbf{2}\}$, we define for a given spin $\sigma \in \{\uparrow,\downarrow\}$:

$$\overline{\sigma} \; := \; \begin{cases} \uparrow & (\sigma = \downarrow) \\ \downarrow & (\sigma = \uparrow). \end{cases} \tag{2.102}$$

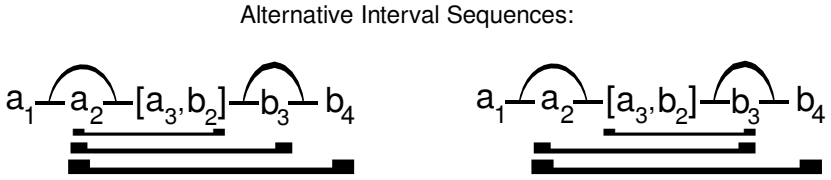

Figure 2.12: The present two diagrams differ only in the horizontal square brackets, which mark the sequences $J(j)_{j=1}^{2n-1}$. The diagrams' common pair formation is reducible with respect to the natural order, but it is irreducible in both of the two orders given by the two different interval sequences. Via a number of, here, four tunneling events, each represented by one of the horizontal lines in the space between neighbouring states, the matrix turns from the initial matrix $|a_3 >< b_2|$ to the final matrix $|a_1 >< b_4|$. The order, in which these events happen, is fixed by the interval sequence $J(j)_{j=1}^{2n-1}$.

The values of the elements $\sigma_M, v_M (M \in \mathcal{P})$ within a diagram

$$\overline{D} \;=\; \left(n, k, J, \mathcal{P}, (a_j)_{j=1}^{k+1}, (b_j)_{j=k}^{2n}, (l_M, \sigma_M, v_M)_{M\in\mathcal{P}}\right) \in \overline{\mathcal{D}} \qquad (2.103)$$

(Def. (D.89)) are, according to the relations (2.96), (2.97), and (2.98), fixed by the choice of the quantum dot states $a_j, b_{j'} \in \{\mathbf{0}, \uparrow, \downarrow, \mathbf{2}\}$, so they don't need to be specified in the figure. To make the depiction of a diagram complete, we include the sequence $J = J(j)_{j=1}^{2n-1} \in \mathcal{J}_{(k)}^{(2n)}$ (Def. (D.77)) of integer intervals in it. We need to take into account all possible choices of J, with respect to which a chosen pair formation $\mathcal{P} \in PF\{1, \ldots, 2n\}$ is irreducible, i.e.: to any $j \in \{1, \ldots, 2n-1\}$ there is at least one $M \in \mathcal{P}$, such, that

$$|M \cap J(j)| = 1. \qquad (2.104)$$

Graphically, we represent J by a sequence of horizontal square brackets appearing below the sequence of quantum dot states, and stretching from $a_{min(J(j))}$ to $b_{max(J(j))}$. The irreducibility of the pair formation $\mathcal{P}$ in (the order given by the sequence) J is recovered in the diagram by the property, that, to any of the horizontal square brackets, there is at least one (bent) tunneling line, which connects a horizontal line *within* the square bracket to a horizontal line *outside* of the square bracket (cp. Fig. 2.12).

In words, we might describe the *tunneling process* in the example of Fig. 2.13 as follows:

1. The initial matrix is $|\mathbf{0} >< \mathbf{0}|$ (cp. vertical square brackets). An electron of spin $\overline{\sigma}$ tunnels halfway from lead l onto the quantum dot; the matrix turns into $|\overline{\boldsymbol{\sigma}} >< \mathbf{0}|$ (cp. first horizontal square bracket).

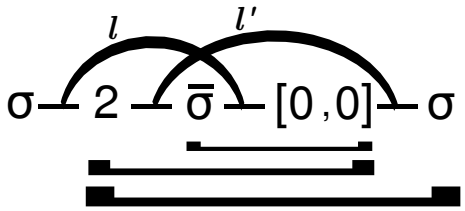

Figure 2.13: By the irreducible tunneling process of the present diagram, an electron of spin σ effectively tunnels onto the quantum dot. We include the lead-index assigned to each pair within the pair formation of the diagram by attaching it to the tunneling line representing that particular pair.

2. An electron of spin σ tunnels halfway from lead l' onto the quantum dot; the matrix is then $|\mathbf{2} >< \mathbf{0}|$ (cp. second horizontal square bracket).

3. The electron of the previous step tunnels fully onto the quantum dot; afterwards the matrix is $|\mathbf{2} >< \boldsymbol{\sigma}|$ (cp. third horizontal square bracket).

4. Finally, the electron of spin $\overline{\sigma}$ tunnels off the quantum dot again; the final matrix is $|\boldsymbol{\sigma} >< \boldsymbol{\sigma}|$ (horizontal square bracket omitted).

Diagram-Counting Scheme

The present transformed diagrams offer an efficient way to find and note all diagrams of – in principle – any given order. For example, to find all sixth order diagrams with initial matrix $|\boldsymbol{\sigma} >< \boldsymbol{\sigma}|$, and final matrix $|\mathbf{0} >< \mathbf{0}|$, applying the transformed version of the diagrams, we would proceed as follows:

1. We note the value of the diagram's parameter $2n = 6$.

2. The value of the diagram's second parameter k is odd, since the overall change of the particle-number in the diagram is -1. Possible values are $k = 1, 3, 5$.

3. To any fixed value $k_0 \in \{1, 3, 5\}$ of k, we note all sequences of quantum dot states $(a_j)_{j=1}^{k_0+1}, (b_j)_{j=k_0}^{6}$ satisfying the following demands:

   - The initial matrix is $|a_{k_0+1} >< b_{k_0}| = |\boldsymbol{\sigma} >< \boldsymbol{\sigma}|$;
   - The final matrix is $|a_1 >< b_{2n}| = |\mathbf{0} >< \mathbf{0}|$;
   - All neighbouring states within the two sequences differ in their particle-number by ± 1.

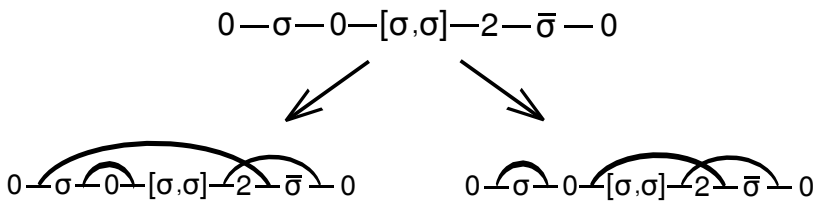

Figure 2.14: In the example of this particular sixth order diagram, there are two ways of choosing a set of tunneling lines.

4. To any of the sequences of quantum dot states we have found in the previous step, we add all sets of tunneling lines, i.e., all pair formations of the horizontal connecting-lines between the quantum dot states, which satisfy the conditions according to Figs. 2.8 , 2.9, and 2.10; cp. also Fig. 2.14.

5. To any of the diagrams, which we have attached a set of tunneling lines to in the previous step, we finally add all interval sequences $J(j)_{j=1}^{5}$ in the form of horizontal square brackets, which the pair formation given by the diagram's particular set of tunneling lines is irreducible in. Because of mirror rule (2.111) we can restrict ourselves to those diagrams whose final square bracket does not contain the very first horizontal line from the left.

We do not apply the present diagram-counting scheme in this work, since we shall take into account only diagrams within a special diagram selection. However, we use the method when we want to find all sixth order diagrams that don't contain the doubly occupied state [20].

2.4.3 Graphic Representation of Conventional Diagrams

In the present section we discuss the depiction of the one form of diagrams which is generally known in the context of irreducible tunneling processes, i.e., from the formal point of view, the elements of the set

$$D \;=\; \left(n, k, S, \mathcal{Q}, (a_j)_{j=1}^{k+1}, (b_j)_{j=k}^{2n}, (l_N, \sigma_N, v_N)_{N\in\mathcal{Q}}\right) \;\in\; \mathcal{D} \qquad (2.105)$$

(Def. (D.92)). Instead of the interval sequence $J \in \mathcal{J}_{(k)}^{(2n)}$, and the pair formation $\mathcal{P} \in \varphi_{(J)}^{-1} PF_{irr}\{1,\ldots,2n\}$ (Def. (D.86)), the conventional diagrams $D \in \mathcal{D}$ rather take the parameters $S \subset \{1,\ldots,2n\}$ with $|S| = k$, and $\mathcal{Q} \in PF_{irr}\{1,\ldots,2n\}$. We depict them as graphic objects in the following way:

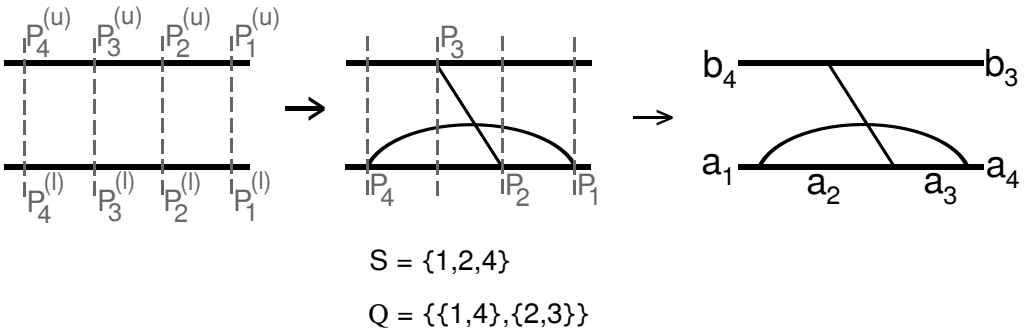

Figure 2.15: The steps by which we construct a diagram $D \in \mathcal{D}$ from the data contained in the tuple $D = \left(n, k, S, \mathcal{Q}, (a_j)_{j=1}^{k+1}, (b_j)_{j=k}^{2n}, (l_N, \sigma_N, v_N)_{N\in\mathcal{Q}}\right)$. In the present example, $2n = 4, |S| = k = 3$.

1. We draw two horizontal lines – which we shall refer to as the *upper* and *lower contour* of the diagram – arranged as opposite sides of a rectangle.

2. We perform a number of $2n$ imaginary vertical cuts through both contours; we count the cuts by convention from the right to the left, and define (without actually marking them in the drawing) the points $P_1^{(u)}, \ldots, P_{2n}^{(u)}$, and $P_1^{(l)}, \ldots, P_{2n}^{(l)}$, as the intersections of these vertical cuts with the upper and lower contour, respectively.

3. For $j \in \{1, \ldots, 2n\}$ we define the point (without actually marking it in the drawing)

$$P_j := \begin{cases} P_j^{(l)} & (j \in S) \\ P_j^{(u)} & (j \in \{1, \ldots, 2n\} \setminus S)\,. \end{cases} \tag{2.106}$$

4. To any $N \in \mathcal{Q}$, with $\mathcal{Q}$ the given pair formation in $PF_{irr}\{1, \ldots, 2n\}$, we connect the points $P_{p(N,<)}$ and $P_{q(N,<)}$ by a simple (bent) line running through the area between the two contours, and, touching the contours only at its ends (Fig. 2.15).

5. The points $P_j, j \in S$, which we shall refer to as the *vertices* of the lower contour, divide the lower contour into a number of $|S| + 1$ segments; to these segments we assign (and attach in the diagram) the quantum dot states $a_1, \ldots, a_{k+1}$, starting from the left end.

6. The points $P_j, j \in \{1, \ldots, 2n\} \setminus S$, which we shall refer to as the vertices on the upper contour, divide the upper contour into a number of

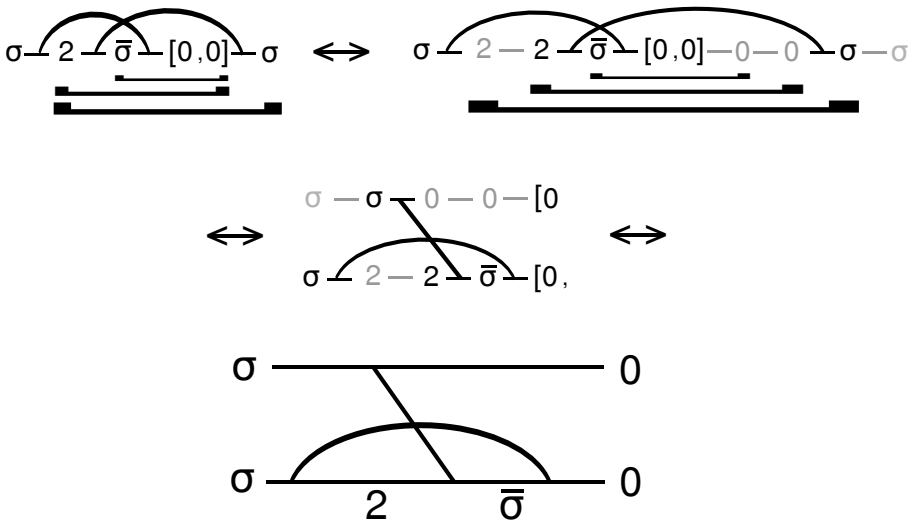

Figure 2.16: The graphic transformation of the diagram in Fig. 2.13 into a diagram of conventional form.

$2n - |S| + 1$ segments; to these segments we assign (and attach in the diagram) the quantum dot states $b_{|S|}, \ldots, b_{2n}$, starting from the right end.

7. The spins and signs $(\sigma_N, v_N)_{N \in \mathcal{Q}}$ contained in the tuple D are fixed by the sequences of quantum dot states $(a_j)_{j=1}^{|S|+1}$, $(b_j)_{j=|S|}^{2n}$ in the sense that, according to the relations (2.96), (2.97), (2.98), at most one choice of these spins and signs yields a non-zero contribution of the diagram D to the kernel; hence, we can omit them in the graphic representation.

8. The lead-indices $l_N, N \in \mathcal{Q}$, on the other hand, can be attached to the tunneling lines; in general we take the sum over all leads to obtain all contributions to the kernel; in this case we shall omit the attachement of a lead-index to a tunneling line.

The two diagram versions D, and $\overline{D} = T_{diag}(D)$, are equivalent; we show their transformation (D.88) graphically by Fig. 2.16.

2.4.4 Diagrammatic Expansion of the Density Matrix Kernel

We note the diagrammatic Expansion of the density matrix kernel shown in App. D, Eq. (D.97)/Def. (D.95):

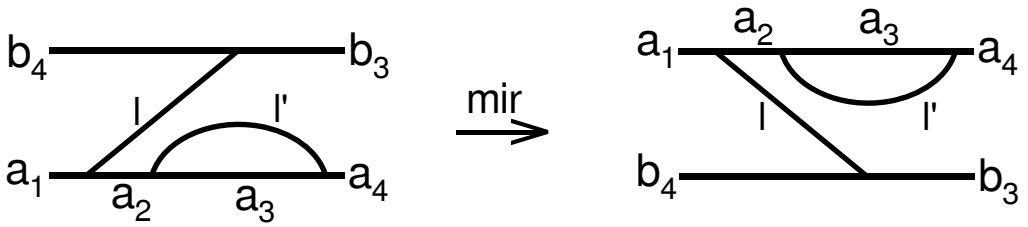

Figure 2.17: Two diagrams mapped to each other by the mirror-map (2.109). The parameters of the diagram D' on the right-hand side, expressed by the parameters of its origin D under the map "mir", are $\left(n', k', S', \mathcal{Q}', \left(a'_j\right)_{j=1}^{k'+1}, \left(b'_j\right)_{j=k'}^{2n}, \left(l'_N, \sigma'_N, v'_N\right)_{N\in\mathcal{Q}}\right)$, where $n' = n, k' = 2n - k, S' = \{1, \ldots, 2n\} \setminus S, \mathcal{Q}' = \mathcal{Q}, \left(l'_N, \sigma'_N, v'_N\right) = \left(l_N, \sigma_N, v_N\right), a'_j = b_{2n+1-j}, b'_j = a_{2n+1-j}$. In the present example, $2n = 4, k = 3, S = \{1, 3, 4\}, \mathcal{Q} = \{\{1, 3\}\{2, 4\}\}$.

$$K(\tau) \;=\; \sum_{D\in\mathcal{D}} K\left(D\right)(\tau) \;=\; \sum_{\overline{D}\in\overline{\mathcal{D}}} K\left(\overline{D}\right)(\tau). \tag{2.107}$$

[For simplicity we simultaneously use the terminology "$K\left(D\right)$", and "$K\left(\overline{D}\right)$", while, rigorously, we would have to distinguish between the two formally different assignments.] The contribution $K\left(D\right)$ of a particular diagram to the kernel is given in Eq. (D.95), and, in Sec. 2.6.3 (Deducing Analytical Expression from Figure), we shall show how we deduce the analytical expression for $K(\overline{D})$ from a graphic representation of the diagram $\overline{D}$.

Mirror Rule

To any diagram

$$D \;=\; \left(n, k, S, \mathcal{Q}, \left(a_j\right)_{j=1}^{k+1}, \left(b_j\right)_{j=k}^{2n}, \left(l_N, \sigma_N, v_N\right)_{N\in\mathcal{Q}}\right) \;\in\; \mathcal{D} \tag{2.108}$$

we can find a partner-diagram by mirroring its graphic representation at a horizontal line, Ref. [21] (cp. Fig. 2.17). At the level of the tuples, we define the mirror-map of diagrams

$$\text{mir}: \quad \mathcal{D} \quad \to \quad \mathcal{D} \tag{2.109}$$

by

$$\begin{aligned}\mathrm{mir}(D) \;:=\; \Big(n, 2n-k, S^c, \mathcal{Q}, (b_{2n+1-j})_{j=1}^{2n-k+1}, (a_{2n+1-j})_{j=2n-k}^{2n}, \\ (l_N, \sigma_N, v_N)_{N\in\mathcal{Q}}\Big),\end{aligned} \tag{2.110}$$

where $S^c := \{1, \ldots, 2n\} \setminus S$, and note the following relation between the contributions to the density matrix kernel (D.97) of a diagram and its mirrored diagram:

$$K\left(\mathrm{mir}(D)\right)(\tau)\ \hat{y} \;=\; \left[K\left(D\right)(\tau)\ \hat{y}\right]^\dagger. \tag{2.111}$$

The present equation, which we shall refer to as *mirror rule*, holds for any self-adjoint operator $\hat{y} : V_\odot \to V_\odot$. We give a proof of mirror rule in App. D.5 (Mirror Rule and Conjugate Diagrams).

2.5 Stationary Density Matrix and Stationary Current

2.5.1 Stationary Density Matrix

Analogously to the definition of the stationary current (cp. Fig. 2.3) we define the *stationary reduced density matrix* of the quantum dot as

$$\hat{\boldsymbol{\rho}} \;:=\; \lim_{\lambda\to 0+}\ \lambda\left\{\mathcal{L}\hat{\rho}_\odot\right\}(\lambda), \tag{2.112}$$

where

$$\left\{\mathcal{L}\hat{\rho}_\odot\right\}(\lambda) \quad := \quad \int_{t_0}^{\infty} dt\ e^{-\lambda(t-t_0)}\ \hat{\rho}_\odot(t), \tag{2.113}$$

the Laplace transform of $\hat{\rho}_\odot(t)$, $t \geq t_0$. [We omit the index "$\odot$" in the variable-name for the stationary reduced density matrix, since we shall not consider any other stationary density matrix, and, because, at a later stage, we shall add further indices to the variable-letter of the present quantity $\hat{\boldsymbol{\rho}}$]. Upon multiplying by λ, and applying the Laplace transform to both sides of the quantum master equation (2.45), we obtain:

$$\lambda \left\{\mathcal{L}\dot{\hat{\rho}}_\odot\right\}(\lambda) \quad = \quad \frac{i}{\hbar}\left[\hat{\boldsymbol{\rho}}(\lambda), \hat{\mathrm{H}}_\odot\right] \; + \; \{\mathcal{L}K\}(\lambda)\hat{\boldsymbol{\rho}}(\lambda), \tag{2.114}$$

where

$$\hat{\boldsymbol{\rho}}(\lambda) \; := \; \lambda\,\{\mathcal{L}\hat{\rho}_\odot\}(\lambda), \tag{2.115}$$

$$\{\mathcal{L}K\}(\lambda) \quad := \quad \int_0^\infty d\tau \; e^{-\lambda\tau} \; K(\tau). \tag{2.116}$$

For a proof of (2.114), we swap the order of the integrations in the integral

$$\begin{aligned} & \int_{t_0}^\infty dt \; e^{-\lambda(t-t_0)} \; \int_{t_0}^t ds \; K(t-s)\hat{\rho}_\odot(s) \\ = \; & \int_{t_0}^\infty ds \; \left\{\int_s^\infty dt \; e^{-\lambda(t-s)} K(t-s)\right\} \; \left[e^{-\lambda(s-t_0)}\hat{\rho}_\odot(s)\right] \\ = \; & (\mathcal{L}K)(\lambda) \; (\mathcal{L}\hat{\rho}_\odot)(\lambda). \qquad \square \end{aligned} \tag{2.117}$$

The quantity $\lim_{\lambda\to 0} \; \lambda \left\{\mathcal{L}\dot{\hat{\rho}}_\odot\right\}(\lambda)$ is the long-term average value of $\dot{\hat{\rho}}_\odot(t)$, and, for finite λ, the relation

$$\lambda \left\{\mathcal{L}\dot{\hat{\rho}}_\odot\right\}(\lambda) \; = \; \lambda^2 \; \{\mathcal{L}\hat{\rho}_\odot\}(\lambda) - \lambda\hat{\rho}_\odot(t_0) \tag{2.118}$$

(integration by parts) holds, and so we conclude

$$\lim_{\lambda\to 0} \; \lambda \left\{\mathcal{L}\dot{\hat{\rho}}_\odot\right\}(\lambda) \; = \; 0. \tag{2.119}$$

With this, Eq. (2.114) reads in the stationary limit:

$$0 \quad = \quad \frac{i}{\hbar}\left[\hat{\boldsymbol{\rho}}, \hat{\mathrm{H}}_\odot\right] \; + \; \boldsymbol{K}\hat{\boldsymbol{\rho}}, \tag{2.120}$$

where

$$\boldsymbol{K} \; := \; \lim_{\lambda\to 0+} \; \{\mathcal{L}K\}(\lambda). \tag{2.121}$$

In the applied part of this work we shall make use of Eq. (2.114) to determine the stationary reduced density matrix $\hat{\boldsymbol{\rho}}$ of the quantum dot by the approximative calculation of $\boldsymbol{K}$. We shall consider only cases where, at any time t,

$$\left[\hat{\rho}_\odot(t), \hat{\mathrm{H}}_\odot\right] \; = \; 0, \tag{2.122}$$

so the Laplace-transformed quantum master equation in the stationary limit reads

$$0 \quad = \quad \boldsymbol{K}\hat{\boldsymbol{\rho}}. \tag{2.123}$$

2.5.2 Current Kernel and Stationary Current

Upon taking the Laplace transform of both sides of the memory equation for the particle-current onto a particular lead $l \in \mathcal{L}$, Eq. (2.50)/(B.10), multiplying with λ, and performing the full trace, as well as the limit $\lambda \to 0$, we obtain the following equation for the stationary current in the definition of Eq. (2.16):

$$\boldsymbol{I_l} \;=\; Tr\left\{\boldsymbol{K_{curr,l}}\hat{\boldsymbol{\rho}}\right\}, \tag{2.124}$$

where in analogy to Defs. (2.116), and (2.121):

$$\begin{aligned} \left\{\mathcal{L}K_{curr,l}\right\}(\lambda) \quad &:= \quad \int_0^\infty d\tau\; e^{-\lambda\tau}\; K_{curr,l}(\tau), \\ \boldsymbol{K_{curr,l}} \quad &:= \quad \lim_{\lambda\to 0+} \left\{\mathcal{L}K_{curr,l}\right\}(\lambda). \end{aligned} \tag{2.125}$$

A diagrammatic analysis of the current kernel $K_{curr,l}(\tau)$ (Def. (B.11)) is performed analogously to the analysis of the density matrix kernel. By the subsets of diagrams (cp. Fig. 2.18)

$$\begin{aligned} \mathcal{D}_l \;:=\; \Big\{ \Big(n, k, S, \mathcal{Q}, (a_j)_{j=1}^{k+1}, (b_j)_{j=k}^{2n}, (l_N, \sigma_N, v_N)_{N\in\mathcal{Q}}\Big) \in \mathcal{D} : \\ 2n \in S,\; l_{N_{2n}(\mathcal{Q})} = l \Big\}, \end{aligned} \tag{2.126}$$

and

$$\begin{aligned} \overline{\mathcal{D}}_l \;:=\; \Big\{ \Big(n, k, J, \mathcal{P}, (a_j)_{j=1}^{k+1}, (b_j)_{j=k}^{2n}, (l_M, \sigma_M, v_M)_{M\in\mathcal{P}}\Big) \in \overline{\mathcal{D}} : \\ k \geq 1, J(2n-1) = \{2, \ldots, 2n\},\; l_{M_1(\mathcal{P})} = l \Big\}, \end{aligned} \tag{2.127}$$

where $M_1(\mathcal{P}) \in \mathcal{P}$ is the one pair $M \in \mathcal{P}$ with $1 \in M$, and $N_{2n}(\mathcal{Q}) \in \mathcal{Q}$ is the one $N \in \mathcal{Q}$ with $2n \in N$, i.e., for any $M \in \mathcal{P}, N \in \mathcal{Q}$:

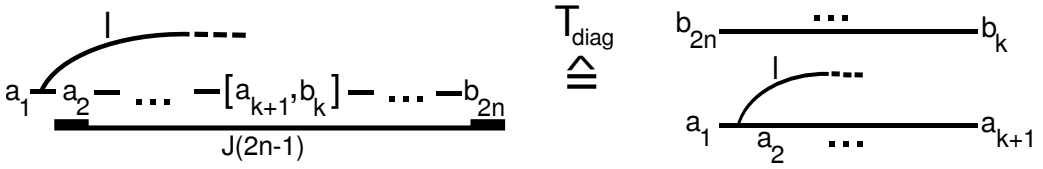

Figure 2.18: Graphic sketch of the properties by which the subsets of diagrams $\overline{\mathcal{D}}_l$, and $\mathcal{D}_l$, respectively, are defined: The diagram on the right-hand side has its final vertex on the lower contour, and the lead-index attached to that tunneling line (representing the pair $N_{2n}(\mathcal{Q})$ (2.129)) which separates the states a_1 and a_2 is l. The corresponding properties of the transformed diagram on the left-hand side are, first, that the horizontal square bracket representing $J(2n-1)$ stretches from a_2 to b_{2n}, and, second, that the one tunneling line (representing the pair $M_1(\mathcal{P})$ (2.128)) which touches the horizontal bar between a_1 and a_2 has lead-index l.

$$M = M_1(\mathcal{P}) \quad :\Leftrightarrow \quad 1 \in M, \tag{2.128}$$

$$N = N_{2n}(\mathcal{Q}) \quad :\Leftrightarrow \quad 2n \in N, \tag{2.129}$$

we obtain the following diagrammatic expansion of $K_{curr,l}$:

$$K_{curr,l}(\tau) \;=\; \sum_{D\in\mathcal{D}_l} K_{curr,l}\,(D)\,(\tau) \;=\; \sum_{\overline{D}\in\overline{\mathcal{D}}_l} K_{curr,l}\,\big(\overline{D}\big)\,(\tau), \tag{2.130}$$

analogously to the expansion of $K(\tau)$ (2.107). [For simplicity we use the same name "$K_{curr,l}$" for two formally different maps.] To any

$$D = \Big(n, k, S, \mathcal{Q}, (a_j)_{j=1}^{k+1}, (b_j)_{j=k}^{2n}, (l_N, \sigma_N, v_N)_{N\in\mathcal{Q}}\Big) \;\in \mathcal{D}_l, \tag{2.131}$$

and any transformed diagram

$$\overline{D} = \Big(n, k, J, \mathcal{P}, (a_j)_{j=1}^{k+1}, (b_j)_{j=k}^{2n}, (l_M, \sigma_M, v_M)_{M\in\mathcal{P}}\Big) \;\in \overline{\mathcal{D}}_l \tag{2.132}$$

we define

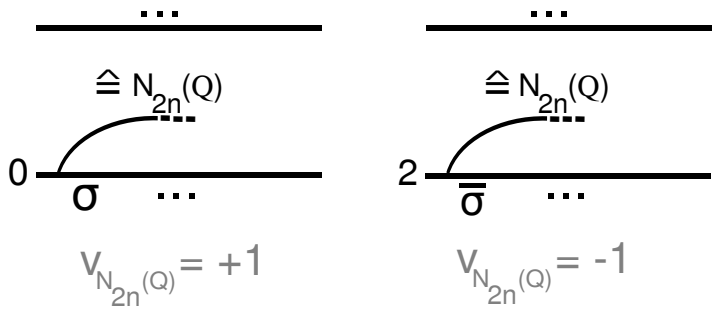

Figure 2.19: The sign $v_{N_{2n}(\mathcal{Q})}$ of a diagram $D \in \mathcal{D}_l$ is positive, if the particle-number of the quantum dot states a_1 and a_2, separated by that tunneling line that corresponds to the pair $N_{2n}(\mathcal{Q})$, *increases* from the left to the right; otherwise it is negative.

$$K_{curr,l}\left(\overline{D}\right) := v_{M_1(\mathcal{P})} K\left(\overline{D}\right), \tag{2.133}$$
$$K_{curr,l}\left(D\right) := v_{N_{2n}(\mathcal{Q})} K\left(D\right), \tag{2.134}$$

with $K(D)$ the contribution of the diagram D to the density matrix kernel (Def. (D.95)).

The Sign $v_{N_{2n}(\mathcal{Q})}$:

Because of the emergence of the factor

$$\langle a_1 |\ \mathrm{d}^{(v_{M_1}(\mathcal{P}))}_{\sigma_{M_1}(\mathcal{P})} a_2 \rangle \tag{2.135}$$

in $\mathrm{sg}^{(1)}\left(\overline{D}\right)$ (Def. (D.39)) we conclude that the relation

$$v_{M_1(\mathcal{P})} \;=\; \langle \hat{\mathrm{N}}_\odot \rangle(a_2) \;-\; \langle \hat{\mathrm{N}}_\odot \rangle(a_1) \tag{2.136}$$

must hold, where $\hat{\mathrm{N}}_\odot$ is the particle-counting operator on the vector space of the quantum dot states, and $\langle \hat{\mathrm{N}}_\odot \rangle(a) := \langle a |\ \hat{\mathrm{N}}_\odot(a) \rangle$, the particle-number of a particular quantum dot state a (cp. Fig. 2.19).

2.5.3 Conjugate Diagrams

For each $a \in \mathcal{B}$, the diagrams contributing to $Tr\left\{\boldsymbol{K_{curr,l}} | a >< a |\right\}$ can be grouped into pairs whose elements give complex conjugate contributions, cp.

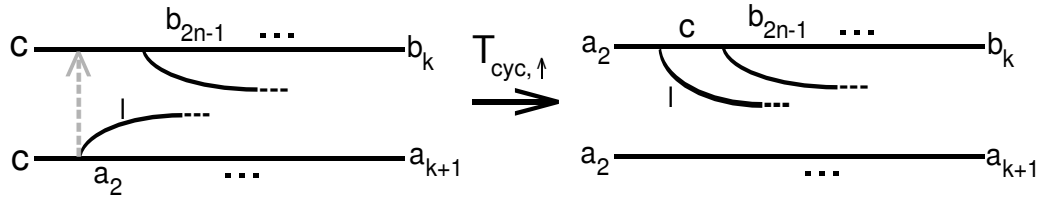

Figure 2.20: The effect of the map $T_{cyc,\uparrow}$ on a diagram $D \in \mathcal{D}_{l,0}$ with final matrix $|c><c|$: The final vertex is shifted from the lower to the upper contour, and the final matrix changes to $|a_2><a_2|$.

Ref. [22]. At the same time, the contribution to the trace $Tr\left\{\boldsymbol{K}|a><a|\right\}$ of the diagrams within these pairs, together with their mirrored diagrams, is zero. Upon defining

$$\begin{aligned}\mathcal{D}^{l} &:= \Big\{ \left(n,k,S,\mathcal{Q},(a_j)_{j=1}^{k+1},(b_j)_{j=k}^{2n},(l_N,\sigma_N,v_N)_{N\in\mathcal{Q}}\right)\in\mathcal{D}: \\ &\qquad 2n\notin S,\ l_{N_{2n}(\mathcal{Q})}=l\Big\} \\ &= \mathrm{mir}\left(\mathcal{D}_l\right),\end{aligned} \tag{2.137}$$

the image of the diagram-set $\mathcal{D}_l$ under mirror-map (2.109), and

$$\begin{aligned}\mathcal{D}_{l,0} &:= \left\{\left(n,k,S,\mathcal{Q},(a_j)_{j=1}^{k+1},(b_j)_{j=k}^{2n},(l_N,\sigma_N,v_N)_{N\in\mathcal{Q}}\right)\in\mathcal{D}_l:\ a_1=b_{2n}\right\}, \\ \mathcal{D}^{l,0} &:= \mathrm{mir}\left(\mathcal{D}_{l,0}\right),\end{aligned} \tag{2.138}$$

$$\begin{aligned}\mathcal{D}^{0} &:= \cup_{l\in\mathcal{L}}\ \mathcal{D}^{l,0}, \\ \mathcal{D}_{0} &:= \cup_{l\in\mathcal{L}}\ \mathcal{D}_{l,0},\end{aligned} \tag{2.139}$$

as well as the map (cp. Figs. 2.20, and 2.21)

$$T_{cyc,\uparrow}:\quad \mathcal{D}_0\ \rightarrow\ \mathcal{D}^0, \tag{2.140}$$

$$\begin{aligned}&\left(n,k,S,\mathcal{Q},(a_j)_{j=1}^{k+1},(b_j)_{j=k}^{2n},(l_N,\sigma_N,v_N)_{N\in\mathcal{Q}}\right) \\ \mapsto\ &\left(n,\tilde{k},\tilde{S},\mathcal{Q},(\tilde{a}_j)_{j=1}^{\tilde{k}+1},\left(\tilde{b}_j\right)_{j=\tilde{k}}^{2n},(l_N,\sigma_N,\tilde{v}_N)_{N\in\mathcal{Q}}\right),\end{aligned}$$

where

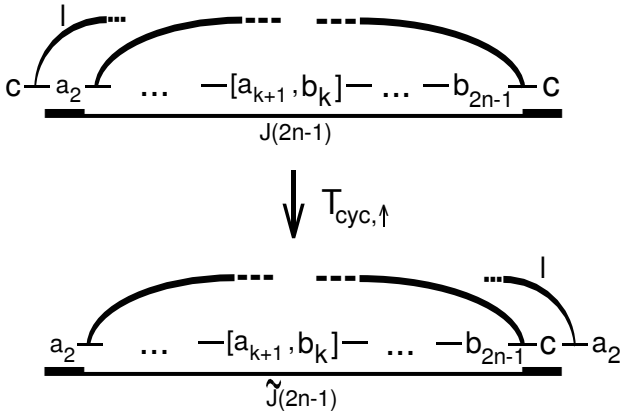

Figure 2.21: The effect of the map $T_{cyc,\uparrow}$ on a diagram in $\mathcal{D}_{l,0}$ in transformed representation. The very first horizontal line appearing to the right of the quantum dot state $a_1 = c$ is moved, together with the corresponding end of that tunneling line which is connected to it, to the right of the state $b_{2n} = c$. The quantum dot state a_1 within the sequence $(a_j)_{j=1}^{k+1}$ is removed on the left side of the diagram, and the state a_2 is added on the right, while the rest of the figure remains unchanged.

$$\begin{aligned} \tilde{k} &:= k-1, \\ \tilde{S} &:= S \setminus \{2n\}, \\ \tilde{a}_j &:= a_{j+1} \quad (j = 1, \ldots, k), \end{aligned} \tag{2.141}$$

and

$$\tilde{b}_j := \begin{cases} b_{j+1} & (j = k-1, \ldots, 2n-1) \\ a_2 & (j = 2n), \end{cases} \tag{2.142}$$

$$\tilde{v}_N := \begin{cases} v_N & (N \neq N_{2n}(\mathcal{Q})) \\ -v_N & (N = N_{2n}(\mathcal{Q})), \end{cases} \tag{2.143}$$

we note that the map $T_{cyc,\uparrow}$ is bijective.

Upon defining

$$\begin{aligned} \mathcal{D}_{l,0,+} &:= \Big\{ \Big(n, k, S, \mathcal{Q}, (a_j)_{j=1}^{k+1}, (b_j)_{j=k}^{2n}, (l_N, \sigma_N, v_N)_{N\in\mathcal{Q}}\Big) \in \mathcal{D}_{l,0} : \\ &\qquad v_{N_{2n}(\mathcal{Q})} = +1 \Big\}, \\ \mathcal{D}_{l,0,-} &:= \mathcal{D}_{l,0} \setminus \mathcal{D}_{l,0,+}, \end{aligned} \tag{2.144}$$

and the composition of maps

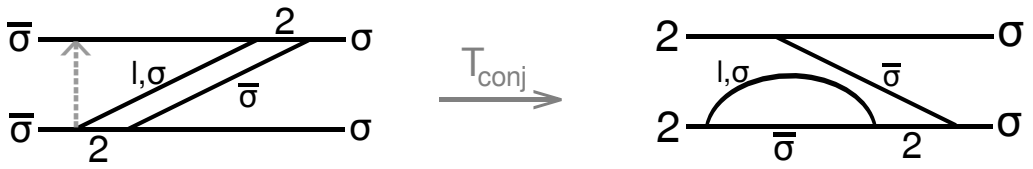

Figure 2.22: The map T_{conj}: The final vertex is shifted to the upper contour, and, second, the diagram is mirrored at a horizontal axis. In the present example, a diagram in $\mathcal{D}_{l,0,+}$ is mapped to a diagram in $\mathcal{D}_{l,0,-}$ (cp. Fig. 2.19).

$$T_{conj} \;:=\; \text{mir} \;\circ\; T_{cyc,\uparrow}: \qquad \mathcal{D}_0 \to \mathcal{D}_0, \tag{2.145}$$

(cp. Fig. 2.22) with "mir" the mirror-map (2.109), we note that T_{conj} is bijective, and

$$\begin{aligned} T_{conj}\left(\mathcal{D}_{l,0,+}\right) &= \mathcal{D}_{l,0,-}\;, \\ T_{conj}\left(\mathcal{D}_{l,0,-}\right) &= \mathcal{D}_{l,0,+}\;. \end{aligned} \tag{2.146}$$

If we take into account any diagram $D \in \mathcal{D}_{l,0,+}$ always together with its conjugate diagram $T_{conj}D$, and apply mirror rule (2.111), we arrive at the expansion

$$Tr\left\{K_{curr,l}(\tau)\hat{y}\right\} \;=\; \sum_{D\in\mathcal{D}_{l,0,+}} 2\; Re\Big(Tr\Big\{K\left(D\right)(\tau)\hat{y}\Big\}\Big), \tag{2.147}$$

which holds for any self-adjoint operator $\hat{y}: V_\odot \to V_\odot$, where $Re(z)$ denotes the real part of a complex quantity z.

Proof:

In App. D.5.2 (Contribution of Conjugate Diagrams to the Kernels) we show that for any $D \in \mathcal{D}_{l,0}$, and any linear map $\hat{y}: V_\odot \to V_\odot$:

$$Tr\Big\{K\left(T_{cyc,\uparrow}D\right)(\tau)\;\hat{y}\Big\} \;=\; (-1)\; Tr\Big\{K\left(D\right)(\tau)\;\hat{y}\Big\}. \tag{2.148}$$

Hence, mirror rule (2.111) implies, that for any self-adjoint $\hat{y} : V_{\odot} \to V_{\odot}$:

$$Tr\Big\{K\left(T_{conj}D\right)(\tau)\hat{y}\Big\} \;=\; (-1)\; Tr\Big\{K\left(D\right)(\tau)\hat{y}\Big\}^{*}, \tag{2.149}$$

where the asterisk denotes the complex conjugate. With relation (2.146) and the expansion (2.130) we arrive at Eq. (2.147). $\square$

2.6 Summary: Application of the Theory

We here give a summary of the steps we shall take in the applied chapter of this work in order to calculate the stationary reduced density matrix $\hat{\boldsymbol{\rho}}$ of the quantum dot as well as the current which flows across it. In particular, we show how we deduce the analytical expression for a particular diagram's contribution to the kernels directly from its graphic representation rather than from Def. (D.67).

2.6.1 Density Matrix

We will consider only such cases where $\hat{\boldsymbol{\rho}}$ is diagonal in the basis $\mathcal{B} = \{\mathbf{0}, \uparrow, \downarrow, \mathbf{2}\}$ (2.91) or, in the case of the spinless quantum dot (2.3), in a corresponding basis $\mathcal{B} = \{\mathbf{0}, \boldsymbol{\sigma}_o\}$. The quantum master equation in the stationary limit reads in these cases:

$$\begin{aligned} 0 \;&=\; \boldsymbol{K}\hat{\boldsymbol{\rho}} \;=\; \boldsymbol{K}\left\{\sum_{a\in\mathcal{B}} \rho_{aa}|a><a|\right\} \\ &=\; \sum_{a\in\mathcal{B}} \rho_{aa}\boldsymbol{K}\left(|a><a|\right), \end{aligned} \tag{2.150}$$

where the matrix elements ρ_{aa} are the eigenvalues

$$\rho_{aa} \;=\; \langle a|\hat{\boldsymbol{\rho}}(a)\rangle \tag{2.151}$$

satisfying

$$\rho_{aa} \;\geq\; 0, \tag{2.152}$$

as well as the normalization condition

$$\sum_{a\in\mathcal{B}} \rho_{aa} \;=\; 1. \tag{2.153}$$

The kernel $\boldsymbol{K}$ maps operators to operators, and so we conclude that for any $b \in \mathcal{B}$:

$$0 \;=\; \sum_{a\in\mathcal{B}} \rho_{aa} \langle b\,|\{\boldsymbol{K}\left(|a><a|\right)\}(b)\rangle \;, \tag{2.154}$$

which amounts to a system of $|\mathcal{B}|$ equations for the same number of unknown quantities ρ_{aa}. The density matrix kernel maps any operator of the form $\sum_{a\in\mathcal{B}} \rho_{aa}|a><a|$ to an operator with zero trace, so the dimension of the image of $\boldsymbol{K}$ is reduced by one, thus ensuring there is a non-trivial solution $\hat{\boldsymbol{\rho}}$ to $\boldsymbol{K}\hat{\boldsymbol{\rho}} = 0$. Correspondingly, the number of independent equations in the present system of equations is $|\mathcal{B}| - 1$, which fixes the solution up to a scalar factor. Finally, the absolute values of the elements ρ_{aa} are determined by the normalization condition (2.153).

To calculate the *kernel elements* $\langle b\,|\{\boldsymbol{K}\left(|a><a|\right)\}(b)\rangle$, we apply the diagrammatic expansion (D.97), taking into account all diagrams with initial matrix $|a><a|$ and final matrix $|b><b|$. We obtain:

$$\langle b\,|\{\boldsymbol{K}\left(|a><a|\right)\}(b)\rangle \;=\; \sum_{D\in\mathcal{D}_{a\to b}} 2\; Re\left\{\langle b\,|\{\boldsymbol{K}(D)\left(|a><a|\right)\}(b)\rangle\right\}, \tag{2.155}$$

with

$$\begin{aligned}\mathcal{D}_{a\to b} \;:=\; \Big\{ \Big(n, k, S, \mathcal{Q}, (a_j)_{j=1}^{k+1}, (b_j)_{j=k}^{2n}, (l_N, \sigma_N, v_N)_{N\in\mathcal{Q}}\Big) \in \mathcal{D} : \\ 2n \in S,\; a_1 = b_{2n} = b,\; a_{k+1} = b_k = a\Big\}\end{aligned} \tag{2.156}$$

(cp. Fig. 2.23).

2.6.2 Current

Once having determined the stationary density matrix $\hat{\boldsymbol{\rho}}$ from the kernel elements of the density matrix kernel, we determine the stationary particle-current $\boldsymbol{I_l}$ onto lead l by inserting the expansion of the current kernel as a sum over $\mathcal{D}_{l,0,+}$ (2.147) into Eq. (2.124):

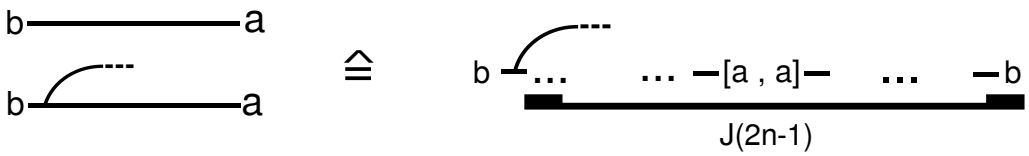

Figure 2.23: Features of the diagrams within the set $\mathcal{D}_{a\to b}$, for given quantum dot states $a, b \in \mathcal{B}$: The initial matrix of the diagram is $|a><a|$, its final matrix is $|b><b|$. The final vertex is on the lower contour; in alternative representation, the final interval of the sequence $J(j)_{j=1}^{2n-1}$ is given by $J(2n-1) = \{2, \ldots, 2n\}$. The contribution to the kernel element $\langle b\,|\{\boldsymbol{K}\,(|a><a|)\}\,(b)\rangle$ of those diagrams with their final vertex on the upper contour, according to mirror rule (2.111), is the complex conjugate of the contribution of the diagram-set $\mathcal{D}_{a\to b}$.

$$\boldsymbol{I_l} \;=\; \sum_{D\in\mathcal{D}_{l,0,+}} 2Re\left\{Tr\left\{\boldsymbol{K}(D)\hat{\boldsymbol{\rho}}\right\}\right\}. \tag{2.157}$$

The summands on the right-hand side of this equation, on the other hand, are determined by the relation

$$Tr\left\{\boldsymbol{K}(D)\hat{\boldsymbol{\rho}}\right\} \;=\; \sum_{a,b\in\mathcal{B}} \rho_{aa}\langle b\,|\{\boldsymbol{K}(D)\,(|a><a|)\}\,(b)\rangle\,, \tag{2.158}$$

where the contributions $\langle b\,|\{\boldsymbol{K}(D)\,(|a><a|)\}\,(b)\rangle$ to the kernel elements of the density matrix kernel have already been calculated at this stage.

2.6.3 Deducing Analytical Expression from Figure

We here show by an example-diagram (Fig. 2.24) how we obtain the analytical expression for a diagram's contribution $\boldsymbol{K}(D)$ to the density matrix kernel more directly from its graphic representation rather than by inserting the parameters of the tuple $D \in \mathcal{D}$ (D.92) into Def. (D.67). At first, we shall note the expression for the time-dependent quantity

$$K(D)(\tau)\hat{y}. \tag{2.159}$$

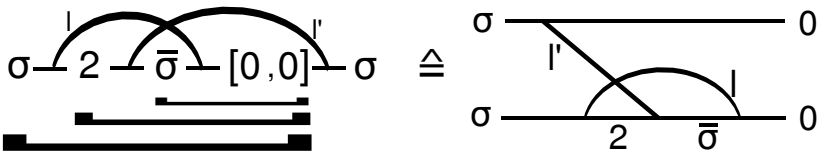

Figure 2.24: A fourth-order diagram representing a tunneling process during which one electron from lead l' effectively tunnels onto the quantum dot, while a second electron fluctuates between the quantum dot and one of the leads.

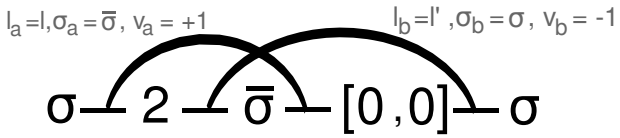

Figure 2.25: Parts of the analytical expression for $\boldsymbol{K}(D)$ depend only on the diagram's sequence of quantum dot states and its pair formation, hence we here focus on the upper part of the diagram. We distinguish the tunneling lines by the indices "a", "b".

Parts Independent of the Interval Sequence J

We begin with those parts of the analytical expression that depend only on the upper part of the diagram in Fig. 2.24 (or else: only the topology of the corresponding conventional diagram), so for the moment we consider only the reduced diagram of Fig. 2.25.

Operator-Part

First, we note the operator

$$|\boldsymbol{\sigma}><\boldsymbol{\sigma}|\ \langle \mathbf{0}|\hat{y}(\mathbf{0})\rangle, \tag{2.160}$$

i.e., the diagram's final matrix, multiplied by the scalar product $\langle \mathbf{0}|\hat{y}(\mathbf{0})\rangle$ – that one part into which $\hat{y}$ enters.

Signs

We note the signs:

$$\mathrm{sign}(\mathcal{P}) \ = -1, \tag{2.161}$$

since there is one intersection of tunneling lines in this diagram;

$$(-1)^{n+k} \ = \ -1, \tag{2.162}$$

since $n = 2$ (the number of tunneling lines), and $k = 3$ (the number of quantum dot states left of the square bracket); and, the two products of scalar products,

$$\underbrace{\langle \boldsymbol{\sigma}|\hat{\mathrm{d}}_{\overline{\sigma}}(\mathbf{2})\rangle\ \langle \overline{\boldsymbol{\sigma}}|\hat{\mathrm{d}}^{\dagger}_{\overline{\sigma}}(\mathbf{0})\rangle}_{tunneling\ line\ a)}\ \underbrace{\langle \mathbf{2}|\hat{\mathrm{d}}^{\dagger}_{\sigma}(\overline{\boldsymbol{\sigma}})\rangle\ \langle \mathbf{0}|\hat{\mathrm{d}}_{\sigma}(\boldsymbol{\sigma})\rangle}_{tunneling\ line\ b)}\ =\ -1 \tag{2.163}$$

(Defs. (2.92), (2.94)), corresponding to the two tunneling lines.

Participation of *Occupied* vs. *Empty* One-Electron Levels in the Leads

Generally, the signs $(v_M)_{M\in\mathcal{P}}$ are determined by comparison of the particle-number of subsequent quantum dot states (cp. Fig. 2.8, Eq. (2.96), and following):

$$\begin{aligned} v_M &= \left\{ \begin{array}{cc} \langle \hat{\mathrm{N}}_{\odot}\rangle \left(a_{p(M)+1}\right) - \langle \hat{\mathrm{N}}_{\odot}\rangle \left(a_{p(M)}\right) & (p(M)\leq k) \\ \langle \hat{\mathrm{N}}_{\odot}\rangle \left(b_{p(M)}\right) - \langle \hat{\mathrm{N}}_{\odot}\rangle \left(b_{p(M)-1}\right) & (k+1\leq p(M)) \end{array} \right\} \\ &= \left\{ \begin{array}{cc} (-1)\left[\langle \hat{\mathrm{N}}_{\odot}\rangle \left(a_{q(M)+1}\right) - \langle \hat{\mathrm{N}}_{\odot}\rangle \left(a_{q(M)}\right)\right] & (q(M)\leq k) \\ (-1)\left[\langle \hat{\mathrm{N}}_{\odot}\rangle \left(b_{q(M)}\right) - \langle \hat{\mathrm{N}}_{\odot}\rangle \left(b_{q(M)-1}\right)\right] & (k+1\leq q(M)) \end{array} \right\}, \end{aligned} \tag{2.164}$$

with $\hat{\mathrm{N}}_{\odot} = \sum_{\sigma}\hat{\mathrm{N}}_{\sigma}$ the particle-counting operator of the quantum dot, and $\langle \hat{\mathrm{N}}_{\odot}\rangle\,(c) := \langle c|\hat{\mathrm{N}}_{\odot}(c)\rangle$ (cp. Def. (2.99)).

To every tunneling line, we have to note one of the functions of energy $\alpha^{(v)}_{l\sigma}(\varepsilon)$ (D.66), which quadratically contain the tunneling coupling, as well as either the Fermi function of contact l for spin σ in case $v = +1$, or one minus this function in case $v = -1$. The function we obtain for a particular tunneling line corresponding to an element $M \in \mathcal{P}$ is

$$\alpha^{\left(sg^{(2)}(M,k)v_M\right)}_{l_M\sigma_M}, \tag{2.165}$$

with $sg^{(2)}\,(M,k) = -1$, if the corresponding tunneling line stretches *over* the pair of square brackets that enclose the states of the diagram's initial matrix, and $sg^{(2)}\,(M,k) = +1$ otherwise (Def. (D.40)). As a consequence, we obtain the function $\alpha^{(+1)}_{l_M\sigma_M}$, in case the tunneling line corresponds to an electron that first tunnels halfway *onto* the quantum dot, and, otherwise, the function $\alpha^{(-1)}_{l_M\sigma_M}$, in case the tunneling line corresponds to an electron that first tunnels halfway *off* the quantum dot (cp. Fig. 2.26). For the example-diagram of Figs. 2.24/ 2.25 we note the functions

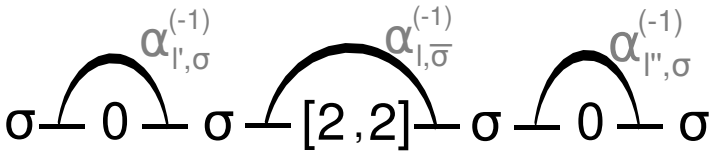

Figure 2.26: In the example of this particular diagram, the tunneling line stretching over the central square brackets represents an electron of spin $\overline{\sigma}$ which tunnels in two steps off the quantum dot; the other two tunneling lines correspond to electrons that first tunnel "halfway" off the quantum dot, and then return. The sign $sg^{(2)}(M,k)\, v_M$ is negative for all of the three tunneling lines in the present figure.

$$\alpha_{l\overline{\sigma}}^{(+1)}(\varepsilon),\ \alpha_{l'\sigma}^{(+1)}(\varepsilon'). \tag{2.166}$$

The product of the two functions (2.166) appears in an integral over the variables $\varepsilon, \varepsilon'$.

Parts Depending on the Interval Sequence J

We now note those parts of the analytical expression for the diagram of Fig. 2.24 that actually depend on the time-ordering.

Time-Integral

We note the integral

$$\frac{1}{\hbar^{2n}}\ \frac{1}{\sqrt{2n-1}}\ \int_{\left\{S^{(2n-1)}=\tau\right\}},$$

over the $2n-2$-dimensional surface $\left\{S^{(2n-1)}=\tau\right\}$ (Fig. 2.6), where in the present case $2n-1=3$, so

$$\left\{S^{(2n-1)}=\tau\right\}\ =\ \left\{(\overline{\tau}_1,\overline{\tau}_2,\overline{\tau}_3):\ \overline{\tau}_j\geq 0 (j=1,2,3),\ \sum_{j=1}^{3}\overline{\tau}_j\ =\tau\right\}. \tag{2.167}$$

The integrand of this time-integral has the general shape

$$\exp\ \left\{\ \frac{i}{\hbar}\sum_{j=1}^{3}\overline{\tau}_j\ \left[\ -\overline{E}_j+\sum_{M\in\mathcal{P}:|M\cap J(j)|=1} w_M\ \varepsilon_M\ \right]\ \right\}. \tag{2.168}$$

Values of the Energies $\overline{E}_j (j = 1, 2, 3)$

The energies $\overline{E}_j$ are given by the differences of energies of quantum dot states,

$$\overline{E}_j \;=\; E_{a_{min(J(j))} b_{max(J(j))}} \;=\; E_{a_{min(J(j))}} - E_{b_{max(J(j))}}. \tag{2.169}$$

The interval $J(j)$ is represented by one of the horizontal square brackets in Fig. 2.24, and the quantum dot state $b_{max(J(j))}$ is the right-most which is still contained in the bracket, while $a_{min(J(j))}$ is the left-most state contained in the bracket. For the present example-diagram of Fig. 2.24 we obtain:

$$\begin{array}{rcl} \overline{E}_1 &=& E_{\overline{\sigma}0}, \\ \overline{E}_2 &=& E_{20}, \\ \overline{E}_3 &=& E_{\sigma 0}. \end{array} \tag{2.170}$$

Values of the Signs w_M

To each $j \in \{1, 2, 3\}$, the sum $\sum_{M \in \mathcal{P}: |M \cap J(j)| = 1} w_M \, \varepsilon_M$ goes over all tunneling lines which connect one of the horizontal lines *within* the space enclosed by the square bracket representing $J(j)$ to one of the horizontal lines *outside* of this space. The signs

$$w_M \;=\; \mathrm{sg}^{(3)}(M, J)\, v_M \tag{2.171}$$

(Eq. (D.67), Def. (D.41)) can be determined by the relation

$$\mathrm{sg}^{(3)}(M, J)\, v_M \;=\; \Delta N(j_0) - \Delta N(j_0 - 1), \tag{2.172}$$

with

$$j_0 \;=\; \min\{j \in \{1, 2, 3\} : \; J(j) \cap M \neq \emptyset\}, \tag{2.173}$$

and

$$\Delta N(j) \;:=\; \langle \hat{\mathrm{N}}_\odot \rangle \left(a_{min(J(j))}\right) - \langle \hat{\mathrm{N}}_\odot \rangle \left(b_{max(J(j))}\right) \quad (j = 1, \ldots, 2n-1), \tag{2.174}$$

the difference between the overall particle-numbers of the quantum dot states $a_{min(J(j))}, b_{max(J(j))}$, or else, in case $j = 0$:

$$\Delta N(0) \;:=\; \langle \hat{\mathrm{N}}_\odot \rangle (a_{k+1}) - \langle \hat{\mathrm{N}}_\odot \rangle (b_k) \tag{2.175}$$

(cp. Fig. 2.27).

For the example-diagram of Fig. 2.24 we note:

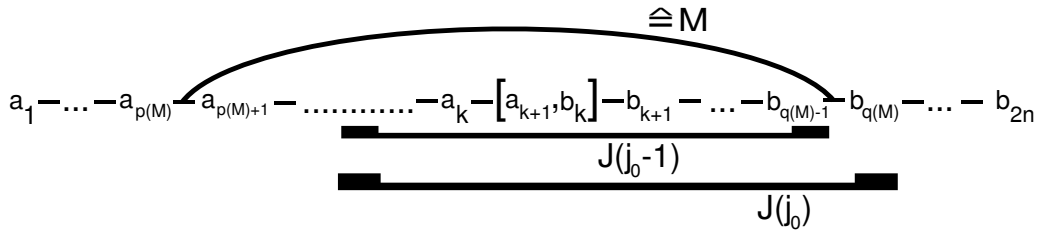

Figure 2.27: To determine the sign $v_M \mathrm{sg}^{(3)}(M,J)$, for a particular element $M \in \mathcal{P}$, we distinguish between four cases (one case each for Figs. 2.8, and 2.9, as well as two sub-cases for Fig. 2.10, where one of the latter sub-cases is sketched by the present figure). In the diagram of the present figure, $\mathrm{sg}^{(3)}(M,J) = +1$, and $v_M = \langle \hat{\mathrm{N}}_\odot \rangle \left(a_{p(M)+1}\right) - \langle \hat{\mathrm{N}}_\odot \rangle \left(a_{p(M)}\right) = \langle \hat{\mathrm{N}}_\odot \rangle \left(b_{q(M)-1}\right) - \langle \hat{\mathrm{N}}_\odot \rangle \left(b_{q(M)}\right)$, and hence, $v_M \mathrm{sg}^{(3)}(M,J) = \Delta N(j_0) - \Delta N(j_0 - 1)$, where the latter equation holds true in all other cases as well.

$$\begin{aligned} \Delta N(0) &= 0, \\ \Delta N(1) &= 1, \\ \Delta N(2) &= 2, \end{aligned} \tag{2.176}$$

so, with Eq. (2.172), we obtain the two signs

$$w_{M_a} = \mathrm{sg}^{(3)}(M_a, J)\, v_{M_a} = +1 = \mathrm{sg}^{(3)}(M_b, J)\, v_{M_b} = w_{M_b}, \tag{2.177}$$

where we distinguish between the two tunneling lines by the indices "a", and "b" as before (Fig. 2.25).

Complete Expression and Laplace Transform

The complete expression for $K(D)(\tau)\hat{y}$ reads

$$\begin{aligned} K(D)(\tau)\hat{y} \quad = \quad & (-1)\, |\boldsymbol{\sigma}><\boldsymbol{\sigma}|\, \langle \mathbf{0}|\hat{y}(\mathbf{0})\rangle \int d\varepsilon \int d\varepsilon'\, \alpha^{(+1)}_{l\bar{\sigma}}(\varepsilon)\, \alpha^{(+1)}_{l'\sigma}(\varepsilon') \\ & \frac{1}{\hbar^4}\frac{1}{\sqrt{3}} \int_{\left\{S^{(3)}=\tau\right\}} \exp\Big(\frac{i}{\hbar}\Big\{ \overline{\tau}_1 \left[\varepsilon - E_{\bar{\sigma}0}\right] + \overline{\tau}_2 \left[\varepsilon + \varepsilon' - E_{20}\right] + \\ & \qquad \overline{\tau}_3 \left[\varepsilon' - E_{\sigma 0}\right] \Big\} \Big) \ . \end{aligned} \tag{2.178}$$

In order to obtain the Laplace transform, we apply the transformation of Fig. 2.6 in backward direction:

$$\int_0^\infty d\tau\; e^{-\lambda\tau}\frac{1}{\sqrt{3}}\int_{\left\{S^{(3)}=\tau\right\}}\exp\left(i\sum_{j=1}^{3}c_j\overline{\tau}_j\right) \tag{2.179}$$

$$= \frac{1}{\sqrt{3}}\int_0^\infty d\tau\;\int_{\left\{S^{(3)}=\tau\right\}}\exp\left(i\sum_{j=1}^{3}\overline{\tau}_j\left[-\lambda+ic_j\right]\right)$$

$$= \int_0^\infty d\overline{\tau}_1\int_0^\infty d\overline{\tau}_2\int_0^\infty d\overline{\tau}_3\;\prod_{j=1}^{3}\exp\left(\overline{\tau}_j\left[-\lambda+ic_j\right]\right),$$

for any set of real coefficients c_1, c_2, c_3. With this, we arrive at the expression

$$\boldsymbol{K}(D)\hat{y} = \frac{-1}{\hbar}\,|\boldsymbol{\sigma}><\boldsymbol{\sigma}|\,\langle\mathbf{0}|\hat{y}(\mathbf{0})\rangle\,\lim_{\eta\to0+}\int\int d\varepsilon d\varepsilon'\;\alpha_{l\overline{\sigma}}^{(+1)}(\varepsilon)\;\alpha_{l'\sigma}^{(+1)}(\varepsilon')$$
$$\frac{1}{\eta+i\left[E_{\overline{\sigma}0}-\varepsilon\right]}\quad\frac{1}{\eta+i\left[E_{20}-\varepsilon-\varepsilon'\right]}\quad\frac{1}{\eta+i\left[E_{\sigma0}-\varepsilon'\right]} \tag{2.180}$$

for the contribution of the example-diagram in Fig. 2.24 to the density matrix kernel in the stationary limit.

Analytical Expression for a Sixth Order Diagram

The analytical expression for the sixth order example-diagram D of Fig. 2.28 contains $n = 3$ coupling functions, correspondingly three integrals, and $2n - 1 = 5$ fractions. The complete expression is

$$\boldsymbol{K}(D)\hat{y} = \frac{+1}{\hbar}\,|\mathbf{1}><\mathbf{1}|\langle\mathbf{0}|\hat{y}(\mathbf{0})\rangle\,\lim_{\eta\to0+}\int\int\int d\varepsilon d\varepsilon' d\varepsilon''\alpha_l^+(\varepsilon)\alpha_{l'}^+(\varepsilon')\alpha_{l''}^+(\varepsilon'')$$
$$\frac{1}{\eta+i\left[E_{01}+\varepsilon\right]}\frac{1}{\eta+i\left[\varepsilon-\varepsilon'\right]}\frac{1}{\eta+i\left[E_{01}+\varepsilon\right]}\frac{1}{\eta+i\left[\varepsilon-\varepsilon''\right]}\frac{1}{\eta+i\left[E_{01}+\varepsilon\right]}. \tag{2.181}$$

We encounter the pre-factor $1/\hbar$ in all orders; the overall sign in the present diagram's expression is given exclusively by $(-1)^{n+k} = (-1)^{3+5} =$

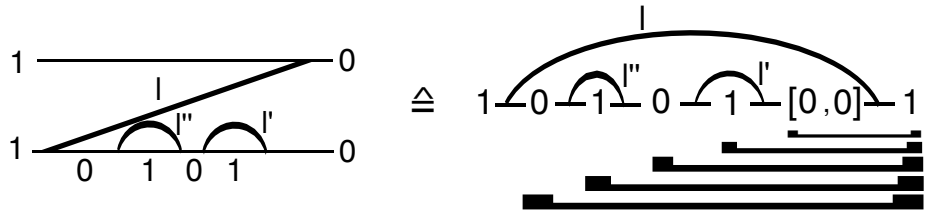

Figure 2.28: A sixth order diagram which we give the analytical expression for in Eq. (2.181) .

+1; the differences of energies of quantum dot states appearing in the denominators are given by Eq. (2.169), while the signs of $\varepsilon = \varepsilon_M, \varepsilon' = \varepsilon_{M'}$, and $\varepsilon'' = \varepsilon_{M''}$, (we refer to the three tunneling lines by M, M', and M'') are given by

$$(-1)\left[\Delta N(j_0) - \Delta N(j_0 - 1)\right], \tag{2.182}$$

with $\Delta N(j)$ defined correspondingly to Eq. (2.174); we here abbreviate $\alpha_l^{(\pm 1)} = \alpha_l^{\pm}$.

2.7 Relation between Kernel Elements and Transition Rates

2.7.1 Transition Rates

At the present stage we interpret the transport theory as follows: For any $b \in \mathcal{B}$ (Sec. 2.5.3 (Conjugate Diagrams)):

$$Tr\left\{\boldsymbol{K}\left(|b><b|\right)\right\} \;=\; 0. \tag{2.183}$$

Hence, we can note the quantum master equation in the form of Eq. (2.154) equivalently by the equality

$$\rho_{bb} \sum_{a\in\mathcal{B}:a\neq b} \boldsymbol{K}_{bb}^{aa} \;=\; \sum_{a\in\mathcal{B}:a\neq b} \rho_{aa} \boldsymbol{K}_{aa}^{bb}, \tag{2.184}$$

holding for every single fixed state $b \in \mathcal{B}$, where we use the abbreviation

$$\boldsymbol{K}_{aa}^{bb} \;:=\; \langle b\,|\{\boldsymbol{K}\left(|a><a|\right)\}(b)\rangle\ . \tag{2.185}$$

The quantities $\boldsymbol{K}_{aa}^{bb}$ actually have the unit $1/s$, and we interpret them as (relative) rates for the transition of the quantum dot from state a to state b

in Eq. (2.184): The left-hand side takes into account the rate and probability of all processes which have the initial state b and a final state $a \neq b$, while the right-hand side takes into account the probability and rate of all processes which have any initial state $a \neq b$, and the final state b. [Generally, we distinguish between the relative rate $\boldsymbol{K}^{bb}_{aa}$, and the absolute rate $\rho_{aa}\boldsymbol{K}^{bb}_{aa}$.] In the stationary configuration, these two contributions to the gain and loss [19] of the probability with which we find the quantum dot in the state b must be equal.

2.7.2 Change of Electron Number on the Leads by a Particular Tunneling Process

For any given quantum dot state $a \in \mathcal{B}$, and any particular lead l we consider again

$$\begin{aligned} Tr\left\{\boldsymbol{K_{curr,l}}|a><a|\right\} &= Tr\left\{\sum_{D\in\mathcal{D}_l}\boldsymbol{K_{curr,l}}(D)|a><a|\right\} \\ &= Tr\left\{\sum_{D\in\mathcal{D}_{l,0}}\boldsymbol{K_{curr,l}}(D)|a><a|\right\} \end{aligned} \tag{2.186}$$

$$= Tr\left\{\sum_{D\in\mathcal{D}_{l,0,+}}\boldsymbol{K_{curr,l}}(D)|a><a| \;+\; \boldsymbol{K_{curr,l}}(T_{conj}D)|a><a|\right\}$$

$$= Tr\left\{\sum_{D\in\mathcal{D}_{l,0,+}}\boldsymbol{K}(D)|a><a| \;-\; \boldsymbol{K}(T_{conj}D)|a><a|\right\}$$

$$\begin{aligned} = \frac{1}{2}\sum_{D\in\mathcal{D}_{l,0,+}} & Tr\Big\{\boldsymbol{K}(D)|a><a| \;+\; \boldsymbol{K}(\mathrm{mir}(D))|a><a|\Big\} \\ & - \; Tr\Big\{\boldsymbol{K}(T_{conj}D)|a><a| \;+\; \boldsymbol{K}\left(\mathrm{mir}(T_{conj}D)\right)|a><a|\Big\}, \end{aligned}$$

according to (2.130) (diagrammatic expansion of the current kernel), (2.138), (2.144) (definition of $\mathcal{D}_{l,0}$, and $\mathcal{D}_{l,0,+}$), (2.134) (definition of $\boldsymbol{K_{curr,l}}(D)$), and according to mirror rule (2.111).

To any diagram

$$\overline{D} \;=\; \left(n, k, J, \mathcal{P}, (a_j)_{j=1}^{k+1}, (b_j)_{j=k}^{2n}, (l_M, \sigma_M, v_M)_{M\in\mathcal{P}}\right) \;\in\; \overline{\mathcal{D}} \tag{2.187}$$

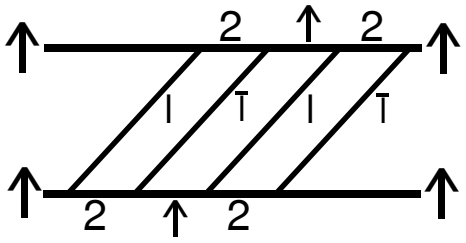

Figure 2.29: The initial and final matrix of the present diagram is $|\uparrow><\uparrow|$. Altogether two electrons tunnel from lead $\bar{l}$ onto the quantum dot, and the same number of electrons tunnel from the quantum dot onto the opposite lead l. Hence, the integer $Z_l(D)$ equals 2 for this particular diagram, while $Z_{\bar{l}}(D) = -2$.

(Def. (D.89)) we define the integer

$$Z_l(\overline{D}) \;:=\; \sum_{M\in\mathcal{P}:\; l_M=l, p(M)\leq k, k+1\leq q(M)} v_M, \tag{2.188}$$

the number of electrons that effectively tunnel onto lead l during the tunneling process represented by the diagram $\overline{D}$ (cp. Fig. 2.10, and the present example-diagram of Fig. 2.29). In conventional diagrams, the number $Z_l(D)$ is given by the number of those tunneling lines connecting the two contours whose lead-index is l, and which represent electrons that tunnel *onto* this lead minus the number of those tunneling lines connecting the two contours whose lead-index is l, and which represent electrons that tunnel *off* this lead.

Applying the relation (2.149), we obtain for any $D \in \mathcal{D}_{0,+}$, with

$$\mathcal{D}_{0,+} \;:=\; \cup_{l\in\mathcal{L}}\, \mathcal{D}_{l,0,+}, \tag{2.189}$$

the equality

$$\begin{aligned} & Tr\Big\{\boldsymbol{K}(D)|a><a| \;+\; \boldsymbol{K}(\mathrm{mir}(D))|a><a|\Big\} \\ =\quad & -\; Tr\Big\{\boldsymbol{K}(T_{conj}D)|a><a| \;+\; \boldsymbol{K}\left(\mathrm{mir}(T_{conj}D)\right)|a><a|\Big\}, \end{aligned} \tag{2.190}$$

and hence:

$$\begin{aligned} & Tr\Big\{\boldsymbol{K}(D)|a><a| \;+\; \boldsymbol{K}(\mathrm{mir}(D))|a><a|\Big\} \\ & -\; Tr\Big\{\boldsymbol{K}(T_{conj}D)|a><a| \;+\; \boldsymbol{K}\left(\mathrm{mir}(T_{conj}D)\right)|a><a|\Big\} \end{aligned} \tag{2.191}$$

$$\begin{aligned} = \quad & 2Z_l(D) \quad Tr\Big\{\boldsymbol{K}(D)|a><a| \;+\; \boldsymbol{K}(\mathrm{mir}(D))|a><a|\Big\} \\ & +\; 2Z_l(T_{conj}D)\; Tr\Big\{\boldsymbol{K}(T_{conj}D)|a><a| \;+\; \boldsymbol{K}\left(\mathrm{mir}(T_{conj}D)\right)|a><a|\Big\} \end{aligned}$$

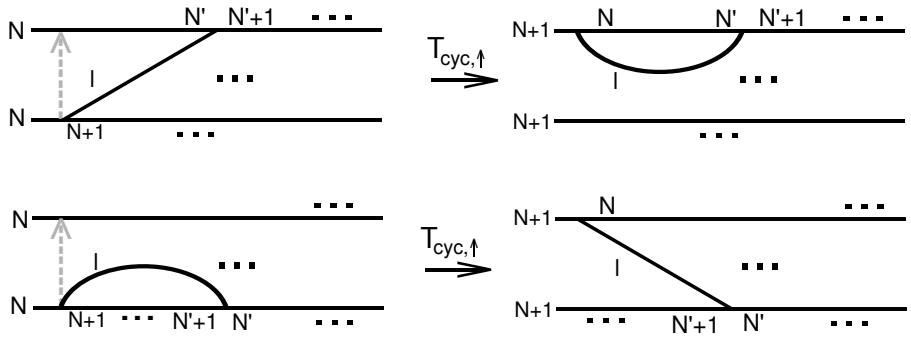

Figure 2.30: For any diagram $D \in \mathcal{D}_{l,0,+}$, the tunneling line containing the final vertex either connects the two different contours, thus representing an electron that effectively tunnels from the quantum dot onto lead l (first line in the present figure), or else it connects the final vertex to another vertex on the lower contour, in which case the corresponding tunneling line in the transformed diagram $T_{conj}D = \mathrm{mir}T_{cyc,\uparrow}D$ represents an electron that effectively tunnels from the lead l onto the quantum dot (second line). In both cases, $Z_l(D) = Z_l(T_{conj}D) + 1$.

for any $D \in \mathcal{D}_{l,0,+}$, since

$$Z_l(D) - Z_l(T_{conj}D) \;=\; 1 \tag{2.192}$$

(cp. Fig. 2.30). For $D \in \mathcal{D}_{\bar{l},0,+}$, obviously $Z_l(D) - Z_l(T_{conj}D) \;=\; 0$, and hence we obtain by inserting (2.191) into Eq. (2.186):

$$Tr\left\{\boldsymbol{K_{curr,l}}|a><a|\right\} \tag{2.193}$$

$$\begin{aligned} = \sum_{D\in\mathcal{D}_{0,+}} & Z_l(D) \quad Tr\Big\{\boldsymbol{K}(D)|a><a| \;+\; \boldsymbol{K}(\mathrm{mir}(D))|a><a|\Big\} \\ & + Z_l(T_{conj}D) Tr\Big\{\boldsymbol{K}(T_{conj}D)|a><a| \;+\; \boldsymbol{K}\left(\mathrm{mir}(T_{conj}D)\right)|a><a|\Big\} \\ = \sum_{D\in\mathcal{D}} & Z_l(D)\; Tr\Big\{\boldsymbol{K}(D)|a><a|\;\Big\}, \end{aligned}$$

so

$$Tr\left\{\boldsymbol{K_{curr,l}}|a><a|\right\} \;=\; \sum_{D\in\mathcal{D}} Z_l(D)\; Tr\Big\{\boldsymbol{K}(D)|a><a|\;\Big\}, \tag{2.194}$$

since every diagram $D \in \mathcal{D}$ with a non-zero contribution to the trace is contained exactly one time in the previous sum. The present expansion of the current kernel $\boldsymbol{K_{curr,l}}$, applying the effective number $Z_l(D)$ of electrons that tunnel onto the lead l in the process represented by D, is analogous to the decomposition (3.15) in Ref. [18], only here we refer to every single diagram, while the contributions of diagrams with equal $Z_l(D)$ are gathered in an extra sum in Ref. [18].

2.7.3 Kernels as Sums over Processes

Throughout this work we consider only cases in which the reduced density matrix of the quantum dot is diagonal in the basis of the eigenstates of the quantum dot's Hamiltonian. Hence, only those diagrams

$$D \;=\; \left(n, k, S, \mathcal{Q}, (a_j)_{j=1}^{k+1}, (b_j)_{j=k}^{2n}, (l_N, \sigma_N, v_N)_{N\in\mathcal{Q}}\right) \tag{2.195}$$

with initial matrix

$$|a_{k+1} >< b_k| \;=\; |a >< a|, \tag{2.196}$$

as well as final matrix

$$|a_1 >< b_{2n}| \;=\; |b >< b|, \tag{2.197}$$

i.e., only the diagrams within the subset $\mathcal{D}_0$ (2.139), and their mirrored diagrams, are relevant. To any $D \in \mathcal{D}_0$ we define the initial and final states of D as

$$\begin{aligned} s_i(D) &:= a_{k+1}, \\ s_f(D) &:= a_1, \end{aligned} \tag{2.198}$$

and we put D and its mirrored diagram $\mathrm{mir}(D)$ together to form one element of the set of "processes"

$$Proc \;:=\; \{\{D, \mathrm{mir}(D)\} :\; D \in \mathcal{D}_0\}\,. \tag{2.199}$$

We define for any $P = \{D, \mathrm{mir}(D)\} \in Proc$:

$$\boldsymbol{K}(P) \;:=\; \sum_{D'\in P} \boldsymbol{K}(D'), \tag{2.200}$$

$$\begin{aligned} s_i(P) &:= s_i(D), \\ s_f(P) &:= s_f(D), \end{aligned} \tag{2.201}$$

for any lead-index l:

$$Z_l(P) \;:=\; Z_l(D), \tag{2.202}$$

as well as for any two states $a, b \in \mathcal{B}$:

$$Proc\{a \to b\} \;:=\; \{P \in Proc:\; s_i(P) = a,\; s_f(P) = b\}\,. \tag{2.203}$$

Noting that, according to mirror rule, for any $P \in Proc\{a \to b\}$, the quantity

$$\boldsymbol{K}(P)^{bb}_{aa} \;:=\; \langle b\,|\{\boldsymbol{K}(P)\,(|a><a|)\}\,(b)\rangle \tag{2.204}$$

is real, we define the relative rate

$$\Gamma(P) \;:=\; \left|K(P)^{bb}_{aa}\right|. \tag{2.205}$$

Additionally, we define

$$Proc_{\geq 0}\{a \to b\} \;:=\; \left\{P \in Proc\{a \to b\}:\; \boldsymbol{K}(P)^{bb}_{aa} \geq 0\right\}, \tag{2.206}$$

$$Proc_{<0}\{a \to b\} \;:=\; \left\{P \in Proc\{a \to b\}:\; \boldsymbol{K}(P)^{bb}_{aa} < 0\right\}, \tag{2.207}$$

and note the diagrammatic expansion of the kernel element $\boldsymbol{K}^{bb}_{aa}$ in the form

$$\boldsymbol{K}^{bb}_{aa} \;=\; \sum_{P \in Proc_{\geq 0}\{a \to b\}} \Gamma(P) \;-\; \sum_{P \in Proc_{<0}\{a \to b\}} \Gamma(P). \tag{2.208}$$

With this, we can rewrite the system of equations (2.184), equivalent to the quantum master equation in the stationary limit, in the form

$$\begin{aligned} &\sum_{a \in \mathcal{B}: a \neq a_0} \left(\sum_{P \in Proc_{\geq 0}\{a_0 \to a\}} \rho_{a_0 a_0} \Gamma(P) \right) + \left(\sum_{P \in Proc_{<0}\{a \to a_0\}} \rho_{aa} \Gamma(P) \right) \\ = &\sum_{a \in \mathcal{B}: a \neq a_0} \left(\sum_{P \in Proc_{\geq 0}\{a \to a_0\}} \rho_{aa} \Gamma(P) \right) + \left(\sum_{P \in Proc_{<0}\{a_0 \to a\}} \rho_{a_0 a_0} \Gamma(P) \right), \\ &(a_0 \in \mathcal{B}). \end{aligned} \tag{2.209}$$

Analogously, applying the expansion (2.194), we can express the traces $Tr\,\{\boldsymbol{K_{curr,l}}|a><a|\}$ by process rates:

$$Tr\left\{\boldsymbol{K_{curr,l}}|a><a|\right\} \quad = \quad (2.210)$$
$$\sum_{b\in\mathcal{B}}\left(\sum_{P\in Proc_{\geq 0}\{a\to b\}} Z_l(P)\Gamma(P)\right) - \left(\sum_{P\in Proc_{<0}\{a\to b\}} Z_l(P)\Gamma(P)\right),$$

and so we obtain the expression

$$\boldsymbol{I_l} \;=\; \sum_{a,b\in\mathcal{B}}\left(\sum_{P\in Proc_{\geq 0}\{a\to b\}} Z_l(P)\rho_{aa}\Gamma(P)\right) - \left(\sum_{P\in Proc_{<0}\{a\to b\}} Z_l(P)\rho_{aa}\Gamma(P)\right) \quad (2.211)$$

for the stationary particle-current $\boldsymbol{I_l} = Tr\left\{\boldsymbol{K_{curr,l}}\hat{\boldsymbol{\rho}}\right\}$ onto lead l.

Zero Net Current:

The sum of the currents $\sum_{l\in\mathcal{L}}\boldsymbol{I_l}$, calculated by performing the sum over l on the right-hand side of Eq. (2.211), is zero, since the quantity

$$Z(P) \;:=\; \sum_{l\in\mathcal{L}} Z_l(P) \quad (2.212)$$

satisfies

$$Z(P) \;=\; \langle\hat{\mathrm{N}}_{\odot}\rangle(s_i(P)) - \langle\hat{\mathrm{N}}_{\odot}\rangle(s_f(P)). \quad (2.213)$$

Upon multiplying every single one of the equations (2.209) by the particle-number $\langle\hat{\mathrm{N}}_{\odot}\rangle(a_0)$ of the quantum dot state a_0, and performing the sum over a_0, we get an equation equivalent to $\sum_{l\in\mathcal{L}}\boldsymbol{I_l} = 0$, where we insert the right-hand side of (2.211) for $\boldsymbol{I_l}$.

2.7.4 Processes with Inversed Time-Direction

To any process $P = \{D, \mathrm{mir}(D)\}, D \in \mathcal{D}_0$, there is a conjugate process P^{conj}, given by the conjugate diagram $T_{conj}D$ (Sec. 2.5.3 (Conjugate Diagrams)), and the mirrored diagram of the latter. If $P \in Proc\{a \to b\}$, then $P^{conj} \in Proc\{a \to c\}$ with $c \neq b$, and

$$\boldsymbol{K}(P)^{bb}_{aa} \;=\; -\,\boldsymbol{K}(P^{conj})^{cc}_{aa} \quad (2.214)$$

(Eq. (2.149)). Hence, the set $Proc_{<0}\{a \to c\}$, with $a, c \in \mathcal{B}$, is in general not empty – the set of all processes with strictly negative contribution $\boldsymbol{K}(P)^{s_f(P)s_f(P)}_{s_i(P)s_i(P)}$ to the kernel is just as rich as the set of all processes with strictly positive contribution.

In Eq. (2.209), we interpret the terms $\rho_{a_0a_0}\Gamma(P)$ with $P \in Proc_{\geq 0}\{a_0 \to a\}, a \neq a_0$, as the contributions to the decrease of $\rho_{a_0a_0}$ caused by processes starting in the state a_0, and ending in the state a – occurring with an absolute rate $\rho_{a_0a_0}\Gamma(P)$; in the same way, we interpret the terms $\rho_{aa}\Gamma(P)$ with $P \in Proc_{\geq 0}\{a \to a_0\}, a \neq a_0$, as the contributions to the increase of $\rho_{a_0a_0}$ caused by processes starting in the state a, and ending in the state a_0 – occurring with an absolute rate $\rho_{aa}\Gamma(P)$. Correspondingly, in Eq. (2.211), the absolute rate $\rho_{aa}\Gamma(P)$ of a process $P \in Proc_{\geq 0}\{a \to b\}$ is multiplied by the number $Z_l(P)$ of electrons effectively transferred onto the lead l during this process to take into account the contribution of this process to the particle-current onto lead l.

Analogously, we might conceive that the terms $\rho_{aa}\Gamma(P)$ with $P \in Proc_{<0}\{a \to a_0\}$, $a \neq a_0$, on the left-hand side of Eq. (2.209) are the absolute rates of processes with logical initial state $s_i(P) = a$ and logical final state $s_f(P) = a_0$, however, evolving in inversed time-direction. Hence, although $\Gamma(P)$ is multiplied by ρ_{aa}, the process contributes to the *increase* of the probability ρ_{aa} and a corresponding *decrease* of the probability $\rho_{a_0a_0}$. In the same way, we might interpret the terms $\rho_{a_0a_0}\Gamma(P)$ with $P \in Proc_{<0}\{a_0 \to a\}$ on the right-hand side of Eq. (2.209) as the absolute rate of processes with logical initial state a_0, and logical final state a, evolving in inversed time-direction – thus representing a contribution to the increase of the probability $\rho_{a_0a_0}$. Within this interpretation, Eq. (2.209) corresponds to the demand that, in spite of all processes contained in the set $Proc$, the quantum dot's density matrix remains stationary.

Finally, in Eq. (2.211), for all processes $P \in Proc_{<0}\{a \to b\}$, the absolute rate $\rho_{aa}\Gamma(P)$ is multiplied by $-Z_l(P)$, which is the effective number of electrons transferred onto the lead l during the process P if, again, we assume that it evolves in inversed time-direction.

Chapter 3

Application: The Dressed-Second-Order Diagram Selection

In the present applied chapter of this work, parts of which have been published in Ref. [17], we describe linear and nonlinear transport across a single impurity Anderson model (SIAM) quantum dot. If the tunnel-coupling is large enough, sequential tunneling processes alone do not suffice to properly describe the transport characteristics. Taking into account all diagrams within the dressed-second-order (DSO) diagram selection – the second order diagrams are dressed by further tunneling lines within these diagrams – we study the effect of subsequent charge- and spin-fluctuations on the tunneling current. By the DSO we describe those resonances in the dynamic conductance versus applied bias, that are observed whenever one of the quantum dot levels meets with one of the leads' chemical potentials, qualitatively correctly - and even *exactly* in the case of the spinless quantum dot. Moreover, in agreement with experimental reality, we find a zero bias anomaly of the differential conductance, and an enhancement of the linear conductance with decreasing temperature in case the SIAM's degenerate level lies below the Fermi level of the contacts. We show that the zero bias resonance-peak splits in the expected way, if a magnetic field is applied. Finally, we consider the case of finite Coulomb-interaction, point out the limitations of the DSO in this case, and compare our data to an experiment.

3.1 Second Order Approximation

Our approximation is an extension of the second order, so we start out with the calculation of the second order diagrams.

Second Order Density Matrix

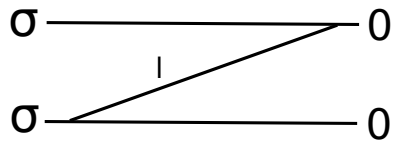

Figure 3.1: The only second order diagram (up to a sum over l, and up to mirrored diagrams) contributing to the kernel element $\mathbf{K}_{00}^{\sigma\sigma}$ is the one shown in the present figure. The diagram's initial matrix is $|\mathbf{0}><\mathbf{0}|$, while its final matrix is $|\boldsymbol{\sigma}><\boldsymbol{\sigma}|$; an electron with spin σ tunnels in two steps (cp. Sec. 2.4.2 (Graphic Representation of Diagrams)) onto the quantum dot in the present diagram.

According to Sec. 2.6.3 (Deducing Analytical Expression from Figure), the contribution of the diagram D in Fig. 3.1 to the density matrix kernel is given by

$$\{\mathcal{L}K(D)\}(\lambda)\hat{y} \;=\; \frac{\langle\mathbf{0}|\hat{y}(\mathbf{0})\rangle}{\hbar}\;|\boldsymbol{\sigma}><\boldsymbol{\sigma}|\;\int d\varepsilon\;\frac{\alpha_{l\sigma}^{+}(\varepsilon)}{\hbar\lambda+i(\varepsilon-E_{\sigma 0})}, \tag{3.1}$$

where we let λ, the argument of the Laplace transform, still be finite. To any two quantum dot states $a, b \in \mathcal{B}$, the quantity E_{ba} is defined as

$$E_{ba} := E_b - E_a, \tag{3.2}$$

the difference between the energies of these two quantum dot states. For brevity we write $\alpha_{l\sigma}^{+} := \alpha_{l\sigma}^{(+1)}$, etc. (cp. Def. (D.66)). To obtain the second order matrix element $\boldsymbol{K}_{00}^{\sigma\sigma}$, we perform the sum over l, insert $\hat{y} = |\mathbf{0}><\mathbf{0}|$, take the limit $\lambda \to 0+$ as in Eq. (E.123), and we take two times the real part of the present operator's coefficient:

$$\boldsymbol{K}_{00}^{\sigma\sigma} \;=\; \frac{2\pi}{\hbar}\alpha_{\sigma}^{+}(E_{\sigma 0}), \tag{3.3}$$

where

$$\alpha_{\sigma}^{\pm} \;:=\; \sum_{l}\alpha_{l\sigma}^{\pm}. \tag{3.4}$$

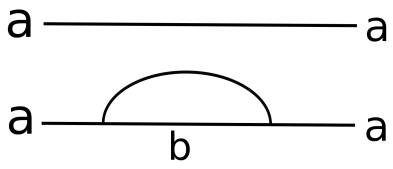

Figure 3.2: Second order diagrams of the present form are conjugates (Sec. 2.5.3 – Conjugate Diagrams) of diagrams contributing to $\boldsymbol{K}_{aa}^{bb}$, $b \neq a$, and hence, implicitly, we already calculated them.

All remaining second order kernel elements $\boldsymbol{K}_{aa}^{bb}$, with $a \neq b$, are obtained from analogous second order diagrams; we note:

$$\begin{aligned} \boldsymbol{K}_{\sigma\sigma}^{00} &= \tfrac{2\pi}{\hbar}\alpha_{\sigma}^{-}(E_{\sigma 0}), \\ \boldsymbol{K}_{\sigma\sigma}^{22} &= \tfrac{2\pi}{\hbar}\alpha_{\overline{\sigma}}^{+}(E_{2\sigma}), \\ \boldsymbol{K}_{22}^{\sigma\sigma} &= \tfrac{2\pi}{\hbar}\alpha_{\overline{\sigma}}^{-}(E_{2\sigma}). \end{aligned} \tag{3.5}$$

Finally, the matrix elements $\boldsymbol{K}_{00}^{22}$, and $\boldsymbol{K}_{22}^{00}$, are zero within the second order.

We here assume that the situation is symmetric with respect to the two spins – in the quantum dot, as well as in the leads – so we use the notation:

$$\begin{aligned} E_{10} &:= E_{\uparrow 0} = E_{\downarrow 0}, \\ E_{21} &:= E_{2\uparrow} = E_{2\downarrow}, \end{aligned} \tag{3.6}$$

$$\begin{aligned} \alpha_l^{\pm} &:= \alpha_{l\uparrow}^{\pm} = \alpha_{l\downarrow}^{\pm}, \\ \alpha_l &:= \alpha_{l\uparrow} = \alpha_{l\downarrow} \end{aligned} \tag{3.7}$$

(cp. Def. (D.60)), and

$$\begin{aligned} \alpha^{\pm} &:= \textstyle\sum_{l\in\mathcal{L}} \alpha_l^{\pm}, \\ \alpha &:= \textstyle\sum_{l\in\mathcal{L}} \alpha_l. \end{aligned} \tag{3.8}$$

By the second order tunneling rates

$$\begin{aligned} \Gamma_{l,01}^{\pm} &:= \tfrac{2\pi}{\hbar}\alpha_l^{\pm}(E_{10}), \\ \Gamma_{l,12}^{\pm} &:= \tfrac{2\pi}{\hbar}\alpha_l^{\pm}(E_{21}), \end{aligned} \tag{3.9}$$

$$\begin{aligned} \Gamma_{01}^{\pm} &:= \tfrac{2\pi}{\hbar}\alpha^{\pm}(E_{10}), \\ \Gamma_{12}^{\pm} &:= \tfrac{2\pi}{\hbar}\alpha^{\pm}(E_{21}), \end{aligned} \tag{3.10}$$

and by the notation

$$\begin{aligned} \Gamma_{01} &:= \Gamma_{01}^{+} + \Gamma_{01}^{-}, \\ \Gamma_{12} &:= \Gamma_{12}^{+} + \Gamma_{12}^{-}, \end{aligned} \tag{3.11}$$

we formulate the stationary density matrix, as well as the current across the quantum dot, in the spin-symmetric case: In this case, the quantum master equation in the stationary limit turns into the following set of two independent equations for the three independent variables ρ_{00}, ρ_{22} and $\rho_{\uparrow\uparrow} = \rho_{\downarrow\downarrow}$:

$$\begin{aligned} 0 &= -\rho_{00}\Gamma^{+}_{01} + \rho_{\sigma\sigma}\Gamma^{-}_{01}, \\ 0 &= +\rho_{\sigma\sigma}\Gamma^{+}_{12} - \rho_{22}\Gamma^{-}_{12} \end{aligned} \tag{3.12}$$

(cp. Eq. (2.154), and (2.184)). By the normalization condition

$$\rho_{00} + 2\rho_{\sigma\sigma} + \rho_{22} = 1 \tag{3.13}$$

we obtain the stationary reduced density matrix

$$\begin{pmatrix} \rho_{00} \\ \rho_{\uparrow\uparrow} \\ \rho_{\downarrow\downarrow} \\ \rho_{22} \end{pmatrix} = \frac{1}{\Gamma^{-}_{12}\Gamma_{01} + \Gamma^{+}_{01}\Gamma_{12}} \begin{pmatrix} \Gamma^{-}_{01}\Gamma^{-}_{12} \\ \Gamma^{+}_{01}\Gamma^{-}_{12} \\ \Gamma^{+}_{01}\Gamma^{-}_{12} \\ \Gamma^{+}_{12}\Gamma^{+}_{01} \end{pmatrix}. \tag{3.14}$$

Second Order Current

We determine the stationary current across the quantum dot by Eq. (2.124),

$$\boldsymbol{I_l} \;=\; Tr\left\{\boldsymbol{K_{curr,l}}\hat{\boldsymbol{\rho}}\right\} \;=\; \sum_{a\in\mathcal{B}} \rho_{aa} Tr\left\{\boldsymbol{K_{curr,l}}\left(|a><a|\right)\right\}, \tag{3.15}$$

where we insert the second order current kernel for $\boldsymbol{K_{curr,l}}$. To determine the traces $Tr\left\{\boldsymbol{K_{curr,l}}\left(|a><a|\right)\right\}$, on the other hand, we apply the diagrammatic expansion

$$Tr\left\{\boldsymbol{K_{curr,l}}|a><a|\right\} \;=\; \sum_{D\in\mathcal{D}_{l,0,+}} 2\; Re\Big(Tr\Big\{\boldsymbol{K}\left(D\right)|a><a|\Big\}\Big) \tag{3.16}$$

according to Eq. (2.147), where the sum goes over all second order diagrams within the diagram-set $\mathcal{D}_{l,0,+}$ (Def. (2.144), cp. Fig. 2.19). For the quantum dot state $a = \mathbf{0}$, and to each spin $\sigma \in \mathcal{S}$, there is one diagram contributing to the sum on the right-hand side of the present equation. In the same way, for the quantum dot state $a = \mathbf{2}$, there is, to each spin σ, one diagram contributing to that sum (Fig. 3.3). Moreover, to each spin σ, there are two second order diagrams contributing to $Tr\left\{\boldsymbol{K_{curr,l}}|\boldsymbol{\sigma}><\boldsymbol{\sigma}|\right\}$ (Fig. 3.4). In summary, we obtain in the spin-symmetric case:

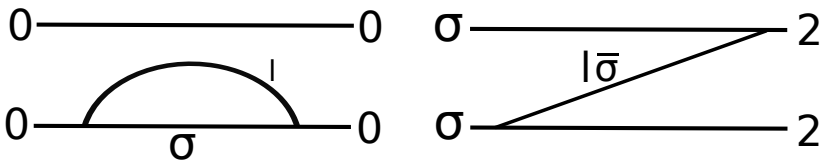

Figure 3.3: The two diagrams of the present figure give the traces $Tr\{\boldsymbol{K_{curr,l}}|\mathbf{0}><\mathbf{0}|\}$, and $Tr\{\boldsymbol{K_{curr,l}}|\mathbf{2}><\mathbf{2}|\}$, respectively.

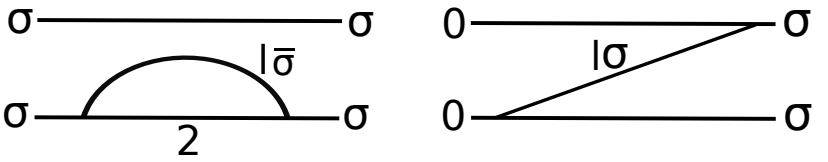

Figure 3.4: Within the diagram-set $\mathcal{D}_{l,0,+}$ (Def. (2.144), cp. Fig. 2.19), we find two diagrams contributing to $Tr\{\boldsymbol{K_{curr,l}}|\boldsymbol{\sigma}><\boldsymbol{\sigma}|\}$.

$$\begin{aligned} Tr\{\boldsymbol{K_{curr,l}}|\mathbf{0}><\mathbf{0}|\} &= -2\Gamma^{+}_{l,01}, \\ Tr\{\boldsymbol{K_{curr,l}}|\mathbf{2}><\mathbf{2}|\} &= 2\Gamma^{-}_{l,12}, \\ Tr\{\boldsymbol{K_{curr,l}}|\boldsymbol{\sigma}><\boldsymbol{\sigma}|\} &= \Gamma^{-}_{l,01}-\Gamma^{+}_{l,12}. \end{aligned} \tag{3.17}$$

Upon inserting the density matrix (3.14), and the tunneling rates (3.17), into Eq. (3.15), we note the stationary second order particle-current onto lead l:

$$\begin{aligned} \boldsymbol{I_l} &= \frac{2}{1+\frac{\Gamma^{+}_{01}\Gamma_{12}}{\Gamma_{01}\Gamma^{-}_{12}}}\left(\kappa_l\Gamma^{+}_{\bar{l},01}-\kappa_{\bar{l}}\Gamma^{+}_{l,01}\right) \\ &+ \frac{2}{1+\frac{\Gamma_{01}\Gamma^{-}_{12}}{\Gamma^{+}_{01}\Gamma_{12}}}\left(\kappa_{\bar{l}}\Gamma^{-}_{l,12}-\kappa_l\Gamma^{-}_{\bar{l},12}\right), \end{aligned} \tag{3.18}$$

where we assume proportional tunneling coupling of the two leads to the quantum dot:

$$\alpha_l = \kappa_l\alpha, \tag{3.19}$$

with $\kappa_l, l\in\mathcal{L}$, positive scalar factors satisfying $\sum_l\kappa_l=1$. As for the spin, we apply the bar over the lead-index l to refer to the one lead opposite to lead l by "$\bar{l}$"; The second order rates $\Gamma^{\pm}_{l,01}$ etc. are given in Eq. (3.9) and following.

The pre-factor of the second line within the right-hand side of Eq. (3.18) is the stationary electron number on the quantum dot, as calculated from the second order density matrix:

$$\frac{2}{1+\frac{\Gamma_{01}\Gamma_{12}^{-}}{\Gamma_{01}^{+}\Gamma_{12}}} \;=\; 0\cdot\rho_{00} \;+\; \sum_{\sigma} 1\cdot\rho_{\sigma\sigma} \;+\; 2\cdot\rho_{22}; \tag{3.20}$$

the pre-factor of the first line of this equation's right-hand side, on the other hand, is two minus the latter stationary electron number on the quantum dot.

Density Matrix and Current for the Spinless Quantum Dot

The theoretically relevant spinless quantum dot has two states: the empty state **0**, and the occupied state **1**; it is coupled to leads whose electrons, in the same way, do not have a spin. Equivalently, for the purpose of a uniform treatment of the SIAM on the one hand, and the spinless quantum dot on the other hand, we can assume that the spin-index has only *one* possible value σ_0, as we do in Def. (2.3). By the notation

$$\begin{array}{rcl} \alpha_l^{(\pm)} & := & \alpha_{l\sigma_0}^{(\pm)}, \\ \alpha^{(\pm)} & := & \alpha_{\sigma_0}^{(\pm)}, \end{array} \tag{3.21}$$

we find – in the same way as in the previous section for the SIAM – the second order matrix elements of the density matrix kernel:

$$\begin{array}{rcl} \boldsymbol{K}_{00}^{11} & = & \frac{2\pi}{\hbar}\alpha^{+}(E_{10}), \\ \boldsymbol{K}_{11}^{00} & = & \frac{2\pi}{\hbar}\alpha^{-}(E_{10}), \end{array} \tag{3.22}$$

with $\boldsymbol{K}_{00}^{00} = -\boldsymbol{K}_{00}^{11}$, $\boldsymbol{K}_{11}^{11} = -\boldsymbol{K}_{11}^{00}$, as well as the second order elements of the current kernel:

$$\begin{array}{rcl} Tr\left\{\boldsymbol{K_{curr,l}}|\mathbf{0}><\mathbf{0}|\right\} & = & -\frac{2\pi}{\hbar}\alpha_l^{+}(E_{10}), \\ Tr\left\{\boldsymbol{K_{curr,l}}|\mathbf{1}><\mathbf{1}|\right\} & = & \frac{2\pi}{\hbar}\alpha_l^{-}(E_{10}). \end{array}$$

Hence, by the tunneling rates

$$\Gamma_l^{\pm} \;:=\; \frac{2\pi}{\hbar}\alpha_l^{\pm}(E_{10}), \tag{3.23}$$

by

$$\Gamma^{\pm} \;:=\; \sum_{l} \Gamma_l^{\pm}, \tag{3.24}$$

as well as by

$$\Gamma \;:=\; \Gamma^{+} + \Gamma^{-}, \tag{3.25}$$

we can express the stationary density matrix:

$$\begin{pmatrix} \rho_{00} \\ \rho_{11} \end{pmatrix} \;=\; \frac{1}{\Gamma} \begin{pmatrix} \Gamma^{-} \\ \Gamma^{+} \end{pmatrix}, \tag{3.26}$$

and the stationary current onto lead l:

$$\boldsymbol{I_l} \;=\; \frac{1}{\Gamma} \left(\Gamma_l^{-} \Gamma_{\bar{l}}^{+} \;-\; \Gamma_l^{+} \Gamma_{\bar{l}}^{-} \right). \tag{3.27}$$

3.2 Dressed-Second-Order Diagrams

3.2.1 Spinless Quantum Dot

We now want to increase the set of diagrams we take into account by "dressing" the second order diagrams by bubbles which represent subsequent charge fluctuations. We begin with the spinless quantum dot (2.3): The diagram selection of the dressed-second-order (DSO) contains diagrams of all orders. As an example, we show two fourth order DSO-diagrams in Fig. 3.5.

Referring to the two fourth order diagrams of Fig. 3.5 by $D_1^{(1)}(l')$, and $D_2^{(1)}(l')$, respectively, we note the sum of their contributions to the density matrix kernel:

$$\begin{aligned} \sum_{j=1}^{2} \{\mathcal{L}K(D_j^{(1)})(l')\}(\lambda)\hat{y} \quad &= \quad \frac{\langle \mathbf{0}|\hat{y}(\mathbf{0})\rangle}{\hbar} \; |\mathbf{1}><\mathbf{1}| \int d\varepsilon \; \frac{\alpha_l^{+}(\varepsilon)}{\hbar\lambda + i(\varepsilon - E_{10})} \\ &\qquad \frac{-1}{\hbar\lambda + i(\varepsilon - E_{10})} \int d\varepsilon' \; \frac{(\alpha_{l'}^{+} + \alpha_{l'}^{-})(\varepsilon')}{\hbar\lambda + i(\varepsilon - \varepsilon')}. \end{aligned} \tag{3.28}$$

We define the diagram-set

$$\mathcal{G}^{(1)}(DSO)(D) \;:=\; \left\{ D_j^{(1)}(l') : \; j = 1, 2; l' \in \mathcal{L} \right\}, \tag{3.29}$$

so $\mathcal{G}^{(1)}(DSO)(D)$ is the set of all diagrams within which the diagram D (in the first line of Fig. 3.5) is dressed by one tunneling line in the form of a bubble. Correspondingly, we define

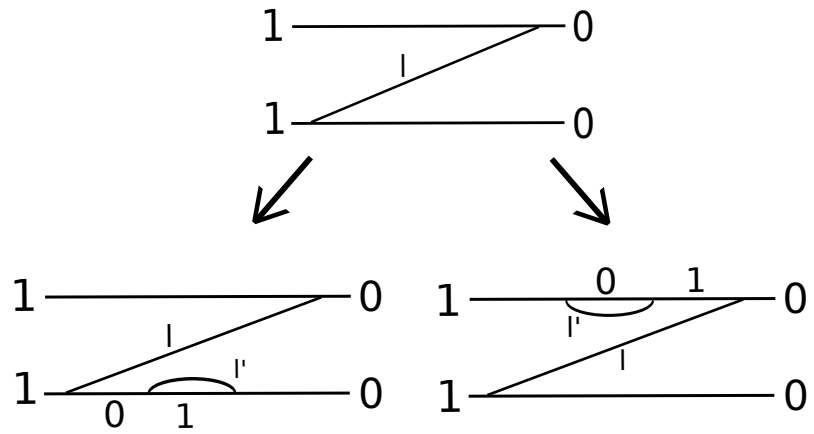

Figure 3.5: The second line of the present figure shows two example-diagrams within which the second order diagram "D" in the first line is dressed by one further tunneling line. In the fourth order DSO-diagram on the left-hand side of the present figure, an electron from lead l' tunnels halfway onto the dot and leaves it again, while, in the diagram on the right-hand side, an electron tunnels halfway from the quantum dot onto lead l', and back.

$$K\left(\mathcal{G}^{(1)}(DSO)(D)\right) \;:=\; \sum_{D'\in\mathcal{G}^{(1)}(DSO)(D)} K(D'), \tag{3.30}$$

the sum of all contributions to the density matrix kernel of diagrams within the set $\mathcal{G}^{(1)}(DSO)(D)$. Upon replacing $\alpha_{l'}^{+}+\alpha_{l'}^{-}=\alpha_{l'}$, and performing the sum over l', $\alpha \;=\; \sum_{l'}\alpha_{l'}$, in (3.28) we find

$$\begin{aligned}\{\mathcal{L}K(\mathcal{G}^{(1)}(DSO)(D))\}(\lambda)\hat{y} \;\;=\;\; & \frac{\langle\mathbf{0}|\hat{y}(\mathbf{0})\rangle}{\hbar}\;|\mathbf{1}><\mathbf{1}|\int d\varepsilon\;\frac{\alpha_l^{+}(\varepsilon)}{\hbar\lambda+i(\varepsilon-E_{10})}\\ & \frac{-1}{\hbar\lambda+i(\varepsilon-E_{10})}\int d\varepsilon'\;\frac{\alpha(\varepsilon')}{\hbar\lambda+i(\varepsilon-\varepsilon')}.\end{aligned} \tag{3.31}$$

Analogously, we express the sum of the contributions to the density matrix kernel of all *sixth* order diagrams "$D_j^{(2)}(l',l'')$", $j\;=\;1,2,3,4,$ in Fig. 3.6:

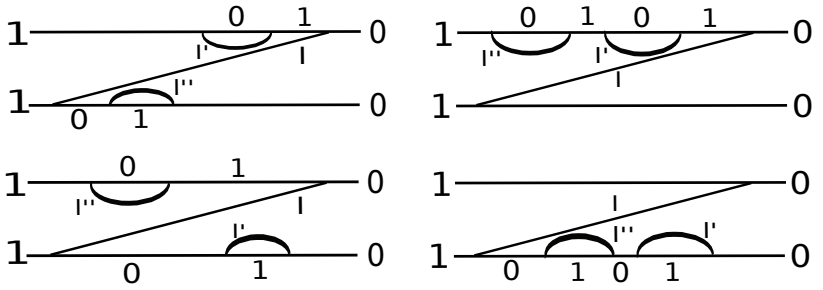

Figure 3.6: The 2×2 possibilities to dress the second order diagram in Fig. 3.5 by two subsequent bubbles, each positioned either on the upper or on the lower contour.

$$\sum_{j=1}^{4} \{\mathcal{L}K(D_j^{(2)})(l',l'')\}(\lambda)\hat{y} = \frac{\langle \mathbf{0}|\hat{y}(\mathbf{0})\rangle}{\hbar} |\mathbf{1}><\mathbf{1}| \int d\varepsilon \, \frac{\alpha_l^+(\varepsilon)}{\hbar\lambda + i(\varepsilon - E_{10})} \frac{-1}{\hbar\lambda + i(\varepsilon - E_{10})} \int d\varepsilon' \, \frac{(\alpha_{l'}^+ + \alpha_{l'}^-)(\varepsilon')}{\hbar\lambda + i(\varepsilon - \varepsilon')} \frac{-1}{\hbar\lambda + i(\varepsilon - E_{10})} \int d\varepsilon'' \, \frac{(\alpha_{l''}^+ + \alpha_{l''}^-)(\varepsilon'')}{\hbar\lambda + i(\varepsilon - \varepsilon'')}. \tag{3.32}$$

Upon defining

$$\mathcal{G}^{(2)}(DSO)(D) := \left\{ D_j^{(2)}(l',l'') : \; j = 1,2,3,4; \; l',l'' \in \mathcal{L} \right\}, \tag{3.33}$$

and

$$K\left(\mathcal{G}^{(2)}(DSO)(D)\right) := \sum_{D' \in \mathcal{G}^{(2)}(DSO)(D)} K(D'), \tag{3.34}$$

we note

$$\{\mathcal{L}K(\mathcal{G}^{(2)}(DSO)(D))\}(\lambda)\hat{y} = \frac{\langle \mathbf{0}|\hat{y}(\mathbf{0})\rangle}{\hbar} |\mathbf{1}><\mathbf{1}| \int d\varepsilon \, \frac{\alpha_l^+(\varepsilon)}{\hbar\lambda + i(\varepsilon - E_{10})} \left(\frac{-1}{\hbar\lambda + i(\varepsilon - E_{10})} \int d\varepsilon' \, \frac{\alpha(\varepsilon')}{\hbar\lambda + i(\varepsilon - \varepsilon')} \right)^2. \tag{3.35}$$

Generally, the number of possibilities to dress the diagram D within the first line of Fig. 3.5 by a number of $n-1$ further tunneling lines in the form

of subsequent bubbles in the manner of Fig. 3.6 is 2^{n-1}, since each bubble can be positioned either on the upper or on the lower contour. We refer to the set of these diagrams by "$\mathcal{G}^{(n-1)}(DSO)(D)$", and note the sum of their contributions to the kernel:

$$\begin{aligned}\{\mathcal{L}K(\mathcal{G}^{(n-1)}(DSO)(D))\}(\lambda)\hat{y} &= \frac{\langle \mathbf{0}|\hat{y}(\mathbf{0})\rangle}{\hbar}\,|\mathbf{1}><\mathbf{1}|\int d\varepsilon\,\frac{\alpha_l^+(\varepsilon)}{\hbar\lambda+i(\varepsilon-E_{10})} \\ &\left(\frac{-1}{\hbar\lambda+i(\varepsilon-E_{10})}\int d\varepsilon'\,\frac{\alpha(\varepsilon')}{\hbar\lambda+i(\varepsilon-\varepsilon')}\right)^{n-1}.\end{aligned} \tag{3.36}$$

In summary, we define $\mathcal{G}(DSO)(D)$ as the set of all diagrams within which the diagram D is dressed by any number of subsequent bubbles:

$$\mathcal{G}(DSO)(D) = \cup_{n=1}^{\infty}\,\mathcal{G}^{(n-1)}(DSO)(D), \tag{3.37}$$

including

$$\mathcal{G}^{(0)}(DSO)(D) := \{D\}, \tag{3.38}$$

and, upon applying the closed expression

$$\sum_{n=1}^{\infty} q^{n-1} = \frac{1}{1-q} \tag{3.39}$$

for a geometric series, we note the sum of the contributions to the kernel of all diagrams within $\mathcal{G}(DSO)(D)$:

$$\begin{aligned}\{\mathcal{L}K(\mathcal{G}(DSO)(D))\}(\lambda)\hat{y} &= \frac{\langle \mathbf{0}|\hat{y}(\mathbf{0})\rangle}{\hbar}\,|\mathbf{1}><\mathbf{1}| \\ &\int d\varepsilon\,\frac{\alpha_l^+(\varepsilon)}{\hbar\lambda+i(\varepsilon-E_{10})+\int d\varepsilon'\,\frac{\alpha(\varepsilon')}{\hbar\lambda+i(\varepsilon-\varepsilon')}}.\end{aligned} \tag{3.40}$$

In the same way as the diagram D (Fig. 3.5), we can dress any other second order diagram contributing to the kernels by subsequent bubbles, e.g., Fig. 3.7. Per definition, any conventional diagram whose pair formation (cp. Fig. 2.4) has the general form of Fig. 3.8 enters into the diagram selection of the DSO. Taking into account all of these diagrams, we obtain the DSO tunneling rates for the spinless quantum dot:

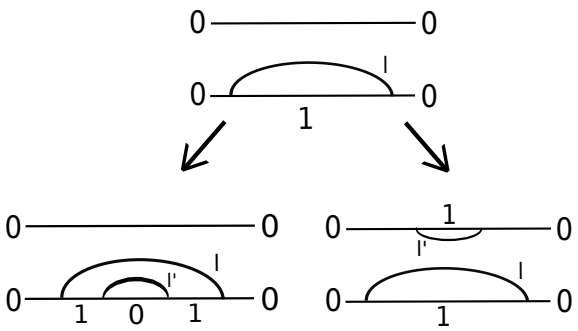

Figure 3.7: Another example of a second order diagram for the spinless quantum dot, and two ways of dressing this diagram by one further tunneling line.

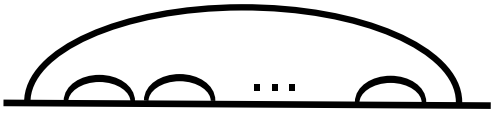

Figure 3.8: The general property, by which we define the DSO-diagram selection. If we project the ends of all tunneling lines in any conventional diagram onto the lower contour, remove all labels and indices from the figure, then only a graphic representation of an irreducible pair formation remains. Within an ordered set of $2n$ elements, a DSO-pair formation connects the first to the last element, while, otherwise, only neighbouring elements are connected to each other.

$$\Gamma_l^{\pm} \;=\; \frac{2\pi}{\hbar}\int d\varepsilon \frac{(\alpha\alpha_l^{\pm})(\varepsilon)}{\pi^2\alpha(\varepsilon)^2 \;+\; \left(\varepsilon+\pi(H\alpha)(\varepsilon)-E_{10}\right)^2}. \tag{3.41}$$

[We take the real part of the integral on the right-hand side of Eq. (3.40). In order to perform the limit $\lambda \to 0$ of this real part, we determine the limit

$$\lim_{\eta\to 0+}\int d\varepsilon' \frac{\alpha(\varepsilon')}{\eta + i(\varepsilon-\varepsilon')} \tag{3.42}$$

analogously to Eq. (E.93), (E.94). We assume that the function $\alpha(\varepsilon)$ is strictly positive around E_{10}, and, in addition, that the term $\pi(H\alpha)(\varepsilon)$ (definition of the Hilbert transformation H in Eq. (E.49)) can be treated as a small correction within $\left(\varepsilon+\pi(H\alpha)(\varepsilon)-E_{10}\right)^2$. Under sensible conditions concerning the functions $\alpha_{l'}^{\pm}$, the limit $\lambda \to 0$ can be performed in the straightforward way.]

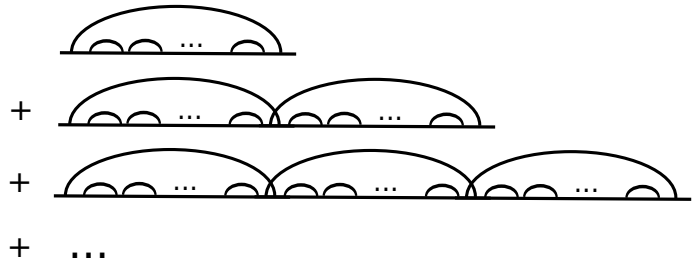

Figure 3.9: The structure of the diagrams within the RTA-selection, illustrated by one-contour diagrams with reduced information (cp. Fig. 3.8). The criterion which RTA-diagrams are defined by is: Any imagined vertical line cutting the diagram in two pieces has at most two intersections with tunneling lines. As a consequence, an RTA-pair formation is a combination of an integer number of DSO-pair formations in the sense of the present figure. In particular, the DSO-diagram selection is contained in the RTA-selection.

The expressions for the density matrix (3.26), as well as the current (3.27), in terms of the rates (3.41) are the same both for the DSO and for the undressed second order. In the case of proportional coupling (3.19), we obtain for the particle-current onto lead l the *exact* result:

$$\boldsymbol{I_l} \;=\; \frac{4\kappa_l\kappa_{\bar{l}}}{h}\int d\varepsilon \frac{\pi^2\left\{\alpha^2(f_{\bar{l}}-f_l)\right\}(\varepsilon)}{\pi^2\alpha(\varepsilon)^2 \;+\; \left(\varepsilon+\pi(H\alpha)(\varepsilon)-E_{10}\right)^2}. \tag{3.43}$$

[Note that we here replace $\hbar$ by $h/2\pi$; moreover, the quantity $4\kappa_l\kappa_{\bar{l}}$ takes the maximum value 1 in the case of symmetric coupling.] In the case of proportional coupling, the result of the DSO – for the tunneling current across the spinless quantum dot – is actually the same as the *exact* [21] result of the resonant tunneling approximation (RTA) (Fig. 3.9). We here note that in the case of zero Coulomb-interaction, $U = 0$ in (2.4), the tunneling current across the SIAM is two times the tunneling current across the spinless quantum dot.

If we consider the chemical potentials $\mu_l, \mu_{\bar{l}}$ entering into the Fermi-functions (D.17) of the two contacts $l, \bar{l}$ to be a function of a bias voltage V_b according to

$$\begin{aligned} \mu_l(V_b) \;&=\; E_F + eV_b, \\ \mu_{\bar{l}}(V_b) \;&=\; E_F, \end{aligned} \tag{3.44}$$

multiply the particle-current onto lead l (3.43) by the negative electron charge $-e$, and take the derivative with respect to the bias, we obtain the differential or dynamic conductance:

$$\frac{d\boldsymbol{I_l}}{dV_b} \;=\; 4\kappa_l\kappa_{\bar{l}}\frac{e^2}{h}\int d\varepsilon\; l(\varepsilon)\; f_{T,\mu_l(V_b)}(\varepsilon), \tag{3.45}$$

with

$$l(\varepsilon) \;:=\; \frac{\pi^2\alpha^2(\varepsilon)}{\pi^2\alpha(\varepsilon)^2 \;+\; \left(\varepsilon+\pi(H\alpha)(\varepsilon)-E_{10}\right)^2}, \tag{3.46}$$

$$f_{T,\mu_l}(\varepsilon) \;:=\; \frac{-1}{k_BT}f'\left(\frac{\varepsilon-\mu_l}{k_BT}\right), \tag{3.47}$$

f the parameter-free Fermi-Dirac distribution (C.78). As far as the coupling function $\alpha(\varepsilon)$ is approximately constant, the function $l(\varepsilon)$ is approximately a lorentzian with width $2\pi\alpha(E_F)$, centered around E_{10}. The second factor within the integral for the differential conductance (3.45), on the other hand, is a strictly positive function with total weight 1 – the integral over the complete real axis is one – and this weight is distributed around the chemical potential μ_l with a width proportional to k_BT. Hence, the differential conductance, considered as a function

$$\frac{d\boldsymbol{I_l}}{dV_b}(\mu_l) \tag{3.48}$$

of μ_l with constant value of the parameter E_{10}, displays a peak for $\mu_l \;=\; E_{10}$. The order of magnitude of this peak's width is determined by the sum of the thermal energy k_BT, and of the tunneling coupling $2\pi\alpha(E_F)$. With these qualitative statements about the transport across the spinless quantum dot we conclude the discussion of the DSO-results in this case.

3.2.2 Dressed-Second-Order for the SIAM with Infinite Coulomb-Interaction

In the case of infinitely large Coulomb-interaction U on the doubly occupied SIAM (2.4), and symmetry with respect to the spin on the quantum dot as well as in the leads, we assume the stationary reduced density matrix in terms of the rates is given by

$$\begin{pmatrix} \rho_{00} \\ \rho_{\uparrow\uparrow} \\ \rho_{\downarrow\downarrow} \end{pmatrix} = \frac{1}{\Gamma_{01}+\Gamma^+_{01}} \begin{pmatrix} \Gamma^-_{01} \\ \Gamma^+_{01} \\ \Gamma^+_{01} \end{pmatrix} \tag{3.49}$$

(cp. Eq. (3.14)), with $\rho_{00} + \sum_\sigma \rho_{\sigma\sigma} = 1$, while the second order stationary current onto lead l (3.18) is reduced to

$$\boldsymbol{I_l} = \frac{2}{1 + \frac{\Gamma^+_{01}}{\Gamma_{01}}} \left(\kappa_l \Gamma^+_{\bar{l},01} - \kappa_{\bar{l}} \Gamma^+_{l,01} \right). \tag{3.50}$$

We do not obtain the latter two formulas as mathematical limits in the case of infinite interaction, but rather apply the following reasoning: For large interaction, practically, any tunneling process, within which the doubly occupied state **2** appears, does not occur. The element ρ_{22} of the stationary reduced density matrix is zero. Hence, we calculate only the relative transition rates between the states $\mathbf{0}, \uparrow$, and $\downarrow$, taking into account only processes within which exclusively these states appear, and, balancing the transitions, we find the probabilities $\rho_{00}, \rho_{\uparrow\uparrow}$, and $\rho_{\downarrow\downarrow}$, as well as the absolute values of the transition rates in the stationary configuration, and thus the current.

Within the DSO-diagram selection, the inclusion of diagrams which contain two opposite spins – as opposed to the DSO for the spinless quantum dot – implies basically only one extension: For example, in any DSO-diagram contributing to the kernel element $K^{\sigma\sigma}_{00}$ there is one additional possible fluctuation of an electron of *opposite* spin $\overline{\sigma}$ (cp. Fig. 3.10). The DSO thus contains spin-fluctuations on the quantum dot in the sense that intermediate matrices within DSO-diagrams can have the form $|\sigma >< \overline{\sigma}|$. Taking into account the altogether three possibilities of fluctuations in any diagram contributing to $K^{bb}_{aa}, a, b \in \{\mathbf{0}, \boldsymbol{\sigma}\}$, we obtain – perfectly analogously to the way in which we derived the DSO tunneling rates for the spinless quantum dot (3.41) – the following DSO tunneling rates for infinite interaction in the spin-symmetric case:

$$\Gamma^\pm_{l,01} \;=\; \frac{2\pi}{\hbar} \int d\varepsilon \frac{(\gamma \alpha^\pm_l)(\varepsilon)}{\pi^2 \gamma(\varepsilon)^2 \;+\; \left(\varepsilon + \pi (H\gamma)(\varepsilon) - E_{10}\right)^2}, \tag{3.51}$$

with $\gamma = \alpha + \alpha^+$.

The same approximation scheme for infinite U has been applied with the RTA [18], taking into account all those diagrams with a pair formation according to Fig. 3.9, which exclusively contain the states $\mathbf{0}, \uparrow, \downarrow$. We compare the result of the DSO to that of the RTA at the level of the linear conductance G – the differential conductance at zero bias. We note:

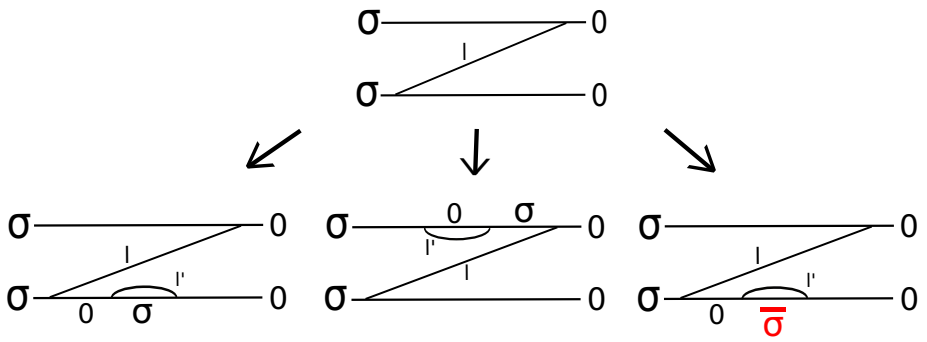

Figure 3.10: A second order diagram with the states **0**, and $\boldsymbol{\sigma}$, and the altogether three possibilities to add to this diagram one further tunneling line according to the definition of DSO-diagrams (cp. Fig. 3.8) in such a way, that the quantum dot state **2** does not appear. Compared to the spinless case (Fig. 3.5), there is one additional possible fluctuation for the SIAM.

$$G^{RTA} = 4\kappa_l\kappa_{\bar{l}}\frac{e^2}{h}2\int d\varepsilon\ \frac{\pi^2\alpha^2(\varepsilon)}{d(\varepsilon)}\ f_{T,E_F}(\varepsilon), \tag{3.52}$$

$$G^{DSO} = 4\kappa_l\kappa_{\bar{l}}\frac{e^2}{h}\left(\frac{2}{1+\frac{\Gamma^+_{01}}{\Gamma_{01}}}\right) \int d\varepsilon\ \frac{\pi^2\left[\alpha(\alpha+\alpha^+)\right](\varepsilon)}{d(\varepsilon)}\ f_{T,E_F}(\varepsilon), \tag{3.53}$$

where $f_{T,E_F}(\varepsilon)$ is given by Def. (3.47), where the integrands' common denominator is

$$d(\varepsilon) := \pi^2(\alpha+\alpha^+)^2(\varepsilon) + (\varepsilon + \pi H(\alpha+\alpha^+)(\varepsilon) - E_{10})^2, \tag{3.54}$$

with $\mu_l = \mu_{\bar{l}} = E_F$, and where we insert the DSO rates for infinite interaction (3.51) for

$$\Gamma^{\pm}_{01} = \sum_l \Gamma^{\pm}_{l,01}. \tag{3.55}$$

Finally,

$$\Gamma_{01} := \Gamma^+_{01} + \Gamma^-_{01} \tag{3.56}$$

as in Eq. (3.11).

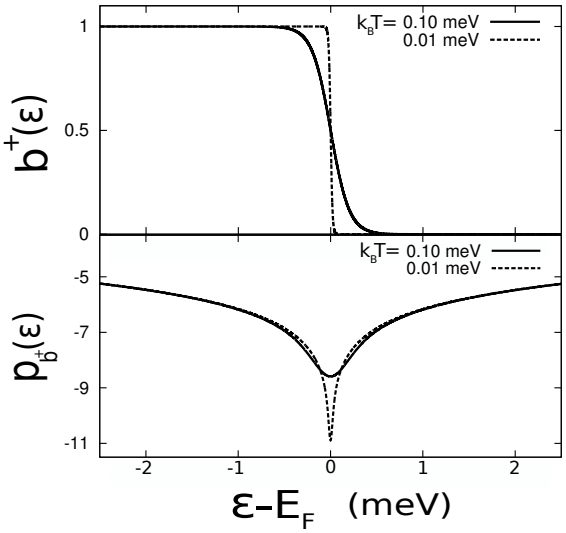

Figure 3.11: Behaviour of the function $\pi H(\alpha^+)(\varepsilon)$ appearing in (3.54) around the Fermi level E_F. We write $\alpha(\varepsilon) = \alpha(E_F)b(\varepsilon)$, with a dimension-less function $b(\varepsilon)$ satisfying $b(E_F) = 1$, and, correspondingly, at zero bias ($\mu_l = \mu_{\bar{l}} = E_F$), $\alpha^+(\varepsilon) = \alpha(E_F)b^+(\varepsilon)$, with $b^+(\varepsilon) = b(\varepsilon)f_l(\varepsilon)$, where f_l is the Fermi function of contact l. We note that $\pi H(b^+)(\varepsilon) = p_{b^+}(\varepsilon) := \int_0^\infty d\omega(b^+(\varepsilon+\omega)-b^+(\varepsilon-\omega))/\omega$; the graph of the function $p_{b^+}(\varepsilon)$ displays a valley around E_F, which becomes narrower for smaller temperatures (lower part of the present figure). The valley's minimum diverges logarithmically with temperature. The *shape* of the valley, however, is independent of temperature and universal as we show in App. F.

Numerical Comparison between RTA and DSO for Infinite U at the Level of the Linear Conductance

The common factor $f_{T,E_F}(\varepsilon)$ in the integrands on the right-hand side of (3.52), and (3.53) sets the focus within the integrals that give the linear conductance on a region of size $\sim k_BT$ around E_F. The function $H(\alpha^+)(\varepsilon)$ appearing in the denominator (3.54), on the other hand, has the property that $H(\alpha^+)(E_F + xk_BT) - H(\alpha^+)(E_F)$ is convergent for $T \to 0$, where the limit

$$\lim_{T\to 0} \left\{ H(\alpha^+)(E_F + xk_BT) - H(\alpha^+)(E_F) \right\} \tag{3.57}$$

is proportional to $\alpha(E_F)$, and otherwise parameter-free. Finally, the term $H(\alpha^+)(E_F)$ is a function of temperature, and it diverges logarithmically to $-\infty$ for $T \to 0$ (cp. Fig. 3.11). We give a proof of the latter two statements in App. F (Universality).

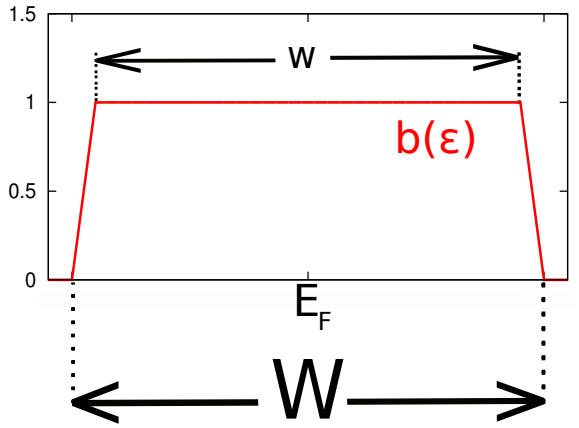

Figure 3.12: Our choice of the shape of the dimension-less function $b(\varepsilon) = \alpha(\varepsilon)/\alpha(E_F)$ for the numerical implementation. We choose $b(\varepsilon)$ to be symmetric, and place the Fermi level E_F in the center. The concrete values we take for the parameters W, and w, of the present figure are $W = 1eV, w = 0.9W$. The continuous cut-off at the edges (or, alternatively, a smooth decay) is necessary to ensure the existence of the Hilbert transforms $H\alpha, H\alpha^+$.

As a consequence, the *shapes* of the linear conductances $G(E_{10})$ for infinite U as function of E_{10} within RTA and DSO are convergent for $T \to 0$. With decreased temperature, the peaks are shifted toward lower energies starting from a value around the Fermi level E_F (Fig. 3.13) – an effect due to the presence of the spin within the SIAM, as opposed to the spinless quantum dot, where the linear conductance does not display this feature (Eq. (3.45)).

Universality and Kondo Temperature in the Infinite U-Case

The DSO-conductance as function of the temperature displays universality in the regime of strong coupling: For a given and fixed value of E_{10}, the linear conductance G becomes a function of the temperature. The function $G(T)$ is expected to display universality in the following sense [23]: There is a temperature T_K such, that G/G_{max} is a parameter-free function of the ratio T/T_K, where G_{max} is the maximum value of the conductance. Both G^{DSO} and G^{RTA} satisfy this demand for energies $E_{10} \ll E_F$.

We derive the universal behaviour of $G^{DSO}(T)$ (and $G^{RTA}(T)$) in App. F. For the temperature T_K – defined by the condition that, at this temperature, the conductance reaches one half of its maximum – we obtain within the DSO:

$$k_B T_K = 7W \exp\left(\frac{E_{10} - E_F}{\alpha(E_F)}\right). \tag{3.58}$$

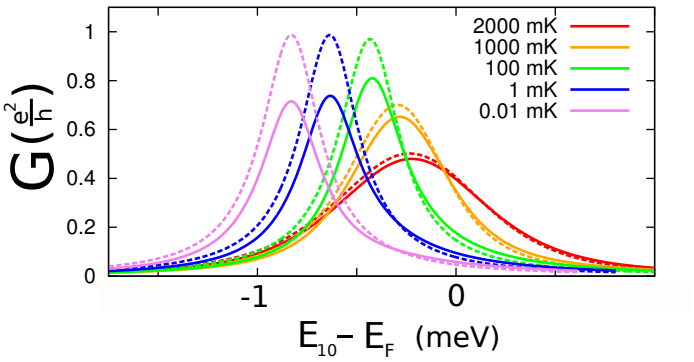

Figure 3.13: Linear conductance G within the DSO for infinite U as a function of the energy difference E_{10} – which corresponds to a plot of G as function of the gate voltage – for different temperatures. The dashed lines show the result for the RTA. We choose the tunneling coupling to be $\alpha(E_F) = 0.042meV$, and the parameter W defining the width of the function $b(\varepsilon)$ (Fig. 3.12) as $W = 1eV$. The same choices we make for a later comparison with an experiment in Sec. 3.2.3 (Linear Conductance at Finite Coulomb-Interaction). For large temperatures, the width of the peak is determined by the thermal energy, and its center is found roughly around the Fermi level. For decreased temperatures, on the other hand, the position of the maximum is shifted, and the width of the peak is proportional to $\alpha(E_F)$. The transition happens at thermal energies $k_BT \approx \alpha(E_F)$. While the logarithmic shift of the peak with the temperature does not stop, the shape of the curve and its maximum value saturate.

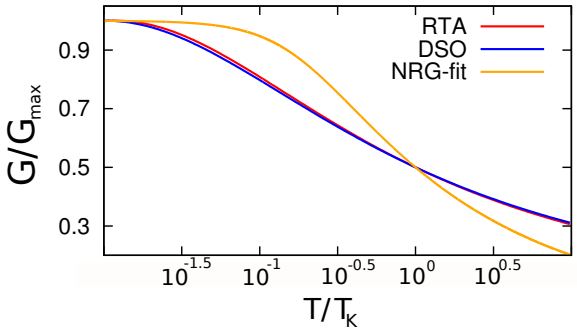

Figure 3.14: Comparison of the parameter-free function $F\left(T/T_K\right)$ which gives $G(T)/G_{max}$ obtained within the DSO (and RTA) to an NRG-fit [23]: All three functions take the value 0.5 at $T = T_K$, and are normalized in such a way that the maximum is one. One feature of the NRG-fit is that, within one power of ten, the linear conductance increases from 50 % to about 95 % of its maximum, while the functions obtained for RTA and DSO grow much less in this interval. As implicitly shown by Fig. 3.13, and unlike the NRG-fit, the parameter-free functions for the RTA and DSO *decrease* again for even smaller values of T/T_K than shown in the present figure. The equation for the NRG-fit is: $G(T) = G_{max}\left(1/\left[(T/T_K')^2 + 1\right]\right)^s$ with $T_K' = T_K/(2^{1/s} - 1)^{1/2}$ so that $G(T_K) = G_{max}/2$; we choose $s = 0.2$.

The pre-factor, which is 7 in the present case, depends on the actual shape of the function b (Fig. 3.12).

The results of App. F (Universality) are valid under the condition:

$$\left\{ \begin{array}{c} k_B T \ll \alpha(E_F) \ll W, \text{ and} \\ 1 \ll \frac{E_F - E_{10}}{\alpha(E_F)} \end{array} \right\}, \tag{3.59}$$

in which case we obtain the expression

$$G^{DSO} = 4\kappa_l \kappa_{\bar{l}} \frac{e^2}{h} F_0^{DSO}\left(c_{1/2} + \ln\frac{T}{T_K}\right), \tag{3.60}$$

where T_K is given by Eq. (3.58), and where the parameter-free function F_0^{DSO} – the function does not take any physical quantities as parameters – is given in Eq. (F.34), App. F.

The DSO linear conductance becomes a universal function of T/T_K in the regime $E_{10} \ll E_F$; at $T = T_K$, $G(T)$ reaches one half of its maximum. In Fig. 3.14 we compare our result for the universal function $G(T/T_K)/G_{max}$ to a curve obtained by numerical renormalization group (NRG) calculations [23]. Our method of analysis within App. F is applicable both to the DSO and the RTA – the resulting formula for T_K deviates only in the pre-factor.

The relation between the quantities $\alpha(E_F)$, which we here use as coupling-parameter, and "Γ", by the use of which T_K is more frequently expressed, e.g. Ref. [18, 23], is

$$\Gamma = 2\pi\alpha(E_F). \tag{3.61}$$

[We note that Γ is the width of the lorentzian (3.46).]

In summary, the DSO clearly fails to describe the regime of low temperature quantitatively correctly. However, it is remarkable that the linear conductance obtained by the DSO displays a universality in a similar way as it is predicted by perfectly different approaches.

Zero Bias Anomaly of the Differential Conductance

We consider now the differential conductance obtained within the DSO at infinite Coulomb-interaction U. We notice that, in the same way as the RTA [22], the approximation produces a zero bias *maximum* of the differential conductance in case E_{10} lies below the Fermi level (shown in Fig. 3.15), which is experimentally well confirmed, and, in addition, a *minimum* in case it lies above or in the vicinity of the Fermi level (not shown); we know of only one experimental observation of the latter minimum [24]. Finally, we study the behaviour of the conductance-peak for smaller and smaller temperatures (Fig. 3.16): The peak splits into two parts, since, as we showed, the differential conductance at zero bias goes to zero with $T \to 0$.

Remark: We here note that the zero bias anomaly contained in the DSO-selection starts to be seen at the sixth order (App. E (Perturbation Theory)). However, upon taking into account *all* sixth order diagrams, the maximum of the differential conductance is even increased, while the minimum in case $E_{10} > E_F$ is no more in the same way as the maximum contained in the complete sixth order [20].

We conclude that the DSO describes the onset of the Kondo peak as well as its evolution for lower and lower temperature qualitatively correctly. Only when the peak splits in two, the DSO starts to fail.

Splitting of the Anomaly in Magnetic Field

By a magnetic field, the SIAM's degenerate level can be split. The application of the DSO for infinite Coulomb-interaction U to the more general case of possibly different energies $E_\uparrow \neq E_\downarrow$ implies only slight changes in the equations. As before, we take into account all possibilities to dress diagrams

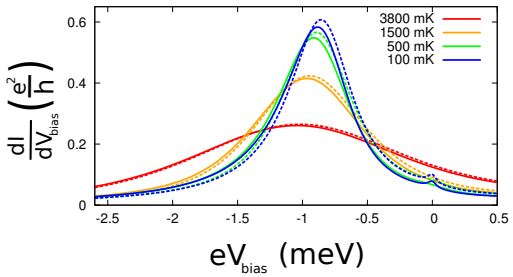

Figure 3.15: The differential conductance versus the bias. We set $E_{10}^{(0)} = E_F - 1meV$ and choose $\alpha(E_F) = 0.042meV, W = 1eV$ as for Fig. 3.13. We fix the position of one of the leads' chemical potentials at the Fermi level, $\mu_l = E_F$, vary only the chemical potential of the opposite lead $\bar{l}$, and define $eV_{bias} = \mu_{\bar{l}} - E_F$. We assume a capacitive coupling between the leads and the quantum dot in such a way that $E_{10}(V_{bias}) = E_{10}^{(0)} + 0.2eV_{bias}$. We see that a hill appears in the graph at zero bias for small temperatures. The dashed lines show the result of the RTA. The zero bias anomaly becomes more and more pronounced with decreasing temperature. The shape of the curve does depend on the capacitive couplings, and on how the window between the two chemical potentials is opened; however, the appearing of the zero bias anomaly does not in principle depend on these choices as one can conclude from the fact that they are irrelevant to the differential conductance at zero bias (3.52), (3.53).

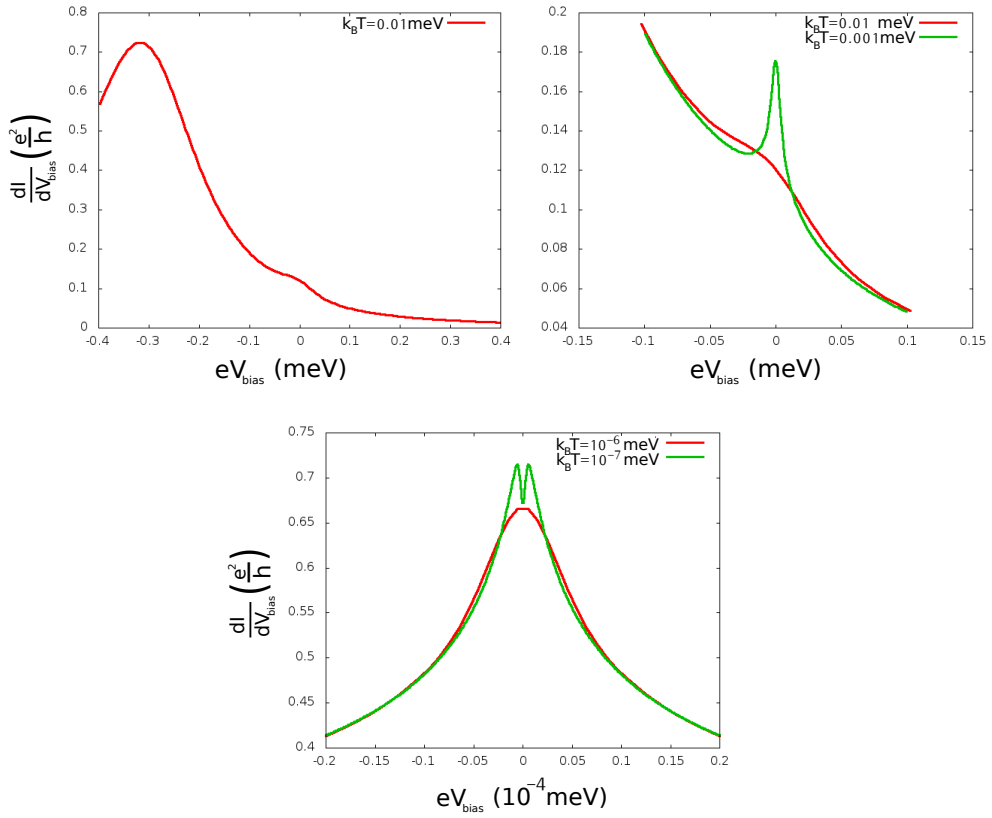

Figure 3.16: Temperature-dependence of the peak in the differential conductance vs. the bias. With decreasing temperature, the peak increases, and finally splits into two parts. At exact zero bias, the conductance goes to zero. [We here choose $E_{10}^{(0)} = E_F - 0.5meV$, $\alpha(E_F) = 0.024meV$.]

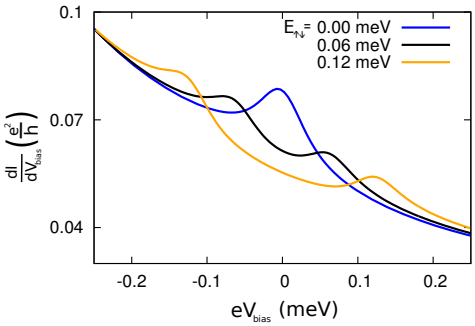

Figure 3.17: Differential conductance vs. the bias for spin-symmetric leads, but not necessarily equal energies $E_\sigma, E_{\overline{\sigma}}$. The zero bias resonance is split if $E_\uparrow \neq E_\downarrow$. We choose the temperature $T = 100mK$, and all remaining parameters as within Fig. 3.15, apart from the spin-dependent energy, $E^{(0)}_{\sigma 0} = E_F - 1meV + E_{\sigma\overline{\sigma}}/2$. We show the graph of the differential conductance for $E_\uparrow = E_\downarrow$, as well as for the two asymmetric cases $E_{\uparrow\downarrow} = 0.06meV$, and $E_{\uparrow\downarrow} = 0.12meV$. The peak in the graph is split in two, where the positions of the resulting peaks differ from zero bias by the energy difference $E_{\uparrow\downarrow}$.

by bubbles sketched in Fig. 3.10, and, by the same method as in Sec. 3.2.2 (Dressed-Second-Order for the SIAM with Infinite Coulomb-Interaction), we obtain in the *not* necessarily spin-symmetric case the rates

$$\Gamma^{\pm}_{l\sigma} = \frac{2\pi}{\hbar}\int d\varepsilon \frac{\alpha^{\pm}_{l\sigma}(\varepsilon)\left(\alpha_\sigma(\varepsilon) + \alpha^{+}_{\overline{\sigma}}(\varepsilon + E_{\overline{\sigma}\sigma})\right)}{\pi^2\left(\alpha_\sigma(\varepsilon) + \alpha^{+}_{\overline{\sigma}}(\varepsilon + E_{\overline{\sigma}\sigma})\right)^2 + \left(\varepsilon - E_{\sigma 0} + p_{\alpha_\sigma}(\varepsilon) + p_{\alpha^{+}_{\overline{\sigma}}}(\varepsilon + E_{\overline{\sigma}\sigma})\right)^2}, \tag{3.62}$$

where (Def. (3.2))

$$E_{\overline{\sigma}\sigma} = E_{\overline{\sigma}} - E_\sigma, \tag{3.63}$$

and where we apply the notation

$$H(g) = \frac{1}{\pi}\, p_g, \tag{3.64}$$

for the Hilbert transform of any function g (Def. (E.49)), as we did also for Fig. 3.11. We see (Fig. 3.17), that the zero bias anomaly is split, and we find two peaks in the graph of the differential conductance vs. the bias at $eV_{bias} \approx \pm E_{\uparrow\downarrow}$, which is in agreement with other theories [22, 25, 26], and observed in experiments [24, 27, 28].

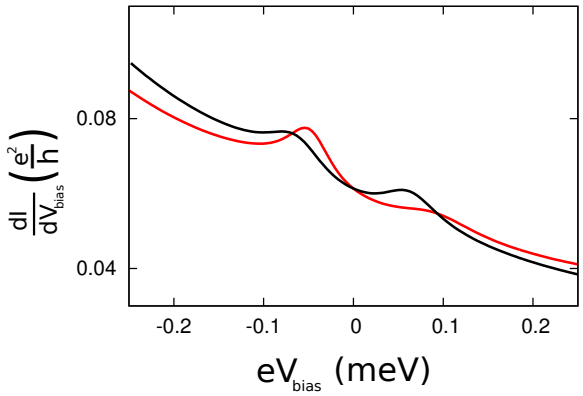

Figure 3.18: An asymmetry of the two different levels' capacitive couplings to the leads has the effect that the split anomaly becomes asymmetric; one of the peaks starts to vanish, while the other one gets sharper. The black line in the present figure has the same data as the graph of the differential conductance vs. the bias for an energy difference of $E_{\uparrow\downarrow} = 0.06meV$ in Fig. 3.17. For the red (grey) line we change the capacitive couplings in such a way that $E_{\uparrow 0}(V_{bias}) = E^{(0)}_{\uparrow 0} + 0.4eV_{bias}$, $E_{\downarrow 0}(V_{bias}) = E^{(0)}_{\downarrow 0} + 0.1eV_{bias}$.

Situations in which only One Peak is Expected

In Ref. [24] a maximum of the differential conductance vs. the bias, close to zero bias, whose position changed slightly with the gate voltage, has been reported. The dependence of the maximum's position on the gate voltage was explained by the conjecture that two different wave functions (not only two different spins) might be involved, so that the assumption of different capacitive couplings of these two levels to the gate electrode – with the effect that the energies of the two levels become gate-dependent – is justified. In this case, analogously to the case where different energies $E_\uparrow \neq E_\downarrow$ are achieved by a magnetic field (Fig. 3.17), one would expect to see two hills in the graph of the differential conductance located symmetrically around zero bias. However, a second maximum was not observed.

We here assume in addition different capacitive couplings of these two levels on the quantum dot to the leads and see that, with growing asymmetry of the capacitive couplings *to the leads*, one of the hills in the differential conductance changes position, becomes wider and much less pronounced (Fig. 3.18). The opposite hill, on the other hand, becomes even sharper, and its position moves closer to zero bias. At the level of the transition rates, Eq. (3.62), we can explain this numerical result as follows:

The integral, which $\Gamma^{\pm}_{l\sigma}$ is given by, changes rapidly with the bias in areas

where

$$\mu_l - \mu_{\bar{l}} \;\approx\; E_{\sigma\bar{\sigma}}, \tag{3.65}$$

since here, by changing the bias, the region of large values of $p_{\alpha^+_{\bar{l}\bar{\sigma}}}(\varepsilon + E_{\bar{\sigma}\sigma})$ leaves or enters the interval $]-\infty, \mu_l]$, over which the integral essentially goes. This leads to the condition "$eV_{bias} \approx \pm E_{\uparrow\downarrow}$" for rapid change of the current with the bias. In the case of different capacitive couplings of the levels to the leads the energy differences $E_{\sigma\bar{\sigma}}$ become a function of the bias. With increasing bias, one of the differences decreases while the other one increases. Thus, one of the peaks gets sharper, while the other one vanishes. The positions are no longer symmetric around zero bias.

Moreover, we notice that also asymmetric *tunnel* coupling can have the effect that one of the maxima in the graph of the differential conductance is getting less pronounced. We can let the coupling functions $\alpha_{l\sigma}(\varepsilon)$, Eq. (D.60), be dependent on the spin as well as on the lead, and thus obtain further independent parameters. We evaluated the differential conductance also in this case (not shown), and we can qualitatively confirm the assumption that different tunnel couplings of the levels to source and drain, too, can be responsible for the observation of only one peak [24].

Finally, we consider another situation where the DSO yields, this time, *in principle* only one peak in the graph of the differential conductance vs. the bias: The energies $E_\uparrow, E_\downarrow$ are in general different, and there are four different, separately variable, chemical potentials $\mu_{l\sigma}$ for each of the leads, and each of the spins. The chemical potentials of the down-spin are kept constant and equal, $\mu_{l\downarrow} = \mu_{\bar{l}\downarrow} =: \mu_\downarrow$; the up-spin chemical potential of one particular lead l_0, too, is kept constant, and only the chemical potential $\mu_{\bar{l_0}\uparrow}$ of the opposite lead is varied. The current is then a function of $eV_{bias} = \mu_{\bar{l_0}\uparrow} - \mu_{l_0\uparrow}$.

A consideration of the question under what condition the rates $\Gamma^\pm_{l\sigma}$ (3.62) change rapidly with the bias yields the condition

$$eV_{bias} \approx E^*_{\uparrow\downarrow} := E^*_\uparrow - E^*_\downarrow, \tag{3.66}$$

where we use the definition $E^*_\sigma := E_{\sigma 0} - \mu_{l_0\sigma}$ for $\sigma = \uparrow, \downarrow$. Indeed, the DSO yields only one peak in the differential conductance as function of the bias located (approximately) at this value of the bias (Fig. 3.19). Experiments with a pseudo spin [29] might be interpreted by the use of the SIAM as we do it here. In agreement with experiment, the DSO predicts the appearing of only one resonance as far as only one of the voltages (only one of the differences $\mu_{l\sigma} - \mu_{\bar{l}\sigma}, \sigma = \uparrow, \downarrow$) is varied.

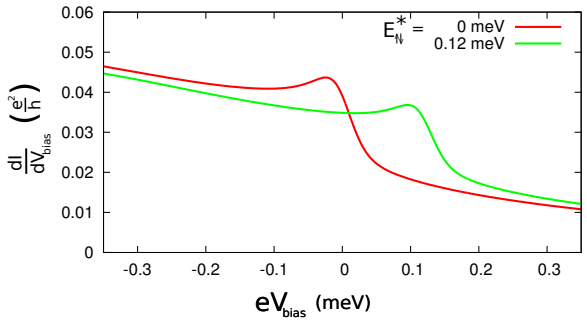

Figure 3.19: The differential conductance as function of the bias in the following situation: The temperature is $T = 100mK$, the capacitive coupling is assumed to be zero; moreover, we choose $\mu_\downarrow = E_F - 0.5meV, \mu_{l_0\uparrow} = E_F + 0.5meV$. The energies $E_{\sigma 0}$ are: $E_{\sigma 0} = \mu_{l_0\sigma} - 1meV + E^*_{\sigma\bar{\sigma}}/2$. The differential conductance displays one resonance located approximately at the value $eV_{bias} \approx E^*_{\uparrow\downarrow}$.

3.2.3 Linear Conductance at Finite Coulomb-Interaction

We finally apply the DSO-diagram selection to the case of finite interaction, so we include the doubly occupied state **2**. We shall compare our results to an experiment [23] at the level of the linear conductance. First of all, we note the DSO tunneling rates $\Gamma^\pm_{l,01}, \Gamma^\pm_{l,12}$ for finite interaction, within which we take into account all possibilities to dress a second order diagram contained in Figs. 3.20, 3.21 . In the spin-symmetric case these rates read:

$$\Gamma^\pm_{l,01} = \frac{2\pi}{\hbar}\int d\varepsilon \frac{\alpha^\pm_l(\varepsilon)\left[(\alpha+\alpha^+)(\varepsilon)+\alpha^+(E_{20}-\varepsilon)\right]}{d_{01}(\varepsilon)}, \tag{3.67}$$

$$\Gamma^\pm_{l,12} = \frac{2\pi}{\hbar}\int d\varepsilon \frac{\alpha^\pm_l(\varepsilon)\left[(\alpha+\alpha^-)(\varepsilon)+\alpha^-(E_{20}-\varepsilon)\right]}{d_{12}(\varepsilon)}, \tag{3.68}$$

with the integrands' denominators

$$\begin{aligned} d_{01}(\varepsilon) := \quad & \pi^2\left[(\alpha+\alpha^+)(\varepsilon)+\alpha^+(E_{20}-\varepsilon)\right]^2 \\ + \quad & \left[\varepsilon + p_{\alpha+\alpha^+}(\varepsilon) - p_{\alpha^+}(E_{20}-\varepsilon) - E_{10}\right]^2, \end{aligned} \tag{3.69}$$

and

$$\begin{aligned} d_{12}(\varepsilon) := \quad & \pi^2\left[(\alpha+\alpha^-)(\varepsilon)+\alpha^-(E_{20}-\varepsilon)\right]^2 \\ + \quad & \left[\varepsilon + p_{\alpha+\alpha^-}(\varepsilon) - p_{\alpha^-}(E_{20}-\varepsilon) - E_{21}\right]^2. \end{aligned} \tag{3.70}$$

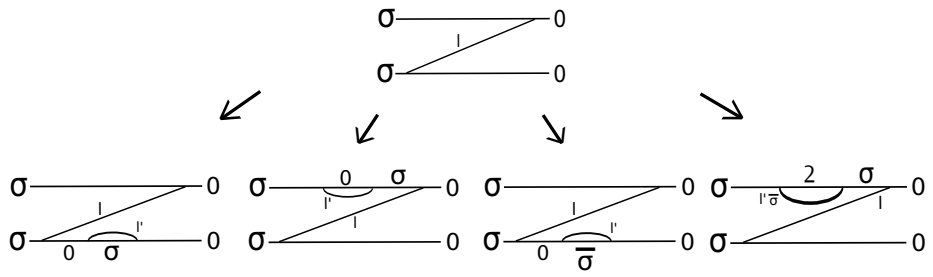

Figure 3.20: A second order diagram contributing to the transition from state **0** to $\boldsymbol{\sigma}$, and the altogether four ways to dress this diagram by one bubble representing a charge fluctuation. Compared to the case of infinite interaction (Fig. 3.10), we here take into account one additional diagram – the one within which the state **2** appears.

From the current at finite U as function of rates, Eq. (3.18), we obtain the differential conductance at zero bias:

$$G^{DSO} = 4\kappa_l\kappa_{\bar{l}}\frac{e^2}{h}\begin{pmatrix} \frac{2}{1+\frac{\Gamma^+_{01}\Gamma_{12}}{\Gamma_{01}\Gamma^-_{12}}} \\ \frac{2}{1+\frac{\Gamma_{01}\Gamma^-_{12}}{\Gamma^+_{01}\Gamma_{12}}} \end{pmatrix} \cdot \begin{pmatrix} \int d\varepsilon \frac{n_{01}(\varepsilon)}{d_{01}(\varepsilon)} f_{T,E_F}(\varepsilon) \\ \int d\varepsilon \frac{n_{12}(\varepsilon)}{d_{12}(\varepsilon)} f_{T,E_F}(\varepsilon) \end{pmatrix}, \tag{3.71}$$

with the integrands' numerators:

$$\begin{aligned} n_{01}(\varepsilon) &:= \pi^2\alpha(\varepsilon)\left[(\alpha+\alpha^+)(\varepsilon)+\alpha^+(E_{20}-\varepsilon)\right], \\ n_{12}(\varepsilon) &:= \pi^2\alpha(\varepsilon)\left[(\alpha+\alpha^-)(\varepsilon)+\alpha^-(E_{20}-\varepsilon)\right], \end{aligned} \tag{3.72}$$

and with $f_{T,E_F}(\varepsilon)$ according to Eq. (3.47).

DSO-Conductance from Weak to Strong Coupling

We model the case of strong and weak tunnel coupling by large and small factors $\alpha(E_F)$. The latter function-value at the Fermi level of the function $\alpha(\varepsilon)$ serves as coupling paremeter (cp. Fig. 3.11). First, we consider the graph of G^{DSO} as function of the gate voltage for different values of the tunnel coupling (Fig. 3.23): In the limit of weak coupling we reproduce the result of the second order, while for larger couplings we observe three effects: The peaks get higher, broader and the positions of the maxima approach each other. For strong couplings the DSO-approximation produces a sharp valley in the center of the present plot (particle-hole symmetric point) which is not observed in experiment. This problem is present also in the RTA for

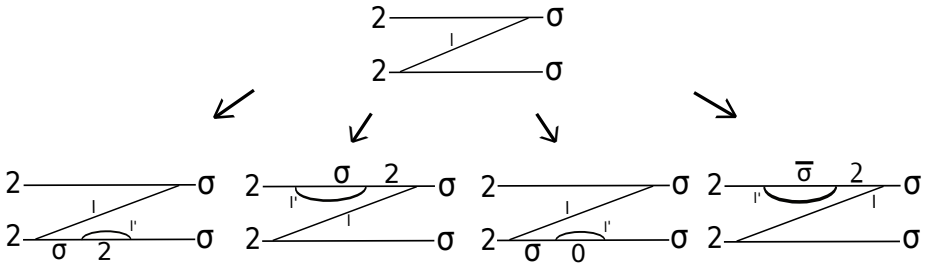

Figure 3.21: A second order diagram which transfers the state $\boldsymbol{\sigma}$ into the state $\mathbf{2}$, and all fourth order diagrams with one bubble dressing this diagram – symmetric to Fig. 3.20. By taking into account only diagrams of the present shape, we actually no more exclusively define the DSO-diagram selection by the demand that the diagrams' pair formations have the form of Fig. 3.8. We here do not take into account any diagrams which include an intersection of tunneling lines (cp. Fig. 3.22).

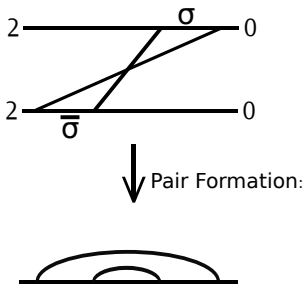

Figure 3.22: A fourth order diagram with an intersection of tunneling lines, however, satisfying the demand that its pair formation is included in the selection of pair formations defined by Fig. 3.8. Upon rigorously applying the definition of the DSO-selection by pair formations to the case of finite interaction, we would obtain the *exact* result in the special case of zero interaction, $U = 0$, at the level of the current – in the same way as the DSO produces the exact result at the level of the current for the spinless quantum dot (Eq. (3.43)). However, to keep the numerical effort lower, we apply the present definition of the DSO for finite U.

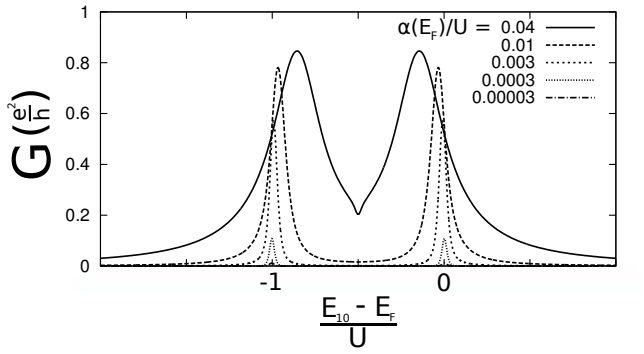

Figure 3.23: Differential conductance at zero bias within the DSO, according to Eq. (3.71), as a function of $(E_{10} - E_F)/U$, with fixed values of U, and E_F, for different tunnel couplings. We choose the Coulomb-interaction to be $U = 1meV$, and the temperature $T = 100mK$. For weak coupling, we see peaks of small height whose width is given by the temperature; the peak positions are quite precisely defined by the resonance conditions $E_{10} = E_F$ (right peak), and $E_{21} = E_F$ (left peak). Upon increasing the coupling, the corrections become more and more important: The width of the hills in the graph increases with $\alpha(E_F)$, and the peak position is shifted by the contributions $p_{\alpha^\pm}(\varepsilon)$ to the denominators ((3.69), (3.70)).

finite U [30, 31]; in addition, an approach by equations of motion displays unphysical independence of temperature at the particle-hole symmetric point [32].

From the Empty Orbital Regime to the Kondo Regime

We now qualitatively compare the DSO for finite U – at the level of the linear conductance as function of the gate voltage and temperature – to an experiment [23]. In this experiment, a small area (diameter $\approx 150nm$) within a two-dimensional electron gas was isolated by electrostatically generated tunneling barriers. In this way, a quantum dot which is tunnel-coupled to leads was formed. Via a gate electrode it is possible to vary E_{10}, and, simultaneously, $E_{21} = E_{10} + U$, where the Coulomb-interaction U remains unaffected by the gate voltage. The linear conductance was measured as a function of the gate voltage and the temperature, and the results were interpreted in terms of the SIAM. The authors distinguish between three different regimes of parameters, depending on whether the level position, i.e., E_{10}, is far below the Fermi energy (here the particle-number is one, *Kondo regime*), in the vicinity of the Fermi level (*mixed valence regime*) or above the Fermi level (*empty orbital regime*). Upon adjusting parameters, we here test the DSO approximation under conditions similar to those in the experiment.

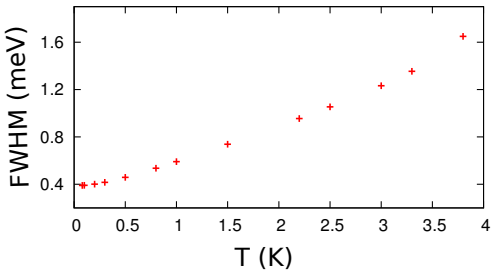

Figure 3.24: Full widths at half maximum (FWHM) of the peaks in Fig. 3.25 as a function of the temperature; the value of $\alpha(E_F)$ is here $0.042meV$. For small temperatures the FWHM saturates at a value of about $0.39meV$ which is in agreement with the value of the saturation width in the experiment [23]. For large temperatures the FWHM increases linearly with T; the graph of the FWHM vs. the temperature in the present figure has positive curvature, since the two peaks in Fig. 3.25 get mixed as we increase the temperature. Hence, we take the saturation width at $T \to 0$ as criterion to adjust the coupling strength to the experiment.

We fit the parameters to the experiment [23] in the following way: The temperatures are given explicitly. The value of the Coulomb-interaction U, too, we take directly from the experiment. To fix the coupling-parameter $\alpha(E_F)$, we plotted $G^{DSO}(E_{10})$ for various values of it (not shown). We determine the coupling-parameter by the demand that the full width at half maximum of the peaks in $G^{DSO}(E_{10})$ is close to the measured values (Fig. 3.24). In the end, we adjust also the scaling factor $4\kappa_l\kappa_{\bar{l}}$ in Eq. (3.71), which contains an asymmetry of the tunneling couplings to source and drain in the case of proportional coupling (Eq. (3.19)), by the demand that the absolute value of the maximum of the linear conductance is approximately equal in theory and experiment.

In Fig. 3.25 we show the graph of the linear conductance G^{DSO} as a function of the gate voltage for different temperatures. We get qualitatively very similar behaviour as in Ref. [23] (Fig. 2): With decreasing temperature, the peaks move towards each other, they get higher, and their widths get smaller and seem to finally saturate.

Finally, for a further comparison we show the dependence of G^{DSO} on the *temperature* for fixed values of E_{10}. To this end, we express E_{10} by its position relative to the Fermi level and divide it by the quantity $\Gamma \approx 0.3meV$, which is applied in Ref. [23] to characterize the strength of the tunnel coupling. The linear conductance $G^{DSO}(T)$ (Fig. 3.26) has the following properties:

- By the use of a logarithmic scale for the temperature T, the graph of $G^{DSO}(T)$ forms a hill.

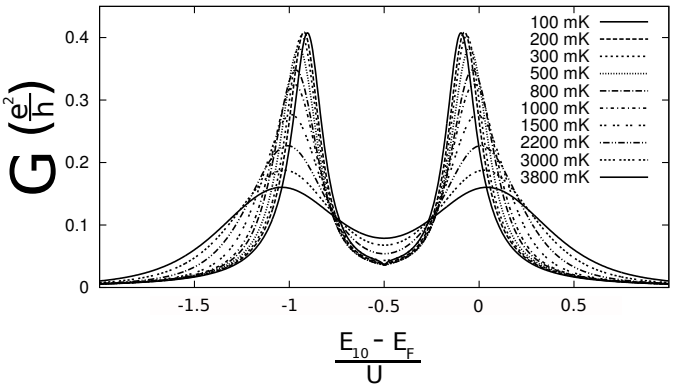

Figure 3.25: Linear conductance G^{DSO} as a function of $(E_{10} - E_F)/U$ – where the values of E_F, and U, are fixed, and where we vary only E_{10}, corresponding to the functional dependence of the linear conductance on the gate voltage V_g – for diverse temperatures . We choose the interaction to be $U = 1.9meV$, the coupling $\alpha(E_F) = 0.042meV$, and the temperatures in agreement with the experiment [23]; the asymmetry of the tunnel couplings to left and right lead, given by κ_l, and $\kappa_{\bar{l}}$ (Eq. (3.19)), we choose as $4\kappa_l\kappa_{\bar{l}} = 0.5$, i.e., we assume an asymmetry of about $\kappa_l : \kappa_{\bar{l}} = 0.17$.

- Inside the empty orbital regime ($\tilde{\varepsilon_0} > 0$), Fig. 3.26 mainly shows the left slope of that hill, while inside the Kondo regime ($\tilde{\varepsilon_0} < -0.5$) we see the right slope.

- Within the range of values contained in Fig. 3.26, $G^{DSO}(T)$ reaches the highest absolute values for $\tilde{\varepsilon_0} \approx -0.6$.

In summary, the behaviour of $G^{DSO}(T)$ for various values of $\tilde{\varepsilon_0}$ is basically in agreement with experiment. A *difference* we observe in the mixed valence regime, where – in experiment – the left slope of $G(T)$ becomes less steep and even turns into a plateau (the curve for $\tilde{\varepsilon_0} = -0.48$ in Fig. 3, Ref. [23]), while $G^{DSO}(T)$ displays a pronounced peak.

With this qualitative comparison of the results of the DSO for finite interaction to an experiment we conclude the present chapter.

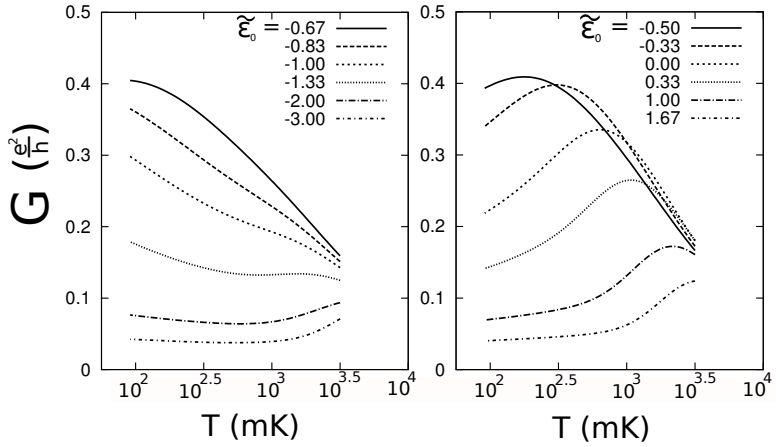

Figure 3.26: A plot of $G^{DSO}(T)$ for different fixed values of the quantity $\tilde{\varepsilon_0} := (E_{10} - E_F)/\Gamma$. [Note that, in this particular plot, we do not take exactly the same but similar values for $\tilde{\varepsilon_0}$ as in Ref. [23].] Within the *empty orbital regime* ($\tilde{\varepsilon_0} > 0$) [the first three lines from below on the right-hand side] we see a decrease of $G^{DSO}(T)$ with decreasing T, at least over a finite interval of temperature-values. Within the mixed valence-, and the Kondo regime, on the other hand, we observe an increase of $G^{DSO}(T)$ with decreasing T. Within the mixed valence regime this latter increase stops at some point, while within the Kondo regime the increase does not terminate within the temperature-range under consideration. However, the increase is strongest, and the absolute values of $G^{DSO}(T)$ are the largest, for $-0.8 \lesssim \tilde{\varepsilon_0} \lesssim -0.5$.

Chapter 4

Conclusions

Within the general-theoretical part of this work, the transport theory, we give an independent derivation of the quantum master equation (Sec. 2.3.2 (Memory Equation for the Reduced Density Matrix and the Current)): Upon noting the time evolution of the density matrix in the interaction picture in the form of a series of integrals (2.26), we define the integrands that give the kernel recursively by multi-commutators, Eq. (2.33). Our method neither depends on the superoperator formalism, nor does it require an integration along the Keldysh-contour (Ref. [15]). Moreover, we rigorously derive and formulate the kernel's diagrammatic expansion. In Sec. 2.7.4 (Processes with inversed Time-Direction) we substantiate the interpretation of tunneling processes with a negative contribution to the kernel – assuming they evolve in inversed time-direction. Finally, we present a novel technique to calculate diagrams in App. E (Perturbation Theory).

In the *applied* Chapter 3, on the other hand, we perform the sum over all diagrams within the dressed-second-order (DSO) diagram selection, first discovered as an instructive selection in Ref. [16]. We show that the DSO is an appropriate tool to address resonant tunneling: It yields the exact result for the current across the spinless quantum dot – so it covers the transition from temperature-broadened to tunnel-broadened conductance peaks. If applied to the single impurity Anderson model, on the other hand, the DSO, as the *resonant tunneling approximation*, contains in addition the experimentally observed shift of the peak position in the the graph of the linear conductance vs. the gate voltage (cp. Figs. 3.13, 3.25).

We find that, in spite of its austerity, the DSO-diagram selection captures the onset of the Kondo resonance, its logarithmic dependence on temperature, its splitting in magnetic field, as well as its behaviour in special experimental situations (Fig. 3.19). The selection's applicability to complex systems has been shown in Ref. [33], where transport across carbon

nanotubes, contacted by ferromagnetic leads, is studied. In addition, the DSO-selection has been extended in Ref. [34], aiming at an improved description of the Kondo resonance. In summary, the DSO-diagram selection is a powerful, simple, and versatile theoretical approach to the tunneling current across quantum dots.

Acknowledgements

The time I spent at the faculty of physics at Universität Regensburg lies now several years behind, and I am grateful that it is a part of my life. I want to thank Milena Grifoni: She had the confidence that a mathematician will contribute substantially to the work of her group; by the resummation and study of the DSO-diagrams as applied to the SIAM she gave me a task fit to my education, and we have had many discussions, no matter under what circumstances (at University, or while running through snowy landscape). Generally, I enjoyed the atmosphere among group members, officemates, colleagues, secretary, and frequently received support, help, advice, encouragement or constructive criticism. Thanks go to Sandra Kolmeder, Abdullah Yar, Sebastian Fries, Dana Darau, Magdalena Marganska-Lyzniak, Sonja Koller, Andrea Donarini, Simone Gutzwiller, Alexander Lopez, Narjes Javadi-Motaghi, Georg Begemann, Sonja Predin, Miriam del Valle, Prakash Parida, Piotr Chudzinski, Johannes Hausinger, Sergey Smirnov, Andreas Scholz, Alois Dirnaichner, Manohar Awasthi, Lizy Lazar, Bhaskaran Muralidharan, and others. In addition, I want to thank my family for encouragement and help. Last not least, thanks go to Deutsche Forschungsgemeinschaft for financial support within the framework of the GRK 1570, and of the SFB 689.

Appendices

Appendix A

Product States

In the present appendix we discuss the product state of two many-electron states, a corresponding product of vector spaces, as well as product operators. This product is implicitly used within this work when we assume that at some initial time t_0 the density matrix of the total system is factored according to $\hat{\rho}(t_0) = \hat{\rho}_R \otimes \hat{\rho}_\odot(t_0)$, Eq. (2.6). Finally, we represent creation- and annihilation operators as product operators – this enables us to take the reduced operator of compositions of the form of (2.53).

A.1 Convention

For simplicity, throughout this work, we consider all quantities to be real or complex numbers, or abstract vectors – without any physical dimension. Physical units, like eV, or constants like the Planck- or the Boltzmann-constant $\hbar$, and k_B, respectively, we treat like purely *numerical* constants, whose actual value is not further specified, unless it is expressed by other units, and constants. Correspondingly, we consider e.g. a one-electron wave function to be a map

$$D \;:=\; \mathbb{R}^3 \times \{\uparrow,\downarrow\} \to \mathbb{C},$$

where the arrows denote the two spin-directions, and, within App. E.2.1 (Diagram Calculations – Theory), we study spaces of functions with the property that sums, as well as products, and convolutions of two functions within these spaces, again, are elements within these spaces.

A.2 Antisymmetric Product of Wave Functions

To any pair of a m- and a n-electron wave function

$$\psi : D^m \to \mathbb{C},\ \varphi : D^n \to \mathbb{C}, \tag{A.1}$$

we can find an antisymmetric product of wave functions [35]

$$\psi \otimes \varphi :\ D^{m+n} \to \mathbb{C}. \tag{A.2}$$

That product satisfies the relation

$$\psi \otimes \varphi \ = \ (-1)^{mn}\ \varphi \otimes \psi, \tag{A.3}$$

and it is associative [$\psi \otimes (\varphi \otimes \lambda) \ = \ (\psi \otimes \varphi) \otimes \lambda$ for any further $\lambda : D^l \to \mathbb{C}$]. For a sequence of one-electron wave functions $\psi_j : D \to \mathbb{C} (j = 1, \ldots, N)$ the antisymmetric product

$$\psi_1 \otimes \cdots \otimes \psi_N \tag{A.4}$$

is the Slater determinant of these functions.

A.3 Vector Spaces constructed by Slater Determinants

Let Φ be a set of a finite number of quadratically integrable and orthonormal one-electron wave functions. To any $N \in \{0, 1 \ldots\}$, let $V_N(\Phi)$ be the set of all linear combinations of N-electron wave functions given by Slater determinants of functions in Φ. We note that, up to scalar multiples, $V_{|\Phi|}(\Phi)$ has only one element, and $V_N(\Phi) = \{0\}$ for even greater particle-number $N > |\Phi|$. We define $V(\Phi)$ as the vector space of all many-electron states constructed from one-electron wave functions contained in Φ, so

$$V(\Phi) \ := \ \{(\psi_N)_{N=0}^{\infty} :\ \text{for all } N \in \mathbb{N}_0 : \psi_N \in V_N(\Phi)\}, \tag{A.5}$$

the set of all sequences of functions $(\psi_N)_{N \in \mathbb{N}_0}$, where each $\psi_N \in V_N(\Phi)$.

To each subset $M \subset \Phi$ we define a product state $\pi(M)$ as the Slater determinant of all one-electron wave functions $\varphi \in M$ in one arbitrarily chosen but fixed order. We note that the states $\pi(M)$, $M \subset \Phi$, form a basis of $V(\Phi)$.

Generally, we consider

$$V_N(\Phi) \subset V(\Phi) \tag{A.6}$$

by the inclusion

$$\begin{aligned} V_N(\Phi) &\to V(\Phi), \\ \psi_N &\mapsto \left(0,\ldots,0,\underbrace{\psi_N}_{\text{site "N"}},0,\ldots\right). \end{aligned} \tag{A.7}$$

In this sense, for $\psi = (\psi_N)_{N\in\mathbb{N}_0} \in V(\Phi)$,

$$\psi = \sum_{N=0}^{\infty} \psi_N. \tag{A.8}$$

A.4 Product Vector Space and Product Operators

If Φ is the disjoint union of subsets $\Phi_1, \Phi_2 \subset \Phi$,

$$\Phi = \Phi_1 \dot{\cup} \Phi_2, \tag{A.9}$$

then

$$V(\Phi) = V(\Phi_1) \otimes V(\Phi_2), \tag{A.10}$$

in the sense of a tensor product, since the elements $\pi(M_1) \otimes \pi(M_2)$, $M_1 \subset \Phi_1, M_2 \subset \Phi_2$, form an orthonormal basis of $V(\Phi)$.

For $j = 1, 2$ let

$$\hat{A}_j : V(\Phi_j) \to V(\Phi_j) \tag{A.11}$$

be a linear map; then, there is a unique operator

$$\hat{A}_1 \otimes \hat{A}_2 : V(\Phi) \to V(\Phi) \tag{A.12}$$

with the property, that for any $\psi \in V(\Phi_1), \varphi \in V(\Phi_2)$, the equality

$$\hat{A}_1 \otimes \hat{A}_2 (\psi \otimes \varphi) = \left(\hat{A}_1 \psi\right) \otimes \left(\hat{A}_2 \varphi\right) \tag{A.13}$$

is satisfied.

If, for each $j = 1, 2$, and $M_j \subset \Phi_j$, the operator $\hat{A}_j$ maps the state $\pi(M_j)$ to (zero or) a linear combination of states with the same particle-number $|M_j|$, then, with Eq. (A.3), the operator product is commutative,

$$\hat{A}_1 \otimes \hat{A}_2 \;=\; \hat{A}_2 \otimes \hat{A}_1; \tag{A.14}$$

in this case, the expression $\underset{j=1,2}{\otimes} \hat{A}_j$, analogous to Eq. (2.7), is well-defined.

A.5 Creation- and Annihilation Operators in Product Space

For $\varphi \in \Phi$, we can define the creation operator $\hat{c}^\dagger_\varphi$ of the one one-electron level that corresponds to the one-electron wave function φ by the multiplication by φ from the left,

$$\begin{array}{rccl} \hat{c}^\dagger_\varphi : & V(\Phi) & \to & V(\Phi), \\ & \alpha & \mapsto & \varphi \otimes \alpha, \end{array} \tag{A.15}$$

and, correspondingly, we may define the annihilation operator $\hat{c}_\varphi$ of the same level φ as the adjoint operator of $\hat{c}^\dagger_\varphi$. Then, for $\varphi_1 \in \Phi_1, \varphi_2 \in \Phi_2$, the following relations between the creation- and annihilation operators $\hat{c}^{(\dagger)}_{\varphi_1}, \hat{c}^{(\dagger)}_{\varphi_2}$, and their restrictions

$$\begin{array}{rcl} \hat{\mathrm{c}}^{(\dagger)}_{\varphi_1} & := & \hat{c}^{(\dagger)}_{\varphi_1}\Big|_{V(\Phi_1)}, \\ \hat{\mathrm{c}}^{(\dagger)}_{\varphi_2} & := & \hat{c}^{(\dagger)}_{\varphi_2}\Big|_{V(\Phi_2)}, \end{array} \tag{A.16}$$

to the sub-spaces $V(\Phi_1), V(\Phi_2)$, respectively, hold:

$$\hat{c}^{(\dagger)}_{\varphi_1} \;=\; \hat{\mathrm{c}}^{(\dagger)}_{\varphi_1} \otimes \hat{1}_{\Phi_2}, \tag{A.17}$$

$$\hat{c}^{(\dagger)}_{\varphi_2} \;=\; \hat{\mathrm{P}}_{\Phi_1} \otimes \hat{\mathrm{c}}^{(\dagger)}_{\varphi_2}, \tag{A.18}$$

where the maps $\hat{1}_{\Phi_2}, \hat{\mathrm{P}}_{\Phi_1}$ are defined as the identity-map on $V(\Phi_2)$, and by

$$\hat{\mathrm{P}}_{\Phi_1} \;:=\; \exp\left(i\pi \hat{\mathrm{N}}_{\Phi_1}\right), \tag{A.19}$$

with

$$\hat{\mathrm{N}}_{\Phi_1} \;:=\; \sum_{\varphi \in \Phi_1} \hat{\mathrm{c}}^\dagger_\varphi \hat{\mathrm{c}}_\varphi, \tag{A.20}$$

the particle-counting operator on $V(\Phi_1)$, respectively.

Appendix B

Memory Equation for the Current

We here derive the memory equation for the current (2.50) by a method analogous to the way in which we derived the quantum master equation (2.45): In the same way as the tunneling Hamiltonian, the current operator (2.15) maps eigenstates of the particle-counting operator of the leads with eigenvalue N to sums of eigenstates with eigenvalues $N-1$, and $N+1$. We note that with Eq. (2.26) we obtain:

$$\begin{aligned} Tr_R\{[\mathcal{W}(t)\hat{I}_l]\hat{\sigma}(t)\} &= \int_{0\leq\tau_1\leq t} U^{(2)}(t,\tau_1)\hat{\sigma}_\odot(0) + \\ &\int\int\int_{0\leq\tau_1\leq\tau_2\leq\tau_3\leq t} U^{(4)}(t,\tau_3,\tau_2,\tau_1)\hat{\sigma}_\odot(0) + \\ &\vdots \quad , \end{aligned} \tag{B.1}$$

where

$$U^{(2n)}(\tau_{2n},\ldots,\tau_1)\hat{y} = Tr_R\left\{[\mathcal{W}(\tau_{2n})\hat{I}_l]\mathcal{L}(\tau_{2n-1})\ldots\mathcal{L}(\tau_1)(\hat{\rho}_R\otimes\hat{y})\right\}, \tag{B.2}$$

with $\mathcal{W}(t)$ the map for the transformation to the interaction picture (2.18), and $\mathcal{L}(t)$ the Liouvillian (2.24).

In analogy to the recursion relation of Eq. (2.31) we define now

$$J^{(2)} := U^{(2)}, \tag{B.3}$$

and

$$
\begin{aligned}
J^{(2n+2)}(\tau_{2n+2},\ldots,\tau_1) \;:=\; & U^{(2n+2)}(\tau_{2n+2},\ldots,\tau_1) \quad - \\
& \Big\{\, J^{(2n)}(\tau_{2n+2},\ldots,\tau_3)A^{(2)}(\tau_2,\tau_1) + \\
& J^{(2n-2)}(\tau_{2n+2},\ldots,\tau_5)A^{(4)}(\tau_4,\ldots,\tau_1) + \\
& \qquad \vdots \\
& J^{(2)}(\tau_{2n+2},\tau_{2n+1})A^{(2n)}(\tau_{2n},\ldots,\tau_1)\Big\}\;,
\end{aligned}
\tag{B.4}
$$

with $A^{(2n)}(\tau_{2n},\ldots,\tau_1)$ given in Eq. (2.30). We rearrange the sum (B.1) analogously to the rearrangement of Eq. (2.34). Making use of Eq. (2.29) [series-expansion of $\hat{\sigma}(t)$ with integrands $A^{(2n)}(\tau_{2n},\ldots,\tau_1)$], we obtain

$$
Tr_R\{[\mathcal{W}(t)\hat{I}_l]\hat{\sigma}(t)\} \quad = \quad \int_0^t ds \quad \kappa_{curr,l}(t,s)\hat{\sigma}_\odot(s), \tag{B.5}
$$

where the integral kernel $\kappa_{curr,l}$ is given by

$$
\begin{aligned}
\kappa_{curr,l}(t,s) \;:=\; & J^{(2)}(t,s) \quad + \\
& \int\int_{s\le s_2\le s_3\le t} J^{(4)}(t,s_3,s_2,s) \quad + \\
& \int\int\int\int_{s\le s_2\le s_3\le s_4\le s_5\le t} J^{(6)}(t,s_5,s_4,s_3,s_2,s) \quad + \\
& \vdots \quad .
\end{aligned}
\tag{B.6}
$$

Now, we perform the back-transformation to the Schrödinger picture according to Eq. (2.21). Applying the relation (2.25), we find

$$
\begin{aligned}
& \mathcal{W}_\odot(-\tau)U^{(2n)}(\tau_{2n},\ldots,\tau_1) \\
= \quad & U^{(2n)}(\tau_{2n}-\tau,\ldots,\tau_1-\tau)\mathcal{W}_\odot(-\tau),
\end{aligned}
\tag{B.7}
$$

and hence

$$
\begin{aligned}
& \mathcal{W}_\odot(-\tau)J^{(2n)}(\tau_{2n},\ldots,\tau_1) \\
= \quad & J^{(2n)}(\tau_{2n}-\tau,\ldots,\tau_1-\tau)\mathcal{W}_\odot(-\tau).
\end{aligned}
\tag{B.8}
$$

As a consequence, the kernel $\kappa_{curr,l}$ has the property

$$
\mathcal{W}_\odot(-s)\kappa_{curr,l}(t,s) \quad = \quad \kappa_{curr,l}(t-s,0)\mathcal{W}_\odot(-s), \tag{B.9}
$$

and we obtain the following memory equation:

$$Tr_R\{\hat{I}_l\hat{\rho}(t)\} \quad = \quad \int_{t_0}^{t} ds \quad K_{curr,l}(t-s)\hat{\rho}_{\odot}(s), \tag{B.10}$$

where the integral kernel $K_{curr,l}$ is given by

$$K_{curr,l}(\tau) \quad := \quad \mathcal{W}_{\odot}(-\tau)\kappa_{curr,l}(\tau,0) \quad = \quad \sum_{n=1}^{\infty} K_{curr,l}^{(2n)}(\tau), \tag{B.11}$$

with

$$K_{curr,l}^{(2)}(\tau) \quad := \quad \mathcal{W}_{\odot}(-\tau)J^{(2)}(\tau,0), \tag{B.12}$$

and for $n \geq 2$:

$$K_{curr,l}^{(2n)}(\tau) \quad := \quad \int \ldots \int_{0\leq s_2\leq\cdots\leq s_{2n-1}\leq\tau} J_{\tau_{(2)}}^{(2n-1)}(s_{2n-1},\ldots,s_2), \tag{B.13}$$

where

$$J_{\tau_{(2)}}^{(2n-1)}(s_{2n-1},\ldots,s_2) \quad := \quad \mathcal{W}_{\odot}(-\tau)J^{(2n)}(\tau,s_{2n-1},\ldots,s_2,0) \tag{B.14}$$

according to Eq. (B.6).

Appendix C

Decomposition of the Integral Kernel

C.1 Expansion of Commutators

We analyze now the kernels appearing in the quantum master equation and in the memory equation for the current, Eq. (2.45) and (2.50), respectively. Because the treatment of both kernels is analogous, we restrict ourselves to the analysis of the density matrix kernel. To study the density matrix kernel $K(\tau)$ (2.46), we go back to the recursive definition of the map $I^{(2n)}(\tau_{2n},\ldots,\tau_1)$ (2.33) whose integral gives $K(\tau)$. Hence, we examine first the map $A^{(2(n-m))}(\tau_{2n},\ldots,\tau_{2m+1})$ (2.30). (For a technical reason, we shall start out with this indexing rather than with "$A^{(2n)}(\tau_{2n},\ldots,\tau_1)$".) Note that for any $0 \leq m < n$, any sequence of times $0 \leq \tau_{2m+1} \cdots \leq \tau_{2n}$, and any linear map $\hat{y}$ operating on $V_\odot$:

$$A^{(2(n-m))}\left(\tau_{2n},\ldots,\tau_{2m+1}\right)\hat{y} \quad = \tag{C.1}$$

$$\begin{aligned} &= \quad Tr_R\Big\{\ \mathcal{L}(\tau_{2n})\ldots\mathcal{L}(\tau_{2m+1})(\hat{\rho}_R\otimes\hat{y})\Big\} \\ &= \quad \frac{(-1)^{n-m}}{\hbar^{2(n-m)}}\quad Tr_R\Big\{\ \Big[\ \hat{H}_T(\tau_{2n}),\ldots[\hat{H}_T(\tau_{2m+1}),\hat{\rho}_R\otimes\hat{y}]\ldots\Big]\ \Big\}\ , \end{aligned}$$

where, for any linear map $\hat{z}$ operating on the state vector space of the total system, we use the abbreviation

$$\hat{z}(\tau) \quad := \quad \mathcal{W}(\tau)\hat{z}, \tag{C.2}$$

with $\mathcal{W}(\tau)$ (2.18) the transformation applied to translate operators to the interaction picture. To make the notation more compact, we write the tunneling Hamiltonian (2.5) in the following analysis as

$$\hat{H}_T \quad = \quad \sum_{\nu \in \mathcal{I}} v_\nu \hat{C}_\nu \hat{D}_\nu, \tag{C.3}$$

with the index set

$$\mathcal{I} \quad := \quad \{(\eta, v) : \eta \in \mathcal{I}_o, v \in \{\pm 1\}\}, \tag{C.4}$$

where

$$\mathcal{I}_o \quad := \quad \{(l, \sigma, \mathbf{k}) : l \in \mathcal{L}, \sigma \in \mathcal{S}, \mathbf{k} \in \mathcal{K}_l\}. \tag{C.5}$$

For any $\nu = ((l, \sigma, \mathbf{k}), v) =: (\eta, v) \in \mathcal{I}$ we define:

$$v_\nu \quad := \quad v, \tag{C.6}$$

and

$$\hat{D}_{\eta,+1} \quad := \quad T_\eta \hat{d}_\sigma, \tag{C.7}$$
$$\hat{D}_{\eta,-1} \quad := \quad T_\eta^* \hat{d}_\sigma^\dagger, \tag{C.8}$$
$$\hat{C}_{\eta,+1} \quad := \quad \hat{c}_\eta^\dagger, \tag{C.9}$$
$$\hat{C}_{\eta,-1} \quad := \quad \hat{c}_\eta. \tag{C.10}$$

Upon expanding the commutator in Eq. (C.1), we obtain:

$$A^{(2(n-m))}(\tau_{2n}, \ldots, \tau_{2m+1})\hat{y} \quad = \tag{C.11}$$

$$\frac{(-1)^{n-m}}{\hbar^{2(n-m)}} \sum_{\nu_{2m+1}, \ldots, \nu_{2n} \in \mathcal{I}} \sum_{S : S \subset \{2m+1, 2m+2, \ldots, 2n\}}$$

$$(-1)^{|S|} \quad v_{\nu_{2m+1}} \ldots v_{\nu_{2n}} \quad Tr_R \Big\{$$

$$\left(\hat{C}_{\nu_{\varphi_S(1)}} \hat{D}_{\nu_{\varphi_S(1)}}\right)(\tau_{\varphi_S(1)})$$

$$\vdots$$

$$\left(\hat{C}_{\nu_{\varphi_S(|S|)}} \hat{D}_{\nu_{\varphi_S(|S|)}}\right)(\tau_{\varphi_S(|S|)})$$

$$(\hat{\rho}_R \otimes \hat{y})$$

$$\left(\hat{C}_{\nu_{\varphi_S(|S|+1)}} \hat{D}_{\nu_{\varphi_S(|S|+1)}}\right)(\tau_{\varphi_S(|S|+1)})$$

$$\vdots$$

$$\left(\hat{C}_{\nu_{\varphi_S(2(n-m))}} \hat{D}_{\nu_{\varphi_S(2(n-m))}}\right)(\tau_{\varphi_S(2(n-m))}) \Big\},$$

where we have applied the formula

$$\left[\hat{z}_N, \left[\hat{z}_{N-1} \dots [\hat{z}_{M+1}, \hat{z}] \dots\right]\right] \quad = \tag{C.12}$$

$$= \sum_{S:S\subset\{M+1,\dots,N\}} (-1)^{N-M-|S|} \left(\hat{z}_{\varphi_S(1)} \dots \hat{z}_{\varphi_S(|S|)}\right) \left(\hat{z}\right) \left(\hat{z}_{\varphi_S(|S|+1)} \dots \hat{z}_{\varphi_S(N-M)}\right).$$

Definition of the Map φ_S:

For any subset $S \subset \{M+1, \dots, N\}$ with a number of $|S|$ elements we define the map

$$\varphi_S = \varphi^{(N)}_{(M+1)_S} : \quad \{1, \dots, N-M\} \quad \to \quad \{M+1, \dots, N\} \tag{C.13}$$

as the one which maps

$$\varphi_S \{1, \dots, |S|\} = S \tag{C.14}$$

in decreasing order, and

$$\varphi_S \{|S|+1, \dots, N-M\} = S^c \tag{C.15}$$

in increasing order, where $S^c := \{M+1, \dots, N\} \setminus S$, so:

$$\begin{aligned} \varphi_S(\quad 1 \quad) &:= \max(S), \quad \text{if } S \neq \emptyset, \\ \varphi_S(j+1) &:= \max\left(S \setminus \{\varphi_S(i) : i = 1, 2, \dots, j\}\right), \\ &\quad \text{for } j \in \{1, 2, \dots, |S|-1\}, \end{aligned} \tag{C.16}$$

and:

$$\begin{aligned} \varphi_S(|S| \ + \ 1) &:= \min(S^c), \quad \text{if } S^c \neq \emptyset, \\ \varphi_S(|S|+j+1) &:= \min\left(S^c \setminus \{\varphi_S(|S|+i) : i = 1, 2, \dots, j\}\right), \\ &\quad \text{for } j \in \{1, 2, \dots, |S^c|-1\}. \end{aligned} \tag{C.17}$$

(For brevity we shall omit the number-indices in "$\varphi^{(N)}_{(M+1)_S}$", and thus write "φ_S" instead, as long as the value of the indices is unambiguous.)

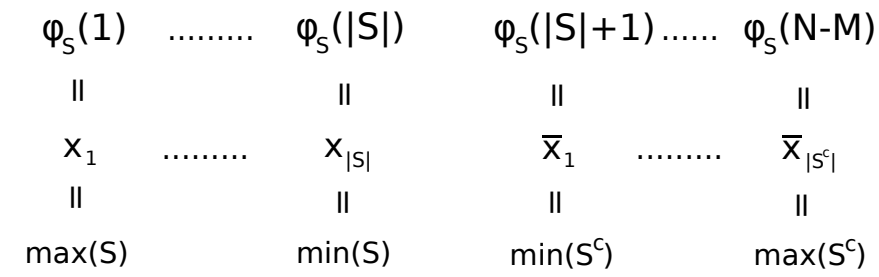

Figure C.1: Let $x_1, \ldots, x_{|S|}$ be a list of the elements of the set $S \subset \{M+1, \ldots, N\}$ in decreasing order, and let $\overline{x}_1, \ldots, \overline{x}_{|S^c|}$ be a list of the elements of the set's complement $S^c := \{M+1, \ldots, N\} \setminus S$ in increasing order. The present figure then shows a complete list of the numbers in the image-set of φ_S in the order in which they are "counted" by the map φ_S.

For the purpose of taking the reduced operator in Eq. (C.11), we define to any $\nu \in \mathcal{I}$:

$$\hat{\mathrm{C}}_\nu := \hat{C}_\nu|_{V_R}, \tag{C.18}$$
$$\hat{\mathrm{D}}_\nu := \hat{D}_\nu|_{V_\odot}, \tag{C.19}$$

and write

$$\hat{C}_\nu = \hat{\mathrm{C}}_\nu \otimes \hat{1}_\odot, \tag{C.20}$$
$$\hat{D}_\nu = \hat{\mathrm{P}}_R \otimes \hat{\mathrm{D}}_\nu, \tag{C.21}$$

where we apply the concrete realization of the present product of operators, as well as of creation- and annihilation operators in App. A (Product States), Eqs. (A.12), (A.15), (A.17), (A.18).

We define the maps

$$\hat{\mathrm{P}}_R : \quad V_R \to V_R, \tag{C.22}$$
$$\hat{1}_\odot : \quad V_\odot \to V_\odot \tag{C.23}$$

as

$$\hat{\mathrm{P}}_R := e^{i\pi \hat{N}_R|_{V_R}}, \tag{C.24}$$

with $\hat{N}_R$ the particle-counting operator of the reservoirs (2.27), and as the identity on $V_\odot$, respectively. In particular,

$$\hat{\mathrm{P}}_R(\psi) \quad = \quad (-1)^N\psi, \text{ if } \hat{N}_R\psi = N\psi. \tag{C.25}$$

With the notation

$$\hat{x}(\tau) \quad := \quad \mathcal{W}_R(\tau)\hat{x}, \tag{C.26}$$
$$\hat{y}(\tau) \quad := \quad \mathcal{W}_\odot(\tau)\hat{y}, \tag{C.27}$$

for linear maps $\hat{x}$ and $\hat{y}$ operating on V_R and on $V_\odot$, respectively, where the transform $\mathcal{W}_R(\tau)\hat{x}$ is defined analogous to the definition of $\mathcal{W}_\odot$ (2.19), i.e.,

$$\mathcal{W}_R(\tau)\hat{x} \quad := \quad e^{\frac{i}{\hbar}\hat{H}_R|_{V_R}\tau} \quad \hat{x} \quad e^{-\frac{i}{\hbar}\hat{H}_R|_{V_R}\tau}, \tag{C.28}$$

we obtain:

$$\left(\hat{C}_\nu\hat{D}_\nu\right)(\tau) \quad = \quad \left[\left(\hat{\mathrm{C}}_\nu\hat{\mathrm{P}}_R\right)(\tau)\right] \otimes \left[\hat{\mathrm{D}}_\nu(\tau)\right]. \tag{C.29}$$

By the anti-commutation relation

$$\hat{\mathrm{C}}_\nu\hat{\mathrm{P}}_R \quad = \quad -\hat{\mathrm{P}}_R\hat{\mathrm{C}}_\nu \tag{C.30}$$

we can rewrite the contributions to the sum within Eq. (C.11) as

$$\begin{aligned}
&(-1)^{|S|} \quad v_{\nu_{2m+1}} \dots v_{\nu_{2n}} \quad Tr_R\Big\{ \\
&\left(\hat{C}_{\nu_{\varphi_S(1)}}\hat{D}_{\nu_{\varphi_S(1)}}\right)(\tau_{\varphi_S(1)}) \dots \left(\hat{C}_{\nu_{\varphi_S(|S|)}}\hat{D}_{\nu_{\varphi_S(|S|)}}\right)(\tau_{\varphi_S(|S|)}) \\
&\qquad (\hat{\rho}_R \otimes \hat{y}) \\
&\left(\hat{C}_{\nu_{\varphi_S(|S|+1)}}\hat{D}_{\nu_{\varphi_S(|S|+1)}}\right)(\tau_{\varphi_S(|S|+1)}) \\
&\qquad \dots \qquad \left(\hat{C}_{\nu_{\varphi_S(2(n-m))}}\hat{D}_{\nu_{\varphi_S(2(n-m))}}\right)(\tau_{\varphi_S(2(n-m))}) \quad \Big\}
\end{aligned}$$

$$
\begin{aligned}
= \quad & (-1)^{|S|} \quad v_{\nu_{2m+1}} \dots v_{\nu_{2n}} \quad (-1)^{n-m} \\
& \exp\left(\frac{i}{\hbar}\left(\tau_{2m+1}\varepsilon_{\nu_{2m+1}} + \dots + \tau_{2n}\varepsilon_{\nu_{2n}}\right)\right) \\
& Tr\Big\{\hat{\mathrm{C}}_{\nu_{\varphi_S(|S|+1)}} \dots \hat{\mathrm{C}}_{\nu_{\varphi_S(2(n-m))}} \\
& \qquad \hat{\mathrm{C}}_{\nu_{\varphi_S(1)}} \dots \hat{\mathrm{C}}_{\nu_{\varphi_S(|S|)}} \quad \hat{\rho}_R\Big\} \\
& \hat{\mathrm{D}}_{\nu_{\varphi_S(1)}}\left(\tau_{\varphi_S(1)}\right) \dots \hat{\mathrm{D}}_{\nu_{\varphi_S(|S|)}}\left(\tau_{\varphi_S(|S|)}\right) \\
& \qquad \hat{y} \\
& \hat{\mathrm{D}}_{\nu_{\varphi_S(|S|+1)}}\left(\tau_{\varphi_S(|S|+1)}\right) \dots \hat{\mathrm{D}}_{\nu_{\varphi_S(2(n-m))}}\left(\tau_{\varphi_S(2(n-m))}\right) \quad , \qquad \text{(C.31)}
\end{aligned}
$$

where we use the cyclicity of the trace, and the relation

$$\hat{\mathrm{C}}_\nu(\tau) \quad = \quad e^{\frac{i}{\hbar}\tau\varepsilon_\nu}\hat{\mathrm{C}}_\nu. \qquad \text{(C.32)}$$

For $\nu = ((l,\sigma,\mathbf{k}),v) \in \mathcal{I}$ (C.4) we define

$$\varepsilon_\nu \quad := \quad v\varepsilon_{l\sigma\mathbf{k}}, \qquad \text{(C.33)}$$

where $\varepsilon_{l\sigma\mathbf{k}}$ are the energies assigned to the electron levels in the reservoirs, Eq. (2.2).

Proof of Eq. (C.32):

Let an element $\nu_0 = ((l_0,\sigma,\mathbf{k}_0),v_0) = (\eta_0,v_0) \in \mathcal{I}$, as well as a subset M of the set $\mathcal{I}_o$ (C.5) of all one-electron levels in the leads be fixed and given. Let the many-electron state "$\pi(M)$" of the leads be defined by the condition that all one-electron levels within M are occupied, while the rest is non-occupied (Sec. A.3). We note:

$$
\begin{aligned}
\hat{\mathrm{C}}_{\nu_0}(\tau)\left(\pi(M)\right) \quad &= \quad \exp\left(\frac{i}{\hbar}\tau\hat{H}_R|_{V_R}\right)\hat{\mathrm{C}}_{\nu_0}\exp\left(-\frac{i}{\hbar}\tau\hat{H}_R|_{V_R}\right)\left(\pi(M)\right) \\
&= \quad \exp\left(\frac{i}{\hbar}\tau\hat{H}_R|_{V_R}\right)\hat{\mathrm{C}}_{\nu_0}\left(\pi(M)\right)\exp\left(-\frac{i}{\hbar}\tau\sum_{\eta\in M}\varepsilon_\eta\right).
\end{aligned}
\qquad \text{(C.34)}
$$

Distinguishing between the cases

$$(v_0 = +1 \text{ and } \eta_0 \in M) \text{ or } (v_0 = -1 \text{ and } \eta_0 \notin M), \qquad \text{(C.35)}$$

and

$$(v_0 = +1 \text{ and } \eta_0 \notin M) \text{ or } (v_0 = -1 \text{ and } \eta_0 \in M), \tag{C.36}$$

we obtain the equality

$$\hat{\mathrm{C}}_{\nu_0}(\tau)\,(\pi(M)) \;=\; \exp\left(\frac{i}{\hbar}\tau\varepsilon_{\nu_0}\right)\hat{\mathrm{C}}_{\nu_0}\,(\pi(M))\,, \tag{C.37}$$

and, thus, Eq. (C.32) is shown. □

C.2 Evaluation of Traces

To evaluate the trace appearing on the right-hand side of Eq. (C.31), we make the present excursion with abstract terms and equations. For any sequence of indices $\mu_1, \ldots, \mu_m \in \mathcal{I}$ (C.4) we abbreviate:

$$\langle \hat{\mathrm{C}}_{\mu_1} \ldots \hat{\mathrm{C}}_{\mu_m} \rangle \quad := \quad Tr\{\hat{\mathrm{C}}_{\mu_1} \ldots \hat{\mathrm{C}}_{\mu_m} \hat{\rho}_R\}. \tag{C.38}$$

Independence of Occupation Probabilities

In the density matrix $\hat{\rho}_R$ (2.7), the probabilities of finding one-electron levels within an arbitrary selection occupied or non-occupied are independent; this independence is contained in Eq. (C.87). We here first show the equality:

$$\langle \hat{\mathrm{C}}_{\nu_1} \ldots \hat{\mathrm{C}}_{\nu_n} \rangle \quad = \quad \sum_{j=2}^{n} (-1)^j \langle \hat{\mathrm{C}}_{\nu_1} \hat{\mathrm{C}}_{\nu_j} \rangle \langle \hat{\mathrm{C}}_{\nu_2} \ldots \hat{\mathrm{C}}_{\nu_{j-1}} \hat{\mathrm{C}}_{\nu_{j+1}} \ldots \hat{\mathrm{C}}_{\nu_n} \rangle, \tag{C.39}$$

which holds for any selection of indices $\nu_1, \ldots, \nu_n \in \mathcal{I}$.

Proof:

Let the left- and right-hand sides of Eq. (C.39) be denoted by $F(\nu_1, \ldots, \nu_n)$ and $G(\nu_1, \ldots, \nu_n)$, respectively; to any index $\nu = ((l, \sigma, \mathbf{k}), v) \in \mathcal{I}$ we define the complementary index:

$$\overline{\nu} \quad := \quad ((l, \sigma, \mathbf{k}), (-1)v). \tag{C.40}$$

We note that, if for any $i_0 \in \{2, \ldots, n-1\}$ we have

$$\nu_{i_0+1} \quad \neq \quad \nu_{i_0}, \overline{\nu}_{i_0}, \tag{C.41}$$

then follows

$$\begin{array}{rcl} F(\nu_1, \ldots, \nu_{i_0-1}, \nu_{i_0}, \nu_{i_0+1}, \nu_{i_0+2}, \ldots, \nu_n) & = & \\ (-1) \quad F(\nu_1, \ldots, \nu_{i_0-1}, \nu_{i_0+1}, \nu_{i_0}, \nu_{i_0+2}, \ldots, \nu_n), & & \end{array} \tag{C.42}$$

as well as

$$\begin{array}{rcl} G(\nu_1, \ldots, \nu_{i_0-1}, \nu_{i_0}, \nu_{i_0+1}, \nu_{i_0+2}, \ldots, \nu_n) & = & \\ (-1) \quad G(\nu_1, \ldots, \nu_{i_0-1}, \nu_{i_0+1}, \nu_{i_0}, \nu_{i_0+2}, \ldots, \nu_n). & & \end{array} \tag{C.43}$$

Hence, we assume without loss of generality that the indices $\nu_1, \ldots, \nu_n$ are ordered (cp. Fig. C.2): There is $k \geq 1$, and a sequence

$$1 < n_1 < n_2 < \cdots < n_k = n, \tag{C.44}$$

such, that with

$$\begin{array}{rcll} m_r & := & n_{r-1} + 1 & (\text{for } r \in \{1, \ldots, k\}, \\ & & & \text{where } n_0 := 0), \end{array} \tag{C.45}$$

and with

$$s_r \quad := \quad n_r - m_r \tag{C.46}$$

we have:

$$\left\{ \begin{array}{c} \text{For any } r \in \{1, \ldots, k\} : \\ \nu_{m_r}, \nu_{m_r+1}, \ldots, \nu_{m_r+s_r} \quad \in \{\nu_{m_r}, \overline{\nu}_{m_r}\}, \end{array} \right\} \tag{C.47}$$

$$\left\{ \begin{array}{c} \text{and for any further } r' \in \{1, \ldots, k\} : \\ r \neq r' \quad \Rightarrow \quad \{\nu_{m_r}, \overline{\nu}_{m_r}\} \cap \{\nu_{m_{r'}}, \overline{\nu}_{m_{r'}}\} \quad = \quad \emptyset. \end{array} \right\} \tag{C.48}$$

In case there is $r \in \{1, \ldots, k\}$, such, that the number of operators

$$t_r \quad := \quad s_r + 1 \quad \text{is odd}, \tag{C.49}$$

we note that both sides of Eq. (C.39) are zero: For any

$$\nu \quad = \quad ((l, \sigma, \mathbf{k}), v) \quad = \quad (\eta, v) \in \mathcal{I} \tag{C.50}$$

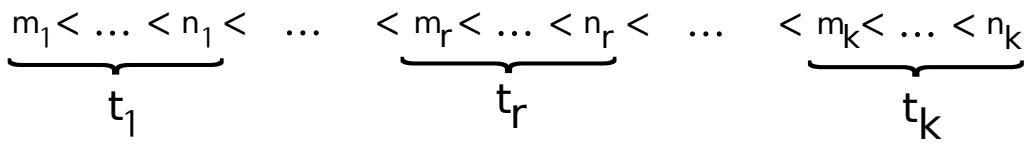

Figure C.2: The numbers $1 = m_1 < \cdots < n_k = n$ in increasing natural order. By our first reduction-step within the proof of Eq. (C.39), we achieve a situation, where the operators $\hat{\mathrm{C}}_{\nu_1} \ldots \hat{\mathrm{C}}_{\nu_n}$ are grouped as follows: There are blocks of indices $m_r, m_r+1, \ldots, n_r$ such, that for any i, j within the same block, the indices $\nu_i, \nu_j \in \mathcal{I}$ (Def. (C.4)) are either complementary or equal, i.e., $\nu_i \in \{\nu_j, \overline{\nu}_j\}$. By further reduction-steps we can assume without restriction of generality, that the number t_r of operators within each block is even, and that, within each block, operators of creation and annihilation appear in alternating order.

we define

$$\hat{\mathrm{N}}_\eta \quad := \quad \hat{c}^\dagger_{l\sigma\mathbf{k}} \hat{c}_{l\sigma\mathbf{k}}|_{V_R}, \tag{C.51}$$

and for $\lambda \in \mathbb{R}$:

$$\mathrm{eig}(\hat{\mathrm{N}}_\eta, \lambda) \quad := \quad \ker\{\hat{\mathrm{N}}_\eta - \lambda \hat{1}_R\}, \tag{C.52}$$

with $\hat{1}_R : V_R \to V_R$ the identity-map on V_R. The relations

$$\begin{aligned} \hat{\mathrm{C}}_{\eta,+1} \left\{ \mathrm{eig}(\hat{\mathrm{N}}_\eta, 0) \right\} &= \mathrm{eig}(\hat{\mathrm{N}}_\eta, 1), && \text{(C.53)} \\ \hat{\mathrm{C}}_{\eta,+1} \left\{ \mathrm{eig}(\hat{\mathrm{N}}_\eta, 1) \right\} &= \{0\}, \\ \hat{\mathrm{C}}_{\eta,-1} \left\{ \mathrm{eig}(\hat{\mathrm{N}}_\eta, 1) \right\} &= \mathrm{eig}(\hat{\mathrm{N}}_\eta, 0), && \text{(C.54)} \\ \hat{\mathrm{C}}_{\eta,-1} \left\{ \mathrm{eig}(\hat{\mathrm{N}}_\eta, 0) \right\} &= \{0\}, \end{aligned}$$

imply, that for any odd number t of elements $v_1, \ldots, v_t \in \{\pm 1\}$ and any $\lambda \in \{0, 1\}$:

$$\hat{\mathrm{C}}_{(\eta,v_1)} \ldots \hat{\mathrm{C}}_{(\eta,v_t)} \left\{ \mathrm{eig}(\hat{\mathrm{N}}_\eta, \lambda) \right\} \quad \perp \quad \mathrm{eig}(\hat{\mathrm{N}}_\eta, \lambda). \tag{C.55}$$

For any $\eta' \in \mathcal{I}_o$ (C.5) with $\eta' \neq \eta$, the operators $\hat{\mathrm{C}}_{\eta',\pm 1}$ map both of the eigenspaces of $\hat{\mathrm{N}}_\eta$ to themselves, hence we obtain under the condition (C.49):

$$F(\nu_1, \ldots, \nu_n) \quad = 0 = \quad G(\nu_1, \ldots, \nu_n). \tag{C.56}$$

Thus, we assume without loss of generality, that each of the numbers of operators t_r (C.49) is even. Note that, if for any $i_0 \in \{2, \ldots, n-1\}$ we have

$$\nu_{i_0+1} \quad = \quad \nu_{i_0}, \tag{C.57}$$

then

$$F(\nu_1, \ldots, \nu_n) \quad = 0 = \quad G(\nu_1, \ldots, \nu_n). \tag{C.58}$$

Hence, we assume additionally without loss of generality, that for any $r \in \{1, \ldots, k\}$ and $i \in \{0, \ldots, s_r - 1\}$ with

$$(r, i) \quad \neq \quad (1, 0), \tag{C.59}$$

the relation

$$\nu_{m_r+i+1} \quad = \quad \overline{\nu}_{m_r+i}. \tag{C.60}$$

is satisfied. Separately, consider the case that

$$\nu_2 = \nu_{m_1+1} \quad = \quad \nu_{m_1} = \nu_1. \tag{C.61}$$

We note that then

$$(\nu_{m_1}, \nu_{m_1+1}, \ldots, \nu_{m_1+s_1}) \quad = \quad (\nu_1, \nu_1, \overline{\nu_1}, \nu_1, \ldots, \overline{\nu_1}, \nu_1), \tag{C.62}$$

and hence

$$\begin{aligned} G(\nu_1, \ldots, \nu_n) \;=\; & \left\langle \hat{\mathrm{C}}_{\nu_1} \hat{\mathrm{C}}_{\nu_1} \right\rangle \left\langle \hat{\mathrm{C}}^\dagger_{\nu_1} \ldots \right\rangle \\ & - \left\langle \hat{\mathrm{C}}_{\nu_1} \hat{\mathrm{C}}^\dagger_{\nu_1} \right\rangle \left\langle \hat{\mathrm{C}}_{\nu_1} \hat{\mathrm{C}}_{\nu_1} \ldots \right\rangle \\ & + \quad \ldots \\ & - \quad \ldots \\ & + \left\langle \hat{\mathrm{C}}_{\nu_1} \hat{\mathrm{C}}_{\nu_1} \right\rangle \left\langle \hat{\mathrm{C}}_{\nu_1} \hat{\mathrm{C}}^\dagger_{\nu_1} \ldots \right\rangle \\ = \; 0 \quad = \quad & F(\nu_1, \ldots, \nu_n). \end{aligned} \tag{C.63}$$

Finally, the equality $F(\nu_1, \ldots, \nu_n) = G(\nu_1, \ldots, \nu_n)$ remains to be shown under the condition that the restrictions according to (C.47), (C.48) with an even number t_r of creation- or annihilation operators of each level, Eq. (C.49), are valid, and that for any $r \in \{1, \ldots, k\}$, and $i \in \{0, \ldots, s_r - 1\}$ the alternation-condition

$$\nu_{m_r+i+1} \quad = \quad \overline{\nu}_{m_r+i}. \tag{C.64}$$

is satisfied. Note that, if we define to any $\eta \in \mathcal{I}_o$:

$$\begin{aligned} E_{\eta,+1} &:= \mathrm{eig}(\hat{\mathrm{N}}_\eta, 1), \\ E_{\eta,-1} &:= \mathrm{eig}(\hat{\mathrm{N}}_\eta, 0), \end{aligned} \tag{C.65}$$

then follows for any $\nu = (\eta, v) \in \mathcal{I}$:

$$\hat{\mathrm{C}}_\nu \hat{\mathrm{C}}_{\overline{\nu}} = \hat{\mathrm{Pr}}_\perp(E_\nu), \tag{C.66}$$

where $\hat{\mathrm{Pr}}_\perp(E_\nu)$ is the orthogonal projector onto E_ν. By the relation (C.75) we obtain:

$$F(\nu_1, \ldots, \nu_n) = Tr\left\{\hat{\mathrm{C}}_{\nu_1}\hat{\mathrm{C}}_{\overline{\nu}_1}\mathrm{Pr}_\perp(E)\,\hat{\rho}_R\right\}, \tag{C.67}$$

$$G(\nu_1, \ldots, \nu_n) = Tr\left\{\hat{\mathrm{C}}_{\nu_1}\hat{\mathrm{C}}_{\overline{\nu}_1}\hat{\rho}_R\right\} \quad Tr\left\{\hat{\mathrm{Pr}}_\perp(E)\,\hat{\rho}_R\right\}, \tag{C.68}$$

with

$$E := E_{\nu_{m_2}} \cap \cdots \cap E_{\nu_{m_k}}. \tag{C.69}$$

Note that the density matrix $\hat{\rho}_R$ of the reservoirs in thermal equilibrium, given by (2.7), and (2.8), has the representation

$$\hat{\rho}_R = \frac{1}{\mathcal{N}} \prod_{\eta \in \mathcal{I}_o} \exp\left(-\beta_\eta \hat{\mathrm{N}}_\eta\right), \tag{C.70}$$

where for $\eta = (l, \sigma, \mathbf{k}) \in \mathcal{I}_o$:

$$\beta_\eta := \frac{1}{k_B T}\left(\varepsilon_{l\sigma\mathbf{k}} - \mu_{l\sigma}\right), \tag{C.71}$$

and

$$\mathcal{N} := \prod_{\eta \in \mathcal{I}_o} \left\{1 + \exp\left(-\beta_\eta\right)\right\}. \tag{C.72}$$

With the notation

$$\beta_\nu := v\beta_\eta \tag{C.73}$$

(for any $\nu = (l, \sigma, \mathbf{k}, v) = (\eta, v) \in \mathcal{I}$) we note

$$\hat{\rho}_R \hat{\mathrm{C}}_\nu = e^{-\beta_\nu}\hat{\mathrm{C}}_\nu \hat{\rho}_R. \tag{C.74}$$

By the cyclicity of the trace, and with the sum-rule

$$\hat{\mathrm{C}}_{\nu_1}\hat{\mathrm{C}}_{\overline{\nu}_1} \quad + \quad \hat{\mathrm{C}}_{\overline{\nu}_1}\hat{\mathrm{C}}_{\nu_1} \quad = \quad \hat{1}_R \tag{C.75}$$

we get the equation

$$\begin{aligned} Tr\left\{\hat{\mathrm{C}}_{\nu_1}\hat{\mathrm{C}}_{\overline{\nu}_1}\mathrm{Pr}_\perp(E)\hat{\rho}_R\right\} \quad &= \quad e^{-\beta_{\nu_1}}\Big[Tr\left\{\hat{\mathrm{Pr}}_\perp(E)\hat{\rho}_R\right\} \\ &- \quad Tr\left\{\hat{\mathrm{C}}_{\nu_1}\hat{\mathrm{C}}_{\overline{\nu}_1}\hat{\mathrm{Pr}}_\perp(E)\hat{\rho}_R\right\}\Big], \end{aligned} \tag{C.76}$$

hence

$$Tr\left\{\hat{\mathrm{C}}_{\nu_1}\hat{\mathrm{C}}_{\overline{\nu}_1}\hat{\mathrm{Pr}}_\perp(E)\hat{\rho}_R\right\} \quad = \quad f(\beta_{\nu_1})\; Tr\left\{\hat{\mathrm{Pr}}_\perp(E)\hat{\rho}_R\right\}, \tag{C.77}$$

where

$$f(x) \quad := \quad \frac{1}{1+e^x} \tag{C.78}$$

is the parameter-free Fermi-Dirac distribution, and in particular for any $\nu \in \mathcal{I}$:

$$\langle\hat{\mathrm{C}}_\nu\hat{\mathrm{C}}_{\overline{\nu}}\rangle \quad := \quad Tr\left\{\hat{\mathrm{C}}_\nu\hat{\mathrm{C}}_{\overline{\nu}}\hat{\rho}_R\right\} \quad = \quad f(\beta_\nu). \tag{C.79}$$

Upon applying Eq. (C.67) and (C.68), we arrive at the equality

$$F(\nu_1,\ldots,\nu_n) \quad = \quad G(\nu_1,\ldots,\nu_n). \quad \square$$

Pair Formations

Let M be a set with an even number of elements, $|M| = 2n$. We define

$$\mathbb{P}_2(M) \quad := \quad \{M' : \quad M' \subset M, |M'| = 2\}, \tag{C.80}$$

as well as the set $PF(M)$ of *pair formations* on M as the set of all selections $\mathcal{P} \subset \mathbb{P}_2(M)$ with the property that M is the disjoint union of all sets in $\mathcal{P}$,

$$PF(M) \; := \; \{\mathcal{P} \subset \mathbb{P}_2(M) : |\mathcal{P}| = n, \cup_{M'\in\mathcal{P}} M' = M\}. \tag{C.81}$$

Let $<$ be a strict total order on the set M (as for example the natural order on a set of real numbers); we define to each $\mathcal{P} \in PF(M)$, and $M' \in \mathcal{P}$:

$$\begin{array}{rcl} p(M',<) & := & \min(M',<), \\ q(M',<) & := & \max(M',<), \end{array} \tag{C.82}$$

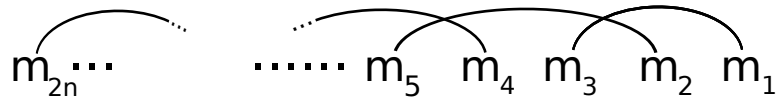

Figure C.3: All the $2n$ elements of the totally ordered set M are arranged along one straight line, according to their order. For each of the elements $M' \in \mathcal{P}$ within a particular pair formation $\mathcal{P} \in PF(M)$, a bent line connecting $p(M', <)$, and $q(M', <)$, is drawn in one chosen half-plane of the paper plane. The total number of intersections of these connecting-lines then differs from the defined quantity $N(\mathcal{P}, <)$ by an even number, and so the pair formation's sign (C.84) can be deduced from a graphic representation.

the minimum and maximum of M' with respect to the order $<$; we define

$$\begin{aligned} N(\mathcal{P}, <) \quad := \quad & |\big\{(M_1, M_2) : \quad M_1, M_2 \in \mathcal{P}, \\ & p(M_1, <) < p(M_2, <) < q(M_1, <) < q(M_2, <)\big\}|, \end{aligned} \tag{C.83}$$

the number of intersections of connecting lines in a graphic representation of the pair formation according to Fig. C.3, and:

$$\mathrm{sign}(\mathcal{P}, <) \quad := \quad (-1)^{N(\mathcal{P}, <)}. \tag{C.84}$$

Analysis of Traces by Pair Formations

Let

$$m_1, m_2, \ldots, m_{2n} \tag{C.85}$$

be the list of all elements in M in strictly increasing order with respect to $<$, and assume we have a sequence of elements

$$\nu_{m_1}, \quad \ldots \quad , \nu_{m_{2n}} \quad \in \mathcal{I}, \tag{C.86}$$

with $\mathcal{I}$ the index set of Def. (C.4). Then, the equality

$$\left\langle \hat{\mathrm{C}}_{\nu_{m_1}} \ldots \hat{\mathrm{C}}_{\nu_{m_{2n}}} \right\rangle = \sum_{\mathcal{P} \in PF(M)} \mathrm{sign}(\mathcal{P}, <) \prod_{M' \in \mathcal{P}} \left\langle \hat{\mathrm{C}}_{\nu_{p(M', <)}} \hat{\mathrm{C}}_{\nu_{q(M', <)}} \right\rangle \tag{C.87}$$

holds.

For a proof of Eq. (C.87), we perform induction over n; for $n = 2$ the equation is obviously true. Note that, if

$$|M| \quad = \quad 2n + 2, \tag{C.88}$$

then we obtain with Eq. (C.39), and the induction hypothesis:

$$\begin{aligned} \left\langle \hat{\mathrm{C}}_{\nu_{m_1}} \dots \hat{\mathrm{C}}_{\nu_{m_{2n+2}}} \right\rangle \quad &= \quad \sum_{j=2}^{2n+2} (-1)^j \left\langle \hat{\mathrm{C}}_{\nu_{m_1}} \hat{\mathrm{C}}_{\nu_{m_j}} \right\rangle \\ &\quad \left\langle \hat{\mathrm{C}}_{\nu_{m_2}} \dots \hat{\mathrm{C}}_{\nu_{m_{j-1}}} \hat{\mathrm{C}}_{\nu_{m_{j+1}}} \dots \hat{\mathrm{C}}_{\nu_{m_{2n+2}}} \right\rangle \end{aligned} \tag{C.89}$$

$$\begin{aligned} &= \quad \sum_{j=2}^{2n+2} (-1)^j \left\langle \hat{\mathrm{C}}_{\nu_{m_1}} \hat{\mathrm{C}}_{\nu_{m_j}} \right\rangle \\ &\quad \sum_{\mathcal{P} \in PF(M \setminus \{m_1, m_j\})} \mathrm{sign}(\mathcal{P}, <) \prod_{M' \in \mathcal{P}} \left\langle \hat{\mathrm{C}}_{\nu_{p(M',<)}} \hat{\mathrm{C}}_{\nu_{q(M',<)}} \right\rangle \\ &= \quad \sum_{j=2}^{2n+2} \quad \sum_{\mathcal{P} \in PF(M \setminus \{m_1, m_j\})} (-1)^j \quad \mathrm{sign}(\mathcal{P}, <) \\ &\quad \prod_{M' \in \mathcal{P}_j} \left\langle \hat{\mathrm{C}}_{\nu_{p(M',<)}} \hat{\mathrm{C}}_{\nu_{q(M',<)}} \right\rangle, \end{aligned}$$

where $\mathcal{P}_j := \mathcal{P} \cup \{\{m_1, m_j\}\}$ for any $\mathcal{P} \in PF(M \setminus \{m_1, m_j\})$. With

$$\begin{aligned} N_1(\mathcal{P}) \quad &:= \quad \left| \{M' \in \mathcal{P} : 1 < p(M', <) < j < q(M', <)\} \right|, \\ N_2(\mathcal{P}) \quad &:= \quad \left| \{M' \in \mathcal{P} : 1 < p(M', <) < q(M', <) < j\} \right|, \end{aligned} \tag{C.90}$$

the equality

$$j - 2 \quad = \quad N_1(\mathcal{P}) + 2N_2(\mathcal{P}) \tag{C.91}$$

holds, and hence

$$(-1)^j \quad = \quad (-1)^{N_1(\mathcal{P})}, \tag{C.92}$$

which implies, that

$$\mathrm{sign}(\mathcal{P}_j, <) \quad = \quad (-1)^j \quad \mathrm{sign}(\mathcal{P}, <). \tag{C.93}$$

In summary, we obtain

$$\left\langle \hat{\mathrm{C}}_{\nu_{m_1}} \dots \hat{\mathrm{C}}_{\nu_{m_{2n+2}}} \right\rangle = \sum_{j=2}^{2n+2} \sum_{\mathcal{P}\in PF(M\setminus\{m_1,m_j\})} \mathrm{sign}(\mathcal{P}_j,<) \prod_{M'\in\mathcal{P}_j} \left\langle \hat{\mathrm{C}}_{\nu_{p(M',<)}} \hat{\mathrm{C}}_{\nu_{q(M',<)}} \right\rangle, \tag{C.94}$$

which makes the induction step for the proof of Eq. (C.87) complete. □

C.3 Irreducibility of Contributions to the Kernel

Within the present Section, we carry out the detailed steps and equations which show that the contributions to the integral kernel are *irreducible*.

Expansion by Pair Formations

We start out with an expansion as sum over pair formations: The map $A^{(2(n-m))}(\tau_{2n},\dots,\tau_{2m+1})$ (C.11, C.31) has a decomposition

$$\begin{aligned} & A^{(2(n-m))}(\tau_{2n},\dots,\tau_{2m+1}) \\ = & \sum_{\mathcal{P}\in PF\{2m+1,\dots,2n\}} A^{(2(n-m))}_{\mathcal{P}}(\tau_{2n},\dots,\tau_{2m+1}), \end{aligned} \tag{C.95}$$

where the sum goes over all pair formations on the set of natural numbers between $2m+1$ and $2n$.

To show this, we apply the result of Eq. (C.87) to the trace on the right-hand side of Eq. (C.31); we obtain:

$$\begin{aligned}
&\Big\langle \hat{\mathrm{C}}_{\nu_{\varphi^{(2n)}_{(2m+1)_S}(|S|+1)}} \dots \hat{\mathrm{C}}_{\nu_{\varphi^{(2n)}_{(2m+1)_S}(2(n-m))}} \\
&\hat{\mathrm{C}}_{\nu_{\varphi^{(2n)}_{(2m+1)_S}(1)}} \dots \hat{\mathrm{C}}_{\nu_{\varphi^{(2n)}_{(2m+1)_S}(|S|)}} \Big\rangle \quad = \\
&\left\langle \hat{\mathrm{C}}_{\nu_{\psi^{(2n)}_{(2m+1)_S}(1)}} \dots \hat{\mathrm{C}}_{\nu_{\psi^{(2n)}_{(2m+1)_S}(2(n-m))}} \right\rangle \quad = \\
&\sum_{\mathcal{P}\in PF\{2m+1,\dots,2n\}} \operatorname{sign}\left(\mathcal{P}, <_{\psi^{(2n)}_{(2m+1)_S}}\right) \\
&\prod_{M'\in\mathcal{P}} \left\langle \hat{\mathrm{C}}_{\nu_{p\left(M',<_{\psi^{(2n)}_{(2m+1)_S}}\right)}} \hat{\mathrm{C}}_{\nu_{q\left(M',<_{\psi^{(2n)}_{(2m+1)_S}}\right)}} \right\rangle,
\end{aligned} \tag{C.96}$$

where for clarity we have now *not* omitted the indices in $\varphi^{(2n)}_{(2m+1)_S} = \varphi_S$ (C.13), and where the map

$$\psi^{(2n)}_{(2m+1)_S}: \quad \{1,\dots,2(n-m)\} \to \{2m+1,\dots,2n\} \tag{C.97}$$

is defined as the composition of maps

$$\psi^{(2n)}_{(2m+1)_S} \quad := \quad \varphi^{(2n)}_{(2m+1)_S} \circ \zeta^{|S|}_{(+)}, \tag{C.98}$$

with $\zeta_{(+)}$ the cyclic permutation

$$\begin{aligned}
\zeta_{(+)}: \quad \{1,\dots,2(n-m)\} &\to \{1,\dots,2(n-m)\}, \\
j &\mapsto \begin{cases} j+1 & (j<2(n-m)) \\ 1 & (j=2(n-m)). \end{cases}
\end{aligned} \tag{C.99}$$

The order $<_{\psi^{(2n)}_{(2m+1)_S}}$ on $\{2m+1,\dots,2n\}$ is defined through the condition

$$l <_{\psi^{(2n)}_{(2m+1)_S}} l' \quad :\Leftrightarrow \quad {\psi^{(2n)}_{(2m+1)_S}}^{-1}(l) < {\psi^{(2n)}_{(2m+1)_S}}^{-1}(l'), \tag{C.100}$$

and for $\mathcal{P}\in PF\{2m+1,\dots,2n\}$, and $M'\in\mathcal{P}$:

$$\begin{aligned}
p\left(M', <_{\psi^{(2n)}_{(2m+1)_S}}\right) &:= \min\left(M', <_{\psi^{(2n)}_{(2m+1)_S}}\right), \\
q\left(M', <_{\psi^{(2n)}_{(2m+1)_S}}\right) &:= \max\left(M', <_{\psi^{(2n)}_{(2m+1)_S}}\right).
\end{aligned} \tag{C.101}$$

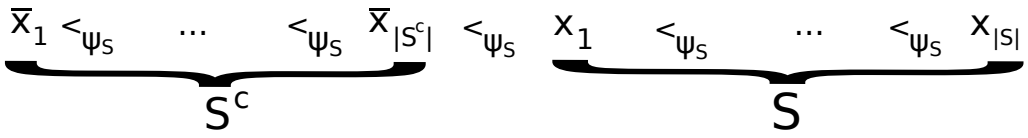

Figure C.4: The order $<_{\psi_S}$ (for brevity we here omit the further indices in $\psi^{(2n)}_{(2m+1)_S} = \psi_S$): For any subset $S \subset \{2m+1, \ldots, 2n\}$, let $\overline{x}_1, \ldots, \overline{x}_{|S^c|}$ be a list of the elements of the set's complement $S^c := \{2m+1, \ldots, 2n\} \setminus S$ in *increasing* natural order, and let the elements of S be listed by $x_1, \ldots, x_{|S|}$ in *decreasing* natural order. The order $<_{\psi_S}$ is then completely defined by the list shown in the present figure.

Inserting the right-hand side of Eq. (C.96) into Eq. (C.31) and (C.11), we obtain:

$$\begin{aligned} & A^{(2(n-m))}(\tau_{2n}, \ldots, \tau_{2m+1}) \qquad \text{(C.102)} \\ = & \sum_{\mathcal{P} \in PF\{2m+1,\ldots,2n\}} A^{(2(n-m))}_{\mathcal{P}}(\tau_{2n}, \ldots, \tau_{2m+1}), \end{aligned}$$

where

$$\begin{aligned} & A^{(2(n-m))}_{\mathcal{P}}(\tau_{2n}, \ldots, \tau_{2m+1})\hat{y} \quad := \qquad \text{(C.103)} \\ & \frac{(-1)^{n-m}}{\hbar^{2(n-m)}} \sum_{\nu_{2m+1},\ldots,\nu_{2n} \in \mathcal{I}} \quad \sum_{S : S \subset \{2m+1, 2m+2, \ldots, 2n\}} \\ & (-1)^{|S|} \quad \exp\left(\frac{i}{\hbar}\left(\tau_{2m+1}\varepsilon_{\nu_{2m+1}} + \cdots + \tau_{2n}\varepsilon_{\nu_{2n}}\right)\right) \\ & \hat{\mathrm{D}}_{\nu_{\varphi^{(2n)}_{(2m+1)_S}(1)}}\left(\tau_{\varphi^{(2n)}_{(2m+1)_S}(1)}\right) \ldots \hat{\mathrm{D}}_{\nu_{\varphi^{(2n)}_{(2m+1)_S}(|S|)}}\left(\tau_{\varphi^{(2n)}_{(2m+1)_S}(|S|)}\right) \\ & \qquad \hat{y} \\ & \hat{\mathrm{D}}_{\nu_{\varphi^{(2n)}_{(2m+1)_S}(|S|+1)}}\left(\tau_{\varphi^{(2n)}_{(2m+1)_S}(|S|+1)}\right) \ldots \hat{\mathrm{D}}_{\nu_{\varphi^{(2n)}_{(2m+1)_S}(2(n-m))}}\left(\tau_{\varphi^{(2n)}_{(2m+1)_S}(2(n-m))}\right) \\ & \operatorname{sign}\left(\mathcal{P}, <_{\psi^{(2n)}_{(2m+1)_S}}\right) \prod_{M' \in \mathcal{P}} \left\langle \hat{\mathrm{C}}_{\nu_{p\left(M', <_{\psi^{(2n)}_{(2m+1)_S}}\right)}} \hat{\mathrm{C}}_{\nu_{q\left(M', <_{\psi^{(2n)}_{(2m+1)_S}}\right)}} \right\rangle. \qquad \square \end{aligned}$$

Factorization of $A^{(2(r-m))}_{\mathcal{P}\cup\mathcal{Q}}(\tau_{2r}, \ldots, \tau_{2m+1})$

Furthermore, a multiplicativity according to

$$
\begin{aligned}
& A_{\mathcal{Q}}^{(2(r-n))}(\tau_{2r},\ldots,\tau_{2n+1}) A_{\mathcal{P}}^{(2(n-m))}(\tau_{2n},\ldots,\tau_{2m+1}) \\
= \;& A_{\mathcal{P}\cup\mathcal{Q}}^{(2(r-m))}(\tau_{2r},\ldots,\tau_{2m+1})
\end{aligned}
\tag{C.104}
$$

is satisfied: For any $0 \leq m < n < r$, for any $\mathcal{P} \in PF\{2m+1,\ldots,2n\}$, and $\mathcal{Q} \in PF\{2n+1,\ldots,2r\}$, for any sequence of times $\tau_{2m+1} \leq \cdots \leq \tau_{2r}$, and for any linear map $\hat{y}$ operating on $V_\odot$ we note:

$$
A_{\mathcal{Q}}^{(2(r-n))}(\tau_{2r},\ldots,\tau_{2n+1}) A_{\mathcal{P}}^{(2(n-m))}(\tau_{2n},\ldots,\tau_{2m+1})\hat{y} \; = \tag{C.105}
$$

$$
\begin{aligned}
& \frac{(-1)^{r-m}}{\hbar^{2(r-m)}} \sum_{\nu_{2m+1},\ldots,\nu_{2r}\in\mathcal{I}} \quad \sum_{S\subset\{2m+1,2m+2,\ldots,2n\}} \quad \sum_{T\subset\{2n+1,2n+2,\ldots,2r\}} \\
& (-1)^{|S|+|T|} \quad \exp\left(\frac{i}{\hbar}\left(\tau_{2m+1}\varepsilon_{\nu_{2m+1}} + \cdots + \tau_{2r}\varepsilon_{\nu_{2r}}\right)\right)
\end{aligned}
$$

$$
\begin{aligned}
& \hat{\mathrm{D}}_{\nu_{\varphi^{(2r)}_{(2n+1)_T}(1)}}\left(\tau_{\varphi^{(2r)}_{(2n+1)_T}(1)}\right) \ldots \hat{\mathrm{D}}_{\nu_{\varphi^{(2r)}_{(2n+1)_T}(|T|)}}\left(\tau_{\varphi^{(2r)}_{(2n+1)_T}(|T|)}\right) \\
& \hat{\mathrm{D}}_{\nu_{\varphi^{(2n)}_{(2m+1)_S}(1)}}\left(\tau_{\varphi^{(2n)}_{(2m+1)_S}(1)}\right) \ldots \hat{\mathrm{D}}_{\nu_{\varphi^{(2n)}_{(2m+1)_S}(|S|)}}\left(\tau_{\varphi^{(2n)}_{(2m+1)_S}(|S|)}\right) \\
& \qquad \hat{y} \\
& \hat{\mathrm{D}}_{\nu_{\varphi^{(2n)}_{(2m+1)_S}(|S|+1)}}\left(\tau_{\varphi^{(2n)}_{(2m+1)_S}(|S|+1)}\right) \ldots \hat{\mathrm{D}}_{\nu_{\varphi^{(2n)}_{(2m+1)_S}(2(n-m))}}\left(\tau_{\varphi^{(2n)}_{(2m+1)_S}(2(n-m))}\right) \\
& \hat{\mathrm{D}}_{\nu_{\varphi^{(2r)}_{(2n+1)_T}(|T|+1)}}\left(\tau_{\varphi^{(2r)}_{(2n+1)_T}(|T|+1)}\right) \ldots \hat{\mathrm{D}}_{\nu_{\varphi^{(2r)}_{(2n+1)_T}(2(r-n))}}\left(\tau_{\varphi^{(2r)}_{(2n+1)_T}(2(r-n))}\right)
\end{aligned}
$$

$$
\begin{aligned}
& \mathrm{sign}\left(\mathcal{P}, <_{\psi^{(2n)}_{(2m+1)_S}}\right) \prod_{M'\in\mathcal{P}} \left\langle \hat{\mathrm{C}}_{\nu_{p\left(M',<_{\psi^{(2n)}_{(2m+1)_S}}\right)}} \hat{\mathrm{C}}_{\nu_{q\left(M',<_{\psi^{(2n)}_{(2m+1)_S}}\right)}} \right\rangle \\
& \mathrm{sign}\left(\mathcal{Q}, <_{\psi^{(2r)}_{(2n+1)_T}}\right) \prod_{M'\in\mathcal{Q}} \left\langle \hat{\mathrm{C}}_{\nu_{p\left(M',<_{\psi^{(2r)}_{(2n+1)_T}}\right)}} \hat{\mathrm{C}}_{\nu_{q\left(M',<_{\psi^{(2r)}_{(2n+1)_T}}\right)}} \right\rangle \quad =
\end{aligned}
$$

$$
\begin{aligned}
&\frac{(-1)^{r-m}}{\hbar^{2(r-m)}} \sum_{\nu_{2m+1},\ldots,\nu_{2r}\in\mathcal{I}} \quad \sum_{S\subset\{2m+1,2m+2,\ldots,2n\}} \quad \sum_{T\subset\{2n+1,2n+2,\ldots,2r\}} \\
&(-1)^{|S|+|T|} \quad \exp\left(\frac{i}{\hbar}\left(\tau_{2m+1}\varepsilon_{\nu_{2m+1}}+\cdots+\tau_{2r}\varepsilon_{\nu_{2r}}\right)\right) \\
&\hat{\mathrm{D}}_{\nu_{\varphi^{(2r)}_{(2m+1)\,S\cup T}(1)}}\left(\tau_{\varphi^{(2r)}_{(2m+1)\,S\cup T}(1)}\right) \ldots\ \hat{\mathrm{D}}_{\nu_{\varphi^{(2r)}_{(2m+1)\,S\cup T}(|S\cup T|)}}\left(\tau_{\varphi^{(2r)}_{(2m+1)\,S\cup T}(|S\cup T|)}\right) \\
&\qquad\qquad \hat{y} \\
&\hat{\mathrm{D}}_{\nu_{\varphi^{(2r)}_{(2m+1)\,S\cup T}(|S\cup T|+1)}}\left(\tau_{\varphi^{(2r)}_{(2m+1)\,S\cup T}(|S\cup T|+1)}\right) \\
&\qquad\qquad\qquad\qquad \ldots\ \hat{\mathrm{D}}_{\nu_{\varphi^{(2r)}_{(2m+1)\,S\cup T}(2(r-m))}}\left(\tau_{\varphi^{(2r)}_{(2m+1)\,S\cup T}(2(r-m))}\right) \\
&\mathrm{sign}\left(\mathcal{P}\cup\mathcal{Q},<_{\psi^{(2r)}_{(2m+1)\,S\cup T}}\right) \\
&\prod_{M'\in\mathcal{P}\cup\mathcal{Q}} \left\langle \hat{\mathrm{C}}_{\nu_{p\left(M',<_{\psi^{(2r)}_{(2m+1)\,S\cup T}}\right)}} \hat{\mathrm{C}}_{\nu_{q\left(M',<_{\psi^{(2r)}_{(2m+1)\,S\cup T}}\right)}} \right\rangle,
\end{aligned}
$$

where the maps $\varphi^{(2n)}_{(2m+1)_S}$ and $\psi^{(2n)}_{(2m+1)_S}$ etc. appearing in the present expressions are defined according to Eq. (C.16) and (C.98); cp. Fig. C.5.

With Def. (C.103) we arrive at the factorization

$$
\begin{aligned}
& A^{(2(r-n))}_{\mathcal{Q}}(\tau_{2r},\ldots,\tau_{2n+1}) A^{(2(n-m))}_{\mathcal{P}}(\tau_{2n},\ldots,\tau_{2m+1}) \\
= \ & A^{(2(r-m))}_{\mathcal{P}\cup\mathcal{Q}}(\tau_{2r},\ldots,\tau_{2m+1}). \qquad \square
\end{aligned} \tag{C.106}
$$

Irreducibility of Contributions

Definition (Irreducibility):
A pair formation $\mathcal{P}\in PF(M)$ on a completely ordered set $M=\{m_1,\ldots,m_{2n}\}$ as in Fig. (C.3) is *irreducible*, if to any pair of two *subsequent* elements $x,y\in M$, with $x<y$, i.e.,

$$
y=\min\left(\left\{x'\in M: x<x'\right\},<\right), \tag{C.107}
$$

there is at least one $M'\in\mathcal{P}$ with $p(M',<)\leq x$, and $y\leq q(M',<)$. Otherwise, we shall call the pair formation *reducible*. $\square$

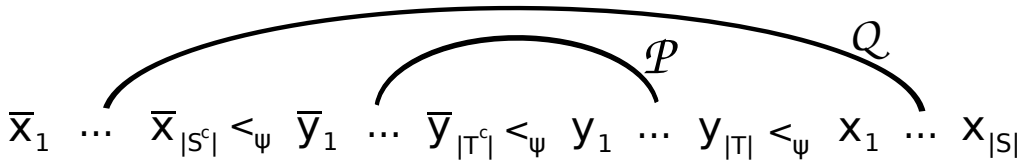

Figure C.5: The order $<_{\psi_{S\cup T}}$ (for brevity we here omit the further indices in $\psi^{(2r)}_{(2m+1)\,S\cup T} = \psi_{S\cup T}$): For any two subsets $S \subset \{2m+1,\ldots,2n\}, T \subset \{2n+1,\ldots,2r\}$, let $\overline{x}_1,\ldots,\overline{x}_{|S^c|}$, and $\overline{y}_1,\ldots,\overline{y}_{|T^c|}$ be a list of the elements of the sets' complements $S^c := \{2m+1,\ldots,2n\} \setminus S$, and $T^c := \{2n+1,\ldots,2r\} \setminus T$, respectively, in *increasing* natural order, and let the elements of S and T be listed by $x_1,\ldots,x_{|S|}$, and $y_1,\ldots,y_{|T|}$, respectively, in *decreasing* natural order. The order $<_{\psi_{S\cup T}}$ is then completely defined by the list shown here. Moreover, for any two pair formations $\mathcal{P} \in PF\{2m+1,\ldots,2n\}, \mathcal{Q} \in PF\{2n+1,\ldots,2r\}$, we deduce from the present figure: $\mathrm{sign}\,(\mathcal{P}\cup\mathcal{Q}, <_{\psi_{S\cup T}}) = \mathrm{sign}\,(\mathcal{P}, <_{\psi_S})\,\mathrm{sign}\,(\mathcal{Q}, <_{\psi_T})$, since the pair formation's sign is obtained from the number of intersection points of connecting lines in a graphic representation (Def. (C.84), Fig. C.3).

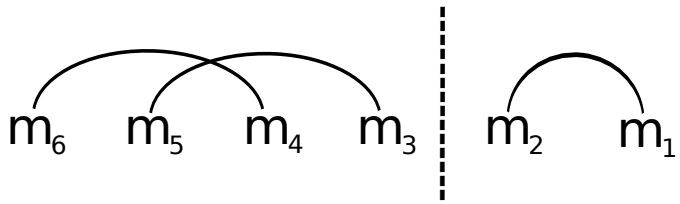

Figure C.6: An example of a reducible pair formation on a set of altogether six elements: We can perform a vertical cut between two subsequent elements (here: m_2 and m_3) which has no intersection with any of the bent lines connecting the elements of the pairs within the pair formation.

Defining $PF_{irr}\{1,\ldots,2n\}$ as the set of all pair formations on $\{1,\ldots,2n\}$ which are irreducible with respect to the natural order, as well as

$$A^{(2n)}_{irr}\left(\tau_{2n},\ldots,\tau_1\right) \;:=\; \sum_{\mathcal{P}\in PF_{irr}\{1,\ldots,2n\}} A^{(2n)}_{\mathcal{P}}\left(\tau_{2n},\ldots,\tau_1\right), \tag{C.108}$$

we can verify by the multiplicativity (C.104) that the maps $A^{(2n)}_{irr}$ satisfy the recursion relation

$$\begin{aligned} A^{(2n+2)}(\tau_{2n+2},\ldots,\tau_1) \;=\; & A^{(2n+2)}_{irr}(\tau_{2n+2},\ldots,\tau_1) \quad + \\ & A^{(2n)}_{irr}(\tau_{2n+2},\ldots,\tau_3)A^{(2)}(\tau_2,\tau_1) \quad + \\ & \quad\vdots \\ & A^{(2)}_{irr}(\tau_{2n+2},\tau_{2n+1})A^{(2n)}(\tau_{2n},\ldots,\tau_1). \end{aligned} \tag{C.109}$$

The equality is obtained by splitting any reducible pair formation $\mathcal{R} \in PF\{1,\ldots,2n+2\}$ into two parts, corresponding to a union

$$\mathcal{R} \;=\; \mathcal{Q}\cup\mathcal{P} \tag{C.110}$$

with $\mathcal{Q}\in PF_{irr}\{2m+1,\ldots,2n+2\}$, $\mathcal{P}\in PF\{1,\ldots,2m\}, 1\le m\le n$. The very same recursion relation (C.109) is satisfied per definition (2.33) also by the maps $I^{(2n)}(\tau_{2n},\ldots,\tau_1)$, whose integrals give the kernel entering into the quantum master equation. Hence, we have

$$I^{(2n)}(\tau_{2n},\ldots,\tau_1) \;=\; A^{(2n)}_{irr}(\tau_{2n},\ldots,\tau_1) \tag{C.111}$$

for any $n=1,2,\ldots$, and we conclude that, to any of the kernel's constituent parts, we can assign (a number n, and) an irreducible pair formation $\mathcal{P}\in PF_{irr}\{1,\ldots,2n\}$, and, vice versa, that any n, and $\mathcal{P}\in PF_{irr}\{1,\ldots,2n\}$, gives a set of contributions to the kernel.

Expansion over Irreducible Pair Formations

From Eq. (C.103) we obtain upon replacing the indices $\nu_{\varphi_S(j)}=\mu_j$:

$$I^{(2n)}(\tau_{2n},\ldots,\tau_1)\hat{y} \quad = \tag{C.112}$$

$$\frac{(-1)^n}{\hbar^{2n}} \quad \sum_{k=0}^{2n} \quad \sum_{S\subset\{1,2,\ldots,2n\}:|S|=k} \quad \sum_{\mu_1,\ldots,\mu_{2n}\in\mathcal{I}}$$

$$(-1)^k \quad \exp\left(\frac{i}{\hbar}\sum_{j=1}^{2n}\tau_{\varphi_S(j)}\varepsilon_{\mu_j}\right)$$

$$\hat{\mathrm{D}}_{\mu_1}\left(\tau_{\varphi_S(1)}\right)\ldots\hat{\mathrm{D}}_{\mu_k}\left(\tau_{\varphi_S(k)}\right) \quad \hat{y} \quad \hat{\mathrm{D}}_{\mu_{k+1}}\left(\tau_{\varphi_S(k+1)}\right)\ldots\hat{\mathrm{D}}_{\mu_{2n}}\left(\tau_{\varphi_S(2n)}\right)$$

$$\sum_{\mathcal{Q}\in PF_{irr}\{1,\ldots,2n\}} \mathrm{sign}\left(\mathcal{Q},<_{\psi_S}\right) \prod_{M'\in\mathcal{Q}} \left\langle \hat{\mathrm{C}}_{\mu_{\varphi_S^{-1}\left(p\left(M',<_{\psi_S}\right)\right)}} \hat{\mathrm{C}}_{\mu_{\varphi_S^{-1}\left(q\left(M',<_{\psi_S}\right)\right)}} \right\rangle,$$

where we abbreviate:

$$\begin{aligned} \varphi_S \quad &:= \quad \varphi^{(2n)}_{(1)\ S}, \\ \psi_S \quad &:= \quad \psi^{(2n)}_{(1)\ S}. \end{aligned} \tag{C.113}$$

For further analysis we define to any pair formation $\mathcal{P}\in PF\{1,\ldots,2n\}$:

$$\varphi_S\mathcal{P} \ := \ \{\varphi_S(M') : \ M'\in\mathcal{P}\}, \tag{C.114}$$

the image pair formation of $\mathcal{P}$ under the map φ_S. We note that

$$\begin{aligned} &\sum_{\mathcal{Q}\in PF_{irr}\{1,\ldots,2n\}} \mathrm{sign}\left(\mathcal{Q},<_{\psi_S}\right) \\ &\qquad \prod_{M'\in\mathcal{Q}} \left\langle \hat{\mathrm{C}}_{\mu_{\varphi_S^{-1}\left(p\left(M',<_{\psi_S}\right)\right)}} \hat{\mathrm{C}}_{\mu_{\varphi_S^{-1}\left(q\left(M',<_{\psi_S}\right)\right)}} \right\rangle = \\ &\qquad \sum_{\mathcal{P}\in\varphi_S^{-1}PF_{irr}\{1,\ldots,2n\}} \mathrm{sign}\left(\varphi_S\mathcal{P},<_{\psi_S}\right) \\ &\qquad \prod_{M'\in\mathcal{P}} \left\langle \hat{\mathrm{C}}_{\mu_{\varphi_S^{-1}\left(p\left(\varphi_S(M'),<_{\psi_S}\right)\right)}} \hat{\mathrm{C}}_{\mu_{\varphi_S^{-1}\left(q\left(\varphi_S(M'),<_{\psi_S}\right)\right)}} \right\rangle = \end{aligned} \tag{C.115}$$

$$= \sum_{\mathcal{P}\in\varphi_S^{-1}PF_{irr}\{1,\ldots,2n\}} \mathrm{sign}\left(\mathcal{P},<_{\zeta^k_{(+)}}\right) \prod_{M'\in\mathcal{P}} \left\langle \hat{\mathrm{C}}_{\mu_{p\left(M',<_{\zeta^k_{(+)}}\right)}} \hat{\mathrm{C}}_{\mu_{q\left(M',<_{\zeta^k_{(+)}}\right)}} \right\rangle,$$

where $\varphi_S^{-1}PF_{irr}\{1,\ldots,2n\}$ is the set of all image pair formations of pair formations within $PF_{irr}\{1,\ldots,2n\}$ under the bijection φ_S^{-1}, where $\zeta_{(+)}$ is the cyclic permutation of $\{1,\ldots,2n\}$ according to Def. (C.99), and where we use relations deduced from Fig. C.7. For any $\mathcal{P}\in PF\{1,\ldots,2n\}$ we note:

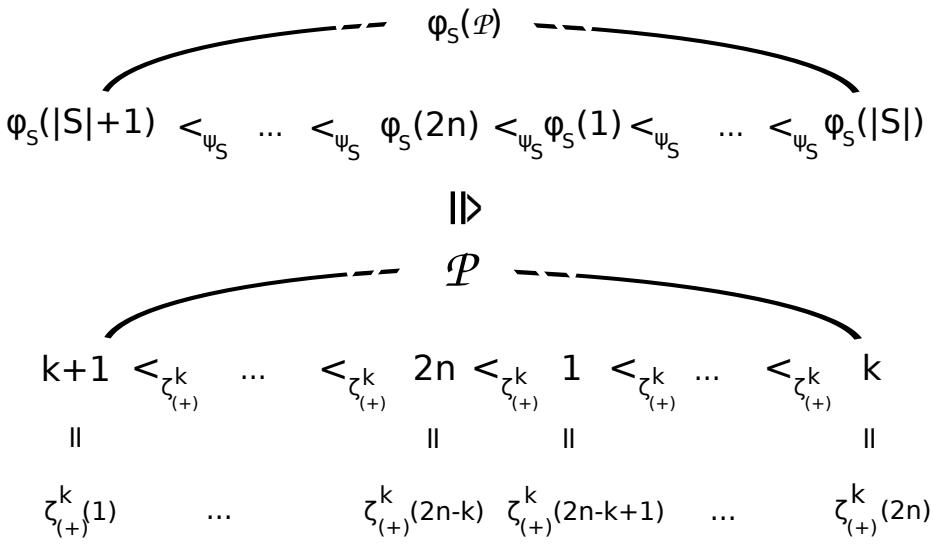

Figure C.7: The graphic representation of any pair formation $\mathcal{P} \in \varphi_S^{-1} PF_{irr}\{1,\ldots,2n\}$ in the order $<_{\zeta^k_{(+)}}$ has the *same* form as the graphic representation of the image-pair formation $\varphi_S(\mathcal{P})$ in the order $<_{\psi_S}$. (Note that, within the present figure, $k = |S|$; the map φ_S is defined by Fig. C.1, while the map ψ_S and the order $<_{\psi_S}$ are given in Eq. (C.98) and (C.100), respectively.) From the equality of the graphic representations we conclude that the corresponding signs of the pair formations are equal, and, in addition, we obtain the equality $\varphi_S\left(p\left(M', <_{\zeta^k_{(+)}}\right)\right) = p\left(\varphi_S(M'), <_{\psi_S}\right)$ for any $M' \in \mathcal{P}$.

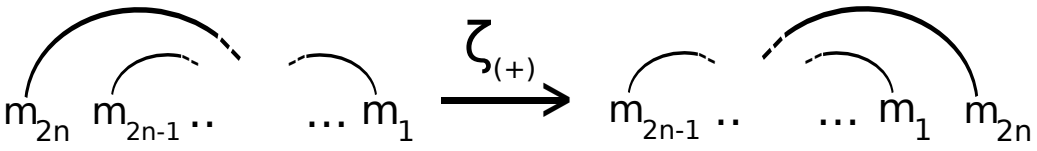

Figure C.8: A permutation cyclic with respect to a particular order does not change the sign of a pair formation in this order, since the number of intersection points of connecting lines is the same before and after the cyclic permutation.

$$\begin{aligned} \operatorname{sign}\left(\mathcal{P}, <_{\zeta_{(+)}^k}\right) &= \operatorname{sign}\left(\mathcal{P}, <\right) \\ &=: \operatorname{sign}\left(\mathcal{P}\right), \end{aligned} \tag{C.116}$$

the sign of $\mathcal{P}$ with respect to the natural order (cp. Fig. C.8). By these manipulations we arrive at

$$\begin{aligned} I^{(2n)}(\tau_{2n},\ldots,\tau_1)\hat{y} \quad = \quad & \\ \frac{(-1)^n}{\hbar^{2n}} \sum_{k=0}^{2n} \sum_{S\subset\{1,2,\ldots,2n\}:|S|=k} \sum_{\mathcal{P}\in\varphi_S^{-1}PF_{irr}\{1,\ldots,2n\}} \sum_{\mu_1,\ldots,\mu_{2n}\in\mathcal{I}} & \\ \operatorname{sign}\left(\mathcal{P}\right)(-1)^k \quad \exp\left(\frac{i}{\hbar}\sum_{j=1}^{2n}\tau_{\varphi_S(j)}\varepsilon_{\mu_j}\right) & \\ \hat{\mathrm{D}}_{\mu_1}\left(\tau_{\varphi_S(1)}\right)\ldots\hat{\mathrm{D}}_{\mu_k}\left(\tau_{\varphi_S(k)}\right) & \\ \hat{y} & \\ \hat{\mathrm{D}}_{\mu_{k+1}}\left(\tau_{\varphi_S(k+1)}\right)\ldots\hat{\mathrm{D}}_{\mu_{2n}}\left(\tau_{\varphi_S(2n)}\right) & \\ \prod_{M'\in\mathcal{P}}\left\langle \hat{\mathrm{C}}_{\mu_{p\left(M',<_{\zeta_{(+)}^k}\right)}}\hat{\mathrm{C}}_{\mu_{q\left(M',<_{\zeta_{(+)}^k}\right)}}\right\rangle. & \end{aligned} \tag{C.117}$$

We recall the definition of the objects appearing in the present equation: For any subset $S \subset \{1,2,\ldots,2n\}$, φ_S is the map defined in Eq. (C.13), while $\varphi_S^{-1}PF_{irr}\{1,\ldots,2n\}$ (cp. Fig. C.9) is the set of all pair formations $\mathcal{P}$ on $\{1,\ldots,2n\}$ whose image under φ_S, i.e., $\{\varphi_S(M') : M' \in \mathcal{P}\}$, is irreducible with respect to the natural order. The indices $\mu_1,\ldots,\mu_{2n}$, specifying the electron levels whose creation- and annihilation operators appear in the following, are taken from the set $\mathcal{I}$ (C.4). The operators $\hat{\mathrm{D}}_{\mu_j}\left(\tau_{\varphi_S(j)}\right)$ are defined according to (C.19, C.27), while the order $<_{\zeta_{(+)}^k}$ on $\{1,\ldots,2n\}$ is given

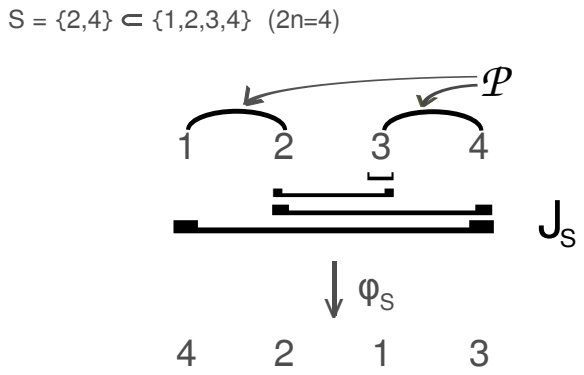

Figure C.9: The condition $\mathcal{P} \in \varphi_S^{-1} PF_{irr}\{1,\ldots,2n\}$ as a property of graphic objects. In the present example of a pair formation $\mathcal{P} \in \varphi_S^{-1} PF_{irr}\{1,\ldots,2n\}$, we have $2n = 4, S = \{2,4\} \subset \{1,2,3,4\}$, hence $\varphi_S(1) = 4, \varphi_S(2) = 2, \varphi_S(3) = 1$, and $\varphi_S(4) = 3$. The pair formation $\mathcal{P}$ is chosen as $\mathcal{P} = \{\{1,2\}\{3,4\}\}$; the condition "$\mathcal{P} \in \varphi_S^{-1} PF_{irr}\{1,\ldots,2n\}$" is equivalent to the demand that, to any $j \in \{1,\ldots,2n-1\}$, there is at least one $M \in \mathcal{P}$ such, that $|J_S(j) \cap M| = 1$, where $J_S(j) := \varphi_S^{-1}\{1,\ldots,j\}$. In the present figure, the integer intervals $J_S(j)$ are depicted by the horizontal square brackets, while the pair formation is indicated by the bent lines, each connecting two numbers. For any of the square brackets representing $J_S(j)$, with $j = 1,2,3$, there is at least one bent line connecting a number *within* $J_S(j)$ to a number *not* contained in $J_S(j)$.

implicitly by Fig. C.7, and explicitly through the cyclic permutation $\zeta_{(+)}$ by the condition

$$l <_{\zeta^k_{(+)}} l' \quad :\Leftrightarrow \quad {\zeta^k_{(+)}}^{-1}(l) < {\zeta^k_{(+)}}^{-1}(l'). \tag{C.118}$$

Appendix D

Complete Decomposition and Diagrammatic Expansion of the Kernel

In this appendix, starting out from Eq. (C.117), we give the detailed steps that lead to a diagrammatic expansion of the kernel: its decomposition into an infinite sum of contributions which we graphically represent by diagrams.

D.1 $K^{(2n)}(\tau)$ as Integral over *Non*-Ordered Times

Representation of the Map $\overline{I}^{(2n)}(\overline{\tau}_{2n-1}, \ldots, \overline{\tau}_0)$

Let $\mathcal{B}$ be an orthonormal basis of the vector space $V_\odot$ of the many-electron states of the quantum dot, which consists of eigenvectors of the quantum dot's Hamiltonian, $\hat{H}_\odot$, Defs. (2.3), (2.4), with corresponding eigenvalues $E_a, a \in \mathcal{B}$. Applying the scalar product "$\langle y|y'\rangle$" of two elements $y, y' \in V_\odot$, we write the operators

$$\begin{aligned} \hat{\mathrm{D}}_\mu(\tau) &= \mathcal{W}_\odot(\tau)\hat{\mathrm{D}}_\mu \\ &= \exp\left(\frac{i}{\hbar}\hat{\mathrm{H}}_\odot t\right)\ \hat{\mathrm{D}}_\mu\ \exp\left(-\frac{i}{\hbar}\hat{\mathrm{H}}_\odot t\right), \end{aligned} \tag{D.1}$$

(Def. (C.27)/ (2.19), with $\hat{\mathrm{H}}_\odot := \hat{H}_\odot\Big|_{V_\odot}$) appearing in Eq. (C.117), as a matrix in the basis $\mathcal{B}$:

$$\hat{\mathrm{D}}_{\mu}(\tau) \quad = \quad \sum_{a,b\in\mathcal{B}} \exp\left(\frac{i}{\hbar}\tau\left(E_a - E_b\right)\right) \langle a|\hat{\mathrm{D}}_{\mu}(b)\rangle \; |a><b|, \tag{D.2}$$

where the linear map $|a><b| : V_{\odot} \to V_{\odot}$ is defined by:

$$|a><b|\,(y) \quad := \quad \langle b|y\rangle a, \tag{D.3}$$

(the vector a multiplied by the scalar $\langle b|y\rangle$) for any $y \in V_{\odot}$. With this, we can rewrite the lines $3-5$ of the right-hand side of Eq. (C.117):

$$\begin{aligned}
&\hat{\mathrm{D}}_{\mu_1}\left(\tau_{\varphi_S(1)}\right) \ldots \hat{\mathrm{D}}_{\mu_k}\left(\tau_{\varphi_S(k)}\right) \\
&\qquad \hat{y} \\
&\hat{\mathrm{D}}_{\mu_{k+1}}\left(\tau_{\varphi_S(k+1)}\right) \ldots \hat{\mathrm{D}}_{\mu_{2n}}\left(\tau_{\varphi_S(2n)}\right) \\
&= \sum_{a_1,a_2,\ldots,a_{k+1}\in\mathcal{B}} \; \sum_{b_k,b_{k+1},\ldots,b_{2n}\in\mathcal{B}} \langle a_{k+1}|\hat{y}(b_k)\rangle \;\; |a_1><b_{2n}| \\
&\quad \prod_{j=1}^{k} \left\langle a_j|\hat{\mathrm{D}}_{\mu_j}(a_{j+1})\right\rangle \;\; \exp\left(\frac{i}{\hbar}\tau_{\varphi_S(j)}\left(E_{a_j} - E_{a_{j+1}}\right)\right) \\
&\quad \prod_{j=k+1}^{2n} \left\langle b_{j-1}|\hat{\mathrm{D}}_{\mu_j}(b_j)\right\rangle \;\; \exp\left(\frac{i}{\hbar}\tau_{\varphi_S(j)}\left(E_{b_{j-1}} - E_{b_j}\right)\right)
\end{aligned} \tag{D.4}$$

(cp. Fig. 2.5). Upon inserting expression (D.4) into Eq. (C.117), the dependence of the summands on the right-hand side of this equation on $\tau_1, \ldots, \tau_{2n}$ is contained in the factor

$$\begin{aligned}
&\exp\left\{\frac{i}{\hbar}\Big[\sum_{j\in S}\tau_j\left(\varepsilon_{\mu_{\varphi_S^{-1}(j)}} + E_{a_{\varphi_S^{-1}(j)}} - E_{a_{\varphi_S^{-1}(j)+1}}\right) + \right. \\
&\qquad \left. \sum_{j\in S^c}\tau_j\left(\varepsilon_{\mu_{\varphi_S^{-1}(j)}} + E_{b_{\varphi_S^{-1}(j)-1}} - E_{b_{\varphi_S^{-1}(j)}}\right) \;\Big]\right\} = \\
&\exp\left\{\frac{i}{\hbar}\Big[\sum_{j\in S}\sum_{l=0}^{j-1}\overline{\tau}_l\left(\varepsilon_{\mu_{\varphi_S^{-1}(j)}} + E_{a_{\varphi_S^{-1}(j)}} - E_{a_{\varphi_S^{-1}(j)+1}}\right) + \right. \\
&\qquad \left. \sum_{j\in S^c}\sum_{l=0}^{j-1}\overline{\tau}_l\left(\varepsilon_{\mu_{\varphi_S^{-1}(j)}} + E_{b_{\varphi_S^{-1}(j)-1}} - E_{b_{\varphi_S^{-1}(j)}}\right) \;\Big]\right\},
\end{aligned} \tag{D.5}$$

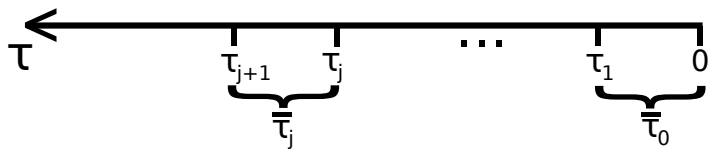

Figure D.1: The relation between the ordered sequence of times $\tau_1, \ldots, \tau_{2n}$, on the one hand, and the sequence $\overline{\tau}_0, \ldots, \overline{\tau}_{2n-1}$, on the other hand.

with

$$\begin{aligned} \overline{\tau}_0 &:= \tau_1, \\ \overline{\tau}_l &:= \tau_{l+1} - \tau_l \quad (l = 1, \ldots, 2n-1). \end{aligned} \tag{D.6}$$

Upon swapping the sums with respect to j and l, we obtain the term

$$\begin{aligned} &\exp\left\{ \frac{i}{\hbar} \sum_{l=1}^{2n} \overline{\tau}_{l-1} \Big[\sum_{j' \in \varphi_S^{-1}(S \cap \{l,\ldots,2n\})} \left(\varepsilon_{\mu_{j'}} + E_{a_{j'}} - E_{a_{j'+1}} \right) \; + \right. \\ &\qquad \left. \sum_{j' \in \varphi_S^{-1}(S^c \cap \{l,\ldots,2n\})} \left(\varepsilon_{\mu_{j'}} + E_{b_{j'-1}} - E_{b_{j'}} \right) \Big] \right\} \\ &= \exp\left\{ \frac{i}{\hbar} \sum_{l=1}^{2n} \overline{\tau}_{l-1} \Big[E_{a_1} - E_{a_{r_S(l)+1}} + \sum_{j=1}^{r_S(l)} \varepsilon_{\mu_j} \; + \right. \\ &\qquad \left. E_{b_{t_S(l)-1}} - E_{b_{2n}} + \sum_{j=t_S(l)}^{2n} \varepsilon_{\mu_j} \Big] \right\} \end{aligned} \tag{D.7}$$

for the dependence of the summands on the right-hand side of Eq. (C.117) on $\overline{\tau}_0, \ldots, \overline{\tau}_{2n-1}$, where

$$\begin{aligned} r_S(l) &:= \max\left\{ \varphi_S^{-1}\left(\{l, \ldots, 2n\} \cap S \right) \cup \{0\} \right\}, \\ t_S(l) &:= \min\left\{ \varphi_S^{-1}\left(\{l, \ldots, 2n\} \cap S^c \right) \cup \{2n+1\} \right\} \end{aligned} \tag{D.8}$$

for $l \in \{1, \ldots, 2n\}$. We note that

$$\begin{aligned} \varphi_S^{-1}\left(S \cap \{l, \ldots, 2n\} \right) &= \{1, \ldots, |S \cap \{l, \ldots, 2n\}|\} \\ &= \{1, \ldots, r_S(l)\}, \end{aligned} \tag{D.9}$$

and

$$\begin{aligned}\varphi_S^{-1}\left(S^c \cap \{l,\ldots,2n\}\right) &= \{2n - |S^c \cap \{l,\ldots,2n\}| + 1,\ldots,2n\} \\ &= \{t_S(l),\ldots,2n\} \qquad \text{(D.10)}\end{aligned}$$

(cp. Fig. C.1).

Letting

$$\begin{aligned}\overline{I}^{(2n)}(\overline{\tau}_{2n-1},\ldots,\overline{\tau}_0) &:= \mathcal{W}_\odot\left(-\sum_{j=1}^{2n}\overline{\tau}_{j-1}\right) \qquad \text{(D.11)} \\ &\quad I^{(2n)}\left(\sum_{j=1}^{2n}\overline{\tau}_{j-1},\ldots,\sum_{j=1}^{2}\overline{\tau}_{j-1},\sum_{j=1}^{1}\overline{\tau}_{j-1}\right),\end{aligned}$$

with $\mathcal{W}_\odot(t)$ (2.19) the transformation applied for the interaction picture, and upon inserting (D.4), as well as (D.7), into Eq. (C.117), we obtain:

$$\overline{I}^{(2n)}(\overline{\tau}_{2n-1},\ldots,\overline{\tau}_0)\hat{y} = \qquad \text{(D.12)}$$

$$\begin{aligned}&\frac{1}{\hbar^{2n}}\sum_{k=0}^{2n}\sum_{S\subset\{1,\ldots,2n\}:|S|=k}\sum_{\mathcal{P}\in\varphi_S^{-1}PF_{irr}\{1,\ldots,2n\}} \\ &\sum_{\mu_1,\ldots,\mu_{2n}\in\mathcal{I}}\sum_{a_1,\ldots,a_{k+1}\in\mathcal{B}}\sum_{b_k,\ldots,b_{2n}\in\mathcal{B}} \\ &\operatorname{sign}(\mathcal{P})\ (-1)^{n+k}\quad \langle a_{k+1}|\hat{y}(b_k)\rangle \quad |a_1><b_{2n}| \\ &\prod_{j=1}^{k}\left\langle a_j\left|\hat{\mathrm{D}}_{\mu_j}(a_{j+1})\right.\right\rangle\prod_{j=k+1}^{2n}\left\langle b_{j-1}\left|\hat{\mathrm{D}}_{\mu_j}(b_j)\right.\right\rangle \\ &\prod_{M'\in\mathcal{P}}\left\langle \hat{\mathrm{C}}_{\mu_{p\left(M',<_{\zeta_{(+)}^k}\right)}}\hat{\mathrm{C}}_{\mu_{q\left(M',<_{\zeta_{(+)}^k}\right)}}\right\rangle \\ &\exp\left\{\frac{i}{\hbar}\sum_{j=1}^{2n}\overline{\tau}_{j-1}\Big[-E_{a_{r_S(j)+1}}+\sum_{i=1}^{r_S(j)}\varepsilon_{\mu_i}\ + \right. \\ &\qquad\left.E_{b_{t_S(j)-1}}+\sum_{i=t_S(j)}^{2n}\varepsilon_{\mu_i}\Big]\right\},\end{aligned}$$

since

$$\mathcal{W}_{\odot}(-\tau)(|a_1><b_{2n}|) = \exp\left(\frac{i}{\hbar}\tau(E_{b_{2n}}-E_{a_1})\right)_{|a_1><b_{2n}|} \quad \text{(D.13)}$$

according to Def. (2.19).

Maximum and Minimum in the Order $<_{\zeta^{\boldsymbol{k}}_{(+)}}$

For $\mathcal{P}\in PF\{1,\ldots,2n\}$ and $M\in\mathcal{P}$ let

$$\begin{array}{rcl} p(M) & := & p(M,<), \\ q(M) & := & q(M,<) \end{array} \quad \text{(D.14)}$$

the minimum and maximum of M in the natural order "$<$". We note that for any $M\in\mathcal{P}, k\in\{0,\ldots,2n\}$:

$$\begin{array}{rcl} q(M)\leq k & \Rightarrow & p\left(M,<_{\zeta^k_{(+)}}\right)=p(M), \\ k+1\leq p(M) & \Rightarrow & p\left(M,<_{\zeta^k_{(+)}}\right)=p(M), \\ p(M)\leq k, k+1\leq q(M) & \Rightarrow & p\left(M,<_{\zeta^k_{(+)}}\right)=q(M), \end{array} \quad \text{(D.15)}$$

(cp. Fig. D.2).

Notation

According to Eq. (C.79) we have:

$$\langle\hat{\mathrm{C}}_{\mu}\hat{\mathrm{C}}_{\nu}\rangle = f(\beta_{\mu})\,\delta_{\nu,\overline{\mu}} \quad \text{(D.16)}$$

for any $\mu,\nu\in\mathcal{I}$, with $\delta_{\nu,\overline{\mu}}$ the Kronecker-Delta, with β_{μ} defined in (C.71), (C.73), and with f the parameter-free Fermi-Dirac distribution (C.78). To any lead-index $l\in\mathcal{L}$, to any spin $\sigma\in\mathcal{S}$, and to $v\in\{\pm1\}$, we define

$$f^{(v)}_{l\sigma}(\varepsilon) := f\left(v\frac{\varepsilon-\mu_{l\sigma}}{k_BT}\right), \quad \text{(D.17)}$$

and for $(l,\sigma,\mathbf{k},v)\in\mathcal{I}$ we write

$$\hat{\mathrm{D}}_{l\sigma\mathbf{k}v} = T^{(v)}_{l\sigma\mathbf{k}}\hat{\mathrm{d}}^{(v)}_{\sigma}, \quad \text{(D.18)}$$

with

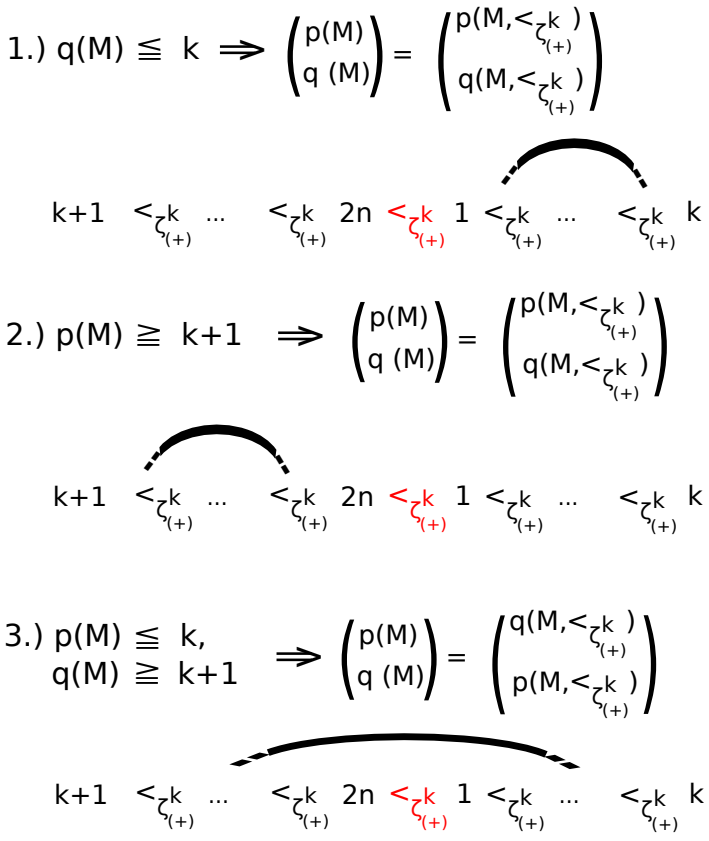

Figure D.2: In order to determine the minimum and maximum in the order $<_{\zeta^k_{(+)}}$ of a set $M \subset \{1, \ldots, 2n\}$ with two elements, $|M| = 2$, we distinguish between three cases.

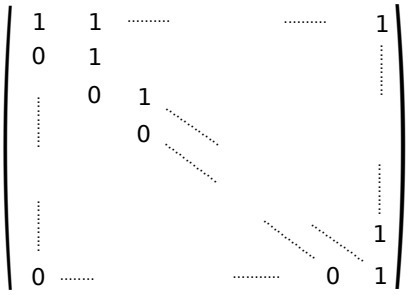

Figure D.3: For any $k \geq 1$, the sum-map $s : \mathbb{R}^k \to \mathbb{R}^k$, $(t_1, \ldots, t_k) \mapsto \left(t_1, \sum_{j=1}^{2} t_j, \ldots, \sum_{j=1}^{k} t_j\right)$ has the constant derivative-matrix with determinant 1 shown here; hence, we can transform integrals according to $\int dt_1 \ldots \int dt_k f\left(s\left(t_1, \ldots, t_k\right)\right) = \int ds_1 \ldots \int ds_k f\left(s_1, \ldots, s_k\right)$.

$$\begin{array}{lcl} T^{(+1)}_{l\sigma\mathbf{k}} & := & T_{l\sigma\mathbf{k}}, \\ T^{(-1)}_{l\sigma\mathbf{k}} & := & T^{*}_{l\sigma\mathbf{k}}, \end{array} \tag{D.19}$$

and

$$\begin{array}{lcl} \hat{\mathrm{d}}^{(+1)}_{\sigma} & := & \hat{d}_{\sigma}\Big|_{V_{\odot}}, \\ \hat{\mathrm{d}}^{(-1)}_{\sigma} & := & \hat{d}^{\dagger}_{\sigma}\Big|_{V_{\odot}}. \end{array} \tag{D.20}$$

Replacement by Integral over Non-Ordered Times

We note that, for $n \geq 2$, the $2n$-th order of the density matrix kernel (2.48) has the representation

$$K^{(2n)}(\tau) \;=\; \int \ldots \int_{0 \leq s_2 \leq \cdots \leq s_{2n-1} \leq \tau} I_{\tau\,(2)}^{(2n-1)}(s_{2n-1}, \ldots, s_2). \tag{D.21}$$

Integrating the latter equation once more, we conclude:

$$\int_0^s d\tau K^{(2n)}(\tau) \;=\; \int \ldots \int_{0 \leq s_2 \leq \cdots \leq s_{2n} \leq s} L(s_{2n}, \ldots, s_2), \tag{D.22}$$

with

$$L(s_{2n}, s_{2n-1}, \ldots, s_2) \;:=\; I_{s_{2n}\,(2)}^{(2n-1)}(s_{2n-1}, \ldots, s_2). \tag{D.23}$$

Upon applying the integral transformations according to Figs. D.3, and 2.6, respectively, we obtain:

$$\begin{aligned}\int_0^s d\tau K^{(2n)}(\tau) &= \int \dots \int_{\overline{\tau}_1+\dots+\overline{\tau}_{2n-1}\leq s} \overline{L}(\overline{\tau}_{2n-1},\dots,\overline{\tau}_1) \qquad \text{(D.24)}\\ &= \int_0^s \frac{d\tau}{\sqrt{2n-1}} \int \dots \int_{\overline{\tau}_1+\dots+\overline{\tau}_{2n-1}=\tau} \overline{L}(\overline{\tau}_{2n-1},\dots,\overline{\tau}_1),\end{aligned}$$

with

$$\overline{L}(\overline{\tau}_{2n-1},\dots,\overline{\tau}_1) \;:=\; L\left(\sum_{j=1}^{2n-1}\overline{\tau}_j, \sum_{j=1}^{2n-2}\overline{\tau}_j, \dots, \sum_{j=1}^{1}\overline{\tau}_j\right), \qquad \text{(D.25)}$$

where the integrals go over the set

$$\left\{S^{(2n-1)} \leq s\right\} := \left\{(\overline{\tau}_{2n-1},\dots,\overline{\tau}_1):\; \overline{\tau}_j \geq 0, \overline{\tau}_1+\dots+\overline{\tau}_{2n-1} \leq s\right\}, \qquad \text{(D.26)}$$

and the $(2n-2)$-dimensional surface

$$\left\{S^{(2n-1)} = \tau\right\} := \left\{(\overline{\tau}_{2n-1},\dots,\overline{\tau}_1):\; \overline{\tau}_j \geq 0, \overline{\tau}_1+\dots+\overline{\tau}_{2n-1} = \tau\right\} \qquad \text{(D.27)}$$

(cp. Fig. 2.6), respectively. We conclude:

$$K^{(2n)}(\tau) \;=\; \frac{1}{\sqrt{2n-1}} \int_{\left\{S^{(2n-1)}=\tau\right\}} \overline{L}(\overline{\tau}_{2n-1},\dots,\overline{\tau}_1). \qquad \text{(D.28)}$$

Inserting the present Defs. of the maps $\overline{L}$, and L, as well as the definition of $I^{(2n-1)}_{\tau_{(2)}}$ (Eq. (2.49)) into the latter equation, we arrive at the following representation of the integral kernel as an integral over non-ordered times:

$$K^{(2n)}(\tau) \;=\; \frac{1}{\sqrt{2n-1}} \int_{\left\{S^{(2n-1)}=\tau\right\}} \overline{I}^{(2n-1)}(\overline{\tau}_{2n-1},\dots,\overline{\tau}_1), \qquad \text{(D.29)}$$

where

$$\overline{I}^{(2n-1)}(\overline{\tau}_{2n-1},\dots,\overline{\tau}_1) \;:=\; \overline{I}^{(2n)}(\overline{\tau}_{2n-1},\dots,\overline{\tau}_1,0), \qquad \text{(D.30)}$$

with $\overline{I}^{(2n)}$ taken from Def. (D.11), the one quantity we give an explicit expression for in Eq. (D.12).

Explicit Expression for $K^{(2n)}(\tau)\hat{y}$

Applying Eq. (D.16) (evaluation of $\langle \hat{\mathrm{C}}_\mu \hat{\mathrm{C}}_\nu \rangle$), as well as the notation (D.14), and (D.20), we obtain from the Eq. (D.12) for $\overline{I}^{(2n)}(\overline{\tau}_{2n-1}, \ldots, \overline{\tau}_0)\hat{y}$ [note that here $\overline{\tau}_0 = 0$ (D.30)] in the case $n \geq 2$:

$$K^{(2n)}(\tau)\hat{y} \;=\; \frac{1}{\sqrt{2n-1}} \int_{\{S^{(2n-1)}=\tau\}} \tag{D.31}$$

$$\frac{1}{\hbar^{2n}} \sum_{k=0}^{2n} \sum_{S\subset\{1,\ldots,2n\}:|S|=k} \sum_{\mathcal{P}\in\varphi_S^{-1} PF_{irr}\{1,\ldots,2n\}}$$
$$\sum_{a_1,\ldots,a_{k+1}\in\mathcal{B}} \sum_{b_k,\ldots,b_{2n}\in\mathcal{B}} \sum_{(\nu_M=(l_M,\sigma_M,\mathbf{k}_M,v_M))_{M\in\mathcal{P}}\in\mathcal{I}^{\mathcal{P}}}$$
$$\mathrm{sign}\,(\mathcal{P})\;\; (-1)^{n+k} \quad \langle a_{k+1}|\hat{y}(b_k)\rangle \quad |a_1><b_{2n}|$$

$$\prod_{M\in\mathcal{P}:q(M)\leq k} \langle a_{p(M)}|\hat{\mathrm{d}}^{(v_M)}_{\sigma_M} a_{p(M)+1}\rangle$$
$$\langle a_{q(M)}|\hat{\mathrm{d}}^{(-v_M)}_{\sigma_M} a_{q(M)+1}\rangle \; A^{(v_M)}_{l_M\sigma_M}(\mathbf{k}_M)$$

$$\prod_{M\in\mathcal{P}:k+1\leq p(M)} \langle b_{p(M)-1}|\hat{\mathrm{d}}^{(v_M)}_{\sigma_M} b_{p(M)}\rangle$$
$$\langle b_{q(M)-1}|\hat{\mathrm{d}}^{(-v_M)}_{\sigma_M} b_{q(M)}\rangle \; A^{(v_M)}_{l_M\sigma_M}(\mathbf{k}_M)$$

$$\prod_{M\in\mathcal{P}:p(M)\leq k,k+1\leq q(M)} \langle a_{p(M)}|\hat{\mathrm{d}}^{(v_M)}_{\sigma_M} a_{p(M)+1}\rangle$$
$$\langle b_{q(M)-1}|\hat{\mathrm{d}}^{(-v_M)}_{\sigma_M} b_{q(M)}\rangle \; A^{(-v_M)}_{l_M\sigma_M}(\mathbf{k}_M)$$

$$\exp\Big\{ \frac{i}{\hbar} \sum_{j=1}^{2n-1} \overline{\tau}_j \Big[E_{b_{t_S(j+1)-1}} - E_{a_{r_S(j+1)+1}}$$
$$+ \sum_{M\in\mathcal{P}:p(M)\notin J_S(j),q(M)\in J_S(j)} v_M\; \varepsilon_{l_M\sigma_M\mathbf{k}_M}$$
$$- \sum_{M\in\mathcal{P}:p(M)\in J_S(j),q(M)\notin J_S(j)} v_M\; \varepsilon_{l_M\sigma_M\mathbf{k}_M} \Big] \Big\},$$

where for any $\nu = (l, \sigma, \mathbf{k}, v) \in \mathcal{I}$:

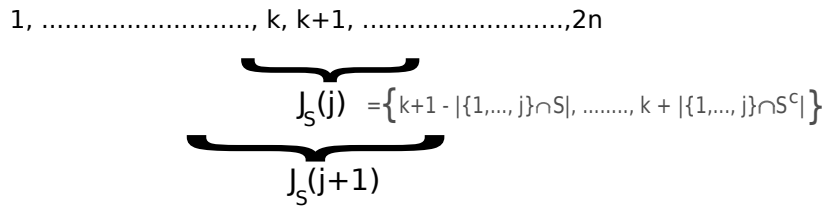

Figure D.4: The sequence $J_S(j)_{j=1}^{2n}$ of intervals of integer numbers, defined through (D.33), (C.13), and (D.8), starts out with $J_S(1) = \{k\}$ or $J_S(1) = \{k+1\}$ [$k = |S|$], grows by one number with every incrementation of j, and terminates with $J_S(2n) = \{1, \ldots, 2n\}$. The direction of the growth of $J_S(j+1)$ compared to $J_S(j)$ depends on whether $j+1 \in S$ or $j+1 \in S^c$.

$$A_{l\sigma}^{(v)}(\mathbf{k}) \;:=\; |T_{l\sigma\mathbf{k}}|^2 \;\; f_l^{(v)}(\varepsilon_{l\sigma\mathbf{k}})\,, \tag{D.32}$$

with $f_l^{(v)}$ taken from Eq. (D.17), and with

$$\begin{aligned} J_S(j) \;&:=\; \{r_S(j+1)+1, \ldots, t_S(j+1)-1\} \\ &=\; \varphi_S^{-1}\{1, \ldots, j\}\,, \end{aligned} \tag{D.33}$$

for any $j \in \{1, \ldots, 2n\}$, with r_S and t_S defined in Eq. (D.8). We note that $J_S(2n) = \{1, \ldots, 2n\}$, and

$$J_S(1) = \begin{cases} |S| & (1 \in S) \\ |S|+1 & (1 \in S^c). \end{cases} \tag{D.34}$$

Since

$$\langle \hat{\mathrm{C}}_\mu \hat{\mathrm{C}}_\nu \rangle \;=\; 0 \quad \text{in case} \quad \nu \neq \overline{\mu}, \tag{D.35}$$

and because of the emergence of the trace

$$\left\langle \hat{\mathrm{C}}_{\mu_{p\left(M', <\zeta_{(+)}^k\right)}} \hat{\mathrm{C}}_{\mu_{q\left(M', <\zeta_{(+)}^k\right)}} \right\rangle \tag{D.36}$$

in (D.12), we here could reduce the sum $\sum_{\mu_1,\ldots,\mu_{2n} \in \mathcal{I}}$ to a sum $\sum_{(\nu_M)_{M\in\mathcal{P}} \in \mathcal{I}^{\mathcal{P}}}$, within which only to each *pair* of numbers $1, \ldots, 2n$ an index in $\mathcal{I}$ is assigned. Correspondingly, we could reduce the sum

$$\sum_{i=1}^{r_S(j+1)} \varepsilon_{\mu_i} \;+\; \sum_{i=t_S(j+1)}^{2n} \varepsilon_{\mu_i} \;=\; -\sum_{i=r_S(j+1)+1}^{t_S(j+1)-1} \varepsilon_{\mu_i} \;=\; -\sum_{i\in J_S(j)} \varepsilon_{\mu_i} \tag{D.37}$$

to a sum over only those pairs $M \in \mathcal{P}$ with $|M \cap J_S(j)| = 1$.

To cover and include the case $n = 1$ in Eq. (D.31), we define

$$\int_{\left\{S^{(1)}=\tau\right\}} F(\overline{\tau}_1) \quad := \quad F(\tau) \tag{D.38}$$

for an arbitrary integrand $F(\overline{\tau}_1)$.

D.2 Replacement of Sums by Integrals

D.2.1 Compact Expression for $K^{(2n)}(\tau)\hat{y}$

By the abbreviations

$$\mathrm{sg}^{(1)}\ \left\{n, k, \mathcal{P},\ (a_j)_{j=1}^{k+1},\ (b_j)_{j=k}^{2n},\ (\sigma_M, v_M)_{M\in\mathcal{P}}\right\} \quad := \tag{D.39}$$

$$\mathrm{sign}(\mathcal{P})\ (-1)^{n+k}$$

$$\prod_{M\in\mathcal{P}:q(M)\le k} \langle a_{p(M)}|\hat{\mathrm{d}}_{\sigma_M}^{(v_M)} a_{p(M)+1}\rangle \quad \langle a_{q(M)}|\hat{\mathrm{d}}_{\sigma_M}^{(-v_M)} a_{q(M)+1}\rangle$$

$$\prod_{M\in\mathcal{P}:k+1\le p(M)} \langle b_{p(M)-1}|\hat{\mathrm{d}}_{\sigma_M}^{(v_M)} b_{p(M)}\rangle \quad \langle b_{q(M)-1}|\hat{\mathrm{d}}_{\sigma_M}^{(-v_M)} b_{q(M)}\rangle$$

$$\prod_{M:p(M)\le k, k+1\le q(M)} \langle a_{p(M)}|\hat{\mathrm{d}}_{\sigma_M}^{(v_M)} a_{p(M)+1}\rangle \quad \langle b_{q(M)-1}|\hat{\mathrm{d}}_{\sigma_M}^{(-v_M)} b_{q(M)}\rangle,$$

$$sg^{(2)}\,(M,k) \ := \begin{cases} 1 & (\text{if } q(M) \le k \text{ or } k+1 \le p(M)) \\ -1 & (\text{else}), \end{cases} \tag{D.40}$$

and

$$\mathrm{sg}^{(3)}\,(M, J_S) := \begin{cases} 1 \ (\exists j \in \{1,\ldots,2n-1\} : p(M) \notin J_S(j), q(M) \in J_S(j)) \\ -1 \ (\exists j \in \{1,\ldots,2n-1\} : p(M) \in J_S(j), q(M) \notin J_S(j)), \end{cases} \tag{D.41}$$

($\exists$: exists) we can rewrite Eq. (D.31) in the more compact form

$$K^{(2n)}(\tau)\hat{y} \ = \ \frac{1}{\sqrt{2n-1}} \int_{\left\{S^{(2n-1)}=\tau\right\}} \tag{D.42}$$

$$\frac{1}{\hbar^{2n}} \sum_{k=0}^{2n} \sum_{S\subset\{1,\ldots,2n\}:|S|=k} \sum_{\mathcal{P}\in\varphi_S^{-1}PF_{irr}\{1,\ldots,2n\}} \sum_{a_1,\ldots,a_{k+1}\in\mathcal{B}} \sum_{b_k,\ldots,b_{2n}\in\mathcal{B}} \sum_{(\nu_M=(l_M,\sigma_M,\mathbf{k}_M,v_M))_{M\in\mathcal{P}}\ \in\mathcal{I}^{\mathcal{P}}}$$
$$\mathrm{sg}^{(1)}\left\{n,k,\mathcal{P},\ (a_j)_{j=1}^{k+1},\ (b_j)_{j=k}^{2n},\ (\sigma_M,v_M)_{M\in\mathcal{P}}\right\}\langle a_{k+1}|\hat{y}(b_k)\rangle \quad |a_1><b_{2n}|$$

$$\left\{\prod_{M\in\mathcal{P}} A_{l_M\sigma_M}^{(v_M sg^{(2)}(M,k))}(\mathbf{k}_M)\right\}\exp\left\{\frac{i}{\hbar}\sum_{j=1}^{2n-1}\overline{\tau}_j\ \left[\ E_{b_{t_S(j+1)-1}}-E_{a_{r_S(j+1)+1}}\right]\right\}$$
$$\exp\left\{\frac{i}{\hbar}\sum_{j=1}^{2n-1}\sum_{M\in\mathcal{P}:|M\cap J_S(j)|=1} v_M\mathrm{sg}^{(3)}(M,J_S)\,\overline{\tau}_j\ \varepsilon_{l_M\sigma_M\mathbf{k}_M}\right\}.$$

D.2.2 Replacement of Sum over Wave Vector

For any $M\in\mathcal{P}$, and for any fixed values of all other appearing parameters, we replace the sum with respect to the wave vector $\mathbf{k}_M$ within the right-hand side of the present equation (D.42), i.e., the sum

$$\sum_{\mathbf{k}_M\in\mathcal{K}_{l_M}} |T_{l_M\sigma_M\mathbf{k}_M}|^2\ f_{l_M\sigma_M}^{(\pm1)}(\varepsilon_{l_M\sigma_M\mathbf{k}_M}) \tag{D.43}$$
$$\exp\left\{\frac{i}{\hbar}\ v_M\mathrm{sg}^{(3)}(M,J_S)\ \ \varepsilon_{l_M\sigma_M\mathbf{k}_M}\ \ [S_M(J_S)(\overline{\tau}_{2n-1},\ldots,\overline{\tau}_1)]\right\},$$

where

$$S_M(J_S)(\overline{\tau}_{2n-1},\ldots,\overline{\tau}_1) \ :=\ \sum_{j\in\{1,\ldots,2n-1\}:|J_S(j)\cap M|=1}\overline{\tau}_j, \tag{D.44}$$

by an integral over a primitive unit cell of the reciprocal lattice of contact l_M (for brevity we shall omit the index "M" now): Let a_1,a_2,a_3 be primitive vectors of the direct lattice of contact l, and, with $N\in\mathbb{N}$, let

$$\left\{\sum_{j=1}^{3}\mu_j a_j:\ \mu_1,\mu_2,\mu_3\in\{0,\ldots,N-1\}\right\} \tag{D.45}$$

be the lattice points of the real and finite lattice of contact l. Let b_1, b_2, b_3 be the primitive vectors of the reciprocal lattice satisfying

$$a_i b_j \;=\; 2\pi\;\delta_{ij}; \tag{D.46}$$

we assume that the set $\mathcal{K}_l$ of allowed wave vectors is given by

$$\mathcal{K}_l \;=\; \left\{\mathbf{k}_{\mu_1,\mu_2,\mu_3}:\; \mu_1,\mu_2,\mu_3 \in \{0,\ldots,N-1\}\right\}, \tag{D.47}$$

with

$$\mathbf{k}_{\mu_1,\mu_2,\mu_3} \;:=\; \sum_{j=1}^{3} \mu_j \frac{1}{N} b_j, \tag{D.48}$$

according to a periodic boundary condition, and consider a sum of the form

$$\sum_{\mathbf{k}\in\mathcal{K}_l} A_{l\sigma}^{(N)}(\mathbf{k})\; F\left(\varepsilon_{l\sigma\mathbf{k}}\right), \tag{D.49}$$

where

$$A_{l\sigma}^{(N)}(\mathbf{k}) \quad :=\quad \left|T_{l\sigma\mathbf{k}}^{(N)}\right|^2, \tag{D.50}$$

where $T_{l\sigma\mathbf{k}}^{(N)}$ are the coefficients of the tunneling Hamiltonian for a finite lead l with a number of N^3 occupied primitive unit cells, and where $F = F(\varepsilon)$ is a continuous function of energy.

We want to replace the sum (D.49) by an integral; to this end, we define the set

$$C_{b_1,b_2,b_3} \;:=\; \left\{\sum_{j=1}^{3}\;\lambda_j\;\frac{1}{N}b_j:\;\lambda_j\in[0,N[\right\}, \tag{D.51}$$

and the map

$$\kappa^{(N)}: \qquad\qquad C_{b_1,b_2,b_3} \;\to\; \mathcal{K}_l \tag{D.52}$$

by the condition, that for any $\mu_j \in \{0,\ldots,N-1\}$, and $\overline{\lambda}_j \in [0,1[$, $j = 1,2,3$:

$$\mathbf{k}_{\mu_1,\mu_2,\mu_3} + \sum_{j=1}^{3} \overline{\lambda}_j \frac{1}{N} b_j \quad\mapsto\quad \mathbf{k}_{\mu_1,\mu_2,\mu_3} \tag{D.53}$$

(cp. Fig. D.5). We note the equality between sum and integral:

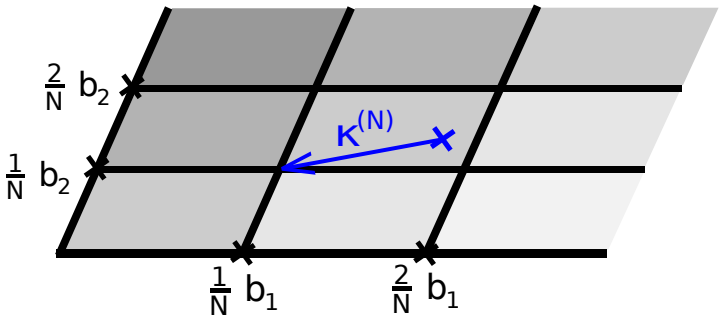

Figure D.5: In the present two-dimensional example, the intersection-points of the black lines mark the elements of the set $\mathcal{K}_l$ according to Eq. (D.47), while the blue arrow depicts the map $\kappa^{(N)}$. We may replace a sum $\sum_{\mathbf{k}\in\mathcal{K}_l} g(\mathbf{k})$ by an integral over C_{b_1,b_2}, assuming that within each of the shaded cells the integrand has the constant value $g(\kappa^{(N)}(\mathbf{k}))/U$, with $U = \frac{1}{N^2}\left|\det\left(b_1, b_2\right)\right|$ the volume of one cell; so, $\sum_{\mathbf{k}\in\mathcal{K}_l} g(\mathbf{k}) = \int_{C_{b_1,b_2}} d\mathbf{k}\; g(\kappa^{(N)}(\mathbf{k}))/U$.

$$\begin{aligned}\sum_{\mathbf{k}\in\mathcal{K}_l} A^{(N)}_{l\sigma}(\mathbf{k})\; F\left(\varepsilon_{l\sigma\mathbf{k}}\right) &= \int_{C_{b_1,b_2,b_3}} d\mathbf{k}\; A^{(N)}_{l\sigma}\left(\kappa^{(\mathbf{N})}\left(\mathbf{k}\right)\right)\; F\left(\varepsilon_{l\sigma\kappa^{(\mathbf{N})}(\mathbf{k})}\right) \\ &\quad \frac{1}{\left|\det\left(b_1, b_2, b_3\right)\right| / \left(N^3\right)} \\ &= \int_{C_{b_1,b_2,b_3}} d\mathbf{k}\; \frac{V}{(2\pi)^3}\left|T^{(N)}_{l\sigma\kappa^{(\mathbf{N})}(\mathbf{k})}\right|^2 F\left(\varepsilon_{l\sigma\kappa^{(\mathbf{N})}(\mathbf{k})}\right),\end{aligned} \tag{D.54}$$

with

$$V \;:=\; N^3\;\left|\det\left(a_1, a_2, a_3\right)\right|, \tag{D.55}$$

the volume of contact l.

We shall assume that, for the band energy $\varepsilon_{l\sigma\mathbf{k}}$, as well as for all other contributions to the present integral's integrand, the variation of their value on a scale given by the distance between neighbouring elements in $\mathcal{K}_l$ is relatively small. With this argument we approximate

$$\frac{V}{(2\pi)^3}\left|T^{(N)}_{l\sigma\kappa^{(\mathbf{N})}(\mathbf{k})}\right|^2 \approx a_{l\sigma}\left(\mathbf{k}\right), \tag{D.56}$$

with $a_{l\sigma}\left(\mathbf{k}\right)$ a continuous function, and

$$\int_{C_{b_1,b_2,b_3}} d\mathbf{k}\ \frac{V}{(2\pi)^3}\left|T^{(N)}_{l\sigma\kappa^{(\mathbf{N})}(\mathbf{k})}\right|^2 F\left(\varepsilon_{l\sigma\kappa^{(\mathbf{N})}(\mathbf{k})}\right) \approx \int_{C_{b_1,b_2,b_3}} d\mathbf{k}\ a_{l\sigma}(\mathbf{k})\, F\left(\varepsilon_{l\sigma\mathbf{k}}\right). \tag{D.57}$$

In summary, we approximate and replace:

$$\sum_{\mathbf{k}\in\mathcal{K}_l}\left|T^{(N)}_{l\sigma\mathbf{k}}\right|^2 F\left(\varepsilon_{l\sigma\mathbf{k}}\right) \approx \int_{C_{b_1,b_2,b_3}} d\mathbf{k}\ a_{l\sigma}(\mathbf{k})\, F\left(\varepsilon_{l\sigma\mathbf{k}}\right) \tag{D.58}$$

for the sums (D.43), with $a_{l\sigma}(\mathbf{k})$ given in Eq. (D.56).

D.2.3 Replacement by Integral over Energy

In a second step, we replace the integral over the primitive unit cell in the reciprocal lattice by an integral with respect to energy, analogously to the method outlined by Fig. 2.6:

$$\int_{C_{b_1,b_2,b_3}} d\mathbf{k}\ a_{l\sigma}(\mathbf{k})\, F\left(\varepsilon_{l\sigma\mathbf{k}}\right) = \int d\varepsilon\ \alpha_{l\sigma}(\varepsilon) F(\varepsilon), \tag{D.59}$$

where

$$\alpha_{l\sigma}(\varepsilon) := \int_{\left\{\mathbf{k}\in C_{b_1,b_2,b_3}:\ \varepsilon_{l\sigma\mathbf{k}}=\varepsilon\right\}} dS\ \frac{a_{l\sigma}(\mathbf{k})}{|\nabla\varepsilon_{l\sigma\mathbf{k}}|}. \tag{D.60}$$

The distance dx between surfaces $\{\varepsilon_{l\sigma\mathbf{k}} = \varepsilon\}$ and $\{\varepsilon_{l\sigma\mathbf{k}} = \varepsilon + d\varepsilon\}$ of constant values ε, and $\varepsilon + d\varepsilon$, of $\varepsilon_{l\sigma\mathbf{k}}$ is locally different and satisfies

$$dx\,|\nabla\varepsilon_{l\sigma\mathbf{k}}| = d\varepsilon, \tag{D.61}$$

with $\nabla\varepsilon_{l\sigma\mathbf{k}}$ the gradient of $\varepsilon_{l\sigma\mathbf{k}}$ considered as a function of $\mathbf{k}$. Hence, for any integrand $g(\mathbf{k})$:

$$\int\int dS dx\ g(\mathbf{k}) = \int d\varepsilon \int_{\{\varepsilon_{l\sigma\mathbf{k}}=\varepsilon\}} dS\ \frac{g(\mathbf{k})}{|\nabla\varepsilon_{l\sigma\mathbf{k}}|}. \tag{D.62}$$

In summary, we obtain for the sum (D.43):

$$\sum_{\mathbf{k}_M \in \mathcal{K}_{l_M}} |T_{l_M\sigma_M\mathbf{k}_M}|^2 \; f^{(\pm 1)}_{l_M\sigma_M}\left(\varepsilon_{l_M\sigma_M\mathbf{k}_M}\right) \tag{D.63}$$
$$\exp\left\{\frac{i}{\hbar}\; v_M \mathrm{sg}^{(3)}\left(M, J_S\right)\; \varepsilon_{l_M\sigma_M\mathbf{k}_M}\;\left[S_M\left(J_S\right)\left(\overline{\tau}_{2n-1},\ldots,\overline{\tau}_1\right)\right]\right\}$$

$$\approx \int d\varepsilon\; \alpha_{l_M\sigma_M}(\varepsilon) f^{(\pm 1)}_{l_M\sigma_M}(\varepsilon)$$
$$\exp\left\{\frac{i}{\hbar}\; v_M \mathrm{sg}^{(3)}\left(M, J_S\right)\; \varepsilon\;\left[S_M\left(J_S\right)\left(\overline{\tau}_{2n-1},\ldots,\overline{\tau}_1\right)\right]\right\},$$

where for any $l \in \mathcal{L}$, and $\sigma \in \mathcal{S}$, the function $\alpha_{l\sigma}(\varepsilon)$ is defined by Eq. (D.60) and the approximation (D.56).

D.3 Diagrammatic Expansion of $K(\tau)$

Performing the replacement according to (D.63) within Eq. (D.42), we obtain the following expansion of the density matrix kernel:

$$\begin{aligned} K(\tau) \;=\; & \sum_{n=1}^{\infty}\sum_{k=0}^{2n}\sum_{S\subset\{1,\ldots,2n\}:|S|=k}\sum_{\mathcal{P}\in\varphi_S^{-1}PF_{irr}\{1,\ldots,2n\}} \\ & \sum_{a_1,\ldots,a_{k+1}\in\mathcal{B}}\;\sum_{b_k,\ldots,b_{2n}\in\mathcal{B}}\;\sum_{(l_M,\sigma_M,v_M)_{M\in\mathcal{P}}\in(\mathcal{L}\times\mathcal{S}\times\{\pm1\})^{\mathcal{P}}} \\ & K\Big\{n,k,J_S,\mathcal{P},(a_j)_{j=1}^{k+1},(b_j)_{j=k}^{2n},(l_M,\sigma_M,v_M)_{M\in\mathcal{P}}, \\ & \left(\alpha^{(v)}_{l\sigma}\right)_{l\in\mathcal{L},\sigma\in\mathcal{S},v\in\{\pm1\}},(E_b-E_a)_{a,b\in\mathcal{B}}\Big\}(\tau), \end{aligned} \tag{D.64}$$

where $\mathcal{B}$ is a basis consisting of eigenvectors of the quantum dot's Hamiltonian $\mathrm{H}_\odot$, and, for each $a \in \mathcal{B}$, the energy E_a is the corresponding eigenvalue.The sequence $J_S(j)_{j=1}^{2n}$ (Def. D.33) of integer intervals is defined according to Fig. D.4, and Fig. C.1, while $\varphi_S^{-1}PF_{irr}\{1,\ldots,2n\}$ is the set of all pair formations of the numbers $\{1,\ldots,2n\}$ whose image under the map

$$\varphi_S:\; \{1,\ldots,2n\} \to \{1,\ldots,2n\} \tag{D.65}$$

(Def. (C.13)) is irreducible (cp. Fig. C.9). We define the functions $\alpha^{(v)}_{l\sigma}(\varepsilon)$ by the product

$$\alpha_{l\sigma}^{(v)}(\varepsilon) \;:=\; \alpha_{l\sigma}(\varepsilon) f_{l\sigma}^{(v)}(\varepsilon), \tag{D.66}$$

where the factor $\alpha_{l\sigma}$ (Def. (D.60), (D.56)) is proportional to the norm-square of the tunneling coupling, and where $f_{l\sigma}^{(+1)}$ $\left(f_{l\sigma}^{(-1)}\right)$ (Def. (D.17)) is the Fermi function of contact l and spin σ at chemical potential $\mu_{l\sigma}$ and temperature T (one minus this function).

For any $n \in \mathbb{N}_1, k \in \{0,\ldots,2n\}, S \subset \{1,\ldots,2n\}$ with $|S| = k$, $\mathcal{P} \in \varphi_S^{-1} PF_{irr}\{1,\ldots,2n\}$, any sequences of states $a_1,\ldots,a_{k+1}, b_k,\ldots,b_{2n} \in \mathcal{B}$, for any family $(l_M,\sigma_M,v_M)_{M\in\mathcal{P}}$ of elements in $\mathcal{L}\times\mathcal{S}\times\{\pm 1\}$, for any family of integrable functions $\left(\gamma_{l\sigma}^{(v)}(\varepsilon)\right)_{l\in\mathcal{L},\sigma\in\mathcal{S},v\in\{\pm1\}}$, any family of energies $(E_{ba})_{a,b\in\mathcal{B}}$, and for any endomorphism $\hat{y} : V_\odot \to V_\odot$ we define:

$$K\Big\{n,k,J_S,\mathcal{P},(a_j)_{j=1}^{k+1},(b_j)_{j=k}^{2n},(l_M,\sigma_M,v_M)_{M\in\mathcal{P}}, \tag{D.67}$$
$$\left(\gamma_{l\sigma}^{(v)}\right)_{l\in\mathcal{L},\sigma\in\mathcal{S},v\in\{\pm1\}},(E_{ba})_{a,b\in\mathcal{B}}\Big\}(\tau)\;\hat{y}$$

$$:= \;\; \langle a_{k+1}|\hat{y}(b_k)\rangle \;\; |a_1><b_{2n}|$$
$$\mathrm{sg}^{(1)}\;\left\{n,k,\mathcal{P},(a_j)_{j=1}^{k+1},(b_j)_{j=k}^{2n},(\sigma_M,v_M)_{M\in\mathcal{P}}\right\}$$

$$\mathrm{I}\left\{n,J_S,\mathcal{P},\left(E_{b_{max(J_S(j))}a_{min(J_S(j))}}\right)_{j=1}^{2n-1},\right.$$
$$\left.\left(\gamma_{l_M\sigma_M}^{\left(sg^{(2)}(M,k)v_M\right)}\right)_{M\in\mathcal{P}},\left(\mathrm{sg}^{(3)}\left(M,J_S\right)v_M\right)_{M\in\mathcal{P}}\right\}(\tau).$$

The maps $\mathrm{sg}^{(1)}, sg^{(2)}, \mathrm{sg}^{(3)}$ are given in Defs. (D.39), (D.40), and (D.41), respectively; for any $n \in \mathbb{N}_1$, $S \subset \{1,\ldots,2n\}, \mathcal{P} \in \varphi_S^{-1} PF_{irr}\{1,\ldots,2n\}$, for any sequence of energies $(E_j)_{j=1}^{2n-1}$, any familiy of integrable functions $(\gamma_M)_{M\in\mathcal{P}}$, and for any family of signs $(w_M)_{M\in\mathcal{P}}$ we define the integral

$$\mathrm{I}\left\{n,J_S,\mathcal{P},\;(E_j)_{j=1}^{2n-1},\;(\gamma_M)_{M\in\mathcal{P}},\;(w_M)_{M\in\mathcal{P}}\right\}(\tau) \;:= \tag{D.68}$$

$$\frac{1}{\hbar^{2n}}\;\frac{1}{\sqrt{2n-1}}\;\int_{\left\{S^{(2n-1)}=\tau\right\}}\;\int_{\mathbb{R}^{\mathcal{P}}}$$

$$\left(\prod_{M\in\mathcal{P}}\gamma_M(\varepsilon_M)\right)\ \exp\left\{\ \frac{i}{\hbar}\sum_{j=1}^{2n-1}\overline{\tau}_j\left[\ E_j + \sum_{M\in\mathcal{P}:|M\cap J_S(j)|=1} w_M\ \varepsilon_M\ \right]\ \right\}.$$

The set $\left\{S^{(2n-1)}=\tau\right\}$ is defined in Eq. (D.27) (cp. Fig. 2.6), while $\mathbb{R}^{\mathcal{P}}$ is the set of all maps $\mathcal{P}\to\mathbb{R}$, or else

$$\mathbb{R}^{\mathcal{P}} \ = \ \{(\varepsilon_M)_{M\in\mathcal{P}}:\ \text{for all } M\in\mathcal{P}:\varepsilon_M\in\mathbb{R} \text{ arbitrary}\}. \tag{D.69}$$

The present integral over $\mathbb{R}^{\mathcal{P}}$ is thus one over a number of n real integration variables $\varepsilon_M, M\in\mathcal{P}$.

D.4 Diagram Versions and Equivalence

We shall collect the majority of the parameters that determine a particular contribution to the density matrix kernel, Eq. (D.67), in a set "$\mathcal{D}$". We refer to the elements of $\mathcal{D}$ as *diagrams*, and, in the main part of this work, we indeed represent them in the form of drawings. There are two directly related versions of diagrams; we here show their equivalence and give the map that transforms them.

D.4.1 Diagram Transformation

Let $n\in\mathbb{N}_1$ and $k\in\{0,\ldots,2n\}$ be fixed and given, let

$$\mathbb{P}^{(2n)}_{(k)} \ := \ \{S\subset\{1,\ldots,2n\}:|S|=k\}\,, \tag{D.70}$$

the set of all subsets of $\{1,\ldots,2n\}$ with a number of k elements; we consider the assignment

$$S\ \left(\in\mathbb{P}^{(2n)}_{(k)}\right)\ \mapsto\ J_S, \tag{D.71}$$

with $J_S=\left(\varphi_S^{-1}\{1,\ldots,j\}\right)_{j=1}^{2n-1}$ the sequence of intervals of natural numbers according to Def. (D.33), and Fig. D.4, and the map

$$\varphi_S:\ \{1,\ldots,2n\}\to\{1,\ldots,2n\} \tag{D.72}$$

given in Fig. C.1.

Bijectivity of the Assignment $S \mapsto J_S$

For fixed and given values of $n \in \mathbb{N}_1$, and $k \in \{0, \ldots, 2n\}$, we show that the assignment (D.71) is injective, and we determine its image, as well as its inverse assignment. We note first that $J_S \in \mathcal{J}^{(2n)}$, with

$$\begin{aligned} \mathcal{J}^{(2n)} \quad := \quad \Big\{ & (J(j))_{j=1}^{2n-1} : \ J(1), \ldots, J(2n-1) \in \mathbb{P}\{1, \ldots, 2n\}, \\ & |J(1)| = 1, \ \forall j \in \{1, \ldots, 2n-2\} : \\ & J(j+1) = J(j) \cup \{\min J(j) - 1\} \ \text{ or} \\ & J(j+1) = J(j) \cup \{\max J(j) + 1\} \Big\}, \end{aligned} \tag{D.73}$$

that

$$J_S(1) \ = \ \begin{cases} \{k\} & (\text{if } 1 \in S) \\ \{k+1\} & (\text{else}), \end{cases} \tag{D.74}$$

and, that

$$S \ = \ \{j \in \{1, \ldots, 2n\} : \ J_S(j) \setminus J_S(j-1) \subset \{1, \ldots, k\}\}, \tag{D.75}$$

where we use the notation

$$\begin{aligned} J_S(0) \quad &:= \quad \emptyset, \\ J_S(2n) \quad &:= \quad \{1, \ldots, 2n\}, \end{aligned} \tag{D.76}$$

since $J_S(j) \setminus J_S(j-1) = \varphi_S^{-1}\{j\}$, and $\varphi_S^{-1}(j) \leq k \Leftrightarrow j \in S$. By the notation

$$\mathcal{J}_{(k)}^{(2n)} \ := \ \Big\{ J \in \mathcal{J}^{(2n)} : \ J(1) \ \in \ \{\{k\}, \{k+1\}\} \Big\} \tag{D.77}$$

we conclude that the assignment (D.71) is injective with an image contained in $\mathcal{J}_{(k)}^{(2n)}$.

At the same time, if we *define* for a given interval sequence $J \in \mathcal{J}_{(k)}^{(2n)}$:

$$S \ := \ \{j \in \{1, \ldots, 2n\} : \ J(j) \setminus J(j-1) \subset \{1, \ldots, k\}\}, \tag{D.78}$$

where

$$\begin{aligned} J(0) \quad &:= \quad \emptyset, \\ J(2n) \quad &:= \quad \{1, \ldots, 2n\}, \end{aligned} \tag{D.79}$$

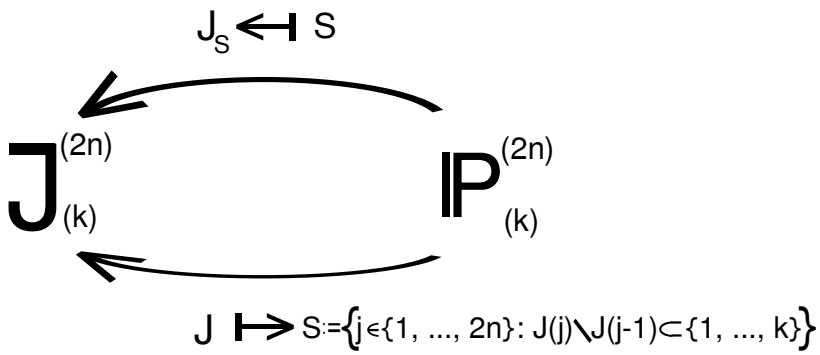

Figure D.6: For any two fixed and given values of $n \in \mathbb{N}$, and $k \in \{0, 1, \ldots, 2n\}$, the assignments (D.71), and (D.78) are bijective, and they are inverse to each other, since, for $S \in \mathbb{P}_{(k)}^{(2n)}$, the set S is recovered in J_S by the relation $S = \{j \in \{1, \ldots, 2n\} : \; J_S(j) \setminus J_S(j-1) \subset \{1, \ldots, k\}\}$.

then $|S| = k$, and $S \subset \{1, \ldots, 2n\}$, so

$$S \; \in \; \mathbb{P}_{(k)}^{(2n)}, \tag{D.80}$$

and for all $j \in \{1, \ldots, 2n\}$:

$$J(j) \; = \; \Big\{ k + 1 - |S \cap \{1, \ldots, j\}| \, , \ldots , k + |S^c \cap \{1, \ldots, j\}| \Big\}, \tag{D.81}$$

with

$$S^c \; := \; \{1, \ldots, 2n\} \setminus S. \tag{D.82}$$

Hence, the assignment $J \mapsto S$ of Def. (D.78), too, is injective. As a consequence,

$$\left|\mathbb{P}_{(k)}^{(2n)}\right| \; \leq \; \left|\mathcal{J}_{(k)}^{(2n)}\right| \; \leq \; \left|\mathbb{P}_{(k)}^{(2n)}\right|, \; \Rightarrow \; \left|\mathcal{J}_{(k)}^{(2n)}\right| = \left|\mathbb{P}_{(k)}^{(2n)}\right|, \tag{D.83}$$

and the assignment (D.71) is bijective with the inverse assignment (D.78). □

Moreover, we conclude from the relation $J_S(j) \; = \; \varphi_S^{-1}\{1, \ldots, j\}$(D.33), that for arbitrary $S, S' \subset \{1, \ldots, 2n\}$ the equivalence

$$J_S \; = \; J_{S'} \; \Leftrightarrow \; \varphi_S \; = \; \varphi_{S'} \tag{D.84}$$

holds, hence the assignment

$$J \ \left(\in \mathcal{J}^{(2n)}\right) \ \mapsto \ \varphi_{(J)} := \varphi_S \text{ with } S \subset \{1,\ldots,2n\}, J_S = J \tag{D.85}$$

is well-defined. We introduce sets $\mathcal{D}'$, and $\overline{\mathcal{D}'}$, of (transformed) *diagrams* as follows:

$$\begin{aligned}
\overline{\mathcal{D}'} \ := \ & \Big\{ \Big(n,k,J,\mathcal{P},(a_j)_{j=1}^{k+1},(b_j)_{j=k}^{2n},(l_M,\sigma_M,v_M)_{M\in\mathcal{P}}\Big) : \\
& n\in\mathbb{N}_1, k\in\{0,\ldots,2n\}, J\in\mathcal{J}^{(2n)}_{(k)}, \\
& \mathcal{P}\in\varphi_{(J)}^{-1}PF_{irr}\{1,\ldots,2n\}, \\
& (a_j)_{j=1}^{k+1}\in\mathcal{B}^{\{1,\ldots,k+1\}}, (b_j)_{j=k}^{2n}\in\mathcal{B}^{\{k,\ldots,2n\}}, \\
& (l_M,\sigma_M,v_M)_{M\in\mathcal{P}}\in(\mathcal{L}\times\mathcal{S}\times\{\pm1\})^{\mathcal{P}}\Big\},
\end{aligned} \tag{D.86}$$

and

$$\begin{aligned}
\mathcal{D}' \ := \ & \Big\{ \Big(n,k,S,\mathcal{Q},(a_j)_{j=1}^{k+1},(b_j)_{j=k}^{2n},(l_N,\sigma_N,v_N)_{N\in\mathcal{Q}}\Big) : \\
& n\in\mathbb{N}_1, k\in\{0,\ldots,2n\}, S\in\mathbb{P}^{(2n)}_{(k)}, \\
& \mathcal{Q}\in PF_{irr}\{1,\ldots,2n\}, \\
& (a_j)_{j=1}^{k+1}\in\mathcal{B}^{\{1,\ldots,k+1\}}, (b_j)_{j=k}^{2n}\in\mathcal{B}^{\{k,\ldots,2n\}}, \\
& (l_N,\sigma_N,v_N)_{N\in\mathcal{Q}}\in(\mathcal{L}\times\mathcal{S}\times\{\pm1\})^{\mathcal{Q}}\Big\}.
\end{aligned} \tag{D.87}$$

We note the bijection

$$\begin{aligned}
& T_{diag}: \ \mathcal{D}' \ \to \ \overline{\mathcal{D}'}, \\
& \Big(n,k,S,\mathcal{Q},(a_j)_{j=1}^{k+1},(b_j)_{j=k}^{2n},(l_N,\sigma_N,v_N)_{N\in\mathcal{Q}}\Big) \ \mapsto \\
& \Big(n,k,J_S,\varphi_S^{-1}\mathcal{Q},(a_j)_{j=1}^{k+1},(b_j)_{j=k}^{2n},\big(l_{\varphi_S(M)},\sigma_{\varphi_S(M)},v_{\varphi_S(M)}\big)_{M\in\varphi_S^{-1}\mathcal{Q}}\Big),
\end{aligned} \tag{D.88}$$

and, to take into account only diagrams with a non-zero contribution to the kernels, we define

$$\overline{\mathcal{D}} \ := \ \left\{\overline{D}\in\overline{\mathcal{D}'}: \ \mathrm{sg}^{(1)}(\overline{D})\neq 0\right\}, \tag{D.89}$$

with

$$\mathrm{sg}^{(1)}(\overline{D}) \;:=\; \mathrm{sg}^{(1)}\left\{n,k,\mathcal{P},(a_j)_{j=1}^{k+1},(b_j)_{j=k}^{2n},(\sigma_M,v_M)_{M\in\mathcal{P}}\right\} \tag{D.90}$$

for

$$\overline{D} \;=\; \left(n,k,J,\mathcal{P},(a_j)_{j=1}^{k+1},(b_j)_{j=k}^{2n},(l_M,\sigma_M,v_M)_{M\in\mathcal{P}}\right) \tag{D.91}$$

(Def. (D.39)), and, correspondingly,

$$\mathcal{D} \;:=\; T_{diag}^{-1}\left(\overline{\mathcal{D}}\right). \tag{D.92}$$

D.4.2 Kernel as Sum over Diagrams

Upon gathering most of the parameters that determine a particular contribution to the sum (D.64) in the transformed diagram $\overline{D}$, we can rewrite Eq. (D.64):

$$K(\tau) \;=\; \sum_{\overline{D}\in\overline{\mathcal{D}}} K\Big\{\overline{D},\left(\alpha_{l\sigma}^{(v)}\right)_{l\in\mathcal{L},\sigma\in\mathcal{S},v\in\{\pm1\}},(E_b-E_a)_{a,b\in\mathcal{B}}\Big\}(\tau), \tag{D.93}$$

where the summands on the right-hand side are defined in Eq. (D.67). In addition, we define to any $D\in\mathcal{D}$, any family $\left(\gamma_{l\sigma}^{(v)}\right)_{l\in\mathcal{L},\sigma\in\mathcal{S},v\in\{\pm1\}}$ of integrable functions, and to any family of energies $(E_{ba})_{a,b\in\mathcal{B}}$:

$$\begin{aligned} K\Big\{D,\left(\gamma_{l\sigma}^{(v)}\right)_{l\in\mathcal{L},\sigma\in\mathcal{S},v\in\{\pm1\}},(E_{ba})_{a,b\in\mathcal{B}}\Big\} \;:=\; \\ K\Big\{T_{diag}D,\left(\gamma_{l\sigma}^{(v)}\right)_{l\in\mathcal{L},\sigma\in\mathcal{S},v\in\{\pm1\}},(E_{ba})_{a,b\in\mathcal{B}}\Big\}, \end{aligned} \tag{D.94}$$

where the right-hand side is given by Eq. (D.67). [For simplicity we use the same name "K" for two formally different maps.]

In cases where we do not focus on the dependence on the energy differences E_b-E_a, or on the functions $\alpha_{l\sigma}^{(v)}$, we shall omit these parameters in the notation and abbreviate:

$$K(D) \;:=\; K\Big\{D,\left(\alpha_{l\sigma}^{(v)}\right)_{l\in\mathcal{L},\sigma\in\mathcal{S},v\in\{\pm1\}},(E_b-E_a)_{a,b\in\mathcal{B}}\Big\}, \tag{D.95}$$

and analogously, for $\overline{D} \in \overline{\mathcal{D}}$,

$$K(\overline{D}) \;:=\; K(T_{diag}^{-1}\overline{D}). \tag{D.96}$$

In summary, we note the expansion of the density matrix kernel as sum over (transformed) diagrams:

$$K(\tau) \;=\; \sum_{D\in\mathcal{D}} K\left(D\right)(\tau) \;=\; \sum_{\overline{D}\in\overline{\mathcal{D}}} K\left(\overline{D}\right)(\tau). \tag{D.97}$$

D.5 Mirror Rule and Conjugate Diagrams

We here give a proof of mirror rule (2.111), and of the relation (2.148), which holds between the contributions of conjugate diagrams (Fig. 2.22) to the kernels.

D.5.1 Proof of Mirror Rule

We show the following general statement: For any family of integrable and real functions $\gamma_{l\sigma}^{(v)}$, for any family of real energy values $(E_{ba})_{a,b\in\mathcal{B}}$ that satisfies

$$E_{ba} + E_{ab} \;=\; 0, \;\; (a,b\in\mathcal{B}), \tag{D.98}$$

and for any self-adjoint linear map $\hat{y} : V_\odot \to V_\odot$, the equality

$$\begin{aligned} &K\Big\{\mathrm{mir}(D), \quad \left(\gamma_{l\sigma}^{(v)}\right)_{l\in\mathcal{L},\sigma\in\mathcal{S},v\in\{\pm1\}}, (E_{ba})_{a,b\in\mathcal{B}}\Big\}(\tau)\;\hat{y} \quad = \\ &\Big[K\Big\{\quad D\quad, \quad \left(\gamma_{l\sigma}^{(v)}\right)_{l\in\mathcal{L},\sigma\in\mathcal{S},v\in\{\pm1\}}, (E_{ba})_{a,b\in\mathcal{B}}\Big\}(\tau)\;\hat{y}\Big]^\dagger \end{aligned} \tag{D.99}$$

holds, with "mir" the mirror-map (2.109), and where the dagger on the right-hand side denotes the adjoint operator (the Hermitian conjugate).

The equation is verified by inserting $T_{diag}\mathrm{mir}D$ into the definition of

$$K\left\{\overline{D}, \left(\gamma_{l\sigma}^{(v)}\right)_{l\in\mathcal{L},\sigma\in\mathcal{S},v\in\{\pm1\}}, (E_{ba})_{a,b\in\mathcal{B}}\right\}(\tau)\;\hat{y} \tag{D.100}$$

(D.67), applying the relation

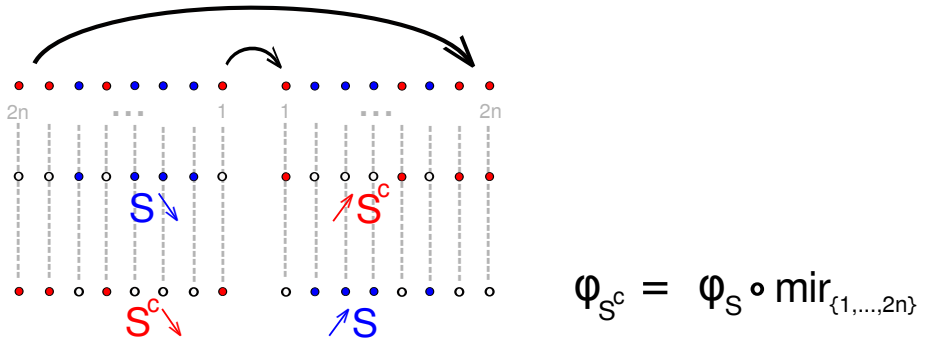

Figure D.7: A list of the numbers $1, \ldots, 2n$, depicted as small circles arranged along one straight line, is mirrored at a vertical axis in the first line of the present figure. The elements of a subset $S \subset \{1, \ldots, 2n\}$ are marked in blue, while the elements of its complement $S^c = \{1, \ldots, 2n\} \setminus S$ are marked in red. The second line of circles, read from the left to the right, shows a list of the numbers $1, \ldots, 2n$ in the order $\varphi_S(1), \varphi_S(2), \ldots, \varphi_S(2n)$, while a list of the same numbers in the order $\varphi_{S^c}(1), \varphi_{S^c}(2), \ldots, \varphi_{S^c}(2n)$ is found in the last line; a comparison of the two lists yields the relation $\varphi_{S^c} = \varphi_S \circ \mathrm{mir}_{\{1,\ldots,2n\}}$.

$$\varphi_{S^c}^{-1} \circ \varphi_S \;=\; \mathrm{mir}_{\{1,\ldots,2n\}} \tag{D.101}$$

(cp. Fig. D.7), where

$$\begin{aligned} \mathrm{mir}_{\{1,\ldots,2n\}} : \quad \{1, \ldots, 2n\} \quad &\to \quad \{1, \ldots, 2n\}, \\ j \quad &\mapsto \quad 2n + 1 - j. \end{aligned} \tag{D.102}$$

We here do not present the lengthy sequence of equalities that explicitly show Eq. (D.99), but rather only note the identities we apply within these manipulations: In particular, we make use of the equalities

$$\mathrm{sign}\,\left(\mathrm{mir}_{\{1,\ldots,2n\}}\mathcal{P}\right) \;=\; \mathrm{sign}\,(\mathcal{P})\,, \tag{D.103}$$

with $\mathcal{P} := \varphi_S^{-1}\mathcal{Q}$ (cp. Fig. C.3), and

$$J_{S^c} = \mathrm{mir}_{\{1,\ldots,2n\}} J_S, \tag{D.104}$$

following from $J_S(j) = \varphi_S^{-1}\{1, \ldots, j\}$ (cp. Fig. D.4). □

D.5.2 Proof of Relation (2.148) (Contribution of Conjugate Diagrams to the Kernels)

From the relation

$$\varphi_{\tilde{S}}^{-1} \circ \varphi_S \;=\; \zeta_{(-1)}, \tag{D.105}$$

with $\tilde{S} := S \setminus \{2n\}$ as in Eq. (2.141), where

$$\zeta_{(-1)} : \quad \{1, \ldots, 2n\} \to \{1, \ldots, 2n\}, \tag{D.106}$$

$$j \mapsto \begin{cases} j-1 & (j \geq 2) \\ 2n & (j = 1), \end{cases}$$

we conclude by inserting $T_{diag} T_{cyc,\uparrow} D$ into Def. (D.67), that for any $D \in \mathcal{D}_{l,0}$ (2.138), any linear map $\hat{y}$ operating on $V_\odot$, for any family of integrable functions $\left(\gamma_{l\sigma}^{(v)}\right)_{l\in\mathcal{L},\sigma\in\mathcal{S},v\in\{\pm1\}}$, and any family of energies $(E_{ba})_{a,b\in\mathcal{B}}$:

$$\begin{aligned} & Tr\Big\{K\big\{T_{cyc,\uparrow} D, \left(\gamma_{l\sigma}^{(v)}\right)_{l\in\mathcal{L},\sigma\in\mathcal{S},v\in\{\pm1\}}, (E_{ba})_{a,b\in\mathcal{B}}\big\}(\tau)\ \hat{y}\Big\} \\ = \; & (-1) Tr\Big\{K\big\{\quad D \quad, \left(\gamma_{l\sigma}^{(v)}\right)_{l\in\mathcal{L},\sigma\in\mathcal{S},v\in\{\pm1\}}, (E_{ba})_{a,b\in\mathcal{B}}\big\}(\tau)\ \hat{y}\Big\}. \quad \square \end{aligned}$$

Appendix E

Perturbation Theory

The present appendix deals with the *perturbative* application of the transport theory: The integral kernel $K(t)$ of the quantum master equation (2.45) has the form $K(t) = \sum_{n=1}^{\infty} K^{(2n)}(t)$ (Eq. (2.46)), where the summand $K^{(2n)}(t)$ contains the tunneling Hamiltonian $\hat{H}_T$, and thus the tunneling coupling, $2n$ times. We here show that

$$\sum_{D\in\mathcal{D}} \int_0^\infty dt\ |K(D)(t)| \quad < \quad \infty \tag{E.1}$$

for sufficiently small value of the coupling-parameter. This implies that the Laplace-transformed kernel $\mathbf{K}$, appearing in Eq. (2.120), is analytic in the coupling-parameter around zero. Hence, the perturbative application of the transport theory is justified for sufficiently small coupling.

In a second part we give the mathematical background for the direct calculation of diagrams, and we determine the contribution of all DSO-diagrams up to sixth order in the coupling, neglecting the doubly occupied state. We analyze the results regarding the temperature-dependence of the linear conductance, and thus find a zero bias anomaly of the dynamic conductance.

E.1 Analyticity of the Integral Kernel in the Coupling-Parameter

E.1.1 Fourier Transforms in the Contributions to the Kernel

For any given diagram

$$\overline{D} \;=\; \left(n, k, J, \mathcal{P}, (a_j)_{j=1}^{k+1}, (b_j)_{j=k}^{2n}, (l_M, \sigma_M, v_M)_{M\in\mathcal{P}}\right) \;\in \overline{\mathcal{D}} \tag{E.2}$$

(D.89), we can write the diagram's contribution to the integral kernel (D.67) as follows:

$$K(\overline{D})(\tau)\hat{y} \qquad = \qquad \langle a_{k+1}|\hat{y}(b_k)\rangle \; |a_1><b_{2n}| \; \mathrm{sg}^{(1)}(\overline{D})$$

$$\frac{1}{\hbar^{2n}}\frac{1}{\sqrt{2n-1}}\int_{\left\{S^{(2n-1)}=\tau\right\}} \int_{\mathbb{R}^{\mathcal{P}}} \exp\left(\frac{i}{\hbar}\sum_{j=1}^{2n-1} \overline{\tau}_j E_j\right)$$
$$\prod_{M\in\mathcal{P}}\left(\gamma_M(\varepsilon_M) \; \exp\left\{\frac{i}{\hbar}\varepsilon_M S_M(J)(\overline{\tau}_{2n-1},\ldots,\overline{\tau}_1)w_M\right\}\right), \tag{E.3}$$

with $\mathrm{sg}^{(1)}(\overline{D})$ the sign defined in (D.39), with

$$E_j \;=\; E_{b_{\max J(j)}} - E_{a_{\min J(j)}}, \tag{E.4}$$

and with γ_M the function

$$\gamma_M \;=\; \alpha_{l_M\sigma_M}^{(sg^{(2)}(M,k)v_M)}. \tag{E.5}$$

The operator $\hat{y}$ is an arbitrary linear map $V_\odot \to V_\odot$, while the sign w_M is given by

$$w_M \;=\; v_M \mathrm{sg}^{(3)}(M, J), \tag{E.6}$$

and $S_M(J)(\overline{\tau}_{2n-1},\ldots,\overline{\tau}_1) = \sum_{j\in\{1,\ldots,2n-1\}:|M\cap J(j)|=1}\overline{\tau}_j$ (Def. (D.44)).

Upon performing the integral over ε_M in (E.3), we obtain a Fourier transform for each $M \in \mathcal{P}$. Applying the definition

$$(\mathcal{F}\gamma)(\tau) \;:=\; \int d\varepsilon \; \gamma(\varepsilon)e^{-i\tau\varepsilon}, \tag{E.7}$$

the integral over ε_M in Eq. (E.3) is

$$(\mathcal{F}\gamma_M)\left(\frac{-1}{\hbar}w_M S_M(J)(\overline{\tau}_{2n-1},\ldots,\overline{\tau}_1)\right). \tag{E.8}$$

Applying the operator norm to $K(\overline{D})(\tau)\hat{y}$, as well as to $K(\overline{D})(\tau)$, we obtain the following estimate for the diagram's contribution to the kernel:

$$\begin{aligned}\left|K(\overline{D})(\tau)\right| \quad &\leq \quad \frac{1}{\hbar^{2n}}\frac{1}{\sqrt{2n-1}}\int_{\left\{S^{(2n-1)}=\tau\right\}} \\ &\prod_{M\in\mathcal{P}}\left|(\mathcal{F}\gamma_M)\left(\frac{-1}{\hbar}w_M S_M(J)(\overline{\tau}_{2n-1},\ldots,\overline{\tau}_1)\right)\right|.\end{aligned} \tag{E.9}$$

E.1.2 Exponential Decay of Fourier Transforms (Assumption)

We *assume* now that the Fourier transforms of all of the functions $\alpha_{l\sigma}^{(v)}$ (D.66) are bounded by an exponential decay, i.e.,

$$\left|\left(\mathcal{F}\alpha_{l\sigma}^{(v)}\right)(\tau)\right| \;\leq\; a\exp(-c|\tau|), \tag{E.10}$$

with $a, c > 0$ independent of τ. Upon inserting this estimate on the right-hand side of Eq. (E.9), we obtain the inequality:

$$\left|K(\overline{D})(\tau)\right| \leq \frac{a^n}{\hbar^{2n}}\frac{1}{\sqrt{2n-1}}\int_{\left\{S^{(2n-1)}=\tau\right\}}\exp\left(\frac{-c}{\hbar}\sum_{M\in\mathcal{P}}S_M(J)(\overline{\tau}_{2n-1},\ldots,\overline{\tau}_1)\right). \tag{E.11}$$

We swap the order of the sums in the exponent:

$$\begin{aligned}\sum_{M\in\mathcal{P}}S_M(J)(\overline{\tau}_{2n-1},\ldots,\overline{\tau}_1) \quad &= \quad \sum_{M\in\mathcal{P}}\sum_{j\in\{1,\ldots,2n-1\}:|M\cap J(j)|=1}\overline{\tau}_j \\ &= \quad \sum_{j=1}^{2n-1}\sum_{M\in\mathcal{P}:|M\cap J(j)|=1}\overline{\tau}_j \\ &= \quad \sum_{j=1}^{2n-1}N_{J(j)}(\mathcal{P})\overline{\tau}_j,\end{aligned} \tag{E.12}$$

with

$$N_{J(j)}(\mathcal{P}) \;:=\; \left|\{M\in\mathcal{P} : |M\cap J(j)| = 1\}\right|, \tag{E.13}$$

the number of pairs $M \in \mathcal{P}$ with the property that exactly one of the pair's elements is contained in the integer interval $J(j)$.

We are interested in the Laplace transform

$$(\mathcal{L}K)(\lambda) \;=\; \int_0^\infty d\tau\; e^{-\lambda\tau} K(\tau), \tag{E.14}$$

and in particular in the limit $\lim_{\lambda\to 0+}(\mathcal{L}K)(\lambda)$, since the Laplace transform of the kernel appears in the equation for the stationary reduced density matrix (2.120). Hence, we consider the integral $\int_0^\infty d\tau \left|K(\overline{D})(\tau)\right|$: Upon applying the integral transformation according to Fig. 2.6 in backward direction, we obtain from (E.11) the estimate:

$$\int_0^\infty d\tau\;\left|K(\overline{D})(\tau)\right| \;\leq\; \frac{1}{\hbar}\,\frac{a^n}{c^{2n-1}}\,\prod_{j=1}^{2n-1}\frac{1}{N_{J(j)}(\mathcal{P})}. \tag{E.15}$$

Taking the sum over all diagrams (D.89) of order $2n$ in the tunneling coupling, we conclude that $K^{(2n)}$ satisfies the inequality

$$\begin{aligned}\int_0^\infty d\tau \left|K^{(2n)}(\tau)\right| \;\leq\; & \sum_{k=0}^{2n} \sum_{a_1,\ldots,a_{k+1},b_k,\ldots b_{2n}\in\mathcal{B}} \sum_{J\in\mathcal{J}_{(k)}^{(2n)}} \sum_{\mathcal{P}\in\varphi_{(J)}^{-1}PF_{irr}\{1,\ldots,2n\}} \\ & \sum_{(l_M)_{M\in\mathcal{P}}\in\mathcal{L}^{\mathcal{P}}} \sum_{(\sigma_M)_{M\in\mathcal{P}}\in\mathcal{S}^{\mathcal{P}}} \sum_{(v_M)_{M\in\mathcal{P}}\in\{\pm 1\}^{\mathcal{P}}}\end{aligned}$$

$$\int_0^\infty d\tau\; |K\underbrace{\left(n,k,J,\mathcal{P},(a_j)_{j=1}^{k+1},(b_j)_{j=k}^{2n},(l_M,\sigma_M,v_M)_{M\in\mathcal{P}}\right)}_{\overline{D}}(\tau)|$$

$$\begin{aligned}\leq\; & \frac{1}{\hbar}\,\frac{(2a)^n}{c^{2n-1}} \sum_{k=0}^{2n} \sum_{a_1,\ldots,a_{k+1},b_k,\ldots b_{2n}\in\mathcal{B}} \sum_{J\in\mathcal{J}_{(k)}^{(2n)}} \sum_{\mathcal{P}\in\varphi_{(J)}^{-1}PF_{irr}\{1,\ldots,2n\}} \\ & \prod_{j=1}^{2n-1}\frac{1}{N_{J(j)}(\mathcal{P})}.\end{aligned} \tag{E.16}$$

In the second step we omit the sums over σ_M, and v_M, since their choice is fixed by the sequences of quantum dot states. The sum over $l \in \mathcal{L}$, on the other hand, is taken into account by the factor 2^n, since we assume there are two leads, so every $l_M, M \in \mathcal{P}$, can take two values.

E.1.3 Combinatorial Intermezzo

We here give an estimate for the sum

$$\sum_{\mathcal{P}\in\varphi_{(J)}^{-1}PF_{irr}\{1,\ldots,2n\}} \prod_{j=1}^{2n-1} \frac{1}{N_{J(j)}(\mathcal{P})}. \tag{E.17}$$

for a fixed and given interval sequence $J \in \mathcal{J}_{(k)}^{(2n)}$ (Def. (D.77)). J is a sequence of integer intervals $J(1) \subset ... \subset J(2n-1) \subset \{1,\ldots,2n\}$ with $|J(j)| = j$. The map $\varphi_{(J)}$, on the other hand, is characterized by the condition

$$\varphi_{(J)}^{-1}\{1,\ldots,j\} \;=\; J(j) \tag{E.18}$$

(Def. (D.85)). Hence, the sum (E.17) goes over all pair formations $\mathcal{P} \in PF\{1,\ldots,2n\}$ which satisfy the condition, that, to any $j \in \{1,\ldots,2n-1\}$, there is a pair $M \in \mathcal{P}$ with

$$|M \cap J(j)| \;=\; 1. \tag{E.19}$$

We now consider one particular pair formation $\mathcal{P}_0 \in \varphi_{(J)}^{-1}PF_{irr}\{1,\ldots,2n\}$ to be fixed and given, and determine the number of (alternative) $\mathcal{P} \in \varphi_{(J)}^{-1}$ $PF_{irr}\{1,\ldots,2n\}$, which produce *the same map* $N_{J(j)}(\mathcal{P})$, i.e., the number of $\mathcal{P}$-s with the property

$$\forall j \in \{1,\ldots,2n-1\}: \;\; N_{J(j)}(\mathcal{P}) \;=\; N_{J(j)}(\mathcal{P}_0). \tag{E.20}$$

To any $j' \in \{1,\ldots,2n\}$ we define

$$x_{j'} \;:=\; \varphi_{(J)}^{-1}(j'); \tag{E.21}$$

then, $J(j) = \{x_1,\ldots,x_j\}$, and the pair formation $\mathcal{P}_0$ is irreducible in the order given by the list $x_1, x_2, \ldots, x_{2n}$ of the elements of $\{1,\ldots,2n\}$ (cp. Fig. E.1).

We consider $N_{J(j)}(\mathcal{P}_0)$ to be a map

$$\begin{aligned} N_J(\mathcal{P}_0): \quad \{1,\ldots,2n-1\} &\;\to\; \{1,2,\ldots\}, \\ j &\;\mapsto\; N_{J(j)}(\mathcal{P}_0). \end{aligned} \tag{E.22}$$

This map has the property that, with every incrementation of the argument, the value of the function changes by ± 1, and that $N_J(\mathcal{P}_0)(2n-1) = N_J(\mathcal{P}_0)(1) = 1$. All information about the map $N_J(\mathcal{P}_0)$ is contained in the subset

$$S^+ \;:=\; \Big\{1\Big\} \cup \Big\{j \in \{2,\ldots,2n-1\} : N_J(\mathcal{P}_0)(j) > N_J(\mathcal{P}_0)(j-1)\Big\}. \tag{E.23}$$

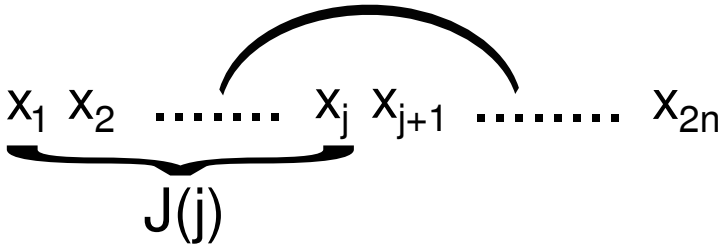

Figure E.1: The elements $x_1, \ldots, x_{2n}$ list the numbers $1, \ldots, 2n$ in the order given by the interval sequence J; to each $J(j), j \leq 2n-1$, there is at least one pair $M \in \mathcal{P}_0$, which connects one element within $J(j)$ to one element outside $J(j)$, as illustrated by the bent line. The map $N_{J(j)}(\mathcal{P}_0)$, on the other hand, counts the number of just these pairs $M \in \mathcal{P}_0$ which share exactly one element with $J(j)$.

In addition, we define $S^- := \{1, \ldots, 2n\} \setminus S^+$. For sure, $|S^+| = |S^-| = n$, and

$$\{1, \ldots, 2n\} = S^+ \cup S^-.$$

We imagine that the elements $x_1, \ldots, x_{2n}$ are listed according to the order of their indices from the left to the right as in Fig. E.1, and we consider an arbitrary pair formation $\mathcal{P}$ which satisfies

$$N_J(\mathcal{P}) \;=\; N_J(\mathcal{P}_0). \tag{E.24}$$

For any $j' \in \{1, \ldots, 2n\}$, let $p_{\mathcal{P}}(j') \in \{1, \ldots, 2n\}$ be defined by the condition

$$\{x_{j'}, x_{p_{\mathcal{P}}(j')}\} \;\in\; \mathcal{P}, \tag{E.25}$$

i.e., to any element $x_{j'}$, its partner $x_{p_{\mathcal{P}}(j')}$ within the pair formation $\mathcal{P}$ is assigned by the map $p_{\mathcal{P}}$ via the indices "j'", and "$p_{\mathcal{P}}(j')$", respectively.

We note that

$$S^+ \;=\; \Big\{\; l \in \{1, \ldots, 2n\} : l < p_{\mathcal{P}}(l) \Big\}\;, \tag{E.26}$$

so the partner of any element x_l, $l \in S^+$, can always be found to the *right* of x_l, while the partner of any $x_{l'}$, $l' \in S^-$, can always be found to the *left* of $x_{l'}$. Thus, the map $N_J(\mathcal{P})$ satisfies the relation

$$N_{J(j)}(\mathcal{P}) \;=\; \big|S^+ \cap \{1, \ldots, j\}\big| - \big|S^- \cap \{1, \ldots, j\}\big|\,. \tag{E.27}$$

We determine the number of alternative pair formations $\mathcal{P}$ which produce the same map $N_J(\mathcal{P})$ as $\mathcal{P}_0$ as follows: We count the elements of the set S^- by a sequence $l_1 < l_2 < \cdots < l_n$ from the left to the right (Fig. E.2).

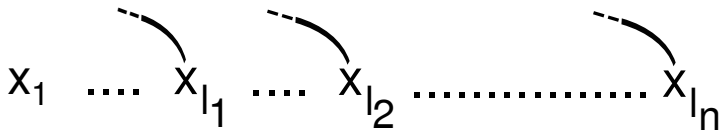

Figure E.2: The elements of the set S^- are counted in increasing order by $l_1 < \cdots < l_n$. In the horizontally arranged list $x_1, \ldots, x_{2n}$, the partner of any of the elements $x_{l_i}, i \in \{1, \ldots, n\}$, is found to the left of x_{l_i}.

Going through the elements of S^- from the left to the right, we notice that, for the first element l_1, we have

$$\left|S^+ \cap \{1, \ldots, l_1\}\right| \;=\; N_{J(l_1)}(\mathcal{P}_0) + 1 \tag{E.28}$$

possibilities to choose a partner within the set $\{1, \ldots, l_1 - 1\}$. For the second element l_2, we have, independently of the particular choice of the partner of l_1,

$$\left|S^+ \cap \{1, \ldots, l_2\}\right| - 1 \;=\; N_{J(l_2)}(\mathcal{P}_0) + 1 \tag{E.29}$$

possibilities to choose a partner: The number $|S^+ \cap \{1, \ldots, l_2\}|$ of all theoretically possible partners is reduced by one by the choice of the partner of l_1. Continuing this procedure of assigning partners to the elements l_i, we notice that in general the number of choices of a partner for l_i is

$$\left|S^+ \cap \{1, \ldots, l_i\}\right| - i + 1 \;=\; N_{J(l_i)}(\mathcal{P}_0) + 1. \tag{E.30}$$

Upon gathering all the possibilities to iteratively choose partners for $l_1, l_2, \ldots, l_n$, we find that the number of pair formations $\mathcal{P}$ with $N_J(\mathcal{P}) = N_J(\mathcal{P}_0)$ is given by the product

$$\prod_{i=1}^{n-1} \left(N_{J(l_i)}(\mathcal{P}_0) + 1\right). \tag{E.31}$$

We want to conclude the present combinatorial intermezzo with an estimate for the sum (E.17). The sum goes over all pair formations $\mathcal{P}$ within the set $\varphi_{(J)}^{-1} PF_{irr}\{1, \ldots, 2n\}$. Hence, we choose a subset

$$\mathcal{S}_{(J)} \;\subset\; \varphi_{(J)}^{-1} PF_{irr}\{1, \ldots, 2n\} \tag{E.32}$$

of pair formations $\mathcal{P}_0$ with the property, that, to any $\mathcal{P} \in \varphi_{(J)}^{-1} PF_{irr}\{1, \ldots, 2n\}$, there is exactly one element $\mathcal{P}_0 \in \mathcal{S}_{(J)}$, so that

$$N_J(\mathcal{P}) \;=\; N_J(\mathcal{P}_0). \tag{E.33}$$

In addition, we define to any $\mathcal{P}_0 \in \mathcal{S}_{(J)}$:

$$Z(\mathcal{P}_0) \;:=\; \left|\left\{\mathcal{P} \in \varphi_{(J)}^{-1} PF_{irr}\{1,\ldots,2n\} :\; N_J(\mathcal{P}) = N_J(\mathcal{P}_0)\right\}\right|. \tag{E.34}$$

We estimate:

$$\sum_{\mathcal{P}\in\varphi_{(J)}^{-1}PF_{irr}\{1,\ldots,2n\}} \prod_{j=1}^{2n-1} \frac{1}{N_{J(j)}(\mathcal{P})} = \sum_{\mathcal{P}_0\in\mathcal{S}_{(J)}} Z(\mathcal{P}_0) \prod_{j=1}^{2n-1} \frac{1}{N_{J(j)}(\mathcal{P}_0)} \tag{E.35}$$

$$\begin{aligned} &= \sum_{\mathcal{P}_0\in\mathcal{S}_{(J)}} \left(\prod_{i=1}^{n-1} \left(N_{J(l_i)}(\mathcal{P}_0)+1\right)\right)\left(\prod_{j=1}^{2n-1} \frac{1}{N_{J(j)}(\mathcal{P}_0)}\right) \\ &\leq \sum_{\mathcal{P}_0\in\mathcal{S}_{(J)}} \left(\prod_{i=1}^{n-1} \left(N_{J(l_i)}(\mathcal{P}_0)+1\right)\right)\left(\prod_{i=1}^{n-1} \frac{1}{N_{J(l_i)}(\mathcal{P}_0)}\right) \\ &\leq 2^{n-1}\left|\mathcal{S}_{(J)}\right|. \end{aligned} \tag{E.36}$$

Any two different elements $\mathcal{P}_0, \mathcal{P}_0' \in \mathcal{S}_{(J)}$ produce different maps $N_J(\mathcal{P}_0) \neq N_J(\mathcal{P}_0')$, and, correspondingly, different sets

$$S^+ \;\neq\; S^{+\prime} \tag{E.37}$$

(Def. (E.23)). Hence, the number $\left|\mathcal{S}_{(J)}\right|$ of elements of the set $\mathcal{S}_{(J)}$ is bounded by the number of all subsets of $\{1,\ldots,2n\}$, which is 2^{2n}. In summary, we note the following estimate for the sum (E.17):

$$\sum_{\mathcal{P}\in\varphi_{(J)}^{-1}PF_{irr}\{1,\ldots,2n\}} \prod_{j=1}^{2n-1} \frac{1}{N_{J(j)}(\mathcal{P})} \;\leq\; 2^{3n}. \tag{E.38}$$

E.1.4 Estimate for $\int_0^\infty d\tau \left|K^{(2n)}(\tau)\right|$

We insert (E.38) into the inequality (E.16). Moreover, we note that, for a fixed and given value of k, the number of possibilities to choose $J \in \mathcal{J}_{(k)}^{(2n)}$ is given by $\left|\mathbb{P}_{(k)}^{(2n)}\right|$, the number of all subsets of $\{1,\ldots,2n\}$ with k elements, since there is a bijective map $\mathbb{P}_{(k)}^{(2n)} \to \mathcal{J}_{(k)}^{(2n)}$ (Fig. D.6). With this, we obtain from (E.16):

$$\int_0^\infty d\tau \left|K^{(2n)}(\tau)\right| \;\leq\; \frac{1}{\hbar}\,\frac{(2a)^n}{c^{2n-1}} \sum_{k=0}^{2n} \sum_{a_1,\ldots,a_{k+1},b_k,\ldots b_{2n}\in\mathcal{B}} \left|\mathbb{P}^{(2n)}_{(k)}\right| \; 2^{3n}. \quad \text{(E.39)}$$

We estimate the number of possibilities to choose quantum dot states $a_j, b_{j'} \in \mathcal{B}$ by

$$|\mathcal{B}|^{2n+2} \;\leq\; 4^{2n+2}, \quad \text{(E.40)}$$

while the sum $\sum_{k=0}^{2n} \left|\mathbb{P}^{(2n)}_{(k)}\right|$ gives 2^{2n}, the number of all subsets of $\{1,\ldots,2n\}$.

In summary, we obtain

$$\int_0^\infty d\tau \left|K^{(2n)}(\tau)\right| \;\leq\; c_1 \left(\frac{a}{c_2}\right)^n, \quad \text{(E.41)}$$

and

$$\sum_{n=1}^{\infty} \int_0^\infty d\tau \left|K^{(2n)}(\tau)\right| \;\leq\; c_1 \sum_{n=1}^{\infty} (a/c_2)^n, \quad \text{(E.42)}$$

with

$$c_1 \;=\; \frac{4^2 c}{\hbar}, \quad \text{(E.43)}$$

$$c_2 \;=\; \frac{c^2}{2^{10}}. \quad \text{(E.44)}$$

The constants $a, c > 0$ are the parameters of an exponentially decaying function, by which the Fourier transforms of the functions $\alpha_{l\sigma}^{(\pm 1)}$ are bounded (E.10). We consider the strength of the tunneling-coupling to be given by a positive scalar which we multiply the tunneling Hamiltonian (2.5) by. We use the square of this scalar as coupling-parameter. The coupling-parameter appears linearly in the functions $\alpha_{l\sigma}^{(\pm 1)}$, and thus, the constant a within the estimate (E.10) is proportional to the coupling-parameter.

The power-series on the right-hand side of (E.42) is absolutely convergent for a sufficiently small *positive* value of the coupling-parameter. As a consequence, for sufficiently small tunneling coupling, the Laplace transform of the kernel,

$$\left(\mathcal{L}K\right)(\lambda) \;=\; \int_0^\infty d\tau\; e^{-\lambda\tau} K(\tau) \quad \text{(E.45)}$$

exists, and in the limit $\lambda \to 0$ it is given by

$$\boldsymbol{K} \;=\; \int_0^\infty d\tau\; K(\tau) \;=\; \sum_{n=1}^{\infty} \int_0^\infty d\tau\; K^{(2n)}(\tau). \tag{E.46}$$

Any truncation of the present series yields an approximation for $\boldsymbol{K}$.

E.2 Diagram Calculations

E.2.1 Theory

Within this appendix we shall calculate diagrams up to sixth order in the tunneling coupling, and the present section serves to provide some theoretical background for this analytical calculation.

Notation:

- For any function f with domain $\mathbb{R}$ we define the mirrored map Sf of f by
$$(Sf)(x) := f(-x). \tag{E.47}$$

- For any function f with domain $\mathbb{R}$, and $x_0 \in \mathbb{R}$, we define the translation $T_{x_0} f$ of f by x_0 as the map
$$(T_{x_0} f)(x) \quad := \quad f(x - x_0). \tag{E.48}$$

- For a smooth and quadratically integrable function $f : \mathbb{R} \to \mathbb{C}$ the Hilbert transform of f is given by
$$Hf(x) \quad := \quad \frac{1}{\pi} \quad \int_0^\infty d\omega \quad \frac{f(x+\omega) - f(x-\omega)}{\omega}. \tag{E.49}$$

- For $x_0 \in \mathbb{R}$, and a smooth function $f : \mathbb{R} \to \mathbb{C}$, we define the map $\delta_{x_0} f : \mathbb{R} \to \mathbb{C}$ as the continuous continuation to $\mathbb{R}$ of the function
$$(\delta_{x_0} f)(x) \quad := \quad \frac{f(x) - f(x_0)}{x - x_0}. \tag{E.50}$$
In particular, let $\delta := \delta_0$. Note that
$$\delta_{x_0} \quad = \quad T_{x_0} \delta T_{-x_0}. \tag{E.51}$$

- For (measurable and) quadratically integrable functions $f, g : \mathbb{R} \to \mathbb{C}$ we define the convolution $f * g$ of f with g by

$$(f * g)(x) \quad := \quad \int_{\mathbb{R}} dy \quad f(y)g(y-x). \tag{E.52}$$

- For $\eta > 0$, and, for example, quadratically integrable $f : \mathbb{R} \to \mathbb{C}$, let the transform $t_\eta f$ of f be defined as

$$t_\eta f \quad := \quad f * l_\eta, \tag{E.53}$$

with l_η the lorentzian

$$l_\eta(x) \quad := \quad \frac{1}{\pi} \quad \frac{\eta}{\eta^2 + x^2}. \tag{E.54}$$

Remark (Translation and Fourier Transformation):

For any quadratically integrable function g, the relation

$$\mathcal{F}T_x g \quad = \quad \mu_x(\mathcal{F}g), \tag{E.55}$$

with μ_x the factor

$$\mu_x(y) \quad := \quad e^{-ixy}, \tag{E.56}$$

holds.

Lemma (Dualism of Spaces):

We define the space of functions $\mathcal{L}$ as the set of all measurable functions $f : \mathbb{R} \to \mathbb{C}$ which decay exponentially. The latter property be defined by the condition that there are $a, b > 0$ such, that for all $x \in \mathbb{R}$:

$$|f(x)| \quad \leq \quad ae^{-b|x|}. \tag{E.57}$$

On the other hand, we define the space of functions $\mathcal{R}$ as the set of all Fourier transforms of functions in $\mathcal{L}$. The explicit definition we use for the Fourier transformation is

$$(\mathcal{F}f)(x) \quad := \quad \int_{\mathbb{R}} dy \quad f(y)e^{-ixy}. \tag{E.58}$$

Examples of elements in $\mathcal{L}$ are, for arbitrary $\eta > 0$,

$$d_\eta(t) \quad := \quad e^{-\eta|t|} \quad \text{and} \quad r_\eta(t) \quad := \quad d_\eta(t)sign(t), \tag{E.59}$$

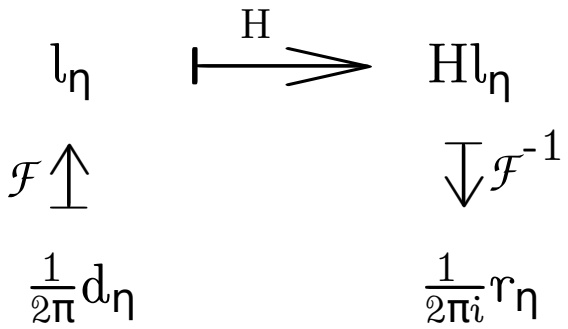

Figure E.3: The image-map of the Hilbert transformation under Fourier transformation is the multiplication by $-i\ sign$.

while the corresponding examples of elements in $\mathcal{R}$ are

$$\mathcal{F}d_\eta \quad = \quad 2\pi l_\eta \quad \text{and} \quad (\mathcal{F}r_\eta)(x) \quad = \quad -2i\frac{x}{\eta^2+x^2} \quad = \quad 2\pi i(Hl_\eta)(x). \tag{E.60}$$

In this particular example, the action of the Hilbert transformation H on a function in $\mathcal{R}$ has, up to a factor, the same effect as the multiplication by the sign of the corresponding exponentially decaying function (Fig. E.3). This is true *in general* and well-known. Nevertheless, it makes sense to verify the equality of maps in the present situation.

All functions in $\mathcal{R}$ are analytic and quadratically integrable. Moreover, it is clear from the definition of the spaces that the latter are copies of each other, as far as the zero-set equivalence is applied in $\mathcal{L}$, the isomorphism is the Fourier transformation. We shall refer to the inverse of the Fourier transformation by $\mathcal{F}^{-1}$. It can be quickly verified that product and convolution of two functions in $\mathcal{L}$ are functions in $\mathcal{L}$. The same holds true for functions in $\mathcal{R}$:

Statement 1: If $f, g \in \mathcal{R}$, then

$$(1a) \quad fg \quad = \quad \mathcal{F}\left[(\mathcal{F}^{-1}f) * (S\mathcal{F}^{-1}g)\right] \quad \in \quad \mathcal{R}, \tag{E.61}$$

$$(1b) \quad f * g \quad = \quad 2\pi \quad \mathcal{F}\left[(\mathcal{F}^{-1}f)(S\mathcal{F}^{-1}g)\right] \quad \in \quad \mathcal{R}. \tag{E.62}$$

As a consequence, for any $\eta > 0$, the transformation t_η maps elements in $\mathcal{R}$ to elements in $\mathcal{R}$. The image of the transformation t_η under Fourier transformation is the multiplication by d_η; moreover,

$$t_{\eta_1} t_{\eta_2} \ = \ t_{\eta_1+\eta_2}, \tag{E.63}$$

and every function $f \in \mathcal{R}$ has the form $f = t_\eta \tilde{f}$ with $\eta > 0, \tilde{f} \in \mathcal{R}$.

Statement 2: The Hilbert transformation H is an endomorphism of $\mathcal{R}$, and the corresponding endomorphism of $\mathcal{L}$ is given by the multiplication with the sign and $-i$,

$$\left(\mathcal{F}^{-1}H\mathcal{F}\right)(\alpha)(t) \quad = \quad -i \quad sign(t)\alpha(t). \tag{E.64}$$

One consequence of this equality, together with the isometry of the Fourier transformation, is, that the Hilbert transformation, too, is isometric with respect to the scalar product of quadratically integrable functions. Generally, for any two real or complex $f, g \in \mathcal{R}$:

$$\int fg = \int (Hf)(Hg). \tag{E.65}$$

Moreover,

$$H^2 \;=\; -1. \tag{E.66}$$

As a further conclusion, we note the equality

$$H\left[fHg + gHf\right] \;=\; HfHg \;-\; fg, \tag{E.67}$$

which we verify by writing each of the products of functions $f(Hg), (Hf)(Hg)$ etc. as the Fourier transform of a convolution of functions according to Eq. (E.61), and by showing the equality of the Fourier back-transforms of both sides of the present equation.

Statement 3: The maps $\delta_{x_0} = T_{x_0}\delta T_{-x_0}, x_0 \in \mathbb{R}$, are endomorphisms of $\mathcal{R}$. In particular, the endomorphism $\mathcal{F}^{-1}\delta\mathcal{F}$ of exponentially decaying functions is given by

$$(\mathcal{F}^{-1}\delta\mathcal{F})(\alpha)(t_0) \;= \begin{cases} -i\int_{t_0}^{\infty} dt\alpha(t) & \text{for } t_0 > 0, \\ \\ i\int_{-\infty}^{t_0} dt\alpha(t) & \text{for } t_0 < 0. \end{cases} \tag{E.68}$$

Proof of Statement 1:

Statement (1a) is verified easily by the convolution theorem for Fourier transforms. In order to show statement (1b), let

$$\begin{array}{rcl} \alpha & := & \mathcal{F}^{-1}f, \\ \beta & := & \mathcal{F}^{-1}g. \end{array} \tag{E.69}$$

We define for arbitrary $\varepsilon > 0$:

$$G_\varepsilon(t) \quad := \quad \frac{1}{\varepsilon\sqrt{\pi}} \quad e^{-(t/\varepsilon)^2}, \tag{E.70}$$

choose a sequence $\varepsilon_n \to 0 \quad (n \to \infty)$, let

$$\begin{array}{rcl} \alpha_n & := & \alpha * G_{\varepsilon_n}, \\ \beta_n & := & \beta * G_{\varepsilon_n}, \end{array} \tag{E.71}$$

and

$$\begin{array}{rcccl} f_n & := & \mathcal{F}\alpha_n & = & f\gamma_n, \\ g_n & := & \mathcal{F}\beta_n & = & g\gamma_n \end{array} \tag{E.72}$$

with $\gamma_n(x) = \exp\left(-\frac{1}{4}(\varepsilon_n x)^2\right)$. For every single $x \in \mathbb{R}$, the equation

$$f * g(x) = \lim_{n\to\infty} f_n * g_n(x) \tag{E.73}$$

holds (Lebesgue). On the other hand, $f_n * g_n$ is integrable and quadratically integrable, and hence

$$f_n * g_n \quad = \quad 2\pi \quad \mathcal{F}(\alpha_n S\beta_n) \quad \in \mathcal{R}. \tag{E.74}$$

[Apply $\mathcal{F}^{-1}$ to the left-hand side.]

For every $x \in \mathbb{R}$, the following equation holds:

$$f_n * g_n(x) \quad = 2\pi \int_{\mathbb{R}} dy \quad e^{-ixy}\alpha_n(y)\beta_n(-y). \tag{E.75}$$

Now, we note that

$$\begin{array}{rcccl} f_n & = & f\gamma_n & \to & f, \\ g_n & = & g\gamma_n & \to & g \end{array} \tag{E.76}$$

in $\|\cdot\|_2$, the norm of the quadratically integrable functions. The isometry of the Fourier transformation implies that also

$$\begin{array}{rcl} \alpha_n & \to & \alpha, \\ \beta_n & \to & \beta \end{array} \tag{E.77}$$

in this norm. As a consequence, we note the convergence of the product

$$\alpha_n S\beta_n \quad \to \quad \alpha S\beta \quad (n \to \infty) \tag{E.78}$$

in the norm $\|\cdot\|_1$ of the absolutely integrable functions. This implies the following convergence of the right-hand side of Eq. (E.75):

$$2\pi \int_{\mathbb{R}} dy \quad e^{-ixy}\alpha_n(y)\beta_n(-y) \qquad \to \qquad 2\pi \quad \mathcal{F}(\alpha S\beta)(x) \quad (n \to \infty). \tag{E.79}$$

With Eq. (E.73) and the definition of α, β follows, for every $x \in \mathbb{R}$,

$$f * g(x) \quad = \quad 2\pi \quad \mathcal{F}\left[(\mathcal{F}^{-1}f)(S\mathcal{F}^{-1}g)\right](x), \tag{E.80}$$

and thus the statement (1b).

Proof of Statements 2,3:

Let $g = \mathcal{F}\beta$ be an arbitrary function in $\mathcal{R}$. We consider the image of g under the Hilbert transformation H, as well as under δ, and, on the other hand, we consider the image of β under $\mathcal{F}^{-1}H\mathcal{F}$, as well under $\mathcal{F}^{-1}\delta\mathcal{F}$.

Statement (1b) implies that

$$g \quad = \quad t_\eta f \quad = \quad f * l_\eta \tag{E.81}$$

with $\eta > 0, f \in \mathcal{R}$. Then,

$$Hg \quad = \quad -\, f * (Hl_\eta) \;\in \mathcal{R}, \tag{E.82}$$

$$\delta g \quad = \quad \frac{1}{-2i}\left\{(fl_\eta) * \mathcal{F}r_\eta \;+\; (f(\mathcal{F}r_\eta)) * l_\eta\right\} \;\in \mathcal{R}. \tag{E.83}$$

Moreover, according to statement (1b):

$$\beta \;=\; \mathcal{F}^{-1}g \quad = \quad d_\eta\, \mathcal{F}^{-1}f, \;\Rightarrow \tag{E.84}$$

$$\mathcal{F}^{-1}H\mathcal{F}\;\beta \quad = \quad -\,i\; r_\eta\; \mathcal{F}^{-1}f \;=\; -\,i\; sign\;\beta. \tag{E.85}$$

Finally, with statements (1a) and (1b):

$$(\mathcal{F}^{-1}\delta\mathcal{F})\beta = \;\frac{-id_\eta}{2}\left\{\; sign\left((\mathcal{F}^{-1}f) * d_\eta\right) \;+\; (\mathcal{F}^{-1}f) * (d_\eta sign)\;\right\}. \tag{E.86}$$

For $t_0 > 0$ we obtain:

$$\begin{aligned}\left\{(\mathcal{F}^{-1}\delta\mathcal{F})\beta\right\}(t_0) \quad &= \quad -\,ie^{-\eta t_0}\int_{t_0}^{\infty} dt\;(\mathcal{F}^{-1}f)(t)e^{-\eta(t-t_0)} \\ &= \quad -\,i\int_{t_0}^{\infty} dt\;\beta(t),\end{aligned} \tag{E.87}$$

the case $t_0 < 0$ is analogous. $\square$

Remarks:

- The convolution of two functions, each of which is bounded by a scalar multiple of $f_0(x) := 1/(1 + |x|)$, is quadratically integrable, since an explicit calculation shows that

$$\int_{\mathbb{R}} |f_0 * f_0|^2 \;<\; \infty. \tag{E.88}$$

- By the residue calculus we note, for arbitrary complex $\tilde{z}, z_1 \ldots, z_N \in \{Im > 0\}$ with strictly positive imaginary part, the equality:

$$\int_{\mathbb{R}} \frac{1}{z+\tilde{z}} \; \frac{1}{z-z_1} \ldots \frac{1}{z-z_N} dz \quad = \quad 2\pi i (-1)^{N+1} \frac{1}{\tilde{z}+z_1} \ldots \frac{1}{\tilde{z}+z_N}. \tag{E.89}$$

Lemma (Extension of the Hilbert Transform):

Let $g \in \mathcal{R}, \varepsilon_1, \ldots, \varepsilon_N \in \mathbb{R}$, $g = t_\eta f$ with $\eta > 0$, and $f \in \mathcal{R}$, be given. Then the limit

$$\begin{aligned} (H_{ext} g) \quad (\varepsilon_1, \ldots, \varepsilon_N) \quad &:= \quad \lim_{\lambda_N \to 0^+} \ldots \lim_{\lambda_1 \to 0^+} \\ \int_{\mathbb{R}} d\omega \quad g(\omega) \quad &\frac{1}{\lambda_1 + i(\omega - \varepsilon_1)} \ldots \frac{1}{\lambda_N + i(\omega - \varepsilon_N)} \end{aligned} \tag{E.90}$$

exists, and it has the representations

$$\begin{aligned} (H_{ext} g)(\varepsilon_1, \ldots, \varepsilon_N) \quad &= \quad (-i)^{N-1} \pi (1 - iH)(\delta_{\varepsilon_{N-1}} \ldots \delta_{\varepsilon_1} g)(\varepsilon_N) \qquad \text{(E.91)} \\ &= \quad \int_0^\infty \ldots \int_0^\infty dt_1 \ldots dt_N \\ &\qquad \mathcal{F}g(t_1 + \cdots + t_N) \exp i(\varepsilon_1 t_1 + \cdots + \varepsilon_N t_N) \\ &= \quad \int_{\mathbb{R}} d\omega \quad f(\omega) \quad \frac{1}{\eta + i(\omega - \varepsilon_1)} \ldots \frac{1}{\eta + i(\omega - \varepsilon_N)}. \end{aligned}$$

Proof:

For $N = 1$, indeed

$$\lim_{\lambda \to 0^+} \int_{\mathbb{R}} d\omega \frac{g(\omega)}{\lambda + i(\omega - \varepsilon)} \quad = \quad \pi (1 - iH)(g)(\varepsilon). \tag{E.92}$$

[We expand the fraction $1/[\lambda + i(\omega - \varepsilon)]$ by the complex conjugate of its denominator. For the real part, we obtain

$$\int_{\mathbb{R}} dx \; \frac{g(\varepsilon + \lambda x)}{1 + x^2} \; \to \; \pi g(\varepsilon) \quad (\lambda \to 0), \tag{E.93}$$

while the imaginary part gives

$$(-i) \int_0^\infty d\omega' \; \frac{g(\varepsilon + \omega')\omega' - g(\varepsilon - \omega')\omega'}{\lambda^2 + \omega'^2} \; \to \; (-i)\pi \; (Hg)(\varepsilon) \tag{E.94}$$

for $\lambda \to 0$.]

In case $N \geq 2$, we write

$$g(\omega) \quad = \quad (\delta_{\varepsilon_1} g)(\omega)(\omega - \varepsilon_1) + g(\varepsilon_1), \tag{E.95}$$

and apply the convergence theorem (Lebesgue), as well as the residue calculus. Repeated use of these manipulations yields

$$(H_{ext} g)(\varepsilon_1, \ldots, \varepsilon_N) \quad = \quad \lim_{\lambda_N \to 0^+} \ldots \lim_{\lambda_1 \to 0^+} \tag{E.96}$$

$$\int d\omega \quad \delta_{\varepsilon_1} g(\omega) \frac{\omega - \varepsilon_1}{\lambda_1 + i(\omega - \varepsilon_1)} \frac{1}{\lambda_2 + i(\omega - \varepsilon_2)} \cdots \frac{1}{\lambda_N + i(\omega - \varepsilon_N)} \quad = \cdots =$$

$$\frac{1}{i^{N-1}} \lim_{\lambda_N \to 0^+} \int d\omega (\delta_{\varepsilon_{N-1}} \ldots \delta_{\varepsilon_1} g)(\omega) \frac{1}{\lambda_N + i(\omega - \varepsilon_N)}$$

$$= \quad (-i)^{N-1} \pi (1 - iH)(\delta_{\varepsilon_{N-1}} \ldots \delta_{\varepsilon_1} g)(\varepsilon_N).$$

For the proof of the second equality in (E.91), we apply $\gamma_n(x) := \exp\left(-\frac{1}{4}(x/n)^2\right)$ to define

$$g_n \quad := \quad \gamma_n g. \tag{E.97}$$

We note that

$$H_{ext} g(\varepsilon_1, \ldots, \varepsilon_N) \quad = \quad \lim_{\lambda_N \to 0^+} \ldots \lim_{\lambda_1 \to 0^+} \quad \lim_{n \to \infty} \tag{E.98}$$

$$\int d\omega \; g_n(\omega) \quad \frac{1}{\lambda_1 + i(\omega - \varepsilon_1)} \cdots \frac{1}{\lambda_N + i(\omega - \varepsilon_N)}$$

$$= [\text{limits}] \quad \int_0^\infty \ldots \int_0^\infty dt_1 \ldots dt_N \quad \mathcal{F} g_n(t_1 + \cdots + t_N)$$

$$e^{-\lambda_1 t_1} \ldots e^{-\lambda_N t_N} \exp i(\varepsilon_1 t_1 + \cdots + \varepsilon_N t_N) \quad \text{(with Fubini)}$$

$$= [\text{limits}] \quad \int_0^\infty dt \quad \mathcal{F} g_n(t) \int_{\left\{(t_1, \ldots, t_N) \in \mathbb{R}^N : t_i \geq 0, \sum_i t_i = t\right\}}$$

$$\frac{1}{\sqrt{N}} \; e^{-\lambda_1 t_1} \ldots e^{-\lambda_N t_N} \exp i(\varepsilon_1 t_1 + \cdots + \varepsilon_N t_N)$$

$$=: [\text{limits}] \quad \int_0^\infty dt \quad (\mathcal{F} g_n)(t) \mu(t) \quad \text{(cp. Fig. 2.6)}$$

$$= \quad \lim_{\lambda_N \to 0^+} \ldots \lim_{\lambda_1 \to 0^+} \quad \int_0^\infty dt \quad (\mathcal{F} g)(t) \mu(t) \quad \text{(continuity in } ||\cdot||_2)$$

$$= \quad \lim_{\lambda_N \to 0^+} \ldots \lim_{\lambda_1 \to 0^+} \quad \int_0^\infty \ldots \int_0^\infty dt_1 \ldots dt_N \quad \mathcal{F} g(t_1 + \cdots + t_N)$$

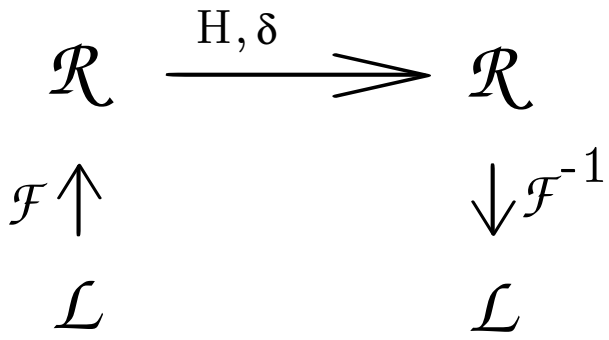

Figure E.4: In our terminology, the Fourier transformation $\mathcal{F}$ maps from $\mathcal{L}$ to $\mathcal{R}$, while the Hilbert transformation, as well as the map δ, are endomorphisms of $\mathcal{R}$.

$$\exp i(\varepsilon_1 t_1 + \cdots + \varepsilon_N t_N) \quad e^{-\lambda_1 t_1} \ldots e^{-\lambda_N t_N}$$
$$= \int_0^\infty \ldots \int_0^\infty dt_1 \ldots dt_N \quad \mathcal{F}g(t_1 + \cdots + t_N) \exp i(\varepsilon_1 t_1 + \cdots + \varepsilon_N t_N)$$

with Lebesgue.

We obtain the last representation of $(H_{ext}g)(\varepsilon_1, \ldots, \varepsilon_N)$ within Eq. (E.91) upon inserting $g = t_\eta f$ into the definition. With Tonelli/Fubini we can swap the order of the integrals; then, we apply Eq. (E.89) to calculate the inner integral. □

Remark (Relation between H and δ_{x_0}):

1. Inserting $\delta_x \delta_y f(t)$ into Def. (E.50), we note the commutation relation

$$\delta_x \delta_y \;=\; \delta_y \delta_x. \tag{E.99}$$

2. For any $f \in \mathcal{R}$, and $x_0 \in \mathbb{R}$, $\delta_{x_0} f$ is Riemann-integrable, and

$$\lim_{R\to\infty} \int_{-R}^{R} \delta_{x_0} f \;=\; \lim_{R\to\infty} \int_{x_0-R}^{x_0+R} \delta_{x_0} f \;=\; \pi\, (Hf)(x_0). \tag{E.100}$$

3. We note that $\delta H = H\delta$, since

$$H\delta \;=\; \mathcal{F}\, \left(\mathcal{F}^{-1} H \mathcal{F}\right) \left(\mathcal{F}^{-1} \delta \mathcal{F}\right)\, \mathcal{F}^{-1}, \tag{E.101}$$

and since $\mathcal{F}^{-1}H\mathcal{F}$ commutes with $\mathcal{F}^{-1}\delta\mathcal{F}$ according to Eq. (E.64), and (E.68). Because, for any $x_0 \in \mathbb{R}$, $T_{x_0}H = HT_{x_0}$, we conclude that generally

$$H\delta_{x_0} \;=\; \delta_{x_0}H. \tag{E.102}$$

4. For any $f \in \mathcal{R}, n \in \mathbb{N}, x_0 \in \mathbb{R}$, we note:

$$\left(\delta^n_{x_0} f\right)(x_0) \;=\; \frac{1}{n!} f^{(n)}(x_0), \tag{E.103}$$

as well as, for any $x \neq x_0$:

$$\left(\delta^n_{x_0} f\right)(x) \;=\; \frac{f(x) - p(f, x_0)_{n-1}(x)}{(x - x_0)^n}, \tag{E.104}$$

where $p(f, x_0)_{n-1}$ is the Taylor polynomial of f around x_0 of degree $n-1$, in particular $p(f, x_0)_{-1} := 0$.

5. As a consequence, the n-th derivative of the Hilbert transform of $f \in \mathcal{R}$ has the representation

$$\begin{aligned}(Hf)^{(n)}(x_0) \;&=\; \frac{n!}{\pi}\int_0^\infty \frac{d\omega}{\omega^{n+1}}\Big\{\;(f - p(f,x_0)_{n-1})(x_0+\omega) \\ &\qquad\qquad + (-1)^{n+1}(f - p(f,x_0)_{n-1})(x_0-\omega)\;\Big\} \\ &=:\; H^{(n)}f(x_0).\end{aligned} \tag{E.105}$$

6. In particular:

$$H^{(0)}f(x_0) \;=\; \frac{1}{\pi}\int_0^\infty \frac{d\omega}{\omega}\left\{f(x_0+\omega) - f(x_0-\omega)\right\}, \tag{E.106}$$

$$H^{(1)}f(x_0) \;=\; \frac{1}{\pi}\int_0^\infty \frac{d\omega}{\omega^2}\left\{f(x_0+\omega) + f(x_0-\omega) - 2f(x_0)\right\}, \tag{E.107}$$

$$H^{(2)}f(x_0) \;=\; \frac{2}{\pi}\int_0^\infty \frac{d\omega}{\omega^3}\left\{f(x_0+\omega) - f(x_0-\omega) - 2\omega f'(x_0)\right\}. \tag{E.108}$$

7. The integrand appearing in $H^{(n)}f(x_0)$ (E.105) has the alternative representation

$$\begin{aligned} & \frac{1}{\omega^{n+1}}\Big\{ \quad (f - p(f,x_0)_{n-1})(x_0+\omega) \\ & \qquad + (-1)^{n+1}(f - p(f,x_0)_{n-1})(x_0-\omega) \Big\} \\ = \quad & \frac{1}{\omega^{n+1}} \int \dots \int_{0\le t_{n+1}\le\dots\le t_1\le\omega} dt_1 \dots dt_{n+1} \\ & \Big(f^{(n+1)}(x_0+t_{n+1}) \; + \; f^{(n+1)}(x_0-t_{n+1}) \Big). \end{aligned} \tag{E.109}$$

Remark (The Integral $I^{RTA}(a,b,c)$):

For any three functions $a, b, c \in \mathcal{R}$ we define

$$I^{RTA}(a,b,c) \; := \; \int_{\mathbb{R}} d\varepsilon \; a(\varepsilon) \; \int_{\mathbb{R}} d\tilde{\varepsilon} \; (\delta_\varepsilon b)(\tilde{\varepsilon}) c(\tilde{\varepsilon}). \tag{E.110}$$

This integral generally appears in the calculation of 6-th order RTA-diagrams (not shown within this work), and in particular in the calculation of the DSO-integral $I(DSO)(6)(f,g,h)$, which we shall carry out within the next section. We here show that the integral is well-defined, that it is symmetric in a and c, and that it is trilinear (linear in each of the three arguments). In addition, since we shall apply the result in the following section, we determine the real part of

$$I^{RTA}\left([1+iH]\,a, [1-iH]\,b, [1+iH]\,c\right), \tag{E.111}$$

with H the Hilbert transformation, in case a, b, c are real.

Right-Hand Side of Eq. (E.110) Well-Defined:
To the function $b \in \mathcal{R}$ we assign the family of functions $(\delta_\varepsilon b)_{\varepsilon\in\mathbb{R}}$ (also in $\mathcal{R}$). For any $\varepsilon \in \mathbb{R}$, the inner integral

$$\int d\tilde{\varepsilon} \; (\delta_\varepsilon b)(\tilde{\varepsilon}) c(\tilde{\varepsilon}) \tag{E.112}$$

exists in the absolute sense; to determine its value, we note:

$$(\delta_\varepsilon b)c \; = \; \delta_\varepsilon(bc) \; - \; b(\varepsilon)\,(\delta_\varepsilon c)\,. \tag{E.113}$$

Thus, with (E.100), the inner integral is

$$\begin{aligned}\int (\delta_\varepsilon b)c &= \int \delta_\varepsilon(bc) \;-\; b(\varepsilon)\int \delta_\varepsilon c \\ &= \pi\;\left[H(bc) - b(Hc)\right](\varepsilon). \end{aligned} \tag{E.114}$$

Since the right-hand side of the present equation is a function in $\mathcal{R}$ (evaluated in ε), we conclude that the integral $I^{RTA}(a,b,c)$ (E.110) is well-defined.

Symmetry $a \leftrightarrow c$: We obtain for the integral's value:

$$\begin{aligned} I^{RTA}(a,b,c) &= \pi\left[\int aH(bc) \;-\; ab(Hc)\right] \qquad\qquad (E.115)\\ &= \pi\left[\int (Ha)\left[HH(bc)\right] \;-\; ab(Hc)\right] \text{(isometry of } H \text{ (E.64))} \\ &= -\pi\left[\int (Ha)bc \;+\; ab(Hc)\right] \qquad \text{(since } HH=-1 \text{ (E.66))}, \end{aligned}$$

and from the last line's representation we conclude that $I^{RTA}(a,b,c)$ is linear in every argument and symmetric in a and c.

Real Part of (E.111):

For real $a,b,c \in \mathcal{R}$ we calculate:

$$Re\left\{I^{RTA}\left([1+iH]\,a,[1-iH]\,b,[1+iH]\,c\right)\right\} \;=$$

$$\begin{aligned} &= I^{RTA}(a,b,c) \;-\; I^{RTA}(Ha,b,Hc) \\ &+ I^{RTA}(Ha,Hb,c) \;+\; I^{RTA}(a,Hb,Hc)\,. \end{aligned} \tag{E.116}$$

Inserting the triple (a,Hb,Hc) into Def. (E.110), we obtain

$$\begin{aligned} I^{RTA}(a,Hb,Hc) &= \int_{\mathbb{R}} d\varepsilon\; a(\varepsilon)\int_{\mathbb{R}} d\tilde{\varepsilon}\;(\delta_\varepsilon(Hb))(\tilde{\varepsilon})(Hc)(\tilde{\varepsilon}) \\ &= \int d\varepsilon\; a(\varepsilon)\int (H(\delta_\varepsilon b))(Hc) \quad \text{(with (E.102))} \\ &= \int d\varepsilon\; a(\varepsilon)\int (\delta_\varepsilon b)c \quad \text{(with (E.65))} \\ &= I^{RTA}(a,b,c). \end{aligned} \tag{E.117}$$

By the symmetry we conclude:

$$\begin{aligned} I^{RTA}(Ha,Hb,c) &= I^{RTA}(c,Hb,Ha) \;=\; I^{RTA}(c,b,a) \\ &= I^{RTA}(a,b,c). \end{aligned} \tag{E.118}$$

Finally, upon inserting the triple (Ha, b, Hc) into the last line of Eq. (E.115), we find:

$$\begin{aligned} -I^{RTA}(Ha,b,Hc) &= \pi\left[\int (HHa)b(Hc) \;+\; (Ha)b(HHc)\right] \\ &= -\pi\left[\int ab(Hc) \;+\; (Ha)bc\right] \quad \text{(with E.66)} \\ &= I^{RTA}(a,b,c). \end{aligned} \tag{E.119}$$

In summary,

$$Re\left\{I^{RTA}\left([1+iH]\,a,[1-iH]\,b,[1+iH]\,c\right)\right\} \;=\; 4\; I^{RTA}\left(a,b,c\right). \qquad \square \tag{E.120}$$

E.2.2 Practice

We here calculate all contributions to the kernels within a certain subselection of diagrams up to sixth order in the tunneling coupling: Neglecting the doubly occupied state, we take into account all DSO-diagrams up to sixth order. This amounts to the calculation of three integrals – one for each order $2n$, $n = 1, 2, 3$. We refer to these integrals by the $2n$-th order DSO pair formation

$$\mathcal{P}_{DSO} = \Big\{\; \{1,2n\},\{2,3\},\{4,5\},\ldots,\{2n-2,2n-1\}\Big\} \;\in PF\{1,\ldots,2n\} \tag{E.121}$$

(cp. Fig. 3.8), or else by a graphic icon of this pair formation. Since imaginary parts cancel in the end, we restrict ourselves to the calculation of the real part and apply the congruence

$$z_1 \equiv z_2 \;:\Leftrightarrow\; Re(z_1) = Re(z_2). \tag{E.122}$$

Second Order Diagram

Let $f \in \mathcal{R}$ be real and integrable; we calculate:

$\mathrm{I}($  $)(\mathrm{f}) :=$

$$\begin{aligned} &= I(DSO)(2)(f) \;:= \\ &= \lim_{\eta\to 0+}\int_{\mathbb{R}} d\omega\; f(\omega)\frac{1}{\eta+i\omega} \;\equiv\; \lim_{\eta\to 0+}\int_{\mathbb{R}} d\omega\; f(\omega)\frac{\eta}{\eta^2+\omega^2} \\ &= \lim_{\eta\to 0+}\int_{\mathbb{R}} d\omega/\eta\; \frac{f\left(\eta\left(\omega/\eta\right)\right)}{1+(\omega/\eta)^2} \;=\; \lim_{\eta\to 0+}\int_{\mathbb{R}} dx\; \frac{f\left(\eta x\right)}{1+x^2} \end{aligned}$$

$$= \pi f(0). \tag{E.123}$$

Fourth Order DSO-Diagram

Let $f, g \in \mathcal{R}$ be real and absolutely integrable; the integral we encounter in the fourth order DSO-diagrams is

$\mathrm{I}($  $)(\mathrm{f},\mathrm{g}) :=$

$$\begin{aligned}
& I(DSO)(4)(f,g) := \qquad\qquad (E.124)\\
= \quad & \lim_{\lambda\to 0+}\int\int d\omega d\omega'\ f(\omega)g(\omega')\frac{1}{\lambda+i\omega}\ \frac{1}{\lambda+i(\omega-\omega')}\ \frac{1}{\lambda+i\omega}\\
= \quad & \int_0^\infty\int_0^\infty\int_0^\infty dt_1dt_2dt_3\ (\mathcal{F}f)(t_1+t_2+t_3)(\mathcal{F}g)(-t_2)\\
= \quad & \lim_{\eta,\eta'\to 0+}\int\int d\omega d\omega'\ f(\omega)g(\omega')\frac{1}{\eta+i\omega}\ \frac{1}{\eta+\eta'+i(\omega-\omega')}\ \frac{1}{\eta+i\omega}
\end{aligned}$$

$$\begin{aligned}
= \quad & \lim_{\eta,\eta'\to 0+}\int\int d\omega d\omega'\ f(\omega)g(\omega')\left(\frac{1}{\eta+i\omega}\right)^2\\
& \frac{1}{2\pi}\int d\varepsilon\frac{1}{\eta+i\omega-i\varepsilon}\ \frac{1}{\eta'-i\omega'+i\varepsilon} \qquad \text{(with } (E.89)\text{)}\\
= \quad & \frac{1}{2\pi}\lim_{\eta,\eta'\to 0+}\int d\varepsilon\ \int d\omega\ f(\omega)\left(\frac{1}{\eta+i\omega}\right)^2\ \frac{1}{\eta+i\omega-i\varepsilon}\\
& \int d\omega'\ g(\omega')\ \frac{1}{\eta'-i\omega'+i\varepsilon} \qquad \text{(with Tonelli/Fubini)}\\
= \quad & \frac{1}{2\pi}\lim_{\eta,\eta'\to 0+}\int d\varepsilon\ H_{ext}(t_\eta f)(0,0,\varepsilon)H_{ext}(t_{\eta'}g)(\varepsilon)^* \quad \text{(with } (E.91)\text{)}.
\end{aligned}$$

At this stage we insert

$$\left.\begin{array}{rcl} f &=& t_{\eta_f}\tilde{f}\\ g &=& t_{\eta_g}\tilde{g}\end{array}\right\} \text{ with } \tilde{f},\tilde{g}\in\mathcal{R},\ \eta_f,\eta_g>0, \tag{E.125}$$

and with (E.63) we rewrite the last line of Eq. (E.124) in the form

$$
\begin{aligned}
& \frac{1}{2\pi} \lim_{\eta,\eta'\to 0+} \int d\varepsilon \; H_{ext}(t_{\eta+\eta_f}\tilde{f})(0,0,\varepsilon) H_{ext}(t_{\eta'+\eta_g}\tilde{g})(\varepsilon)^* \\
= \; & \frac{1}{2\pi} \lim_{\eta,\eta'\to 0+} \int d\varepsilon \int d\omega \; \tilde{f}(\omega) \left(\frac{1}{\eta+\eta_f+i\omega}\right)^2 \; \frac{1}{\eta+\eta_f+i\omega-i\varepsilon} \\
& \int d\omega' \; \tilde{g}(\omega') \; \frac{1}{\eta'+\eta_g-i\omega'+i\varepsilon} \qquad \text{(with (E.91))} \\
= \; & \frac{1}{2\pi} \int d\varepsilon \int d\omega \; \tilde{f}(\omega) \left(\frac{1}{\eta_f+i\omega}\right)^2 \; \frac{1}{\eta_f+i\omega-i\varepsilon} \\
& \int d\omega' \; \tilde{g}(\omega') \; \frac{1}{\eta_g-i\omega'+i\varepsilon} \qquad \text{(E.126)}
\end{aligned}
$$

with Lebesgue, since

$$
\int\int\int d\varepsilon d\omega d\omega' \left| \tilde{f}(\omega)\tilde{g}(\omega') \left(\frac{1}{\eta_f+i\omega}\right)^2 \; \frac{1}{\eta_f+i\omega-i\varepsilon} \; \frac{1}{\eta_g-i\omega'+i\varepsilon} \right| < \infty. \tag{E.127}
$$

We verify the latter absolute integrability by first performing the integral over ε:

$$
\begin{aligned}
& \int d\varepsilon \left| \frac{1}{\eta_f+i\omega-i\varepsilon} \; \frac{1}{\eta_g-i\omega'+i\varepsilon} \right| \qquad \text{(E.128)} \\
= \; & \int d\varepsilon \left| \frac{1}{\eta_f+i(\varepsilon-\omega)} \right| \; \left| \frac{1}{\eta_g+i(\varepsilon-\omega+\omega-\omega')} \right| \\
= \; & \int d\overline{\varepsilon} \left| \frac{1}{\eta_f+i\overline{\varepsilon}} \right| \; \left| \frac{1}{\eta_g+i(\overline{\varepsilon}-(\omega'-\omega))} \right| \\
\leq \; & c_f c_g \int d\overline{\varepsilon} \; f_0(\overline{\varepsilon}) \; f_0(\overline{\varepsilon}-(\omega'-\omega)) \; = \; c_f c_g \; (f_0 * f_0)(\omega'-\omega),
\end{aligned}
$$

with appropriate constants $c_f, c_g > 0$. The function $f_0 * f_0$ is quadratically integrable (E.88), and so, upon inserting the present estimate into the integral (E.127), we obtain

$$
\begin{aligned}
& \int\int\int d\varepsilon d\omega d\omega' \left| \tilde{f}(\omega)\tilde{g}(\omega') \left(\frac{1}{\eta_f+i\omega}\right)^2 \; \frac{1}{\eta_f+i\omega-i\varepsilon} \; \frac{1}{\eta_g-i\omega'+i\varepsilon} \right| \\
\leq \; & c_f c_g \int\int d\omega d\omega' \left| \tilde{f}(\omega)\tilde{g}(\omega') \left(\frac{1}{\eta_f+i\omega}\right)^2 \right| \; (f_0 * f_0)(\omega'-\omega) \\
\leq \; & c_f c_g \; \|\tilde{g}\|_2 \; \|f_0 * f_0\|_2 \int d\omega \left| \tilde{f}(\omega) \left(\frac{1}{\eta_f+i\omega}\right)^2 \right| \; < \; \infty, \qquad \text{(E.129)}
\end{aligned}
$$

since $\tilde{f}, \tilde{g}$ are quadratically integrable. We conclude from (E.126):

$$\begin{aligned} & \frac{1}{2\pi} \lim_{\eta,\eta'\to 0+} \int d\varepsilon \; H_{ext}(t_\eta f)(0,0,\varepsilon) H_{ext}(t_{\eta'} g)(\varepsilon)^* \\ = \quad & \frac{1}{2\pi} \int d\varepsilon \; H_{ext}(f)(0,0,\varepsilon) H_{ext}(g)(\varepsilon)^*, \end{aligned} \tag{E.130}$$

and so, going back to Eq. (E.124):

$$\begin{aligned} I(DSO)(4)(f,g) \quad &= \quad \frac{-\pi}{2} \int d\varepsilon \; (1-iH)\delta\delta(f)(\varepsilon) \; (1+iH)(g)(\varepsilon) \\ & \qquad\qquad\qquad\qquad \text{(with } (E.91)\text{)} \\ &\equiv \quad -\pi \int d\varepsilon \; \delta\delta(f)(\varepsilon)(g)(\varepsilon) \\ & \qquad \text{(we take the real part; isometry of } H\text{).} \end{aligned} \tag{E.131}$$

Upon applying the equality

$$(\delta\delta f)g \;=\; \delta\delta(fg) \;-\; f(0)\delta\delta g \;-\; (\delta f)(0)\delta g, \tag{E.132}$$

as well as the Riemann-integrability (E.100), we obtain for the right-hand side of Eq. (E.131):

$$-\pi \int (\delta\delta f)g \;=\; -\pi^2 \big\{ \; H\left(\delta(fg)\right) - fH(\delta g) - (\delta f)Hg \big\} \; (0). \tag{E.133}$$

Finally, upon commuting H and δ (E.102), we arrive at

$$I(DSO)(4)(f,g) \;\equiv\; \pi^2 \big\{ \; f(Hg) - H\left(fg\right) \big\}' \; (0). \tag{E.134}$$

Sixth Order DSO-Diagram

We calculate, for arbitrary real-valued and integrable $f, g, h \in \mathcal{R}$, the integral

$\mathrm{I}\big($  $\big)(\mathfrak{f},\mathfrak{g},\mathfrak{h}) :=$

$$\begin{aligned} I(DSO)(6)(f,g,h) \quad := \quad & \lim_{\eta\to 0+} \int\int\int \; f(\omega) g(\omega') h(\omega'') \\ & \left(\frac{1}{\eta + i\omega}\right)^3 \frac{1}{\eta + i(\omega - \omega')} \quad \frac{1}{\eta + i(\omega - \omega'')} \end{aligned} \tag{E.135}$$

$$= \lim_{\eta,\eta',\eta''\to 0+} \int\int\int f(\omega)g(\omega')h(\omega'') \left(\frac{1}{\eta+i\omega}\right)^3 \frac{1}{\eta+\eta'+i(\omega-\omega')} \frac{1}{\eta+\eta''+i(\omega-\omega'')}$$

$$= \frac{1}{(2\pi)^2} \lim_{\eta,\eta',\eta''\to 0+} \int\int\int d\omega d\omega' d\omega'' \int\int d\varepsilon d\tilde{\varepsilon}\ f(\omega)g(\omega')h(\omega'') \left(\frac{1}{\eta+i\omega}\right)^3 \frac{1}{\eta+i\omega-i\varepsilon} \frac{1}{\eta'-i\omega'+i\varepsilon} \frac{1}{\eta+i\omega-i\tilde{\varepsilon}} \frac{1}{\eta''-i\omega''+i\tilde{\varepsilon}}$$

$$= \frac{\lim_{\eta,\eta',\eta''\to 0+}}{(2\pi)^2} \int\int d\varepsilon d\tilde{\varepsilon}\ (H_{ext}t_\eta f)(0,0,0,\varepsilon,\tilde{\varepsilon})(H_{ext}t_{\eta'}g)(\varepsilon)^*(H_{ext}t_{\eta''}h)(\tilde{\varepsilon})^*$$

At this stage we perform the limit with respect to η, η', η''; we write

$$\left.\begin{array}{rcl} f &=& t_{\eta_f}\tilde{f} \\ g &=& t_{\eta_g}\tilde{g} \\ h &=& t_{\eta_h}\tilde{h} \end{array}\right\} \text{ with } \tilde{f},\tilde{g},\tilde{h} \in \mathcal{R},\ \eta_f,\eta_g,\eta_h > 0, \tag{E.136}$$

analogously to (E.125). Analogously to (E.127), we note that

$$\int\int\int d\omega d\omega' d\omega'' \int\int d\varepsilon d\tilde{\varepsilon} \left|\tilde{f}(\omega)\tilde{g}(\omega')\tilde{h}(\omega'') \left(\frac{1}{\eta_f+i\omega}\right)^3\right| \left|\frac{1}{\eta_f+i\omega-i\varepsilon} \frac{1}{\eta_g-i\omega'+i\varepsilon} \frac{1}{\eta_f+i\omega-i\tilde{\varepsilon}} \frac{1}{\eta_h-i\omega''+i\tilde{\varepsilon}}\right| < \infty, \tag{E.137}$$

and so, going back to Eq. (E.135), we conclude:

$$\begin{aligned} & I(DSO)(6)(f,g,h) \\ =\ & \frac{1}{(2\pi)^2} \int\int d\varepsilon d\tilde{\varepsilon}\ (H_{ext}f)(0,0,0,\varepsilon,\tilde{\varepsilon})(H_{ext}g)(\varepsilon)^*(H_{ext}h)(\tilde{\varepsilon})^* \\ =\ & \frac{\pi}{4} \int\int d\varepsilon d\tilde{\varepsilon}\ \delta_\varepsilon\delta\delta\delta(1-iH)f(\tilde{\varepsilon})\ (1+iH)g(\varepsilon)\ (1+iH)h(\tilde{\varepsilon}) \end{aligned}$$

$$\begin{aligned} =\ & \frac{\pi}{4}\ I^{RTA}((1+iH)g, \delta\delta\delta(1-iH)f, (1+iH)h) \quad \text{(Def. (E.110))} \\ \equiv\ & \pi\ I^{RTA}(g, \delta\delta\delta f, h) \qquad \text{(we take the real part; Eq. (E.120))} \\ =\ & \pi \int d\varepsilon\ g(\varepsilon) \int\ (\delta_\varepsilon\delta\delta\delta f)\, h. \end{aligned} \tag{E.138}$$

Upon applying the relation

$$(\delta_\omega a)b \;=\; \delta_\omega(ab) - a(\omega)\delta_\omega b, \tag{E.139}$$

as well as the Riemann-integrability (E.100), we get for the inner integral:

$$\int\; (\delta_\varepsilon \delta\delta\delta f)\, h \;=\; \pi \left\{ H\left[(\delta\delta\delta f)\, h\right] - (\delta\delta\delta f)\, H\left[h\right] \right\}(\varepsilon). \tag{E.140}$$

As a consequence, with the isometry of the Hilbert transformation (E.65),

$$\pi\; I^{(RTA)}\,(g, \delta\delta\delta f, h) \;\;=\;\; -\,\pi^2 \int (\delta\delta\delta f)\, \underbrace{\left[(Hg)h + g(Hh)\right]}_{=:\; b}, \tag{E.141}$$

and by the relation

$$(\delta\delta\delta f)b = \delta\delta\delta(fb) - f(0)\delta\delta\delta b - (\delta f)(0)\delta\delta b - (\delta\delta f)(0)\delta b \tag{E.142}$$

we obtain:

$$\int (\delta\delta\delta f)b \;=\; \frac{\pi}{2} \left\{ H(fb) \;-\; f(Hb) \right\}''(0). \tag{E.143}$$

Inserting $b = (Hg)h + g(Hh)$, we note:

$$\pi I^{(RTA)}\,(g, \delta\delta\delta f, h) \;\;=\;\; \frac{\pi^3}{2} \left\{ fH\left[(Hg)h + gHh\right] - H\left(f\left[(Hg)h + g(Hh)\right]\right) \right\}''(0). \tag{E.144}$$

Upon applying relation (E.67), and going back to Eq. (E.138), we arrive at the equality:

$$I(DSO)(6)(f,g,h) \;\equiv\; \frac{\pi^3}{2} \Big\{ f\left(HgHh - gh\right) \;-\; H\left[f(hHg + gHh)\right] \Big\}''(0). \tag{E.145}$$

E.3 Application: Sixth Order DSO with Infinite U

In the present section we give the results for the density matrix and current as obtained within the sixth order DSO, applied to the SIAM with infinite Coulomb-interaction U. We calculated the emerging diagrams theoretically in the previous section, and we here note the results in terms of the multilinear forms of that section. Finally, we consider in particular the temperature-dependence of the linear conductance (the differential conductance at zero

bias) G. An analysis shows that $G(T)$ diverges logarithmically to $+\infty$ with $T \to 0$ in case the Anderson model's degenerate level lies below the Fermi level of the contacts.

E.3.1 Sixth Order Rates

In the same way as within the *complete* dressed-second-order for infinite Coulomb-interaction, Eqs. (3.49), and (3.50), we write the stationary density matrix and current as function of rates $\Gamma_l^{\pm}$:

$$\begin{pmatrix} \rho_{00} \\ \rho_{\uparrow\uparrow} \\ \rho_{\downarrow\downarrow} \end{pmatrix} = \frac{1}{\Gamma + \Gamma^+} \begin{pmatrix} \Gamma^- \\ \Gamma^+ \\ \Gamma^+ \end{pmatrix}, \tag{E.146}$$

and

$$\begin{aligned} \boldsymbol{I_l} &= \frac{1}{2}\left(\boldsymbol{I_l} - \boldsymbol{I_{\bar{l}}}\right) \\ &= \rho_{00}(\Gamma_{\bar{l}}^+ - \Gamma_l^+) \; + \; \rho_{\sigma\sigma}(\Gamma_l^- - \Gamma_{\bar{l}}^-), \end{aligned} \tag{E.147}$$

where

$$\Gamma^{\pm} \; = \; \sum_l \Gamma_l^{\pm}, \tag{E.148}$$

and $\Gamma := \Gamma^+ + \Gamma^-$. For simplicity we here assume symmetry with respect to spin within the quantum dot as well as within the leads; moreover, we assume equal coupling functions $\alpha_l(\varepsilon)$ (Def. (D.60)) for both leads,

$$\alpha_l \; = \; \alpha_{\bar{l}}. \tag{E.149}$$

The rates $\Gamma_l^{\pm}$, on the other hand, are given by the sum of all contributions of DSO-diagrams up to sixth order to

$$-\frac{1}{2} Tr\left\{\boldsymbol{K_{curr,l}} |\mathbf{0}><\mathbf{0}|\right\}, \tag{E.150}$$

and to

$$Tr\left\{\boldsymbol{K_{curr,l}} |\boldsymbol{\sigma}><\boldsymbol{\sigma}|\right\}, \tag{E.151}$$

respectively. Hence, we shall insert

$$\Gamma_l^{\pm} \; = \; \Gamma_l^{\pm}(DSO, III), \tag{E.152}$$

where

$$\Gamma_l^{\pm}(DSO,III) \;:=\; \Gamma_l^{\pm}(DSO,2)+\Gamma_l^{\pm}(DSO,4)+\Gamma_l^{\pm}(DSO,6), \qquad \text{(E.153)}$$

and where, to each $n = 1, 2, \ldots,$ $\Gamma_l^{\pm}(DSO, 2n)$ is the contribution of all DSO-diagrams of order $2n$ to (E.150), and to (E.151), respectively.

The Rates $\Gamma_l^{\pm}(DSO, 2n)(n = 1, 2, 3)$:

With Fig. 3.1, and with Eq. (3.1), the second order contribution to the DSO rate $\Gamma_l^{\pm}(DSO)$ is

$$\begin{aligned}
\Gamma_l^{\pm}(DSO,2) &= \frac{2}{\hbar}\, Re\, \lim_{\eta\to 0}\int d\varepsilon\, \frac{\alpha_l^{\pm}(\varepsilon)}{\eta + i(\varepsilon - E_{10})} \\
&= \frac{2}{\hbar}\, Re\, \lim_{\eta\to 0}\int d\omega\, \frac{T_{-E_{10}}\alpha_l^{\pm}(\omega)}{\eta + i\omega} \\
&= \frac{2\pi}{\hbar}\, T_{-E_{10}}\alpha_l^{\pm}(0) \;=\; \frac{2\pi}{\hbar}\, \alpha_l^{\pm}(E_{10}), \qquad \text{(E.154)}
\end{aligned}$$

where we have applied the translation $T_{-E_{10}}$ (E.48), and the result of Eq. (E.123). For the fourth order contribution to $\Gamma_l^{\pm}(DSO)$ we obtain according to Eq. (3.28), and with Figs. 3.5, 3.10:

$$\begin{aligned}
\Gamma_l^{\pm}(DSO,4) &= \frac{2}{\hbar}\, Re\, \lim_{\eta\to 0}\int d\varepsilon\, \frac{\alpha_l^{\pm}(\varepsilon)}{\eta + i(\varepsilon - E_{10})} \\
&\qquad \frac{-1}{\eta + i(\varepsilon - E_{10})}\int d\varepsilon'\, \frac{\gamma(\varepsilon')}{\eta + i(\varepsilon - \varepsilon')}
\end{aligned}$$

$$\begin{aligned}
&= \frac{2}{\hbar}\, Re\, \lim_{\eta\to 0}\int\int d\omega d\omega'\, \frac{(-1)(T_{-E_{10}}\alpha_l^{\pm})(\omega)(T_{-E_{10}}\gamma)(\omega')}{(\eta + i\omega)^2(\eta + i(\omega - \omega'))} \\
&= \frac{2\pi^2}{\hbar}\left\{H\left((T_{-E_{10}}\alpha_l^{\pm})(T_{-E_{10}}\gamma)\right) - (T_{-E_{10}}\alpha_l^{\pm})H(T_{-E_{10}}\gamma)\right\}'(0) \\
&= \frac{2\pi^2}{\hbar}\left\{H\left(\alpha_l^{\pm}\gamma\right) - \alpha_l^{\pm}(H\gamma)\right\}'(E_{10}), \qquad \text{(E.155)}
\end{aligned}$$

where we use the notation $\gamma := \alpha + \alpha^+$, and where we inserted the result (E.134) of the integral calculation (E.124). Finally, with Eq. (3.36), with Fig. 3.10, and upon applying the translation $T_{-E_{10}}$ to all of the appearing functions, we obtain for the sixth order contribution to $\Gamma_l^{\pm}(DSO)$:

$$\begin{aligned}\Gamma_l^{\pm}(DSO,6) &= \frac{2}{\hbar}\, Re \lim_{\eta\to 0} \int d\varepsilon\, \frac{\alpha_l^{\pm}(\varepsilon)}{\eta + i(\varepsilon - E_{10})} \\ &\quad \left(\frac{-1}{\eta + i(\varepsilon - E_{10})} \int d\varepsilon'\, \frac{\gamma(\varepsilon')}{\eta + i(\varepsilon - \varepsilon')}\right)^2 \\ &= \frac{2}{\hbar}\, I(DSO)(6)\left(T_{-E_{10}}\alpha_l^{\pm}, T_{-E_{10}}\gamma, T_{-E_{10}}\gamma\right) \qquad \text{(E.156)}\end{aligned}$$

with Def. (E.135). By the result (E.145) for the calculation of the general integral $I(DSO)(6)(f,g,h)$ we arrive at

$$\Gamma_l^{\pm}(DSO)(6) \;=\; \frac{\pi^3}{\hbar}\Big\{\alpha_l^{\pm}\left((H\gamma)^2 - \gamma^2\right) \;-\; 2H\left[\alpha_l^{\pm}\gamma H\gamma\right]\Big\}''(E_{10}). \qquad \text{(E.157)}$$

In summary, the sixth order rates within the DSO-selection are given by $\Gamma_l^{\pm}(DSO,III) \;=\; \Gamma_l^{\pm}(DSO,2) + \Gamma_l^{\pm}(DSO,4) + \Gamma_l^{\pm}(DSO,6)$, where

$$\begin{aligned}\Gamma_l^{\pm}(DSO)(2) &= \frac{2}{\hbar}\,\pi\alpha_l^{\pm}(E_{10}), \qquad \text{(E.158)}\\ \Gamma_l^{\pm}(DSO)(4) &= \frac{2}{\hbar}\,\pi^2\left\{H(\alpha_l^{\pm}(\alpha+\alpha^+)) \;-\; \alpha_l^{\pm}H(\alpha+\alpha^+)\right\}'(E_{10}) \\ &= \frac{2}{\hbar}\, Bil(DSO)(\alpha_l^{\pm}, \alpha+\alpha^+), \qquad \text{(E.159)}\end{aligned}$$

and

$$\begin{aligned}\Gamma_l^{\pm}(DSO)(6) &= \frac{2}{\hbar}\,\pi^3\Big\{ \quad \alpha_l^{\pm}H\Big[(\alpha+\alpha^+)H(\alpha+\alpha^+)\Big] \\ &\qquad\qquad - \quad H\Big[\alpha_l^{\pm}(\alpha+\alpha^+)H(\alpha+\alpha^+)\Big]\Big\}''(E_{10}) \\ &= \frac{2}{\hbar}\, Tril(DSO)(\alpha_l^{\pm}, \alpha+\alpha^+, \alpha+\alpha^+). \qquad \text{(E.160)}\end{aligned}$$

The bilinear map $Bil(DSO): \mathcal{R}\times\mathcal{R}\to\mathbb{C}$ is given by

$$Bil(DSO)(f,g) \quad = \quad \pi^2\left\{H(fg) \quad - \quad f(Hg)\right\}'(E_{10}), \qquad \text{(E.161)}$$

while the trilinear map $Tril(DSO):\ \mathcal{R}\times\mathcal{R}\times\mathcal{R}\to\mathbb{C}$ is given by

$$\begin{aligned}Tril(DSO)(f,g,h) &= \frac{\pi^3}{2}\Big\{f(Hg)(Hh) - fgh \\ &\qquad -H\Big[fg(Hh) + f(Hg)h\Big]\Big\}''(E_{10}). \qquad \text{(E.162)}\end{aligned}$$

We implicitly assume that the functions $\alpha_l^{\pm}$ are contained in the set $\mathcal{R}$ (Sec. E.2.1 (Diagram Calculations – Theory)), and we have applied relation (E.67) for Eq. (E.160).

E.3.2 Temperature-Dependence of Sixth Order Current and Conductance – Theory

Next, we want to analyze the temperature-dependence of the sixth order rates, and in particular of the conductance obtained from the sixth order current (E.147). To this end we formulate and prove the following technical remark and lemma:

Remark (T-Dependence of Derivatives of Fermi Function):

All of the derivatives of the parameter-free Fermi function $f(x) = 1/(1+e^x)$ decay exponentially: For all $n \geq 1$ there is $K_n > 0$ such, that for all $x \in \mathbb{R}$:

$$|f^{(n)}(x)| \quad \leq \quad K_n e^{-|x|}. \tag{E.163}$$

As a consequence, the following statement about the Fermi function at chemical potential μ_l, and temperature T,

$$f_l(\varepsilon) \quad := \quad f\left(\frac{\varepsilon - \mu_l}{k_B T}\right), \tag{E.164}$$

holds: For arbtitrary fixed and given $n \geq 0$, and $r > 0$, there is a constant $const(n,r)$ such, that for all $\varepsilon \in \mathbb{R}$ with $|\varepsilon - \mu_l| \geq r$, and, *independently* of $T > 0$:

$$|f_l^{(n)}(\varepsilon)| \quad \leq \quad const(n,r). \tag{E.165}$$

In particular, the limit $\lim_{T\to 0} f_l^{(n)}(\varepsilon)$ exitsts for all $n \geq 0$, and $\varepsilon \neq \mu_l$.

Proof:

For $n \geq 1$, $f^{(n)}(x)$ is a linear combination of terms of the form

$$(1+e^x)^{k_+}(1+e^{-x})^{k_-}, \tag{E.166}$$

with integers $k_+, k_- \leq -1$. Hence, $|f^{(n)}(x)| \leq K_n e^{-|x|}$, with K_n independent of x. For any fixed $\varepsilon \neq \mu_l$ with $|\varepsilon - \mu_l| \geq r$:

$$\begin{aligned} \left|f_l^{(n)}(\varepsilon)\right| \quad &= \quad \left|\frac{1}{(\varepsilon-\mu_l)^n}\left(\frac{\varepsilon-\mu_l}{k_BT}\right)^n f^{(n)}\left(\frac{\varepsilon-\mu_l}{k_BT}\right)\right| \\ &\to \quad 0 \ (T \to 0), \text{ and} \\ &\leq \quad \frac{1}{r^n}\sup\left\{\left|x^n K_n e^{-|x|}\right| : \ x \in \mathbb{R}\right\} \ =: const(n,r). \end{aligned} \tag{E.167}$$

Lemma (T-Dependence of $\Gamma_l^{\pm}(DSO,III)$ and $G(DSO,III)$):

Let $\gamma \in \mathcal{R}$, $m \in \{1,2,\dots\}$, $\mu_1,\dots,\mu_m \in \mathbb{R}$ be arbitrarily given. For $T>0$, and $j=1,2,\dots,m$, we define

$$f_j(\varepsilon) \quad := \quad f\left(\frac{\varepsilon-\mu_j}{k_BT}\right), \tag{E.168}$$

where f is the parameter-free Fermi function, and consider any natural $n \geq 0$ fixed and given. Then, the following statements hold:

i) For all $\varepsilon \in \mathbb{R} \setminus \{\mu_1,\dots,\mu_m\}$ the limit

$$\lim_{T\to 0} \quad H^{(n)}(\gamma f_1 \dots f_m)(\varepsilon) \tag{E.169}$$

(Def. (E.105)) exists. Moreover, for arbitrary $r>0$, there is a constant $c>0$ *independent* of T such, that for all $\varepsilon \in \mathbb{R}$ with

$$\min\{|\varepsilon-\mu_j| : j=1,\dots,m\} \quad \geq \quad r \tag{E.170}$$

the inequality

$$|H^{(n)}(\gamma f_1 \dots f_m)(\varepsilon)| \quad \leq \quad c \tag{E.171}$$

holds.

ii) Let $\kappa \in \{0,1,\dots\}$, $f_1'(\varepsilon) = \frac{df_1}{d\varepsilon}(\varepsilon)$. Then, for all $\varepsilon \in \mathbb{R} \setminus \mu_1$, the limit

$$\lim_{T\to 0} \quad H^{(n)}(\gamma f_1' f_1^{\kappa})(\varepsilon) \tag{E.172}$$

exists.

iii) Additional properties of regularity and decay imply that, for a function $\alpha \in \mathcal{R}$, also $\alpha f_0 \in \mathcal{R}$, where

$$f_0(\varepsilon) \quad := \quad f\left(\frac{\varepsilon-\mu_0}{k_BT}\right), \tag{E.173}$$

where $f(x) = 1/(1+e^x)$ is the parameter-free Fermi function, and where temperature T and chemical potential μ_0 are arbitrary (Ref. [20], App. A). We consider natural numbers $\kappa_1,\dots,\kappa_m \in \{0,1,\dots\}$ to be given. Then, the limit

$$\lim_{T\to 0} \quad H^{(n)}\left[\gamma f_1^{\kappa_1} \dots f_m^{\kappa_m} \quad H(\alpha f_0)\right](\varepsilon) \tag{E.174}$$

exists for all $\varepsilon \in \mathbb{R} \setminus \{\mu_0,\mu_1,\dots,\mu_m\}$.

iv) In addition to the functions α, and f_0, of the previous statement iii), let $\kappa \in \{0, 1, \dots\}$, and $T_0 > 0$ be arbitrarily given. Then, for all $\varepsilon \in \mathbb{R} \setminus \mu_0$:

$$\begin{array}{ccccc} & H^{(n)}\left[\gamma(-f_0')f_0^\kappa \quad H(\alpha f_0)\right] & (\varepsilon) & & \\ \overset{T\to 0}{\equiv} & \frac{n!}{\pi^2} \quad \frac{(\alpha\gamma)(\mu_0)}{\kappa+1} & \frac{1}{(\mu_0-\varepsilon)^{n+1}} & \ln\left(\frac{T}{T_0}\right), & \text{(E.175)} \end{array}$$

where we define the present congruence by the property that the difference between the two functions of the temperature on the left-, and on the right-hand sides of the congruence-sign, respectively, is convergent as $T \to 0$; $\ln := \exp^{-1}$.

Proof of Statement i):

Let $r > 0$ and $\varepsilon \in \mathbb{R}$ with

$$\min\{|\varepsilon - \mu_j| : j = 1, \dots, m\} \quad \geq \quad r$$

be given. By Eq. (E.109) we decompose

$$H^{(n)}g(\varepsilon) \quad = \qquad \text{(E.176)}$$

$$\begin{array}{lllll} \frac{n!}{\pi} & \int_0^{r/2} \frac{d\omega}{\omega^{n+1}} & \int\dots\int_{0\le t_{n+1}\le\dots\le t_1\le\omega} & & \\ & & \left\{g^{(n+1)}(\varepsilon + t_{n+1}) \quad + \quad g^{(n+1)}(\varepsilon - t_{n+1})\right\} & & \end{array}$$

$$\begin{array}{lllll} + & \frac{n!}{\pi} & \int_{r/2}^\infty \frac{d\omega}{\omega^{n+1}} \left\{-p(g,\varepsilon)_{n-1}(\varepsilon+\omega) \quad + \quad (-1)^n p(g,\varepsilon)_{n-1}(\varepsilon-\omega)\right\} & & \\ + & \frac{n!}{\pi} & \int_{r/2}^\infty \frac{d\omega}{\omega^{n+1}} \left\{ \quad g(\varepsilon+\omega) \quad + \quad (-1)^{n+1} g(\varepsilon-\omega) \quad \right\}, & & \end{array}$$

with

$$g \quad := \quad \gamma f_1 \dots f_m. \qquad \text{(E.177)}$$

The integrand of the integral over $[0, r/2]$ is pointwise convergent, which can be seen from the alternative representation of this integrand (Eq. (E.109)). Moreover, to every $l \in \{0, 1, \dots\}$ there is $c_l > 0$ such, that for all $x \in \mathbb{R}$ with

$$\min\{|x - \mu_j| : j = 1, \dots, m\} \quad \geq \quad r/2 \qquad \text{(E.178)}$$

the inequality

$$|g^{(l)}(x)| \quad \leq \quad c_l \tag{E.179}$$

holds independently of the value of the temperature T (Eq. (E.165)). In particular, the integrand of the integral over $[0, r/2]$ within Eq. (E.176) is bounded by

$$\frac{2c_{n+1}}{(n+1)!}, \tag{E.180}$$

so the integral is convergent for $T \to 0$ with Lebesgue. Moreover, note that the upper bound for its value,

$$\frac{c_{n+1}}{n+1}\frac{r}{\pi}, \tag{E.181}$$

does depend on r, but that it is independent of the temperature T, as well as of the value of the initially given ε.

The numerator of the second contributing integral within Eq. (E.176), the first integral over $[r/2, \infty[$, is a polynomial in the integration variable ω of degree smaller or equal $n-1$. Its coefficients are obtained from the derivatives of g in ε. Hence, they are convergent with $T \to 0$, and upper bounds for their absolute values are obtained from the constants $c_l (l = 0, \ldots, n-1)$ chosen above.

What remains to be shown is the convergence of the contribution

$$\begin{aligned} & \frac{n!}{\pi} \quad \int_{r/2}^{\infty} \quad \frac{d\omega}{\omega^{n+1}} \quad \{ \; g(\varepsilon+\omega) \quad + \quad (-1)^{n+1} g(\varepsilon-\omega) \} \\ = \quad & \frac{n!}{\pi} \quad \int_{\mathbb{R}} \quad d\omega \quad g(\varepsilon+\omega) \quad \frac{\mathbf{1}_{\mathbb{R}\setminus B_{r/2}(0)}(\omega)}{\omega^{n+1}} \end{aligned} \tag{E.182}$$

with $T \to 0$, and the existence of an upper bound which is independent of the temperature T, and of ε. However, the integrand of the latter integral is pointwise convergent, an integrable upper bound of the integrand is given by

$$|\gamma(\varepsilon+\omega)| \quad \frac{\mathbf{1}_{\mathbb{R}\setminus B_{r/2}(0)}(\omega)}{|\omega|^{n+1}}, \tag{E.183}$$

and so an upper bound for the integral independent of temperature and the value of ε is obtained by the Cauchy-Schwarz inequality:

$$\begin{aligned} & \left| \frac{n!}{\pi} \quad \int_{\mathbb{R}} \quad d\omega \quad g(\varepsilon+\omega) \quad \frac{\mathbf{1}_{\mathbb{R}\setminus B_{r/2}(0)}(\omega)}{\omega^{n+1}} \right| \\ \leq \quad & \frac{n!}{\pi} \quad \|\gamma\|_2 \quad \left\| \omega \mapsto \frac{\mathbf{1}_{\mathbb{R}\setminus B_{r/2}(0)}(\omega)}{\omega^{n+1}} \right\|_2 . \end{aligned} \tag{E.184}$$

Proof of Statement ii):

We let $\varepsilon \in \mathbb{R} \setminus \mu_1$ be given. Let

$$r \quad := \quad |\mu_1 - \varepsilon|, \tag{E.185}$$

and decompose $H^{(n)}g(\varepsilon)$ as in the proof of statement i), where now

$$g \quad := \quad \gamma f_1' f_1^\kappa. \tag{E.186}$$

The convergence of the integral over $[0, r/2]$ within the sum (E.176), as well as the convergence of the first integral over $[r/2, \infty[$, is seen in the same way as in the proof of statement i).

Hence, we consider only the contribution

$$\begin{aligned} & \frac{n!}{\pi} \quad \int_{\mathbb{R}} \quad d\omega \quad \gamma(\varepsilon+\omega) \quad \frac{\mathbf{1}_{\mathbb{R}\setminus B_{r/2}(0)}(\omega)}{\omega^{n+1}} \quad (f_1' f_1^\kappa)(\varepsilon+\omega) \\ = \quad & \frac{n!}{\pi} \quad \int_{\mathbb{R}} \quad dx \quad h(x) \quad (f_1' f_1^\kappa)(x), \end{aligned} \tag{E.187}$$

with

$$h(x) \quad := \quad \gamma(x) \quad \frac{\mathbf{1}_{\mathbb{R}\setminus B_{r/2}(0)}(x-\varepsilon)}{(x-\varepsilon)^{n+1}}. \tag{E.188}$$

We note that the function h is bounded and smooth on $\mathbb{R}\setminus]\varepsilon - r/2, \varepsilon + r/2[$. Upon applying an integral transformation the integral turns into

$$\frac{n!}{\pi} \quad \int_{\mathbb{R}} dz \quad f'(z) f^\kappa(z) \quad h(\mu_1 + k_B T z). \tag{E.189}$$

The integrand of this integral is pointwise convergent for $T \to 0$, and an integrable upper bound is given by $||h||_\infty |f'(z)|$, so the convergence follows with Lebesgue.

Proof of Statement iii):

Let $\varepsilon \in \mathbb{R} \setminus \{\mu_0, \ldots, \mu_m\}$ be given. We define

$$r \quad := \quad \min\{|\varepsilon - \mu_j| : \quad j = 0, \ldots, m\}, \tag{E.190}$$

$$g \quad := \quad \gamma f_1^{\kappa_1} \ldots f_m^{\kappa_m} \quad H(\alpha f_0), \tag{E.191}$$

and decompose $H^{(n)}g(\varepsilon)$ as in the proof of statement i), Eq. (E.176). Note that, according to our assumption, $\alpha f_0 \in \mathcal{R}$, hence for arbitrary $l \geq 0$: $H(\alpha f_0)^{(l)} = H^{(l)}(\alpha f_0)$ – the l-th derivative of $H(\alpha f_0)$ is obtained by applying the transformation $H^{(l)}$ (Def. (E.105)) to αf_0. Part i) of the present lemma yields thus statements about the derivatives of $H(\alpha f_0)$:

For any $\varepsilon' \neq \mu_0$, the limit

$$\lim_{T \to 0} H^{(l)}(\alpha f_0)(\varepsilon') \tag{E.192}$$

exists, and, to any $r' > 0$, there is a constant $c_{r',l} > 0$ such, that for all $\varepsilon' \in \mathbb{R}\backslash]\mu_0 - r', \mu_0 + r'[$:

$$\left| H^{(l)}(\alpha f_0)(\varepsilon') \right| \;\leq\; c_{r',l}. \tag{E.193}$$

We conclude that the first and the second integral contributing to $H^{(n)}g(\varepsilon)$ within the decomposition (E.176) are convergent for $T \to 0$.

The third and last integral is

$$\begin{aligned} & \frac{n!}{\pi} \quad \int_{r/2}^{\infty} \quad \frac{d\omega}{\omega^{n+1}} \quad \{g(\varepsilon+\omega) + (-1)^{n+1} g(\varepsilon-\omega)\} \\ = \quad & \frac{n!}{\pi} \quad \int_{\mathbb{R}} \quad d\omega \quad \left(\gamma f_1^{\kappa_1} \dots f_m^{\kappa_m}\right)(\omega) \quad \frac{\mathbf{1}_{\mathbb{R}\backslash B_{r/2}(\varepsilon)}(\omega)}{(\omega-\varepsilon)^{n+1}} \quad H(\alpha f_0)(\omega) \\ = \quad & \frac{n!}{\pi} \quad \int_{\mathbb{R}} \quad d\omega \quad h(\omega) \quad H(\alpha f_0)(\omega), \end{aligned} \tag{E.194}$$

with

$$h(\omega) \;:=\; \left(\gamma f_1^{\kappa_1} \dots f_m^{\kappa_m}\right)(\omega) \quad \frac{\mathbf{1}_{\mathbb{R}\backslash B_{r/2}(\varepsilon)}(\omega)}{(\omega-\varepsilon)^{n+1}}. \tag{E.195}$$

Note that h, as well as αf_0, are pointwise convergent for $T \to 0$, and because this pointwise convergence is bounded by a square-integrable function, the convergence is satisfied also in the $\| \quad \|_2$-norm. The Hilbert transformation is isometric with respect to this norm, so $H(\alpha f_0)$ is convergent in $\| \quad \|_2$. With Cauchy-Schwarz follows the convergence of the integral of the product $h\ H(\alpha f_0)$.

Proof of Statement iv):

We let $\varepsilon \in \mathbb{R} \setminus \mu_0$,

$$r \quad := \quad |\varepsilon - \mu_0|, \tag{E.196}$$

$$g \quad := \quad \gamma(-f_0')f_0^{\kappa} \quad H(\alpha f_0), \tag{E.197}$$

and decompose $H^{(n)}g(\varepsilon)$ in the same way as for the proof of statement i), Eq. (E.176). We note that the first two integrals within the decomposition (E.176) are convergent for $T \to 0$. The third integral is

$$\frac{n!}{\pi} \quad \int_{\mathbb{R}} d\omega \quad \left[(-f_0')f_0^{\kappa} \quad H(\alpha f_0)\right](\omega) \quad h(\omega) \tag{E.198}$$

with

$$h(\omega) \quad := \quad \gamma(\omega) \quad \frac{\mathbf{1}_{\mathbb{R}\backslash B_{r/2}(\varepsilon)}(\omega)}{(\omega-\varepsilon)^{n+1}}. \tag{E.199}$$

After a transformation the integral reads

$$\frac{n!}{\pi}\int_{\mathbb{R}} dx \quad (-f'(x))f^{\kappa}(x)\; H(\alpha f_0)(\mu_0 + xk_BT)\; h(\mu_0 + xk_BT). \tag{E.200}$$

As we shall show in App. F (Universality), the difference

$$\gamma_T(x) \quad := \quad H(\alpha f_0)(\mu_0 + xk_BT) \quad - \quad H(\alpha f_0)(\mu_0) \tag{E.201}$$

is pointwise convergent for $T \to 0$, so for each arbitrary value of x, the limit $\lim_{T\to 0}\gamma_T(x)$ exists. Moreover, there is a constant $c > 0$ such, that for all $x \in \mathbb{R}$, and $T \in]0, T_0]$:

$$|\gamma_T(x)| \quad \leq \quad c|x|. \tag{E.202}$$

To show the latter statement, we represent

$$\gamma_T(x_0) \quad = \quad \int_0^{x_0} dx \quad \gamma_T'(x), \text{ and} \tag{E.203}$$

$$\gamma_T'(x) \quad = \quad \frac{1}{\pi}\int_0^{\infty} dy \quad G_{x,T}(y), \tag{E.204}$$

where

$$G_{x,T}(y) \quad := \quad \frac{1}{y^2}\left\{F_{x,T}(y) + F_{x,T}(-y) - 2F_{x,T}(0)\right\}, \tag{E.205}$$

$$F_{x,T}(z) \quad := \quad \alpha(\mu_0 + k_BT(x+z)) \quad f(x+z). \tag{E.206}$$

The integrand $G_{x,T}$ is pointwise convergent for $T \to 0$, and there is an integrable map

$$G_{T_0} : \quad]0, \infty[\to \mathbb{R} \tag{E.207}$$

such, that for all $x \in \mathbb{R}$, $T \in]0, T_0]$:

$$|G_{x,T}| \quad \leq \quad G_{T_0} \tag{E.208}$$

pointwise. To obtain such an upper bound for $|G_{x,T}|(y)$, we distinguish between the cases $y \leq 1$ and $y > 1$. We represent

$$\begin{aligned} & F_{x,T}(y) + F_{x,T}(-y) - 2F_{x,T}(0) \\ = \quad & \int\int_{0\leq t_2\leq t_1\leq y} \left(F''_{x,T}(t_2) + F''_{x,T}(-t_2)\right) \end{aligned} \tag{E.209}$$

in case $y \leq 1$, while for $y > 1$ we estimate: $|G_{x,T}|(y) \leq \frac{4}{y^2}\left\|\alpha\right\|_{\infty}$.

It follows from the pointwise convergence of γ_T (E.201), and from the estimate (E.202), that the integral

$$\frac{n!}{\pi} \quad \int_{\mathbb{R}} dx \quad (-f'(x))f^{\kappa}(x) \quad \gamma_T(x) \quad h(\mu_0 + xk_BT). \tag{E.210}$$

is convergent for $T \to 0$. Hence, the congruence

$$\begin{aligned} & \frac{n!}{\pi} \int_{\mathbb{R}} dx \quad (-f'(x))f^{\kappa}(x)\ H(\alpha f_0)(\mu_0 + xk_BT)\ h(\mu_0 + xk_BT) \\ \overset{T\to 0}{\equiv} \quad & \frac{n!}{\pi}\ H(\alpha f_0)(\mu_0) \int_{\mathbb{R}} dx\ (-f'(x))f^{\kappa}(x)\ h(\mu_0 + xk_BT) \end{aligned} \tag{E.211}$$

holds, so we have slightly simplified the integral (E.200) whose logarithmic divergence with $T \to 0$ we want to show.

Now, we want to prove the relation

$$H(\alpha f_0)(\mu_0) \quad \overset{T\to 0}{\equiv} \quad \frac{\alpha(\mu_0)}{\pi} \ln\left(\frac{T}{T_0}\right) : \tag{E.212}$$

We represent

$$\frac{d}{dT} H(\alpha f_0)(\mu_0) \quad = \frac{\pi^{-1}}{T} \int_{\mathbb{R}} dx \quad (-f'(x))\alpha(\mu_0 + k_BTx), \tag{E.213}$$

and for $T' \in]0, T_0]$:

$$\begin{aligned} & H(\alpha f_0)(\mu_0)|^{T=T'} \quad - \quad \frac{\alpha(\mu_0)}{\pi} \ln\left(\frac{T'}{T_0}\right) \\ = \quad & H(\alpha f_0)(\mu_0)|^{T=T_0} \quad - \quad \frac{k_B}{\pi} \int_{T'}^{T_0} dT \int_{\mathbb{R}} dx \\ & \qquad (-f'(x))x(\delta_{\mu_0}\alpha)(\mu_0 + k_BTx), \end{aligned} \tag{E.214}$$

where the latter integral is convergent for $T' \to 0$.

Finally, we note

$$\begin{aligned} & \frac{n!}{\pi}\ \frac{\alpha(\mu_0)}{\pi} \ln\left(\frac{T}{T_0}\right) \quad \int_{\mathbb{R}} dx\ (-f'(x))f^{\kappa}(x)\ h(\mu_0 + xk_BT) \\ \overset{T\to 0}{\equiv} \quad & \frac{n!}{\pi}\ \frac{\alpha(\mu_0)}{\pi} \ln\left(\frac{T}{T_0}\right) \quad \int_{\mathbb{R}} dx\ (-f'(x))f^{\kappa}(x)\ h(\mu_0), \end{aligned} \tag{E.215}$$

since

$$\begin{aligned} & \left|\ln\frac{T}{T_0}\right| \quad \int_{\mathbb{R}} dx\ (-f'(x))f^{\kappa}(x)\ |h(\mu_0 + xk_BT) - h(\mu_0)| \\ \leq \quad & \left|\ln\frac{T}{T_0}\right| \quad k_BT \quad ||\delta_{\mu_0}h||_{\infty} \int_{\mathbb{R}} dx\ (-f'(x))f^{\kappa}(x)|x| \\ \to \quad & 0\ (T \to 0) \end{aligned} \tag{E.216}$$

with de l'Hospital.

In summary,

$$\begin{array}{cccc} & H^{(n)}\,[\gamma(-f_0')f_0^{\kappa} & H(\alpha f_0)] & (\varepsilon) \\ \overset{T\to 0}{\equiv} & \dfrac{n!}{\pi^2} & \dfrac{(\alpha\gamma)(\mu_0)}{\kappa+1}\,\dfrac{1}{(\mu_0-\varepsilon)^{n+1}} & \ln\left(\dfrac{T}{T_0}\right). \end{array} \qquad \square \quad \text{(E.217)}$$

E.3.3 Temperature-Dependence of Sixth Order Current and Conductance – Practice

The lemma of the previous section implies the existence of the zero temperature limit

$$\lim_{T\to 0}\Gamma_l^{\pm}(DSO,III), \tag{E.218}$$

of the rates $\Gamma_l^{\pm}(DSO,III)$ (Eqs. (E.158), (E.159), and (E.160)) within the sixth order DSO for infinite U in case

$$E_{10} \quad \neq \quad \mu_l,\mu_{\bar{l}}: \tag{E.219}$$

In particular, the lemma's statement i) (E.169) implies the existence of the zero temperature limit of the fourth order contribution $\Gamma_l^{\pm}(DSO,4)$ (E.159), while statements i) and iii) (E.174) imply the existence of the zero temperature limit of the sixth order contribution $\Gamma_l^{\pm}(DSO,6)$ (E.160). As a consequence, the zero temperature limits

$$\lim_{T\to 0}\hat{\boldsymbol{\rho}}, \text{ and } \lim_{T\to 0}\boldsymbol{I_l},$$

of density matrix (E.146), and current (E.147) also exist.

Linear Conductance within the Sixth Order DSO

Expressed by the bilinear and trilinear forms (E.161), and (E.162), the sixth order current $I_l(DSO,III)$ for infinite interaction U reads:

$$\begin{aligned} I_l(DSO,III) \quad = \\ \\ \frac{2}{\hbar}\Big\{\ \pi(\alpha_{\bar{l}}^{+}-\alpha_l^{+})(E_{10}) \ +\ Bil(DSO)(\alpha_{\bar{l}}^{+}-\alpha_l^{+},\alpha+\alpha^{+}) \\ +\ Tril(DSO)(\alpha_{\bar{l}}^{+}-\alpha_l^{+},\alpha+\alpha^{+},\alpha+\alpha^{+})\ \Big\}\,\rho_{00} \quad + \\ \frac{2}{\hbar}\Big\{\ \pi(\alpha_l^{-}-\alpha_{\bar{l}}^{-})(E_{10}) \ +\ Bil(DSO)(\alpha_l^{-}-\alpha_{\bar{l}}^{-},\alpha+\alpha^{+}) \\ +\ Tril(DSO)(\alpha_l^{-}-\alpha_{\bar{l}}^{-},\alpha+\alpha^{+},\alpha+\alpha^{+})\ \Big\}\,\rho_{\sigma\sigma}. \end{aligned} \tag{E.220}$$

We let the chemical potentials be a function of a bias voltage V_b according to

$$\mu_l \;=\; \mu_l(V_b) \;=\; E_F + \lambda_l e V_b, \tag{E.221}$$

with dimension-less constants $\lambda_l > 0, \lambda_{\bar{l}} < 0$ satisfying $\lambda_l - \lambda_{\bar{l}} = 1$, so that

$$\mu_l(V_b) \;-\; \mu_{\bar{l}}(V_b) \;=\; eV_b. \tag{E.222}$$

We determine the linear conductance G by differentiating the particle-current, multiplied by the electron charge $-e$, with respect to the bias, and by evaluating this derivative in particular at zero bias:

$$G(DSO, III) \;=\; \frac{d(-e)I_l(DSO, III)}{dV_b}\bigg|^{V_b=0}. \tag{E.223}$$

We obtain:

$$\begin{aligned} G(DSO, III) \quad &= \\ \frac{4\pi e^2}{h}\,[\rho_{00} + \rho_{\sigma\sigma}]\,\Big\{\; &\pi(\alpha_l f_{T,E_F})(E_{10}) \;+\; Bil(DSO)(\alpha_l f_{T,E_F}, \alpha + \alpha^+) \\ &+ Tril(DSO)(\alpha_l f_{T,E_F}, \alpha + \alpha^+, \alpha + \alpha^+)\;\Big\} \end{aligned} \tag{E.224}$$

with

$$f_{T,E_F}(\varepsilon) \quad := \quad \frac{-1}{k_B T} f'\left(\frac{\varepsilon - E_F}{k_B T}\right) \quad = \quad \frac{\partial}{\partial\varepsilon}(1 - f)\left(\frac{\varepsilon - E_F}{k_B T}\right) \tag{E.225}$$

according to (3.47). Note that the function f_{T,E_F} is positive, has total weight one, and that its weight is distributed over a region around the Fermi level E_F whose size is proportional to $k_B T$.

Divergence of $G(DSO, III)$ with $T \to 0$

We investigate the dependence of $G(DSO, III)$ on the temperature as $T \to 0$. We assume, that

$$E_{10} \quad \neq \quad E_F, \tag{E.226}$$

and consider in particular the divergent contribution

$$\begin{aligned} &(\rho_{00} + \rho_{\sigma\sigma}) \quad Tril(DSO)(\alpha_l f_T, \alpha + \alpha^+, \alpha + \alpha^+) \\ \overset{T\to 0}{\equiv}\; &(\rho_{00} + \rho_{\sigma\sigma})(-\pi^3) H\left[\alpha_l f_T (\alpha + \alpha^+) H(\alpha + \alpha^+)\right]''(E_{10}) \end{aligned} \tag{E.227}$$

(Def. (E.162)).

By the statements (ii) (E.172), and (iv) (E.175), of the previous section's lemma we conclude:

$$G(DSO,III) \quad \stackrel{T\to 0}{\equiv} \quad \frac{e^2\pi^2}{h}(\rho_{00}+\rho_{\sigma\sigma}) \quad \frac{6\alpha^3(E_F)}{(E_{10}-E_F)^3} \quad \ln\left(\frac{T}{T_0}\right). \tag{E.228}$$

Thus, the linear conductance obtained by the sixth order DSO for infinite Coulomb-interaction U diverges logarithmically to plus infinity with $T \to 0$ in case $E_{10} < E_F$, and it diverges logarithmically to minus infinity if $E_{10} > E_F$.

Upon taking into account *all* diagrams for the SIAM at infinite U up to sixth order, the divergence to plus infinity in case $E_{10} < E_F$ is still present, and the pre-factor of the logarithm is increased. On the other hand, in the case $E_{10} > E_F$, the pre-factor of the logarithmic term no more contains the probability ρ_{00}, but only $\rho_{\sigma\sigma}$ [20]. Hence, the logarithmic divergence is much weaker in the case $E_{10} > E_F$ within the exact sixth order.

Conclusion

The current I_l across a quantum dot as function of the bias V_b can be represented as

$$I_l \;=\; \begin{cases} \int_0^{V_b} dV_b' \; \frac{dI_l}{dV_b}(V_b') & (V_b > 0) \\ -\int_{V_b}^0 dV_b' \; \frac{dI_l}{dV_b}(V_b') & (V_b < 0) \end{cases} . \tag{E.229}$$

We showed that, within the approximation of the sixth order DSO for infinite Coulomb-interaction, the zero temperature limit of the current I_l exists, as long as the energy of the quantum dot level is different from both chemical potentials $E_{10} \neq \mu_l, \mu_{\bar{l}}$. In particular, *at zero bias*, the differential conductance dI_l/dV_b diverges logarithmically to plus infinity with $T \to 0$, if the energy E_{10} lies below the Fermi level. Hence, the divergence of the differential conductance at zero bias can be only a singular behaviour, and we can expect to see a peak in the graph of dI_l/dV_b vs. the bias around zero bias, logarithmically getting more and more pronounced with $T \to 0$.

Appendix F

Universality in the Temperature-Dependence of G

In the present appendix we analyze the expressions for the linear conductance for infinite Coulomb-interaction obtained within the DSO (3.53), as well as within the RTA (3.52). Our aim is to represent the expressions for the conductance by functions which take a small number of scalar arguments, and which are otherwise parameter-free, and in this sense universal (cp. Fig. 3.14). On the way to this, we show the existence of the zero temperature limit $\lim_{T\to 0}\{p_{b^+}(E_F + xk_BT) - p_{b^+}(E_F)\}$ (cp. Fig. 3.11), and give its parameter-free representation (Fig. F.1). Moreover, we show that $p_{b^+}(E_F)$ diverges logarithmically with temperature as $T \to 0$.

For a start, we concentrate on the expression

$$G^{RTA} = 4\kappa_l\kappa_{\bar{l}}\frac{e^2}{h}2 \int d\varepsilon \; \frac{\pi^2\alpha^2(\varepsilon)}{d(\varepsilon)} \; f_{T,E_F}(\varepsilon). \tag{F.1}$$

for the conductance within the RTA (3.52), where the denominator is $d(\varepsilon) := \pi^2(\alpha + \alpha^+)^2(\varepsilon) + (\varepsilon + p_{\alpha+\alpha^+}(\varepsilon) - E_{10})^2$. We here study only the relative conductance $G(T)/G_{max}$, and so we analyze only the integral-part of the present expression. To this end, we write the coupling function $\alpha(\varepsilon)$ as the product

$$\alpha(\varepsilon) \;=\; \alpha(E_F)b(\varepsilon) \tag{F.2}$$

(cp. Fig. 3.12), and divide both the numerator and denominator of the integrand within the present equation (F.1) by $\alpha(E_F)^2$. Moreover, we write $\varepsilon = E_F + xk_BT$, and integrate with respect to x instead of ε.

The integral is concentrated in a region of few multiples of the thermal energy around E_F, hence, it is justified to estimate $b(\varepsilon) = 1$, and $p_b(\varepsilon) =$

$p_b(E_F)$; $p_b(E_F)$ here is zero since we choose the function $b(\varepsilon)$ to be symmetric around E_F (Fig. 3.12). Upon applying these modifications we obtain the integral:

$$\int d\varepsilon \; \frac{\pi^2\alpha^2(\varepsilon)}{d(\varepsilon)} \; f_{T,E_F}(\varepsilon) \;=\; \int dx \frac{-\pi^2 f'(x)}{\pi^2(1+f(x))^2+\phi^2(x)}, \tag{F.3}$$

where we use the abbreviation

$$\phi(x) := x\frac{k_BT}{\alpha(E_F)} + \frac{E_F - E_{10}}{\alpha(E_F)} + p_{b^+}(E_F + xk_BT), \tag{F.4}$$

and where the function b^+ is given by $b^+(\varepsilon) = b(\varepsilon)f\left((\varepsilon - E_F)/k_BT\right)$ (cp. Fig. 3.11), with f the parameter-free Fermi function (Eq. (C.78)).

Logarithmic Divergence of $p_{b^+}(E_F)$:

We now analyze the behaviour of the function $p_{b^+}(E_F + xk_BT)$, and, first of all, we consider its depencence on the temperature in $x = 0$. We obtain for the *derivative* of $p_{b^+}(E_F)$ with respect to the temperature:

$$\begin{aligned} & \frac{d}{dT}\, p_{b^+}(E_F) \\ = \;& \frac{d}{dT}\int_0^\infty d\omega \frac{b(E_F+\omega)f\left(\frac{\omega}{k_BT}\right) - b(E_F-\omega)f\left(\frac{-\omega}{k_BT}\right)}{\omega} \\ = \;& \frac{1}{T}\int_{\mathbb{R}} dx(-f')(x)b(E_F+xk_BT) \;\approx\; \frac{1}{T}, \end{aligned} \tag{F.5}$$

provided that, within a range of few multiples of k_BT around the Fermi level, the approximation

$$b(\varepsilon) \;\approx\; 1 \tag{F.6}$$

holds. We conclude that, for temperatures T' below some fixed value T_0, at which the present approximation is satisfied:

$$p_{b^+}(E_F)\big|^{T=T'} \;\approx\; p_{b^+}(E_F)\big|^{T=T_0} \;+\; \ln\left(\frac{T'}{T_0}\right). \tag{F.7}$$

The Pointwise Limit $\lim_{T\to 0}\{p_{b^+}(E_F + xk_BT) - p_{b^+}(E_F)\}$:

Next, we consider the difference

$$p_{b^+}(E_F + xk_BT) - p_{b^+}(E_F) \;=$$

$$\begin{aligned}\int_0^\infty \tfrac{dy}{y} \quad & \{(b(E_F + k_B T(x+y))f(x+y) \\ & -b(E_F + k_B Ty)f(y) \\ & -b(E_F + k_B T(x-y))f(x-y) \\ & +b(E_F - k_B Ty)f(-y)\}. \end{aligned} \tag{F.8}$$

For every single value of y, the limit $T \to 0$ can be taken. We suppose that the zero temperature limit of the present integral exists, and that it is given by the integral of the pointwise limit,

$$\begin{aligned} g(x) := \quad \int_0^\infty \tfrac{dy}{y} \quad & \{f(x+y) - f(y) \\ & -f(x-y) + f(-y)\}. \end{aligned} \tag{F.9}$$

For the proof we want to apply Lebesgue's convergence theorem, so we need to determine an integrable upper bound for the integrand within (F.8) which is independent of the temperature T – below some arbitrary but finite value T_0. To this end, we note the abstract form of the integrand:

$$\frac{1}{y}\left\{(AB)(x+y) - (AB)(y) - (AB)(x-y) + (AB)(-y)\right\}, \tag{F.10}$$

where

$$A(z) := b(E_F + k_B Tz), \tag{F.11}$$

$$B(z) := f(z). \tag{F.12}$$

Moreover, we decompose the integral (F.8) according to $\int_0^\infty = \int_0^1 + \int_1^\infty$, since the two different intervals make different treatments necessary.

Integrable Upper Bound over $]0,1]$:

We group the terms within (F.10) according to

$$\frac{1}{y}\left\{(AB)(x+y) - (AB)(x-y)\right\} \tag{F.13}$$

$$- \quad \frac{1}{y}\left\{(AB)(y) - (AB)(-y)\right\}, \tag{F.14}$$

and consider the present two differences separately. Upon adding and subtracting the mixed terms $A(x+y)B(x-y)$, and $A(y)B(-y)$, respectively, we see that there is even a constant upper bound within this interval. The conditions to be satisfied by the function $b(\varepsilon)$ are as follows:

- The function $b(\varepsilon)$ is bounded, $|b(\varepsilon)| \leq b_\infty$, b_∞ independent of ε.
- The function satisfies a Lipschitz condition of the form:

$$|b(\varepsilon) - b(\varepsilon')| \leq L\,|\varepsilon - \varepsilon'|\,, \tag{F.15}$$

  L independent of ε and ε'.

We note that the Fermi function, too, has these two properties. Moreover, a lorentzian, any other function within the space $\mathcal{R}$ (App. E.2.1 (Diagram Calculations – Theory)), or the function b sketched in Fig. 3.12 has the present two properties.

Integrable Upper Bound over $[1,\infty[$:

To determine an integrable upper bound for the integrand of the integral (F.8) over $[1,\infty[$, which is independent of $T \in]0, T_0]$, T_0 sufficiently small, we group those terms with equal sign in front of y into pairs. We add and subtract the mixed term $A(x+y)B(y)$ to estimate that part of the integrand with positive sign in front of y by

$$\begin{aligned} & \frac{1}{y}\; b(E_F + k_B T(x+y))\;\; |f(x+y) - f(y)| \\ + \;\; & \frac{1}{y}\; f(y)\;\; |b(E_F + k_B T(x+y)) - b(E_F + k_B T y)|\,, \end{aligned} \tag{F.16}$$

while we estimate that part with a negative sign in front of y by

$$\begin{aligned} & \frac{1}{y}\; b(E_F + k_B T(x-y))\;\; |f(x-y) - f(-y)| \\ + \;\; & \frac{1}{y}\; f(-y)\;\; |b(E_F + k_B T(x-y)) - b(E_F - k_B T y)|\,. \end{aligned} \tag{F.17}$$

The first line within the expression (F.16) is bounded by $B/y\,|f(x+y) - f(y)|$, which is integrable, because:

$$\begin{aligned} \frac{|f(x+y) - f(y)|}{y} &\overset{y\geq 1}{\leq} |f(x+y) - f(y)| \\ &\leq \underbrace{\max\{|f'(z)| : |z-y| \leq |x|\}}_{=:m_x(y)}\,|x|\,. \end{aligned} \tag{F.18}$$

Since the value of x is fixed during the present considerations, and because the Fermi function's derivative f' decays exponentially, $m_x(y)$ is integrable.

To determine an integrable upper bound for the second line within (F.16) we define

$$L_>(\varepsilon) := sup\left\{\frac{|b(\varepsilon'') - b(\varepsilon')|}{\varepsilon'' - \varepsilon'} : \varepsilon \leq \varepsilon' < \varepsilon''\right\}. \tag{F.19}$$

We estimate then:

$$\begin{aligned} & \frac{1}{y}\ f(y)\ \ |(b(E_F + k_BT(x+y)) - b(E_F + k_BTy))| \\ \leq\ & \frac{|x|}{y^2}\,[E_F + k_BT(y - |x|) - E_F + k_BT|x|] \\ & L_>(E_F + k_BT(y - |x|)), \end{aligned} \tag{F.20}$$

for which we multiplied and divided the left-hand side by $k_BT\,|x|\,y$. We note that the value of the square bracket within the present estimate is k_BTy, that for sure $L_>(\varepsilon) \leq L$ (Eq. (F.15)), and make the additional assumption that the function $\varepsilon L_>(\varepsilon)$ is bounded over any interval which has a lower bound, i.e., for any ε_0:

$$L^>(\varepsilon_0) := sup\,\{|\varepsilon L_>(\varepsilon)| : \varepsilon \geq \varepsilon_0\}\ \ <\ \ \infty. \tag{F.21}$$

This present assumption is satisfied whenever the derivative of the function $b(\varepsilon) \in \mathcal{R}$ decays at least like $1/(1 + |\text{argument}|)$, or else, also for the choice of the function $b(\varepsilon)$ according to Fig. 3.12.

Exploiting these properties, we obtain for arbitrary temperatures $T \in]0, T_0]$, with T_0 some arbitrary but fixed value, the upper bound

$$\frac{|x|}{y^2}\,\{L\,(|E_F| + |x|k_BT_0) + L^>\,(E_F - |x|k_BT_0)\} \tag{F.22}$$

for the expression (F.20), and hence for the second line within (F.16). This upper bound is integrable with respect to y over the interval $[1, \infty[$, and independent of the temperature $T \in]0, T_0]$.

We have found an integrable upper bound for the expression (F.16), finally independent of $T > 0$. We treat the expression (F.17) analogously. To this end, we introduce functions $L_<(\varepsilon)$, and $L^<(\varepsilon)$, symmetric to $L_>(\varepsilon)$ (F.19), and $L^>(\varepsilon)$ (F.21), assuming the function $\varepsilon L_<(\varepsilon)$ is bounded over any interval of the form $]-\infty, \varepsilon_0]$, analogous to the assumption (F.21).

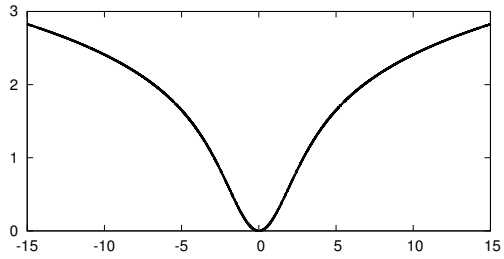

Figure F.1: A plot of the function $g(x)$ defined by Eq. (F.9), i.e., the normalized shape of the functions $p_{b^+}(\varepsilon)$ around the Fermi level in units of the thermal energy (cp. Fig. 3.11). The growth of $g(x)$ is logarithmic in the sense that $xg'(x) \to 1 \quad (|x| \to \infty)$ (not shown within this work).

In summary, we showed the existence of an integrable upper bound for the integrand within the integral (F.8), which is finally independent of $T > 0$.

With Lebesgue we conclude:

$$p_{b^+}(E_F + k_B T x) - p_{b^+}(E_F) \;\to\; g(x) \quad (T \to 0) \tag{F.23}$$

for arbitrary x, where the limit $g(x)$ is given by Def. (F.9). We show the graph of the function $g(x)$ in Fig. F.1.

Approximation for the Integral (F.3):

Earlier, we noticed that the dependence of $p_{b^+}(E_F)$ on the temperature is logarithmic. Putting the two equations (F.7), and (F.23), together, we approximate:

$$p_{b_T^+}(E_F + x k_B T) \;\approx\; p_{b^+_{T_{\alpha(E_F)}}}(E_F) + ln\left(\frac{T}{T_{\alpha(E_F)}}\right) + g(x), \tag{F.24}$$

where the temperature $T_{\alpha(E_F)}$ is defined by the condition

$$k_B T_{\alpha(E_F)} \;=\; \alpha(E_F). \tag{F.25}$$

[To emphasize the fact that the function b^+ has the parameter T, we here add the temperature T as index, and write "b_T^+".] Upon inserting the present approximation into the integral (F.3) we obtain:

$$\begin{aligned}\phi(x) &\approx x\frac{T}{T_{\alpha(E_F)}} + ln\left(\frac{T}{T_{\alpha(E_F)}}\right) + g(x) \\ &\quad + \frac{E_F - E_{10}}{\alpha(E_F)} + p_{b^+_{T_{\alpha(E_F)}}}(E_F). \end{aligned} \tag{F.26}$$

We now define a reference value for E_{10}, "$\overline{E}_{10}$", by the demand that the value of the second line within the present expression is zero for $E_{10} = \overline{E}_{10}$. The integral (F.3) has then the form

$$\int d\varepsilon \; \frac{\pi^2\alpha^2(\varepsilon)}{d(\varepsilon)} \; f_{T,E_F}(\varepsilon) \;\approx\; F^{RTA}\left(\frac{E_{10} - \overline{E}_{10}}{\alpha(E_F)}, \frac{k_BT}{\alpha(E_F)}\right), \tag{F.27}$$

where the definition of F^{RTA} is

$$F^{RTA}(a,b) := \int dx \frac{-\pi^2 f'(x)}{\pi^2(1+f(x))^2 + \phi^2_{a,b}(x)}, \tag{F.28}$$

with

$$\phi_{a,b}(x) := g(x) - a + xb + \ln(b). \tag{F.29}$$

Approximation for G^{DSO}:

The corresponding integral within the formula for G^{DSO} (Eq. (3.53)) can be represented in an analogous way:

$$G^{DSO} \approx 4\kappa_l\kappa_{\bar{l}}\frac{e^2}{h}\left(\frac{2}{1+\frac{\Gamma^+_{01}}{\Gamma_{01}}}\right) F^{DSO}\left(\frac{E_{10} - \overline{E}_{10}}{\alpha(E_F)}, \frac{k_BT}{\alpha(E_F)}\right), \tag{F.30}$$

where the DSO rates $\Gamma^{\pm}_{01} = \sum_l \Gamma^{\pm}_{l,01}$ are given by (3.51), where

$$F^{DSO}(a,b) := \int dx \frac{-\pi^2 f'(x)(1+f(x))}{\pi^2(1+f(x))^2 + \phi^2_{a,b}(x)}, \tag{F.31}$$

and where

$$\overline{E}_{10} := E_F + \alpha(E_F) p_{b^+_{T_{\alpha(E_F)}}}(E_F). \tag{F.32}$$

The factor $\left(2/\left(1+\frac{\Gamma^+_{01}}{\Gamma_{01}}\right)\right) = 1+\rho_{00}$ (Eq. (3.49)) is two minus the particle-number on the quantum dot, and thus a function of the rates – still containing the temperature. However, for temperatures $k_BT \ll \alpha(E_F)$, the tunneling rates become essentially independent of the temperature, so we can focus on the temperature-dependence of the rest. The integral with respect to x contains the derivative of the Fermi function, and is thus concentrated on an interval around zero, whose length's order of magnitude is one. Therefore, we can, in the case of small temperatures compared to $\alpha(E_F)$, $k_BT \ll \alpha(E_F)$, neglect the linear term within $\phi_{a,b}(x)$ (F.29), and estimate

$$\begin{aligned} G^{DSO} &\approx 4\kappa_l\kappa_{\bar{l}}\frac{e^2}{h}(1+\rho_{00}) \\ &\quad F_0^{DSO}\left(-\frac{E_{10}-\overline{E}_{10}}{\alpha(E_F)}+\ln\frac{T}{T_{\alpha(E_F)}}\right), \end{aligned} \tag{F.33}$$

with

$$F_0^{DSO}(c) := \int dx \frac{-\pi^2 f'(x)(1+f(x))}{\pi^2(1+f(x))^2+(g(x)+c)^2}. \tag{F.34}$$

Kondo Temperature

We note that

$$\lim_{|c|\to\infty} F_0^{DSO}(c) = 0, \tag{F.35}$$

and, generally, $F_0^{DSO}(c) > 0$. Let "c_{max}" be the one value of c for which the function $F_0^{DSO}(c)$ reaches its maximum, and let "$c_{1/2} > c_{max}$" be defined by the condition

$$F_0^{DSO}(c_{1/2}) = 1/2F_0^{DSO}(c_{max}). \tag{F.36}$$

We define the temperature T_K by the demand $c = c_{1/2}$, where we insert

$$c = -\frac{E_{10}-\overline{E}_{10}}{\alpha(E_F)}+\ln\frac{T}{T_{\alpha(E_F)}} \tag{F.37}$$

(cp. Eq. (F.33)), so

$$\begin{aligned} T_K &:= e^{c_{1/2}}\exp\left(\frac{E_{10}-E_F}{\alpha(E_F)}\right) \\ &\quad T_{\alpha(E_F)}\exp\left(-p_{b^+_{T_{\alpha(E_F)}}}(E_F)\right). \end{aligned} \tag{F.38}$$

The second line depends on the tunneling coupling $\alpha(E_F)$; however, this dependence is weak, since the quantity $p_{b_T^+}(E_F)$ depends logarithmically on the temperature (Eq. (F.7)).

As long as $\alpha(E_F) \ll W$, the quantity

$$\exp\left(-p_{b^+_{T_{\alpha(E_F)}}}(E_F)\right) \tag{F.39}$$

is proportional to the width W, as introduced in Fig. 3.12. Hence, also T_K is proportional to W under this condition, so we arrive at $k_B T_K = 7W \exp\left(\left(E_{10} - E_F\right)/\alpha(E_F)\right)$ (Eq. (3.58) within Sec. 3.2.2 (Dressed Second Order for the SIAM with Infinite Coulomb-Interaction)), where we obtain the factor "7" numerically.

Bibliography

[1] J.C. Fisher, and I. Giaever, *Tunneling Through Thin Insulating Layers*, Journal of Applied Physics **70**, 172 (1961).

[2] H. R. Zeller, and I. Giaever, *Tunneling, Zero-Bias Anomalies, and Small Superconductors*, Physical Review **181**, 789 (1969).

[3] L.Y.L. Shen, and J.M. Rowell, *Zero-Bias Tunneling Anomalies – Temperature, Voltage, and Magnetic Field Dependence*, Physical Review **165**, 566 (1968).

[4] J.M. Thijssen, and H.S.J. Van der Zant, *Charge transport and single-electron effects in nanoscale systems*, Physica Status Solidi b, **245**, 1455 (2008).

[5] S. Sapmaz, P. Jarillo-Herrero, J. Kong, C. Dekker, L.P. Kouwenhoven, and H.S.J. van der Zant, *Electronic excitation spectrum of metallic carbon nanotubes*, Physical Review B **71**, 153402 (2005).

[6] H. Park, J. Park, A.K.L. Lim, E.H. Anderson, A.P. Alivisatos, and P.L. McEuen, *Nanomechanical oscillations in a single-C_{60} transistor*, Nature (London) **407**, 57 (2000).

[7] N.B. Zhitenev, H. Meng, and Z. Bao, *Conductance of Small Molecular Junctions*, Physical Review Letters **88**, 226801 (2002).

[8] A.V. Kretinin, H. Shtrikman, D. Goldhaber-Gordon, M. Hanl, A. Weichselbaum, J. von Delft, T. Costi, and D. Mahalu, *Spin-$\frac{1}{2}$ Kondo effect in an InAs nanowire quantum dot: Unitary limit, conductance scaling, and Zeeman splitting*, Physical Review B **84**, 245316 (2011).

[9] Y. Teratani, R. Sakano, T. Hata, T. Arakawa, M. Ferrier, K. Kobayashi, and A. Oguri, *Field-induced SU(4) to SU(2) Kondo crossover in a half-filling nanotube dot: Spectral and finite-temperature properties*, Physical Review B **102**, 165106 (2020).

[10] Karl Blum, *Density Matrix: Theory and Applications,* Plenum Press, New York (1996).

[11] B.M. de Souza Melo, L.G.G.V. Dias da Silva, A.R. Rocha, and C. Lewenkopf, *Quantitative comparison of Anderson impurity solvers applied to transport in quantum dots*, Journal of Physics: Condensed Matter **32**, 095602 (2020).

[12] M. Lavagna, *Transport through an interacting quantum dot driven out-of-equilibrium*, Journal of Physics: Conference Series **592**, 012141 (2015).

[13] N.S. Wingreen, and Y. Meir, *Anderson model out of equilibrium: Noncrossing-approximation approach to transport through a quantum dot*, Physical Review B **49**, 11040 (1994).

[14] K.G. Wilson, *The renormalization group: Critical phenomena and the Kondo problem*, Reviews of Modern Physics **47**, 773 (1975).

[15] C. Timm, *Tunneling through molecules and quantum dots: Master-equation approaches*, Physical Review B **77**, 195416 (2008).

[16] S. Koller, M. Grifoni, and J. Paaske, *Sources of negative tunneling magnetoresistance in multilevel quantum dots with ferromagnetic contacts*, Physical Review B **85**, 045313 (2012).

[17] J. Kern, and M. Grifoni, *Transport across an Anderson quantum dot in the intermediate coupling regime,* The European Physical Journal B, **86**, 384 (2013).

[18] H. Schoeller, *Transport Theorie für wechselwirkende Quantenpunkte*, Habilitationsschrift Universität Karlsruhe, KIT-Bibliothek, URN: urn:nbn:de:swb:90-AAA440978 (1997).

[19] S. Koller, *Spin phenomena and higher order effects in transport across interacting quantum-dots*, Ph.D. Thesis, Universitätsverlag Regensburg, Dissertationsreihe Physik, URN: urn:nbn:de:bvb:355-epub-136334, DOI: 10.5283/epub.13633 (2010).

[20] J. Kern, *A perturbation theory for the Anderson model*, arXiv:1302.6511v2 [cond-mat.str-el] (2014).

[21] J. König, *Resonanztunneln in mesoskopischen Systemen*, Diplomarbeit (Universität Karlsruhe), Universität Duisburg-Essen – Jürgen König – list of publications, Universität Karlsruhe (1995).

[22] J. König, J. Schmid, H. Schoeller, and G. Schön, *Resonant tunneling through ultrasmall quantum dots: Zero-bias anomalies, magnetic-field dependence, and boson-assisted transport*, Physical Review B **54**, 16820 (1996).

[23] D. Goldhaber-Gordon, J. Göres, M.A. Kastner, Hadas Shtrikman, D. Mahalu, and U. Meirav, *From the Kondo Regime to the Mixed-Valence Regime in a Single-Electron Transistor*, Physical Review Letters **81**, 5225 (1998).

[24] J. Schmid, J. Weis, K. Eberl, and K.v. Klitzing, *A quantum dot in the limit of strong coupling to reservoirs*, Physica B **256-258**, 182 (1998).

[25] Y. Meir, N.S. Wingreen, and P.A. Lee, *Low-Temperature Transport Through a Quantum Dot – The Anderson Model Out of Equilibrium*, Physical Review Letters **70**, 2601 (1993).

[26] S. Schmitt, and F.B. Anders, *Nonequilibrium Zeeman Splitting in Quantum Transport through Nanoscale Junctions*, Physical Review Letters **107**, 056801 (2011).

[27] D.C. Ralph, and R.A. Buhrman, *Kondo-Assisted and Resonant Tunneling via a Single Charge Trap: A Realization of the Anderson Model Out of Equilibrium*, Physical Review Letters **72**, 3401 (1994).

[28] C.H.L. Quay, J. Cumings, S.J. Gamble, R. de Picciotto, H. Kataura, and D. Goldhaber-Gordon, *Magnetic field dependence of the spin-1/2 and spin-1 Kondo effects in a quantum dot*, Physical Review B **76**, 245311 (2007).

[29] U. Wilhelm, J. Schmid, J. Weis, and K. v. Klitzing, *Experimental evidence for spinless Kondo effect in two electrostatically coupled quantum dot systems*, Physica E **14**, 385 (2002).

[30] J.N. Pedersen, and A. Wacker, *Tunneling through nanosystems: Combining broadening with many-particle states*, Physical Review B **72**, 195330 (2005).

[31] O. Karlström, C. Emary, P. Zedler, J.N. Pedersen, C. Bergenfeldt, P. Samuelsson, T. Brandes, and A. Wacker, *A diagrammatic description of the equations of motion, current and noise within the second-order von Neumann approach*, Journal of Physics A: Mathematical and Theoretical **46**, 065301 (2013).

[32] V. Kashcheyevs, A. Aharony, and O. Entin-Wohlman, *Applicability of the equations-of-motion technique for quantum dots,* Physical Review B **73**, 125338 (2006).

[33] A. Dirnaichner, M. Grifoni, A. Prüfling, D. Steiniger, A.K. Hüttel, and C. Strunk, *Transport across a carbon nanotube quantum dot contacted with ferromagnetic leads: Experiment and nonperturbative modeling*, Physical Review B **91**, 195402 (2015).

[34] D. Mantelli, *Analytical and numerical study of quantum impurity systems in the intermediate and strong coupling regimes*, Ph.D. Thesis, URN: urn:nbn:de:bvb:355-epub-341352, DOI: 10.5283/epub.34135 (2016).

[35] J. Kern, *Tunneling Hamiltonian*, arXiv:1302.1391v2 [cond-mat.str-el] (2013).